Princeton University

Department of
Mechanical and
Aerospace Engineering

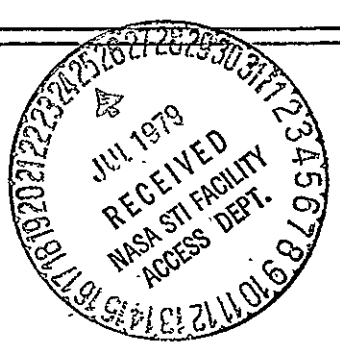

THE INFLUENCE OF FEEDBACK ON THE AEROELASTIC BEHAVIOR OF TILT PROPROTOR AIRCRAFT INCLUDING THE EFFECTS OF FUSELAGE MOTION

by

H. C. Curtiss, Jr.
T. Komatsuzaki
J. J. Traybar

Department of Mechanical and Aerospace Engineering
Princeton University
Princeton, N. J. 08544

Technical Report No. 1441

Final Technical Report
September 1, 1976 to January 31, 1978

NASA-Ames Grant No. NSG-2181

Principal Investigator: H. C. Curtiss, Jr.

NASA Technical Officer: J. P. Rabbott, NASA Ames

July 1979

ABSTRACT

Feedback techniques are employed to examine the influence of various physical design parameters on the aeroelastic stability of tilt proprotor aircraft. In addition, the influence of single loop feedbacks to improve the stability of the system are considered. Reduced order dynamic models are employed where appropriate to promote physical insight. The influence of fuselage freedom on the aeroelastic stability is examined as well as the influence of the airframe flexibility on the low frequency modes of motion relevant to the stability and control characteristics of the vehicle.

TABLE OF CONTENTS

NOMENCLATURE

Conventional helicopter notation is followed in this report. Quantities are made dimensionless using air density, ρ, rotor rotational velocity, Ω, and rotor radius, R. The nondimensionalization is implied by the notation , e.g., the inflow ratio $\frac{V}{\Omega R}$ is written as V. Inertial properties normalized by $\frac{N}{2} I_b$ are denoted by $( )^*$. Quantities are defined when introduced in the text or in Appendix I. The notation is identical to that of References 1 and 2.

INTRODUCTION

One of the critical problem areas related to the design and development of low disc loading tilting proprotor aircraft has been associated with eliminating the occurrance of aeroelastic instabilities at high cruise flight speeds. Owing to the importance of this problem area many studies have been conducted related to this complex problem[1-12].

This report examines a number of aspects of this problem, the aeroelastic stability characteristics of tilting proprotor aircraft in cruise flight including the effects of fuselage motion. It has generally been found that a large number of degrees of freedom, as well as precise modelling of the elastic properties of the rotor system are required in order to predict all of the relevant aeroelastic phenomena[3]. It has also been shown that these models agree well with experiment[9,12]. The high order of these models makes it difficult to obtain physical insight into the significant parameters influencing the dynamic characteristics.

One of the objectives of this study was to employ automatic control techniques to examine the feasibility of using relatively simple feedbacks to improve the dynamic stability characteristics of the wing-proprotor system. It was also expected that through the use of these techniques it would be possible to obtain insight into the manner in which various physical parameters influence the dynamics of this complex aeroelastic system.

Many of the studies referred to above have been concerned with the dynamics of the wing prop-rotor system with the wing root assumed rigidly fixed, and therefore also of interest in this study was the influence of the fuselage degrees of freedom. The equations of motion of the vehicle were

extended to include the effects of the rigid fuselage degrees of freedom in a previous study[13]. The equations of motion for the complete vehicle system employed in this report are presented in References 2 and 13.

A further objective of this study was to examine the effect of the flexibility of the wing proprotor on the dynamic stability characteristics of the vehicle as related to stability and control, and to examine the influence of body motion feedbacks as might be used for altering the stability and control characteristics of the aircraft on the aeroelastic stability of the vehicle. Experience on helicopters has indicated that body motion feedbacks can influence rotor system stability[14].

The analytical model employed in the analysis presented is given by the equations of motion for the wing proprotor system presented in Reference 2. Appendix I presents the equations of motion taken from Reference 1. These equations of motion represent proprotor blade bending by an uncoupled model and are of simpler form than the model of Reference 2. The reduced degree of freedom models discussed in the first part of this report are based on the model of Appendix I. The refined equations of motion of Reference 2 taken with those of Reference 13 are employed for the analysis of the fuselage free case. The modifications to the model of Reference 2, to account for body degrees of freedom are presented in Reference 13.

Since one of the objectives of this study was to obtain physical insight into the dynamics of this vehicle, simplified dynamic models, based on Reference 1, are discussed in some detail prior to examining

the complete system. The reference physical parameters employed in this study are those of the Bell XV-15 presented in Reference 15. In some cases these parameters are varied from their reference values to obtain insight into the effects of changes in design parameters since other proprotor aircraft designs have been considered[1,12].

The topics covered in this report are as follows: First, the isolated rotor dynamics are discussed in cruise flight in order to obtain insight into the flapping and lagging dynamics of the proprotor. The discussion is largely concerned with the cyclic modes of motion. Cyclic proprotor flapping for the configuration of interest is a rigid blade motion owing to the gimbal mounting of the rotor, and cyclic lagging involves the first in-plane bending mode. Owing to the polar symmetry inherent in this problem, the method of complex coordinates is employed (Ref. 16) to reduce the order of the physical system from eighth to fourth order. Then the model is increased in order by allowing shaft flexibility. In order to obtain insight into this increased order system, first the dynamics of the proprotor on a flexible mounting is examined assuming that the support characteristics are isotropic. This allows retention of the method of complex coordinates and permits again a reduction in order of the system by a factor of two. The real physical system is then examined by relaxing the requirement that the support is isotropic. Various feedbacks are examined for the complete system indicating that certain decouplings exist with respect to the collective and cyclic motions of the rotor and their coupling to the wing motion. Then the fuselage degrees of freedom are relaxed and the dynamics of

the complete system with symmetric fuselage motion is considered in some detail. Consideration is also given to the use of reduced order dynamic models for the prediction of the motion of the vehicle relevant to its stability and control characteristics.

A general arrangement drawing of the reference aircraft, the Bell XV-15 is shown in Figure 1.5.

ISOLATED PROPROTOR DYNAMICS

In this section the dynamic characteristics of an isolated proprotor are examined with emphasis on high inflow conditions. Thus it is assumed that the support system of the proprotor is rigid and the dynamics of proprotor flapping and lagging motion are examined. The equations of motion development is presented in Appendix I.

The proprotor physical characteristics employed for this study are essentially those of the Bell XV-15 and are listed in Table I[3,15]. This aircraft has a gimballed rotor with a soft flapping spring ($\nu_\beta^2 = 1.0355$) so that its flapping motion is essentially that of an articulated rotor. The cyclic lag frequency, given in the Table, is the first flexible mode of the blade which in cruise flight is primarily lag bending (Ref. 3). The frequency of this mode, as well as the relative proportion of flap and lag bending associated with the mode, is influenced by the trim airspeed as a result of the blade pitch variation required to trim the aircraft. As can be seen from Reference 3 it is essentially a lag mode at flight speeds above 300 knots. Therefore in the following it is referred to as a lag mode and the small component of flap bending is neglected.

The complete equations of motion for the physical system assuming that the blade modes are uncoupled, taken from Reference 1, are given in Appendix I. The four degrees of freedom of interest in this section are the two components of gimbal motion or flapping, β_{1c} and β_{1s} and the two components of lag bending amplitude, ζ_{1c} and ζ_{1s}. The equations

General;

$N = 3$

$R = 12.5$ ft

$\Omega = 48$ rad/sec

$I_b = 105$ slug×ft^2

$\gamma = 3.83$

$\sigma = .089$

$a = 5.7$

$h = .342$

For Cyclic Motion ;	For Collective Motion	
	Constant RPM Case	With RPM DOF
$\nu_\beta^2 = 1.0355$ (*1)	$\nu_{\beta_o} = 1.85$	(←)
$\nu_\zeta = 1.33$ (*2).	$\nu_{\zeta_o} = \nu_\zeta$	$\nu_{\zeta_o} = 0$
$I_\beta^* = I_{\beta\alpha}^* = 1.0$	$I_{\beta_o}^* = .779$	(←)
$I_\zeta^* = .670$	$I_{\zeta_o}^* = .670$	$I_{\zeta_o}^* = 1.0$
$S_\zeta^* = 1.035$		

(*1): @ $\Omega = 48$ rad/sec

(*2): @ $V = .844$ & $\Omega = 48$ rad/sec

Table I. Description of the Rotor Used for Numerical Examples.

of motion can be written as

$$[A_{11}] \begin{Bmatrix} \beta_{1c} \\ \beta_{1s} \\ \zeta_{1c} \\ \zeta_{1s} \end{Bmatrix} = [B_{11}] \begin{Bmatrix} \theta_{1c} \\ \theta_{1s} \\ \alpha_g \\ \beta_g \end{Bmatrix} \tag{1}$$

where $[A_{11}]$ $[B_{11}]$ are given in Appendix I.

Since the cruise flight condition is of interest the matrices A_{11} and B_{11} possess certain symmetry properties which can be employed to reduce the order of this system from eighth order to fourth order. A set of complex coordinates are defined[13],

$$\begin{aligned} \bar{\beta} &= \beta_{1c} + i\,\beta_{1s} & \bar{\zeta} &= \zeta_{1c} + i\,\zeta_{1s} \\ \bar{\theta} &= \theta_{1c} + i\,\theta_{1s} & \bar{g} &= \alpha_g - i\,\beta_g \end{aligned} \tag{2}$$

Now by multiplying the second of equations (1) by i and adding to the first and multiplying the fourth equation by i and adding to the third we obtain two second-order equations with complex coefficients in place of four second-order equations with real coefficients. The equations of motion in this form are

$$\left[\begin{array}{c|c} s^2 - (\bar{M}_{\dot{\beta}} + 2i)\,s + (\nu_\beta^2 - 1) + i\,\bar{M}_{\dot{\beta}} & \bar{M}_{\dot{\zeta}}\,(s - i) \\ \hline -\bar{Q}_{\dot{\beta}}\,(s - i) & s^2 + (\bar{Q}_{\dot{\zeta}} - 2i)\,s + (\nu_\zeta^2 - 1) - i\,\bar{Q}_{\dot{\zeta}} \end{array}\right] \begin{Bmatrix} \bar{\beta} \\ \bar{\zeta} \end{Bmatrix} = \left[\begin{array}{c|c} \bar{M}_\theta & iV\bar{M}_\mu \\ \hline \bar{Q}_\theta & iV\bar{Q}_\mu \end{array}\right] \begin{Bmatrix} \bar{\theta} \\ \bar{g} \end{Bmatrix} \tag{3}$$

where

$$\bar{M}_{(.)} = \frac{\gamma M_{(\cdot)}}{I^*_\beta} \qquad \bar{Q}_{(\ )} = \frac{\gamma Q_{(\ )}}{I^*_\zeta}$$

The coordinates $\bar{\beta}$ and $\bar{\zeta}$ are essentially complex multiblade coordinates and as such are expressed with respect to a fixed or non-rotating reference frame. The equations of motion can be effectively converted to a non-rotating frame and also incidentally, the complex coefficients removed, by defining a new operational variable

$$\bar{s} = s - i$$

Substitution of this relationship into equation (3) yields a simpler form of the equations of motion,

$$\begin{bmatrix} (\Delta_\beta)_{uc} & \bar{M}_{\dot{\zeta}}\,\bar{s} \\ -\bar{Q}_{\dot{\beta}}\,\bar{s} & (\Delta_\zeta)_{uc} \end{bmatrix} \begin{Bmatrix} \bar{\beta} \\ \bar{\zeta} \end{Bmatrix} = \begin{bmatrix} \bar{M}_\theta & iV\bar{M}_\mu \\ \bar{Q}_\theta & iV\bar{Q}_\mu \end{bmatrix} \begin{Bmatrix} \bar{\theta} \\ \bar{g} \end{Bmatrix} \qquad (4)$$

where

$$(\Delta_\beta)_{uc} = \bar{s}^2 - \bar{M}_{\dot{\beta}}\,\bar{s} + \nu_\beta^2$$

$$(\Delta_\zeta)_{uc} = \bar{s}^2 + \bar{Q}_{\dot{\zeta}}\,\bar{s} + \nu_\zeta^2$$

These quadratic factors give the uncoupled flap and lag eigenvalues of the proprotor with respect to a rotating frame. The eigenvalues are shown in Figure 1 as a function of advance ratio. Approximate expressions for the aerodynamic coefficients $\bar{M}_{\dot{\beta}}$ and $\bar{Q}_{\dot{\zeta}}$ are given in Reference 1,

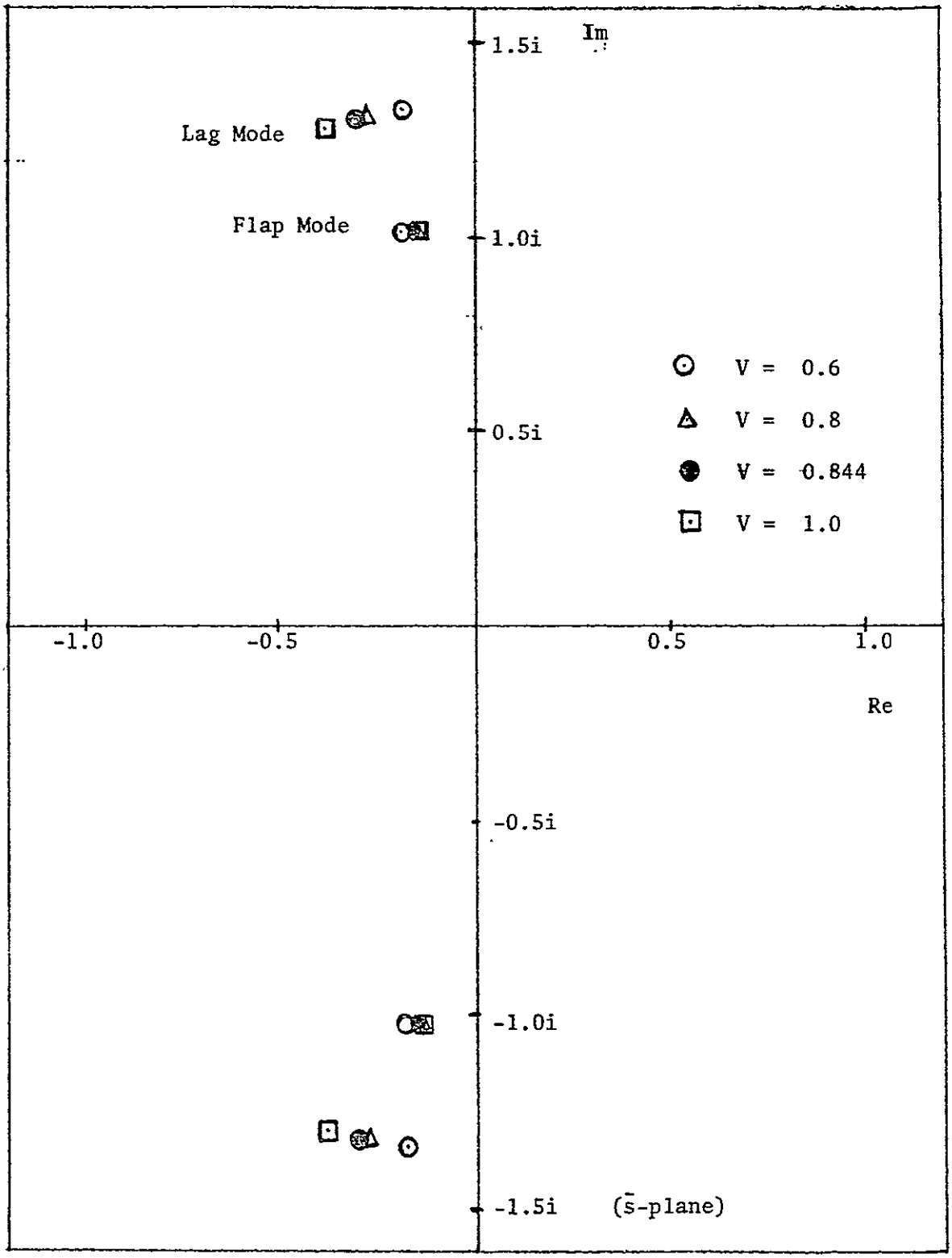

Figure 1. Uncoupled Flap and Lag Characteristic Roots (Cyclic Modes) Rotating Frame.

FIG 1.

$$M_{\dot{\beta}} \cong -\frac{\cos\phi}{8}$$

$$Q_{\dot{\zeta}} \cong \frac{\sin^2\phi}{8\cos\phi}$$

where the effective radius approximation has been employed to obtain simple expressions for the aerodynamic derivatives. The inflow angle ϕ is related to the advance ratio by

$$V = \frac{3}{4} \tan\phi$$

Thus from Figure 1, it can be seen that the flap damping, which is proportional to $M_{\dot{\beta}}$ decreases with increasing advance ratio and the lag damping, $Q_{\dot{\zeta}}$ increases.

As the model is complicated by more degrees of freedom it is convenient to retain the original form of the equations given by equation (3). The eigenvalues for this system are readily found from the relationships between the two operational variables $\bar{s}$ and s and thus the fixed frame dynamics are found by adding i to the eigenvalues of equation (4) giving the values shown in Figure 2.

1.) Uncoupled Flapping Motion with Feedback

First we examine the uncoupled flap dynamics in further detail especially as regards the response characteristics as a function of advance ratio and the influence of cyclic feedback on the flapping response.

The uncoupled flapping equation of motion is given by

$$\{s^2 - (\bar{M}_{\dot{\beta}} + 2i)\, s + i\, M_{\dot{\beta}}\}\ \bar{\beta} = \bar{M}_{\theta}\, \bar{\theta} + iV\bar{M}_{\mu}\, \bar{g} \qquad (5)$$

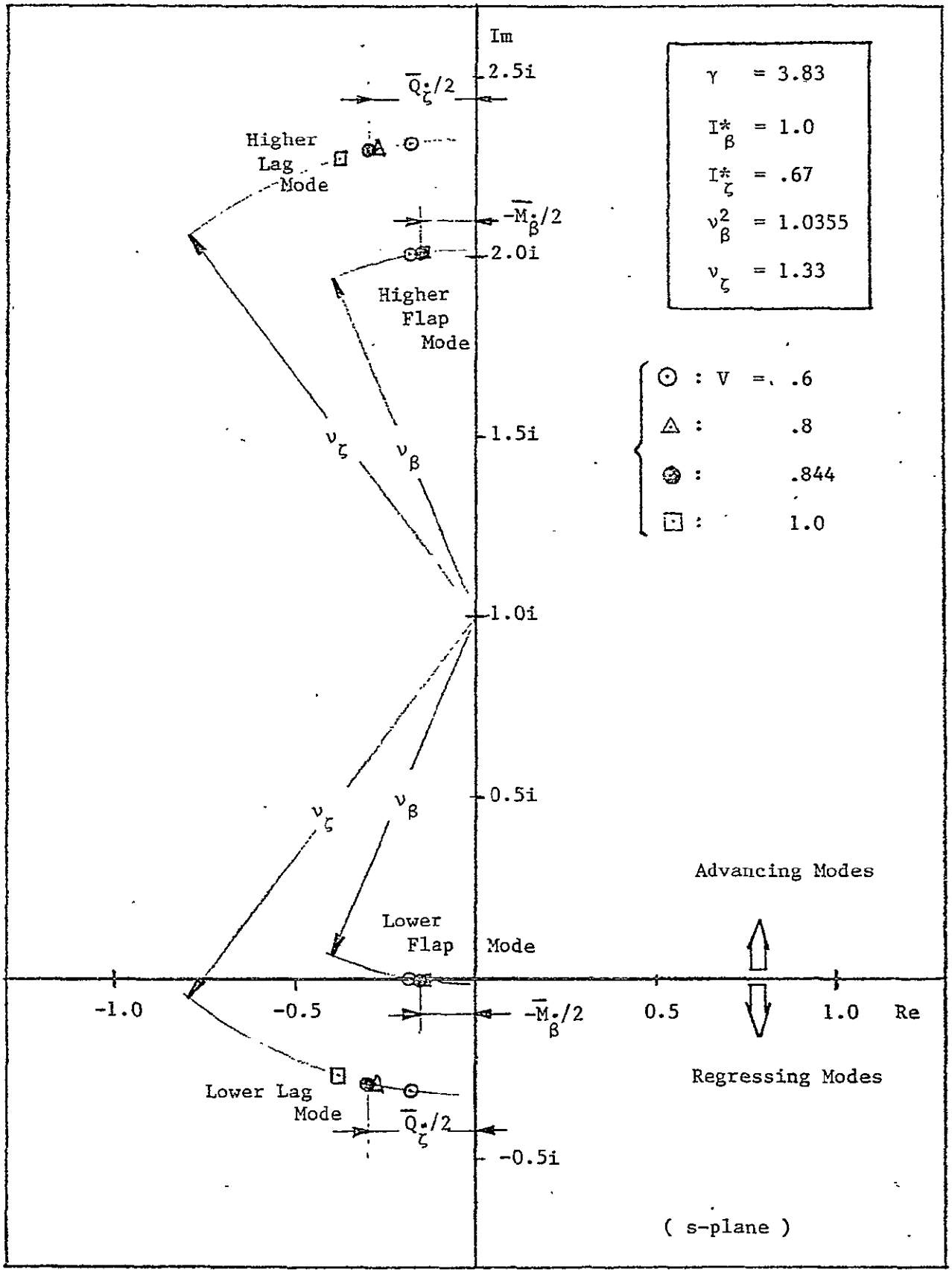

Figure 2. Uncoupled Flap and Lag Characteristic Roots (Cyclic Modes), Fixed Frame.

The influence of the weak flapping spring as represented by ν_β has been neglected since its influence is small. The approximate expressions for M_θ and M_μ are given by Reference 1 as

$$M_\theta = \frac{1}{8 \cos \phi}$$

$$M_\mu = \frac{\sin \phi}{6}$$

Thus the steady state flapping response to cyclic and gust inputs is given by

$$\bar{\beta}_{ss} = - i \left\{ \frac{M_\theta}{M_{\dot{\beta}}} \bar{\theta} + \frac{i V M_\mu}{M_{\dot{\beta}}} \bar{g} \right\} \tag{6}$$

In terms of the approximate aerodynamic derivatives, equation (6) can be expressed as

$$\bar{\beta}_{ss} \cong \frac{i}{\cos^2 \phi} \bar{\theta} - \tan^2 \phi \, \bar{g} \tag{7}$$

Thus; the flapping amplitude per unit cyclic increases with inflow angle proportional to $\cos^{-2} \phi$ and the flapping response to gust inputs grows as $\tan^2 \phi$. At an advance ratio of 1 (355 knots) using the equivalent radius approximation, the flapping amplitude per unit control deflection is 2.76 degrees per degree, and the flapping response due to a gust is 1.76 degrees per degree. The amplitude continues to grow rapidly with advance ratio as shown in Figure 3.

Flapping feedbacks can be used to reduce the sensitivity of the rotor. Two possible flapping feedbacks considered are a δ_3 hinge or

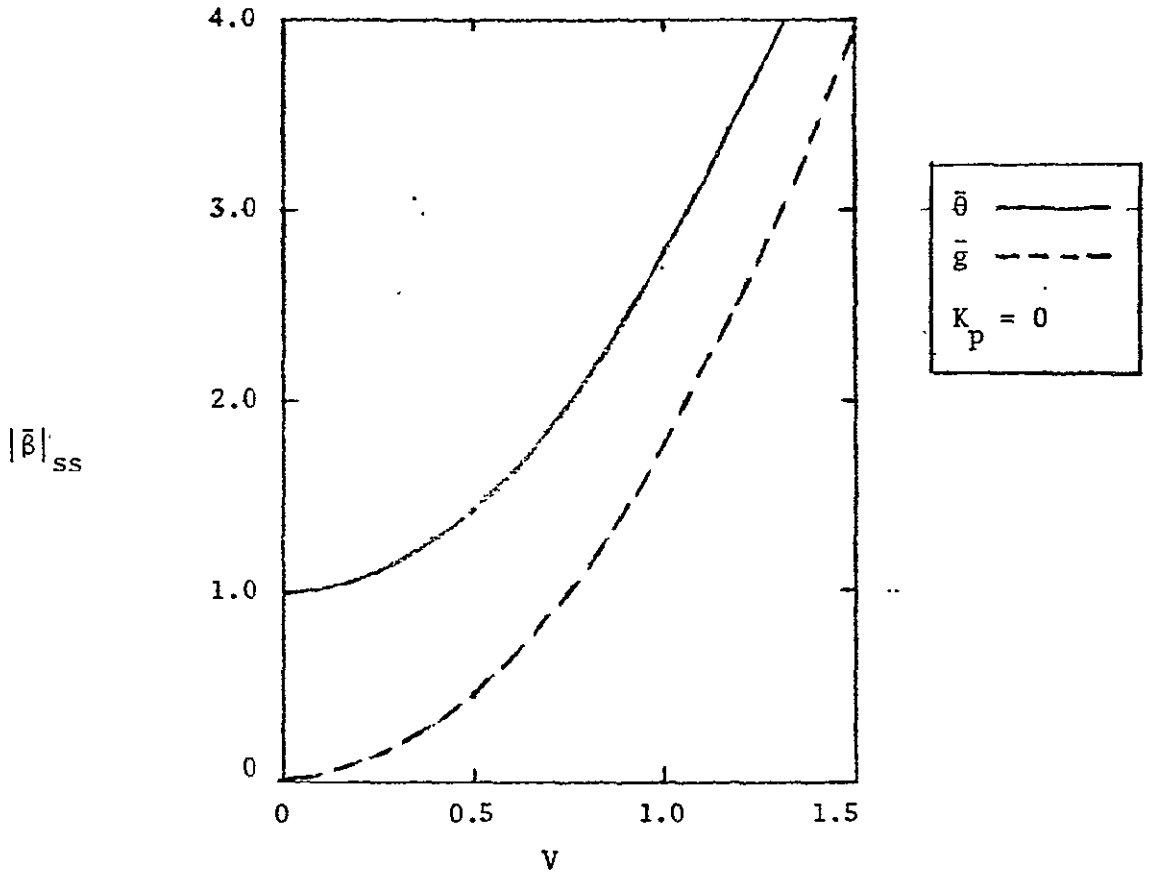

Figure 3. Steady State Flapping Response to Unit Cyclic Pitch and Gust Input as a Function of Advance Ratio.

or pitch-flap coupling with the gearing denoted by K_p, and an Oemichen type feedback where the pitch of one blade is controlled by the flap angle of an adjacent blade and the gearing is expressed as K_o. In overall rotor plane sense, the Oemichen hinge is equivalent to a feedback which is 90^o out of phase compared to the effect of the δ_3 hinge. In complex notation, these two feedbacks can be expressed compactly as,

$$\bar{\theta} = (-K_p + iK_o)\,\bar{\beta} \tag{8}$$

A root locus can be sketched as shown in Figure 4 showing the influence of these two feedbacks on the flapping dynamics. Of particular interest are the flapping stability limits and the amplitude reduction possible through the use of these feedbacks. Inserting the feedback law into equation (5)

$$\{s^2 - (\bar{M}_{\dot{\beta}} + 2i)\,s + i\,(\bar{M}_{\dot{\beta}} - \bar{M}_{\theta}\,K_o) + \bar{M}_{\theta}\,K_p\}\,\bar{\beta} = iV\bar{M}_{\mu}\bar{g} \tag{9}$$

The influence on the flapping amplitude is given by the steady state solution to this equation

$$\frac{\bar{\beta}}{\bar{g}} = \frac{i\,V\,\dfrac{M_{\mu}}{M_{\dot{\beta}}}}{i\left(1 - \dfrac{\bar{M}_{\theta}}{\bar{M}_{\dot{\beta}}}K_o\right) + \dfrac{\bar{M}_{\mu}}{\bar{M}_{\dot{\beta}}}K_p} \tag{10}$$

Substituting the equivalent radius approximation for the aerodynamic derivatives, the ratio of flapping to gust input amplitude is

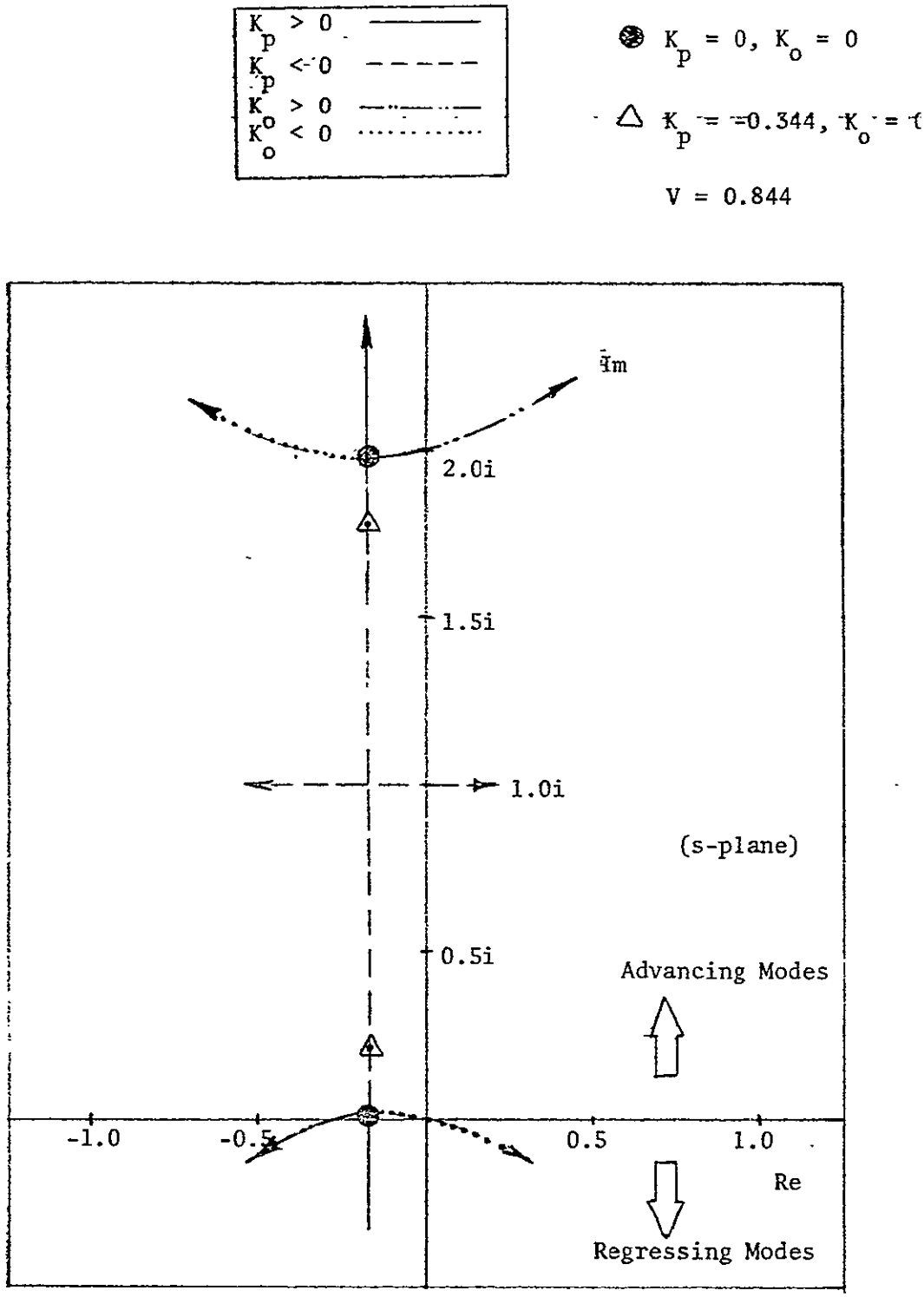

Figure 4. Root Locus Showing Influence of δ_3 and Oemichen Feedback on Flapping Dynamics.

$$\frac{\bar{\beta}}{\bar{g}} = \frac{\tan^2 \phi}{\left\{\left(1 + \frac{K_o}{\cos^2 \phi}\right)^2 + \left(\frac{-K_p}{\cos^2 \phi}\right)^2\right\}^{\frac{1}{2}}} \qquad (11)$$

This indicates that the amplitude reduction due to the δ_3 effect (K_p) is independent of the sign of the pitch-flap coupling and in addition that both feedbacks become more effective as the advance ratio or inflow angle increases.

The gearing ratios or feedback gains are limited by stability considerations. It can be shown that the stability boundaries determined from equation (9) are given by

$$1 + \frac{\gamma}{8} \cos \phi \left(\frac{K_p}{\cos^2 \phi}\right)^2 - \left(\frac{K_o}{\cos^2 \phi}\right)^2 > 0$$

Thus for the δ_3 feedback only the stability boundary is given by

$$K_p = -\frac{8}{\gamma} \cos \phi$$

and for the Øemichen feedback alone

$$K_o = \cos^2 \phi$$

Figure 5 shows the amplitude reduction which can be achieved by these two feedbacks, as well as the stability boundaries, indicating the effectiveness of these two feedbacks.

The effectiveness of pitch-flap coupling in reducing the flapping amplitude can be seen.

2.) Flap-Lag Coupling

We now return to the complete set of flap-lag equations to examine the influence of flap lag coupling arising from the terms $\bar{M}_\zeta$ and $\bar{Q}_\beta$.

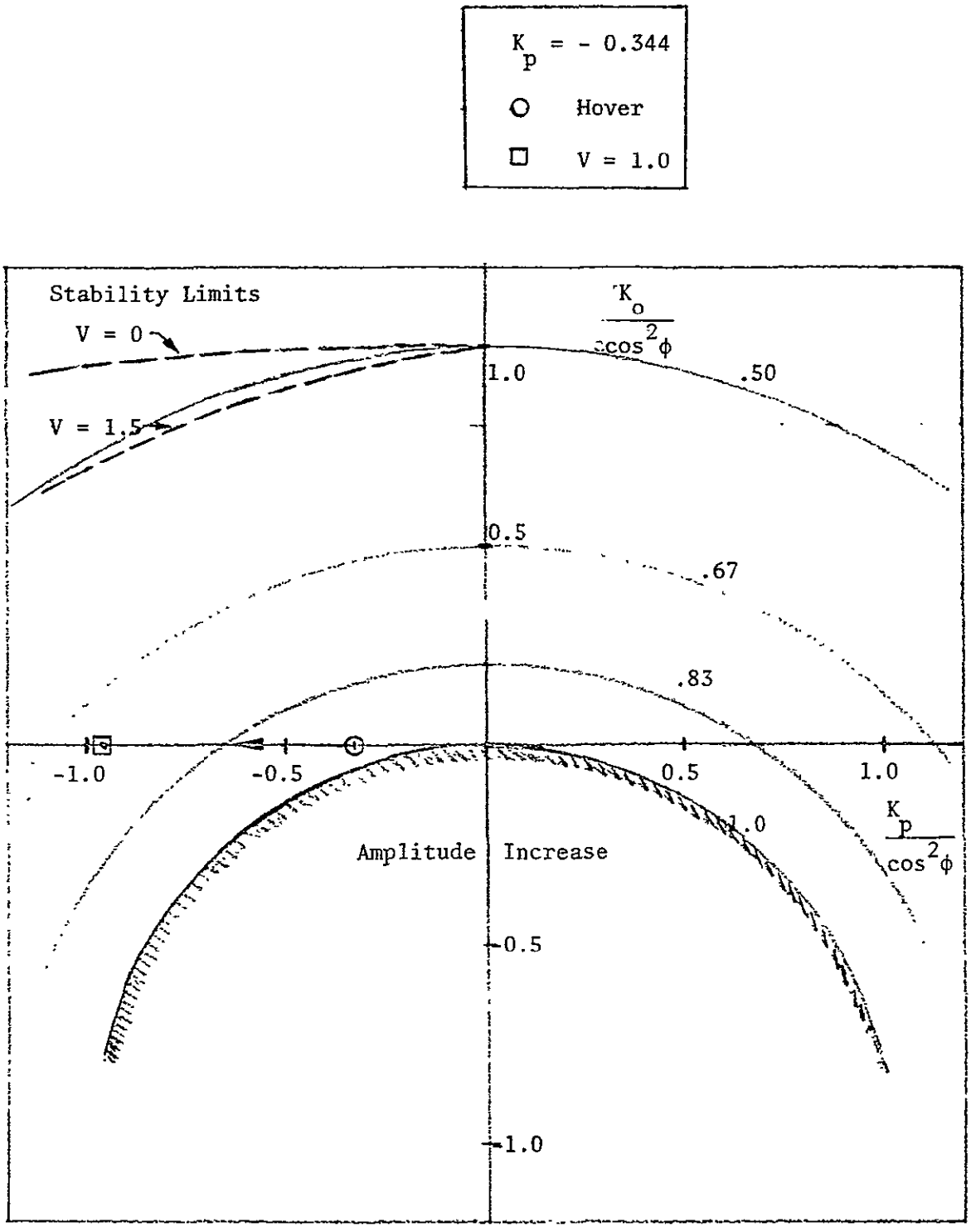

Figure 5. Relative Amplitude Reduction, δ_3 and Oemichen Feedback.

The coupled characteristic equation for the flap-lag motion can be written as in terms of the operational variable $\bar{s}$

$$\Delta_{\beta + \zeta} = (\Delta_{\beta})_{uc} (\Delta_{\zeta})_{uc} + \bar{M}_{\zeta} \bar{Q}_{\beta} \bar{s}^2 \qquad (12)$$

Root locus techniques can be employed to illustrate the influence of the coupling terms. Figure 6 shows the effect of this coupling term on the modes of motion in the non-rotating frame. It can be seen that the coupling between the modes destabilizes the flap mode and stabilizes the lag mode.

The proprotor is also equipped with a δ_3 hinge or pitch-flap coupling. This hinge causes additional coupling between the flap and lag motion resulting in a change in the eigenvalues of the coupled flap-lag motion as shown in Figure 7 at the reference advance ratio V = 0.844. It can be seen that a negative value of K_p (up flap causes and increase in pitch) stabilizes the lightly damped mode and the value for the vehicle (K_p = - 0.344) at this flight condition produces the maximum damping for the lightly damped flap mode. A further source of coupling arises from torsional flexibility of the blades. This effect can be approximately treated as a pitch-lag coupling[3]. For a more precise approach the coupled equations of Reference 2 are required. Figure 8 shows the effect of pitch-lag coupling on the eigenvalues indicating that the negative value (corresponding to a pitch reduction with increasing lag angle) reduces the damping of the lightly damped flap mode. The trend indicated is that expected from experience with helicopter rotors, although because of the fact that the flap mode has less damping it is this mode that is

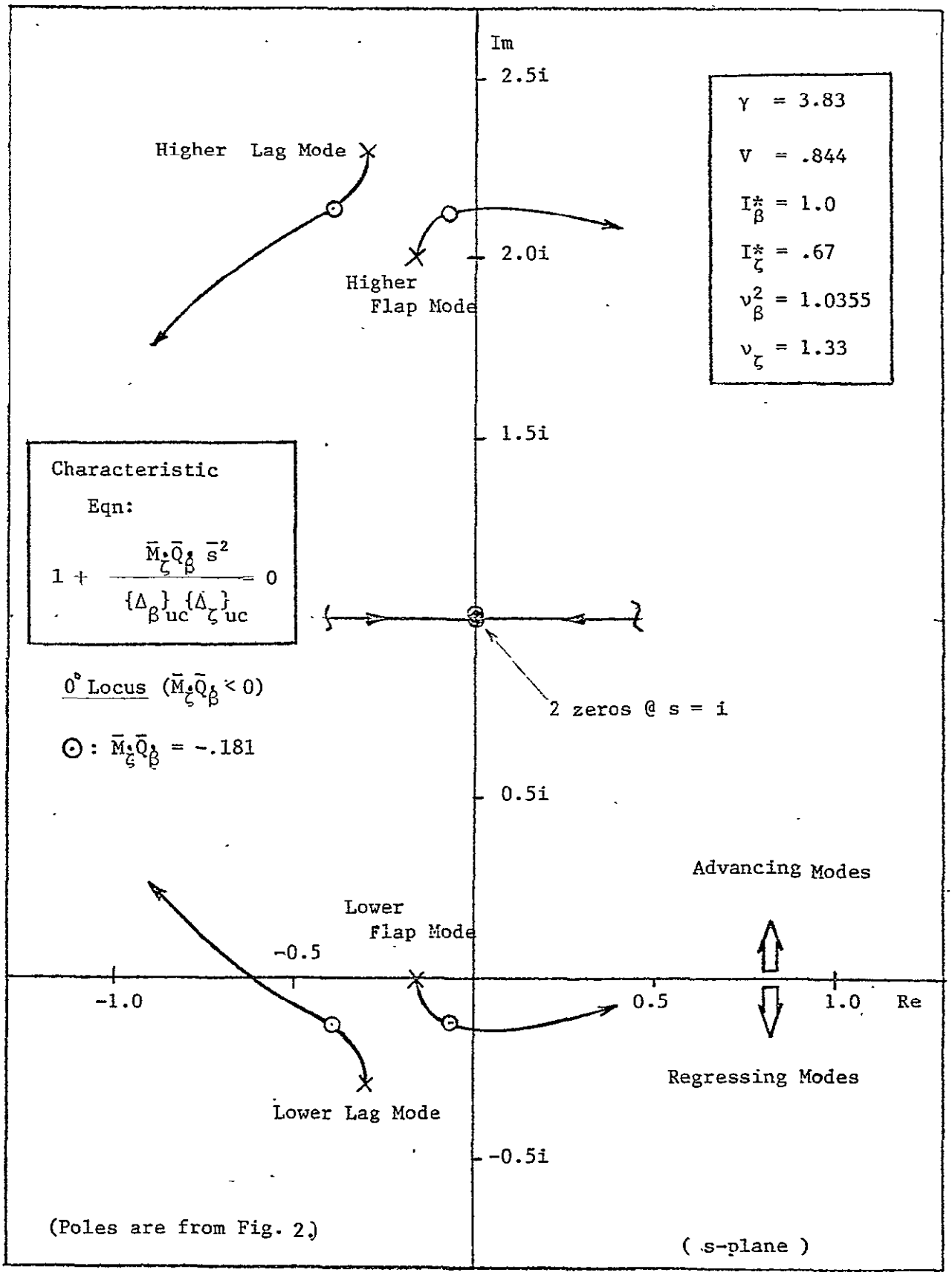

Figure 6. Influence of Flap-Lag Coupling on Flap-Lag Dynamics (Cyclic Modes)

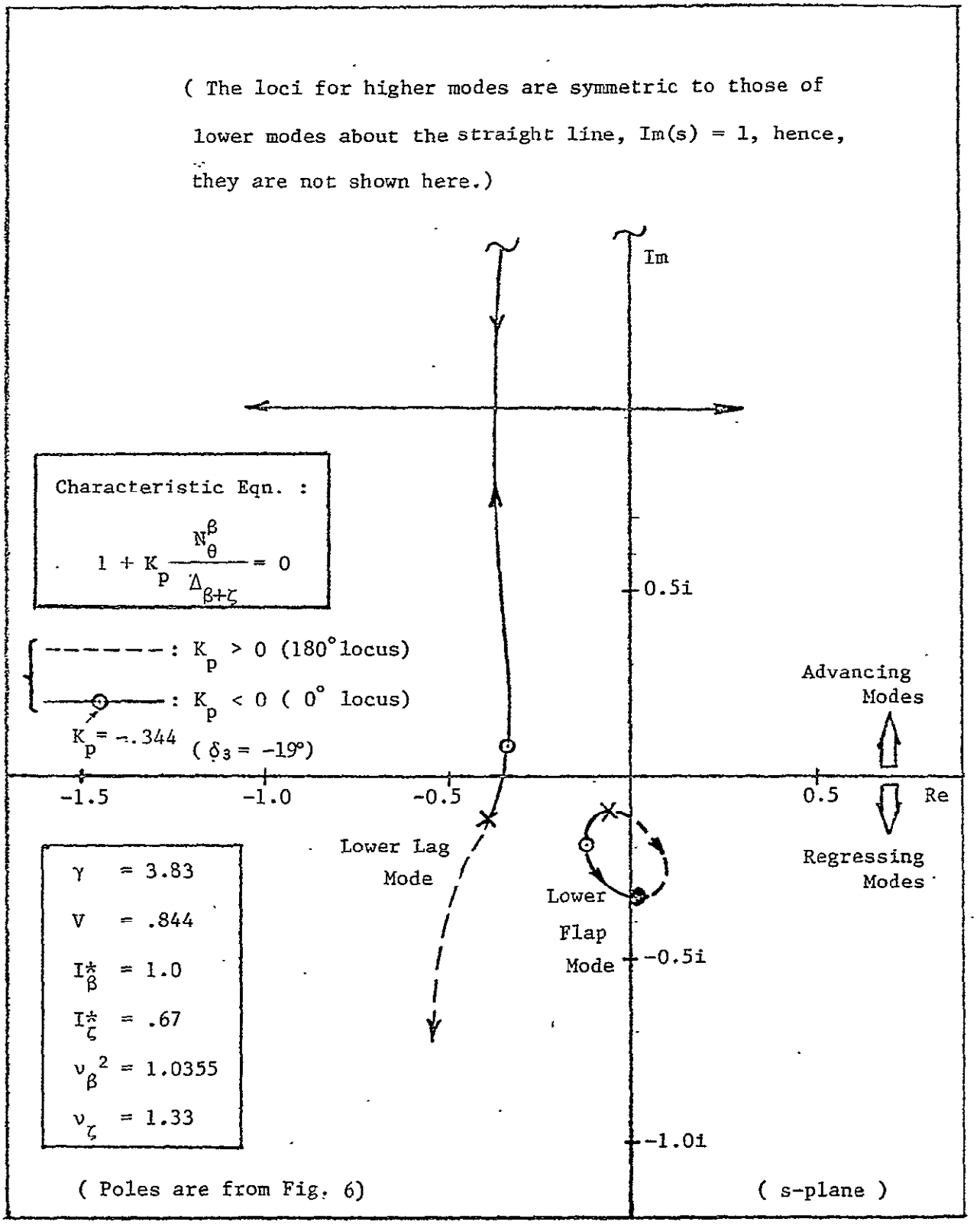

Figure 7. Influence of Pitch-Flap Coupling on Flap-Lag Dynamics (Cyclic Modes)

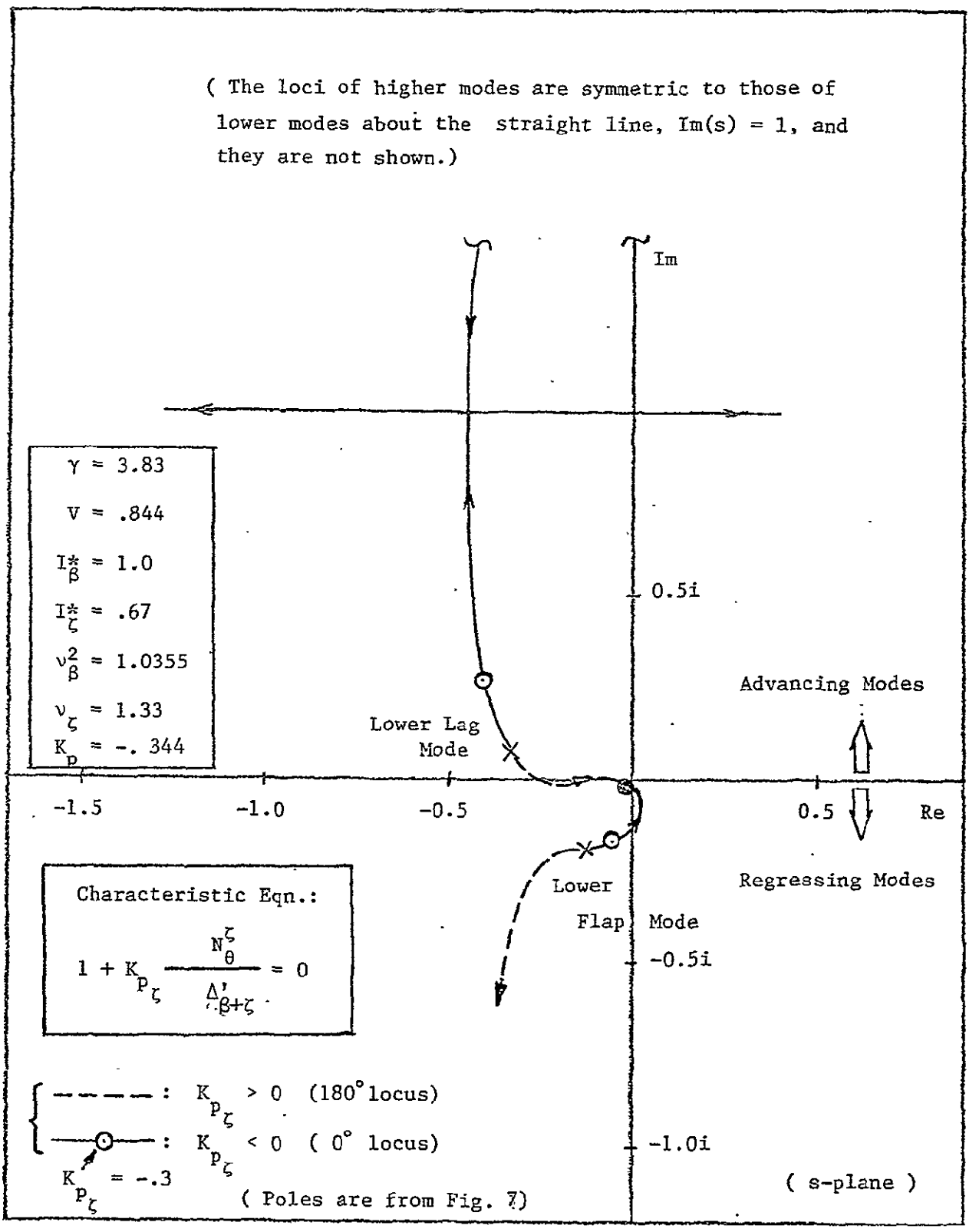

Figure 8. Influence of Pitch-Lag Coupling on Flap-Lag Dynamics (Cyclic Modes)

destabilized by this coupling in contrast to the helicopter at low inflow where the lag damping is small and therefore it is the lag mode which is destablized[17].

This completes the discussion of the isolated rotor cyclic dynamics. The collective flap and lag dynamics are also of interest. The collective motions can be treated separately from the cyclic motions. It should also be noted that the collective flapping is an elastic mode owing to the fact that the rotor is gimballed and each blade is not free to flap individually.

3.) Collective Flap-Lag Motion

The equations of motion describing the collective flap-lag dynamics are quite similar to the cyclic equations of motion expressed in terms of the modified operational variable $\bar{s}$. The major difference arises from the fact that the collective flap mode is an elastic mode with a natural frequency, $\nu_{\beta_o} = 1.85$. Pitch-flap and pitch-lag coupling are present. The effect of a gust disturbance enters in a somewhat different fashion. In addition, an additional degree of freedom, the rotor RPM must be included. In principle, the complete equation of motion for the rotor RPM degree of freedom would involve consideration of the drive train and engine governor dynamics[19]. It has been shown that these influences are not particularly significant and that the major effects of the rotor RPM degree of freedom can be examined through the study of two limiting cases: constant RPM, i.e., the case of a perfect engine/governor system; and autorotation, where the rotor speed perturbation is determined by the aerodynamic forces acting on the rotor.

With the constant RPM assumption, the elastic lag mode is excited,

however with the RPM as a degree of freedom this mode is not important. Consider the following two equations of motion, one describing the elastic lag motion,

$$I^*_{\zeta_o} (\ddot{\zeta}_o - \ddot{\alpha}_z) + I^*_{\zeta_o} \nu^2_{\zeta_o} \zeta_o = \Delta Q \tag{13}$$

and the other the torque balance,

$$I^*_{\zeta_{o\alpha}} \ddot{\zeta}_o - I^*_o \ddot{\alpha}_z = \left(\frac{C_Q}{a\alpha}\right)_o + \Delta Q \tag{14}$$

α_z is the shaft rotation or RPM degree of freedom.

Now if the lag mode shape is assumed to be $\eta_{\zeta_o} = r$, then

$$I^*_{\zeta_{o\alpha}} = I^*_o = I^*_{\zeta_o}$$

Equation (13) reduces to,

$$\ddot{\zeta}_o - \ddot{\alpha}_z + \nu^2_{\zeta_o} \zeta_o = \frac{1}{I^*_o} \Delta Q \tag{15}$$

If the steady state torque is zero, equation (14) is,

$$\ddot{\zeta}_o - \ddot{\alpha}_z = \frac{1}{I^*_o} \Delta Q \tag{16}$$

Comparison of these two equations of motion indicates that $\zeta_o = 0$ and therefore if the RPM degree of freedom (α_z) is present, then the elastic mode degree of freedom (ζ_o) is not excited. Consequently the two cases considered are: RPM constant with elastic flapping and elastic lag, and RPM free with elastic flapping and no elastic lag.

The equations of motion in the RPM fixed case are

$$\begin{bmatrix} (\Delta_{\beta_o})_{uc} & \tilde{M}_{\dot{\zeta}} s \\ -\tilde{Q}_{\dot{\beta}} s & \{\Delta_{\zeta_o}\}_{uc} \end{bmatrix} \begin{Bmatrix} \beta_o \\ \zeta_o \end{Bmatrix} = \begin{bmatrix} \tilde{M}_\theta & V\tilde{M}_\lambda \\ \tilde{Q}_\theta & V\tilde{Q}_\lambda \end{bmatrix} \begin{Bmatrix} \theta_o \\ u_g \end{Bmatrix} \tag{17}$$

where

$$\begin{aligned} (\Delta_{\beta_o})_{uc} &= s^2 - \tilde{M}_{\dot{\beta}}\, s + \nu_{\beta_o}^2 \\ (\Delta_{\zeta_o})_{uc} &= s^2 + \tilde{Q}_{\dot{\zeta}}\, s + \nu_{\zeta_o}^2 \end{aligned} \tag{18}$$

where

$$\tilde{M}_{(\,)} = \frac{\gamma M_{(\,)}}{I^*_{\beta_o}} \qquad \tilde{Q}_{(\,)} = \frac{\gamma Q_{(\,)}}{I^*_{\zeta_o}}$$

Figure 9 shows the effect of the aerodynamic coupling as well as pitch-flap and pitch-lag coupling. The basic flap-lag coupling arising from aerodynamics as well as the pitch-flap coupling act to reduce the damping of the collective flap mode. Pitch-lag coupling has only a small effect on the collective flap mode, and reduces the frequency of the collective lag mode.

The free RPM case can be treated by taking $\nu_{\zeta_o} = 0$ and considering the second motion variable as Ω_s rather than ζ_o, i.e., $\Omega_s = -\dot{\zeta}_o$. Note that since there is no spring in the RPM equation the order of the system is reduced by 1. The uncoupled RPM mode has only one eigenvalue, $s = -\tilde{Q}_{\dot{\zeta}}$.

Figure 10 shows the effect of coupling in the RPM free case. Both in the case of the aerodynamic coupling and the pitch-flap coupling, the general trend is to reduce the natural frequency of the collective flap mode and produce only a minor change in the time constant associated with the RPM degree of freedom. Pitch-lag coupling is not present in the case with the RPM degree of freedom.

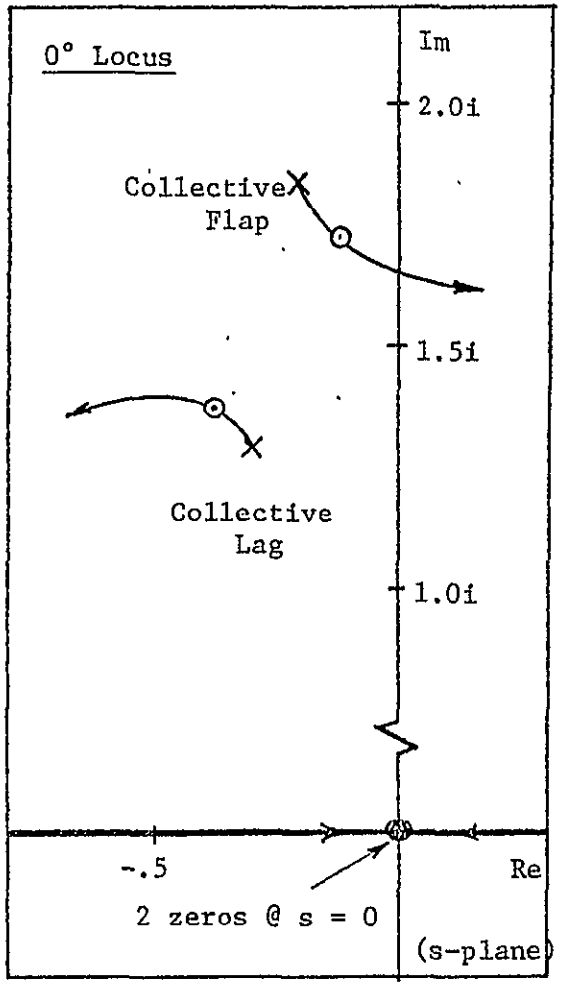

(a) Influence of Flap-Lag Coupling

⊙: $\tilde{M}_\zeta$, $\tilde{Q}_\beta$ = -.233

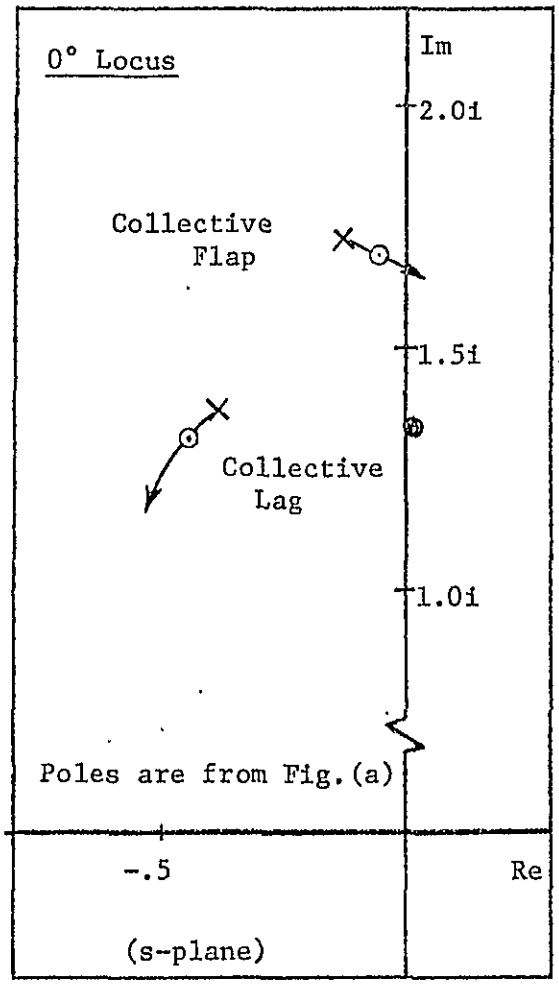

(b) Influence of Pitch-Flap Coupling;

⊙: K_p = -.344

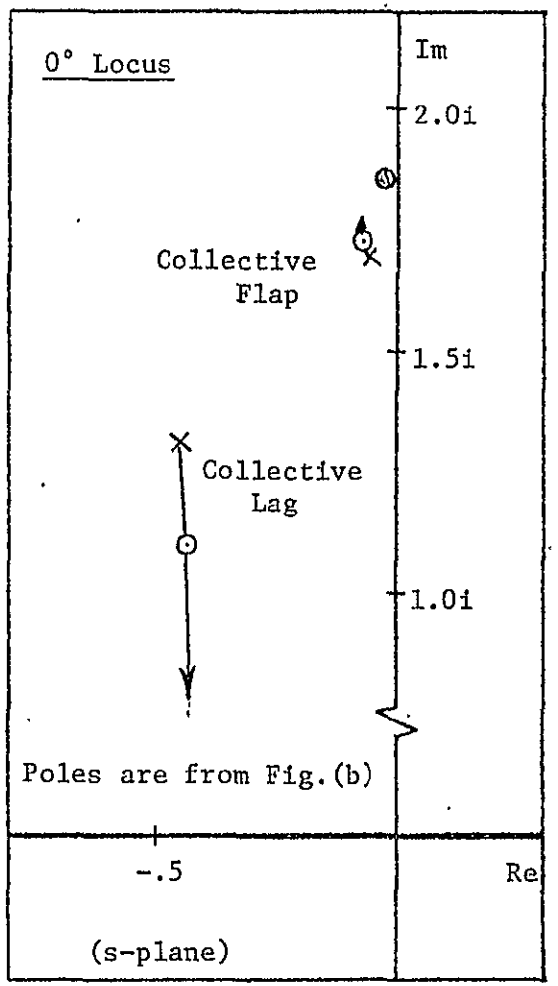

(c) Influence of Pitch-Lag Coupling (with K_p = -.344);

⊙ : K_{p_ζ} = -.3

V = .844, γ = 3.83, $I^*_{\beta_o}$ = .779,

$I^*_{\zeta_o}$ = .67, ν_{β_o} = 1.85, ν_{ζ_o} = 1.33

Figure 9. Collective Flap and Lag Motion Dynamics

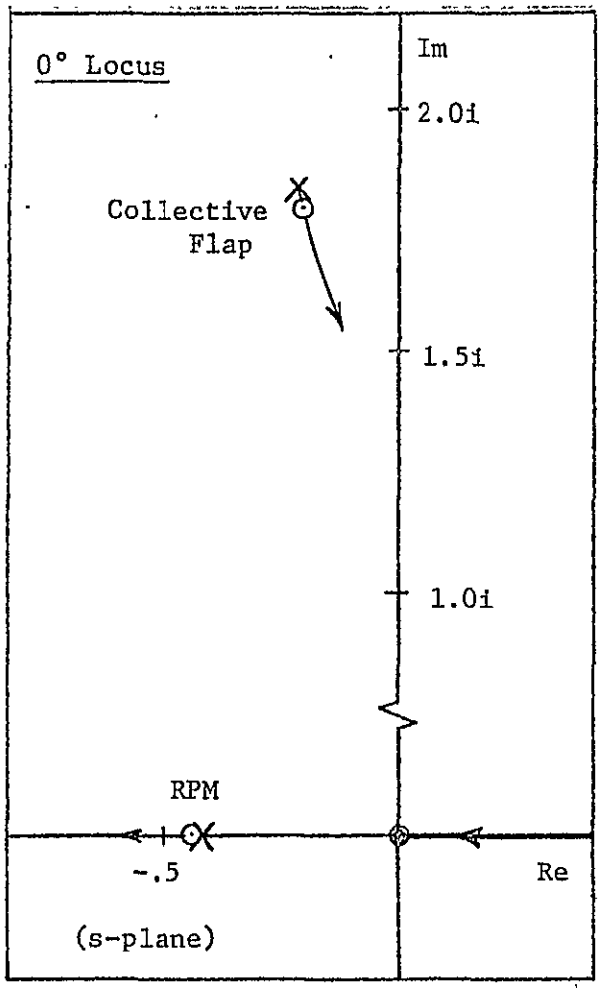

(a) Influence of Coupling;

$\odot$: $\tilde{M}_{\zeta}\tilde{Q}_{\beta} = -.166$

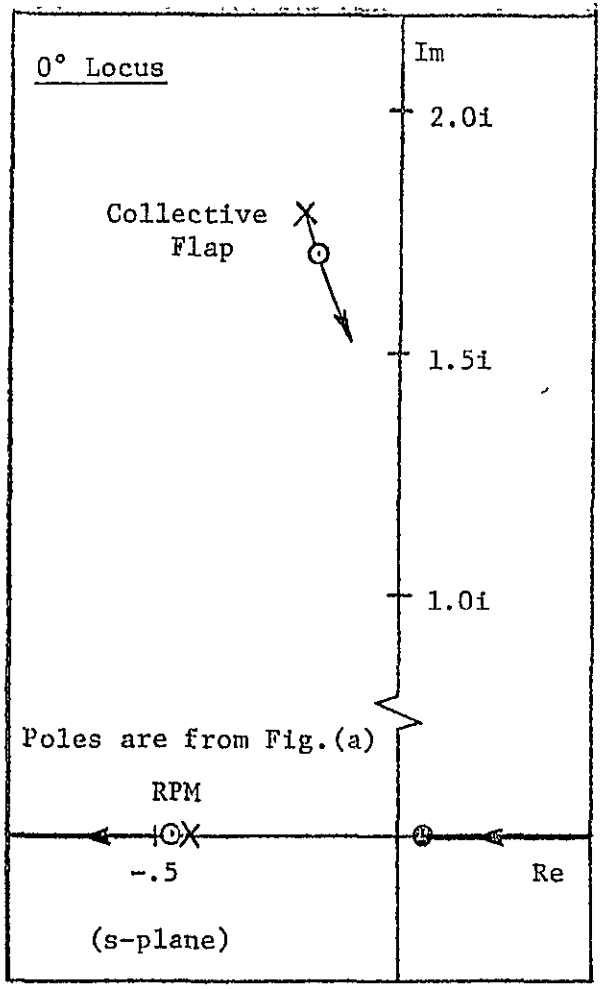

(b) Influence of Pitch-Flap Coupling;

$\odot$: $K_p = -.344$

Figure 10. Collective Flap and Shaft RPM Motion Dynamics

$V = .844, \quad \gamma = 3.83, \quad I^*_{\beta_o} = .779$

$I^*_{\zeta} = 1.0, \quad \nu_{\beta_o} = 1.85, \quad \nu_{\zeta_o} = 0$

This section has considered the isolated proprotor dynamics which enter into the vehicle dynamics. In axial flight, the cyclic modes can be separated from the collective modes.

In contrast to the helicopter which operates at low inflow, it should be noted that the cyclic flap mode has a lower damping than the cyclic lag mode. As the wing/support dynamics are introduced in the next section, recalling the characteristics of these isolated modes will be helpful in interpreting the changes which occur in the flexible wing case.

PROPROTOR WITH ISOTROPIC SUPPORT

In order to promote physical insight into the aeroelastic stability of the wing/proprotor system, in this section the dynamic stability characteristics of the proprotor on a two degree of freedom isotropic flexible support is considered before examining the specific physical system under consideration. That is, for the actual aircraft the aeroelastic flexibility of the wing is modelled by torsion, chordwise bending and spanwise bending modes. In this section we only allow the support two elastic degrees of freedom and assume that the inertial and stiffness properties are the same in both directions. The approximate model permits the use of the complex coordinate transformation employed in the previous section to be extended to the case with a flexible support and helps to promote physical insight into the dynamic characteristics of this complex system.

It should be noted that with this support model, the collective rotor degrees of freedom will not be involved in the problem, as they are primarily coupled to fore and aft translation of the proprotor shaft as shown later.

Thus, in general, we are considering a system with two cyclic flap degrees of freedom, two cyclic lag degrees of freedom, and two directions of support bending. Only aerodynamic forces produced by the proprotor are included. The use of complex coordinates reduces this physical system from a twelfth order system to a sixth order system.

Introducing the equality of the inertial, damping, and spring characteristics of the support into the equations of motion given in

Appendix I, such that

$$I_p^* = I_{py}^* = I_{px}^*$$

$$C^* = C_x^* = C_y^* \qquad (19)$$

$$K^* = K_x^* = K_y^*$$

and introducing a complex coordinate describing shaft motion as

$$\bar{\alpha} = \alpha_y - i\,\alpha_x \quad .$$

The equations of motion for the three complex degrees of freedom can be written as

$$\left[\begin{array}{c|c|c} (\Delta_\beta)_{uc} & \bar{M}_{\dot{\zeta}}\,(s - i) & -s^2 + [\bar{M}_{\dot{\beta}} + i\,(2 + h\,\bar{M}_\mu)]\,s - i\,V\bar{M}_\mu \\ \hline -\bar{Q}_{\dot{\beta}}\,(s - i) & (\Delta_\zeta)_{uc} & i\,h\,(\frac{S_\zeta^*}{I_\zeta^*})\,s^2 + (\bar{Q}_{\dot{\beta}} + i\,h\,\bar{Q}_\mu)\,s - i\,V\bar{Q}_\mu \\ \hline i\,h\,\bar{H}_{\dot{\beta}}\,(s - i) & -i\,h\,(\frac{S_\zeta^*}{I^*})\,s^2 & \\ + \frac{I_\beta^*}{I^*}\,(\nu_\beta^2 - 1) & -i\,h\,\bar{H}_{\dot{\zeta}}\,(s - i) & (\Delta_\alpha)_{uc} \end{array}\right] \left\{\begin{array}{c} \bar{\beta} \\ \bar{\zeta} \\ \bar{\alpha} \end{array}\right\}$$

$$= \left[\begin{array}{cc} \bar{M}_\theta & iV\bar{M}_\mu \\ \bar{Q}_\theta & iV\bar{Q}_\mu \\ -i\,h\,\bar{H}_\theta & hV\bar{H}_\mu \end{array}\right] \left\{\begin{array}{c} \bar{\theta} \\ \bar{g} \end{array}\right\} \qquad (20)$$

where $\frac{I_{\beta_\alpha}^*}{I_\beta^*} \cong 1$ and

$$\bar{M}_{(\,)} = \frac{\gamma M_{(\,)}}{I^*_\beta} \qquad \bar{Q}_{(\,)} = \frac{\gamma Q_{(\,)}}{I^*_\zeta} \qquad \bar{H}_{(\,)} = \frac{\gamma H_{(\,)}}{I^*}$$

$$I^* = I^*_p + 2\, M^*_b\, h^2$$

The uncoupled dynamics in each degree of freedom are

$$\begin{aligned}
(\Delta_\beta)_{uc} &= s^2 - (\bar{M}_{\dot\beta} + 2i)\, s + (\nu^2_\beta - 1) + i\, \bar{M}_{\dot\beta} \\
(\Delta_\zeta)_{uc} &= s^2 + (\bar{Q}_{\dot\zeta} - 2i)\, s + (\nu^2_\zeta - 1) - i\, \bar{Q}_{\dot\zeta} \qquad (21) \\
(\Delta_\alpha)_{uc} &= \Delta_p + (h^2 H_\mu - i\, h\, \bar{H}_{\dot\beta})\, s - h\, V\bar{H}_\mu
\end{aligned}$$

where

$$\Delta_p = s^2 + 2\,\zeta_p\omega_p\, s + \omega^2_p$$

with

$$\omega^2_p = \sqrt{\frac{K^*}{I^*}}\,, \quad 2\,\zeta_p\omega_p = \frac{C^*}{I^*}$$

It can be readily seen that the equations of motion reduce to equations (4) when $\bar{\alpha} = 0$.

First we examine the dynamics of the system with flapping and support degrees of freedom, then consider the influence of the lag degrees of freedom.

Thus, eliminating the lag degrees of freedom from equations (20) the equations of motion are,

$$\left[\begin{array}{c|c}
(\Delta_\beta)_{uc} & -s^2 + (\bar{M}_{\dot\beta} + i\,(2 + h\bar{M}_\mu))\, s - i\, V\bar{M}_\mu \\
\hline
i\, h\, \bar{H}_{\dot\beta}\,(s - i) + \dfrac{I^*_\beta}{I^*}(\nu^2_\beta - 1) & (\Delta_\alpha)_{uc}
\end{array}\right]
\left\{\begin{array}{c} \bar{\beta} \\ \bar{\alpha} \end{array}\right\} =$$

$$\left[\begin{array}{cc}
\bar{M}_\theta & iV\bar{M}_\mu \\
-\,i\, h\, \bar{H}_\theta & h\, V\bar{H}_\mu
\end{array}\right]
\left\{\begin{array}{c} \bar{\theta} \\ \bar{g} \end{array}\right\} \qquad (22)$$

The characteristic equation for this system can be expressed in terms of the characteristic equation for an articulated rotor system and a rigid propeller system as

$$\Delta_{\beta + \alpha} = (\Delta_{\beta + \alpha})_{fa} + (\nu_\beta^2 - 1)\ (\Delta_\alpha)_{rp} \tag{23}$$

where $(\Delta_{\beta + \alpha})_{fa}$ is the characteristic equation for the articulated system

$$(\Delta_{\beta+\alpha})_{fa} = (\Delta_\beta)_{uc}\ (\Delta_\alpha)_{uc} \Big|_{\nu_\beta = 1} + i\ h\ H_{\dot{\beta}}\ (s - i)\ [s^2 - (\bar{M}_{\dot{\beta}} + i\ (2 + h\bar{M}_\mu))\ s + i\ V\bar{M}_\mu] \tag{24}$$

and $(\Delta_\alpha)_{rp}$ is the characteristic equation for the rigid system,

$$(\Delta_\alpha)_{rp} = (\Delta_\alpha)_{uc} + \frac{I_\beta^*}{I^*}\ [s^2 - (\bar{M}_{\dot{\beta}} + i\ (2 + h\bar{M}_\mu))\ s + i\ V\bar{M}_\mu] \tag{25}$$

It is interesting to note from the form of these two expressions that $\bar{H}_{\dot{\beta}}$ is the term responsible for coupling in the articulated case, and the ratio of blade to pylon inertia is responsible in the rigid propeller case. In both instances, the polynomial associated with the effects of coupling is the same and in a rather general sense can be thought of as containing the effects responsible for the whirl flutter instability as will be shown.

First, the simpler problem of the dynamic behavior of a rigid propeller described by equation (25) is examined. This leads to the classical problem of whirl flutter[6]. I_β^* may be taken as 1, and

the characteristic equation for the rigid case can be written as,

$$(\Delta_\alpha)_{rp} = \Delta_p + \frac{1}{I^*}\left(s^2 + \{h^2\gamma H_\mu - \gamma M_{\dot\beta} - 2i\}\, s - (hV\gamma H_\mu - iV\gamma M_\mu)\right) = 0 \qquad (26)$$

It is convenient to use root locus techniques to illustrate the effect of the aerodynamic terms on the dynamics of the rigid propeller. By considering ζ_p and ω_p fixed and varying the inertia, I*, we can examine the related importance of the aerodynamic terms in causing whirl flutter. The poles of the system are given by Δ_p and with $\frac{1}{I^*}$ as the gain, the root loci shown in Figure 11 for three values of support frequency can be drawn. The pylon dynamics are shown, consisting of an advancing mode and a regressing mode. As the inertia is decreased, the roots move towards the complex zeros given by the quadratic factor in equation (26). One of the complex zeros lies in the right half plane, moving farther to the right as the advance ratio is increased as shown in the diagram. The reduction in inertia (or conversely the increase is the aerodynamic terms) causes the regressing mode to become unstable thus, giving rise to whirl flutter. The advancing mode is stabilized by the coupling. Raising the support frequency also produces a stabilizing tendency.

The zero in the right half plane lies there as a result of the term $iV\gamma M_\mu$ and thus it is possible to identify this term as the source of the whirl instability; it is interesting to note that this term increases rapidly with inflow angle, i.e., from Reference 1,

$$VM_\mu \propto \tan\phi \sin\phi$$

indicating that the onset of this instability tends to occur rapidly with increasing airspeed. As in more conventional flutter, the solution is to increase the stiffness of the mounting system, to reduce the effect of aerodynamics.

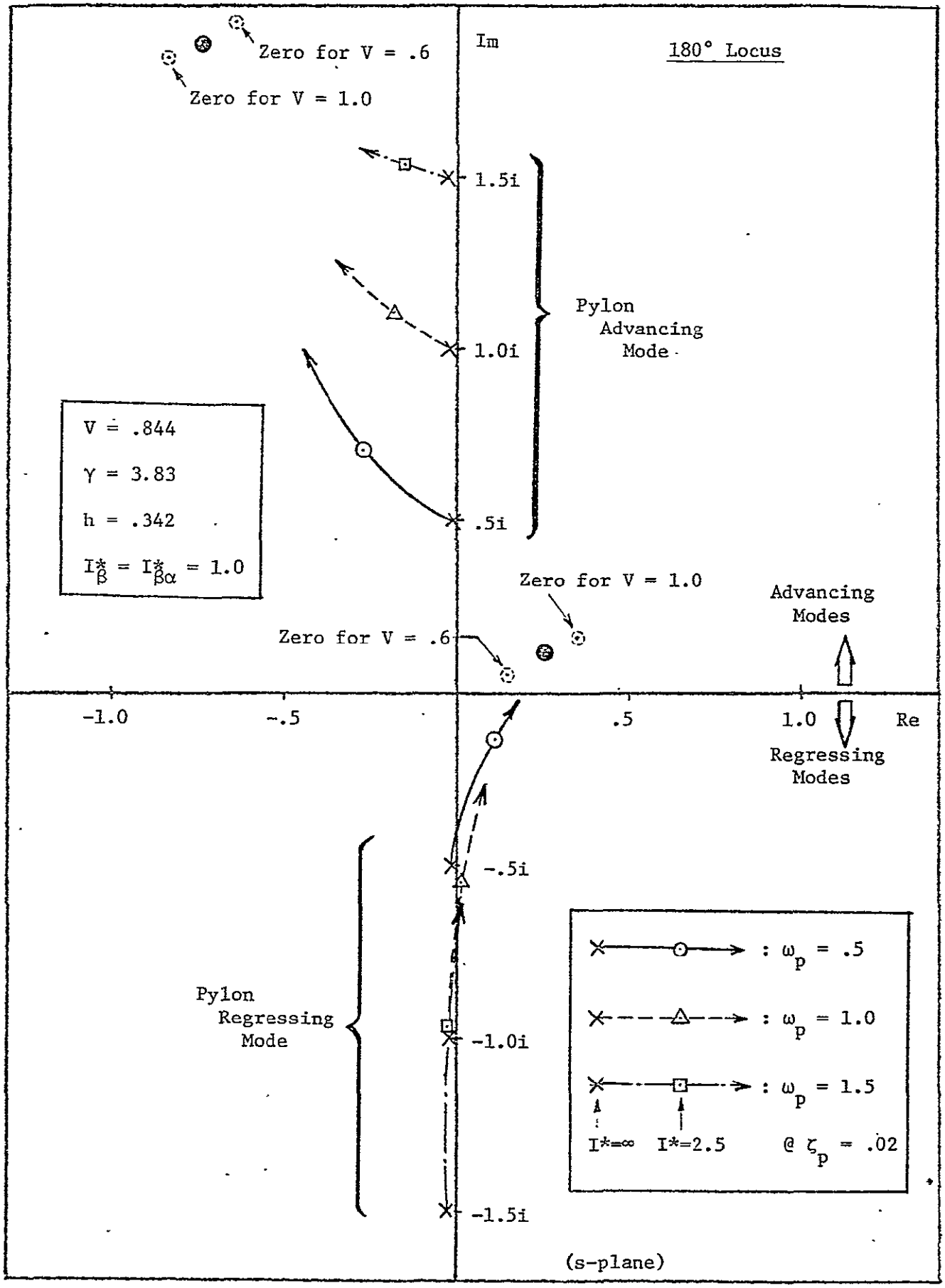

Figure 11. Root Locus: Influence of I* on Pylon Dynamics; Isotropic Pylon with Rigid Propeller; cf. Eqn. (26)

Now we turn to fully articulated case to see the contrast with the rigid case. Equation (24) is expressed as

$$(\Delta_{\beta} + \alpha)_{fa} = \{\Delta_{\beta_{uc}}\}_{\nu_{\beta}=1} \Delta_p + \frac{N_{fa}}{I^*} \tag{27}$$

where

$$\begin{aligned} N_{fa} = [(\Delta_{\beta})_{uc}]_{\nu_{\beta}=1} \{(h^2 \gamma H_{\mu} - ih\gamma H_{\dot{\beta}})\, s - hV\gamma H_{\mu}\} \\ + ih\gamma H_{\dot{\beta}}\,(s - i)[s^2 - \{\bar{M}_{\dot{\beta}} + i\,(2 + h\bar{M}_{\mu})\}\, s + iV\bar{M}_{\mu}] \end{aligned} \tag{28}$$

A root locus showing the influence of the support inertia on the modes of motion is shown in Figure 12. Again it may be noted that the critical case is the one with the lowest support frequency. The trend with Lock number, γ, is also shown, emphasizing the important role that the aerodynamic terms play in the instability.

Now insight into the aerodynamic terms responsible for the instability can be seen by dropping the term $H_{\dot{\beta}}$ from equation (28). If $H_{\dot{\beta}} = 0$ in the fully articulated case, the blade flapping dynamics are uncoupled and only the support dynamics are influenced by inertia variation. Figure 13 shows this root locus. Comparison of Figures 12 and 13 indicate the important role of $H_{\dot{\beta}}$ in causing the whirl instability. It is also interesting to note that in the articulated case, the instability occurs in both the advancing and regressing modes as shown by Figure 12. The location of one zero near the higher flap mode results in the fact that this root locus is essentially symmetric about the real axis giving a root locus diagram that is more conventional in appearance than in the rigid propeller case. That is, the influence of coupling is similar in both the advancing and regressing modes. It should be noted that $H_{\dot{\beta}}$ is of the opposite sign from its value for conventional helicopter flight (low inflow) since it is equal to

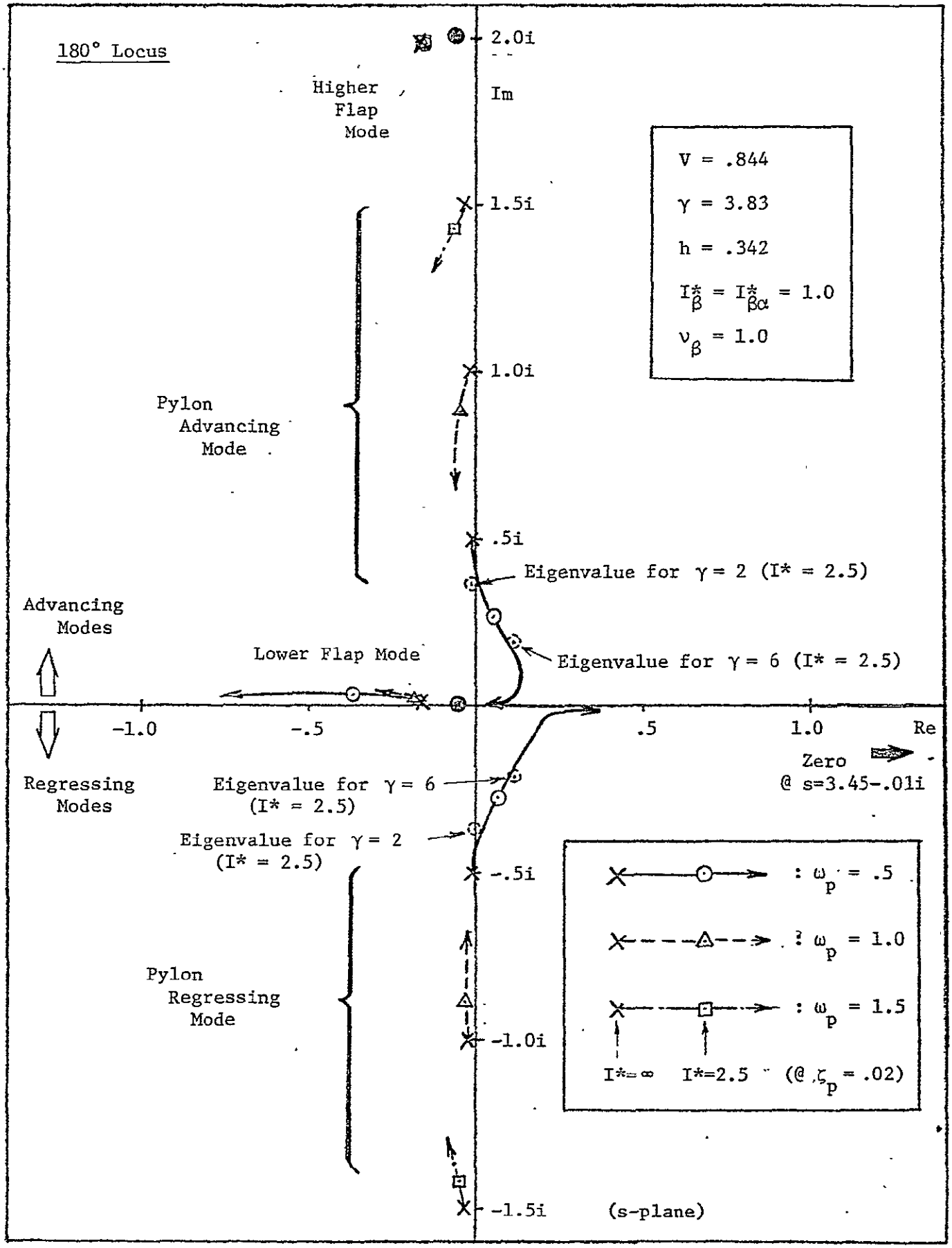

Figure 12. Root Locus: Influence of I* on Coupled Dynamics; Isotropic Pylon with Gimballed Rotor; cf. Eqn. (27).

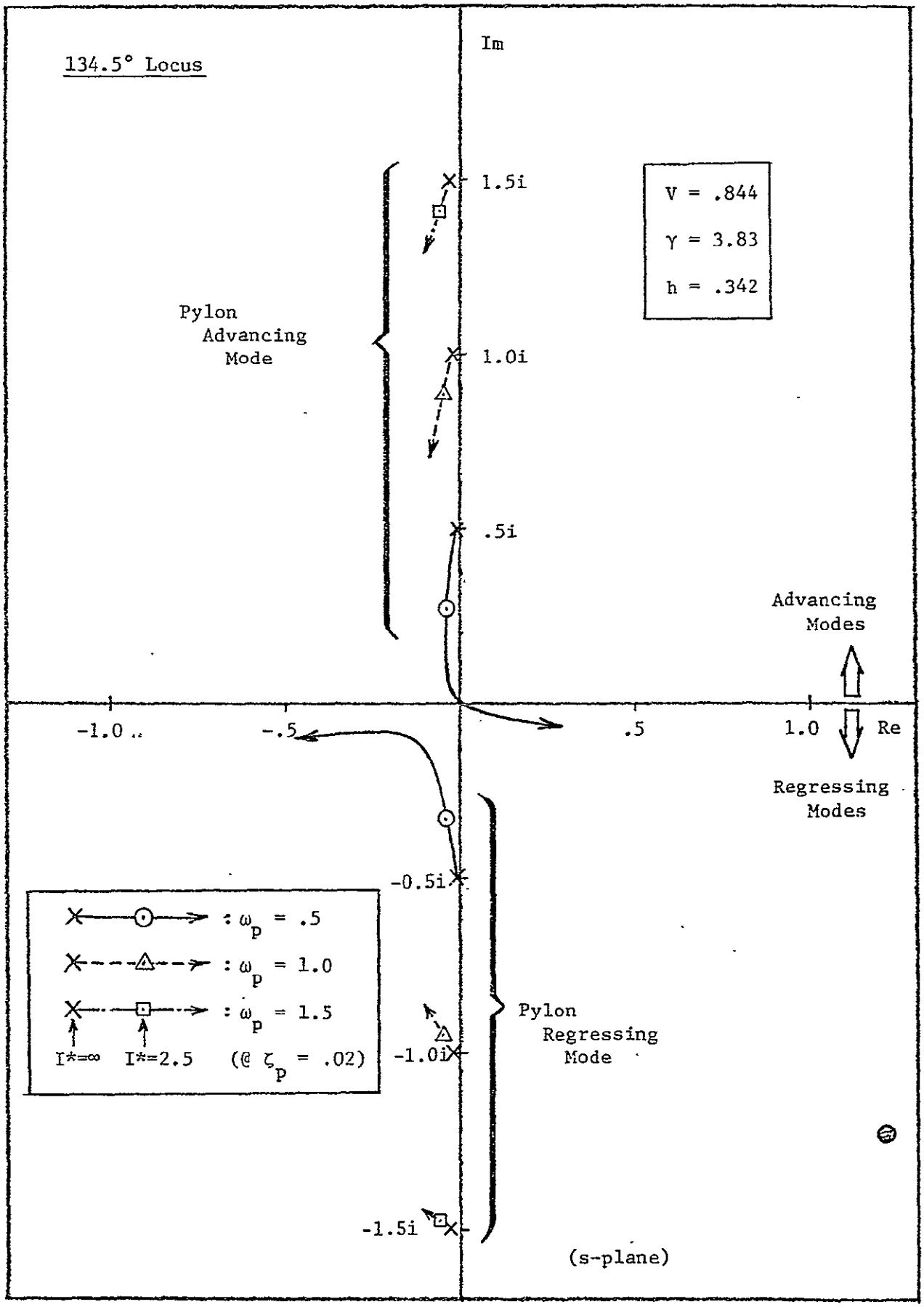

Figure 13. Root Locus: Influence of I* on Uncoupled Pylon Dynamics ($H_{\dot{\beta}} = 0$) for Isotropic Pylon; cf. Eqn. (28).

$$H_{\dot{\beta}} \cong - \frac{\sin \phi}{6} + \frac{C_T}{a\sigma}$$

and therefore at high inflow conditions, the first term dominates. The negative sign corresponds to an unstable damping term at high inflow as comparison of Figures 12 and 13 indicates. With low support stiffness, the effect of $H_{\dot{\beta}}$ can be seen to directly move the roots into the right half plane. Further insight into the fully articulated case can be obtained by considering an approximate factorization of N_{fa}. This polynomial can be written as

$$\begin{aligned} N_{fa} = h^2 \gamma H_\mu [\{\Delta_\beta\}_{uc}]_{\nu_\beta = 1} \{s - \frac{V}{h}(1 - \frac{H_{\dot{\beta}}}{VH_\mu})\} \\ + h^2 \gamma H_{\dot{\beta}} \tilde{M}_\mu (s - i) \{s - \frac{V}{h}(1 - \frac{M_{\dot{\beta}}}{VM_\mu})\} \end{aligned} \tag{29}$$

The simplified forms of the aerodynamic derivatives (Reference 1) give

$$\frac{H_{\dot{\beta}}}{VH_\mu} \cong \frac{M_{\dot{\beta}}}{VM_\mu} \cong - \frac{1}{3V^2}$$

so that

$$\begin{aligned} N_{fa} \cong h^2 \gamma H_\mu \{s - \frac{V}{h}(1 + \frac{1}{3V^2})\} \{s^2 - (2i + M_{\dot{\beta}}(1 - \frac{H_{\dot{\beta}} M_\mu}{H_\mu M_{\dot{\beta}}}) s \\ + i M_{\dot{\beta}} (1 - \frac{H_{\dot{\beta}} M_\mu}{H_\mu M_{\dot{\beta}}}) \end{aligned} \tag{30}$$

Using the effective radius approximation

$$\frac{H_{\dot{\beta}} M_\mu}{H_\mu M_{\dot{\beta}}} = \frac{16}{27}$$

giving

$$N_{fa} \cong h^2 \gamma H_\mu \{(s - \frac{V}{h}(1 + \frac{1}{3V^2})(s - \frac{11}{54} M_{\dot{\beta}})(s - (2i + \frac{11}{54} M_{\dot{\beta}})\} \qquad (31)$$

The approximate zeros given by this approximate factorization agree well with the exact factorization of N_{fa} based on equation (28).

The last factor in equation (31) gives the zero very near the higher flap mode, the second factor gives the zero near the origin, and the first factor is responsible for the zero in the right half plane which may be viewed as the source of the instability, arising from $H_{\dot{\beta}}$ in effect.

Now we examine the influence of ν_β, the flap frequency, on the stability of the system. Figure 14 shows the influence of the flap frequency on the stability for three levels of pylon stiffness. Again with the high pylon stiffness, the dynamic system is stable and the effect of flap frequency is small. At a pylon frequency ratio of 1.5 the effect of ν_β is essentially to raise the blade flapping frequency as would be expected from the uncoupled system. In the low pylon stiffness case, the effect is markedly different, with the variation in ν_β causing primarily a damping change in the pylon and lower flap modes. In fact, it can be seen that there is an optimum flap frequency in the sense that the damping of the pylon mode and the damping of the lower flap mode can be maximized by a suitable choice of ν_β as suggested in Reference 7. For this numerical example the system is stable for $1.07 < \nu_\beta < 1.18$. This figure also shows that the effect of the weak flapping spring on the Bell rotor is small and that the dynamic characteristics of the system essentially correspond to the freely flapping rotor.

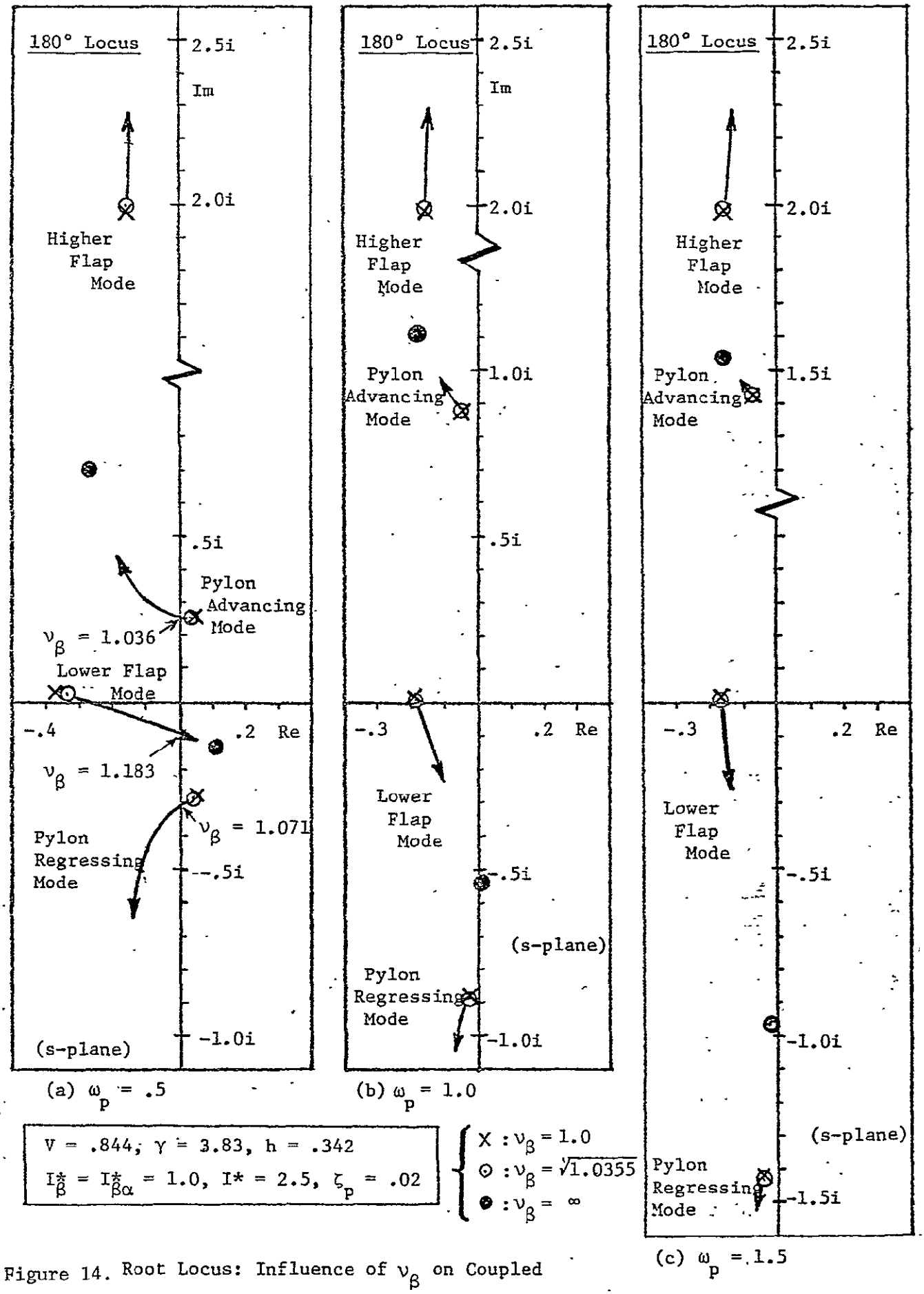

Figure 14. Root Locus: Influence of ν_β on Coupled Dynamics for Isotropic Pylon

We now consider the influence of adding the lag degrees of freedom. The characteristic equation given by expanding equations (20) can be expressed in the following form

$$\Delta_{\beta + \zeta + \alpha} = \Delta_{\beta + \zeta} \Delta_p - \frac{1}{I^*} \left\{ \frac{(S_\zeta^* h)^2}{I_\zeta^*} s^6 + ... \right\} \qquad (32)$$

where $\Delta_{\beta + \zeta}$ is the characteristic equation for the coupled flap-lag motion and Δ_p is defined as before. If the inertia characteristic I* is infinitely large then the dynamics are given by $\Delta_{\beta + \zeta}$ and Δ_p, the former associated with the isolated rotor cyclic motion and the latter with the pylon. The root locus shown in Figure 15 presents the influence of pylon inertia on the dynamics of the system with the lag motion degree of freedom for the fully articulated case. The regressing modes are not particularly influenced by the coupling and the instability which occurs in the pylon advancing mode is quite similar to the case without the lag degree of freedom (Fig. 12) indicating that while the lag is required to obtain a detailed description of the dynamics, it does not play an essential role in the whirl flutter instability. There also appears to be no particular tendency towards an air resonance instability undoubtedly as a result of the high lag damping. Figure 16 shows the effect of blade coupling (blade pitch-flap and pitch-lag effects) which produces no essential change in the root locus diagram. Figures 12 and 14 appear to depict the essential contributing features to the instability. With a pylon frequency of 1.5, there appears to be little likelihood of an instability for the parameter ranges examined.

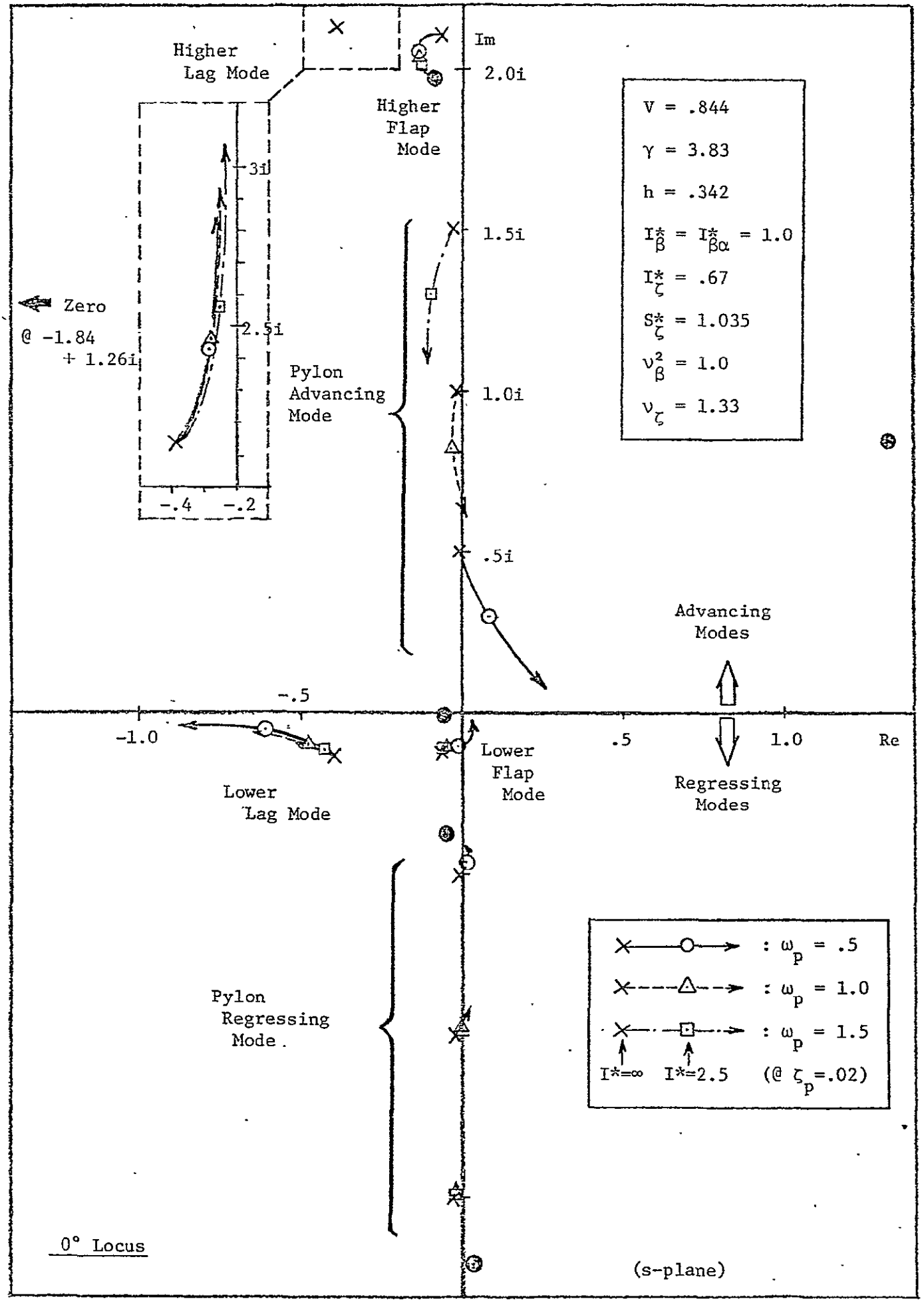

Figure 15. Root Locus: Influence of I* on Coupled Dynamics for Isotropic Pylon; With Cyclic Lag Degree of Freedom

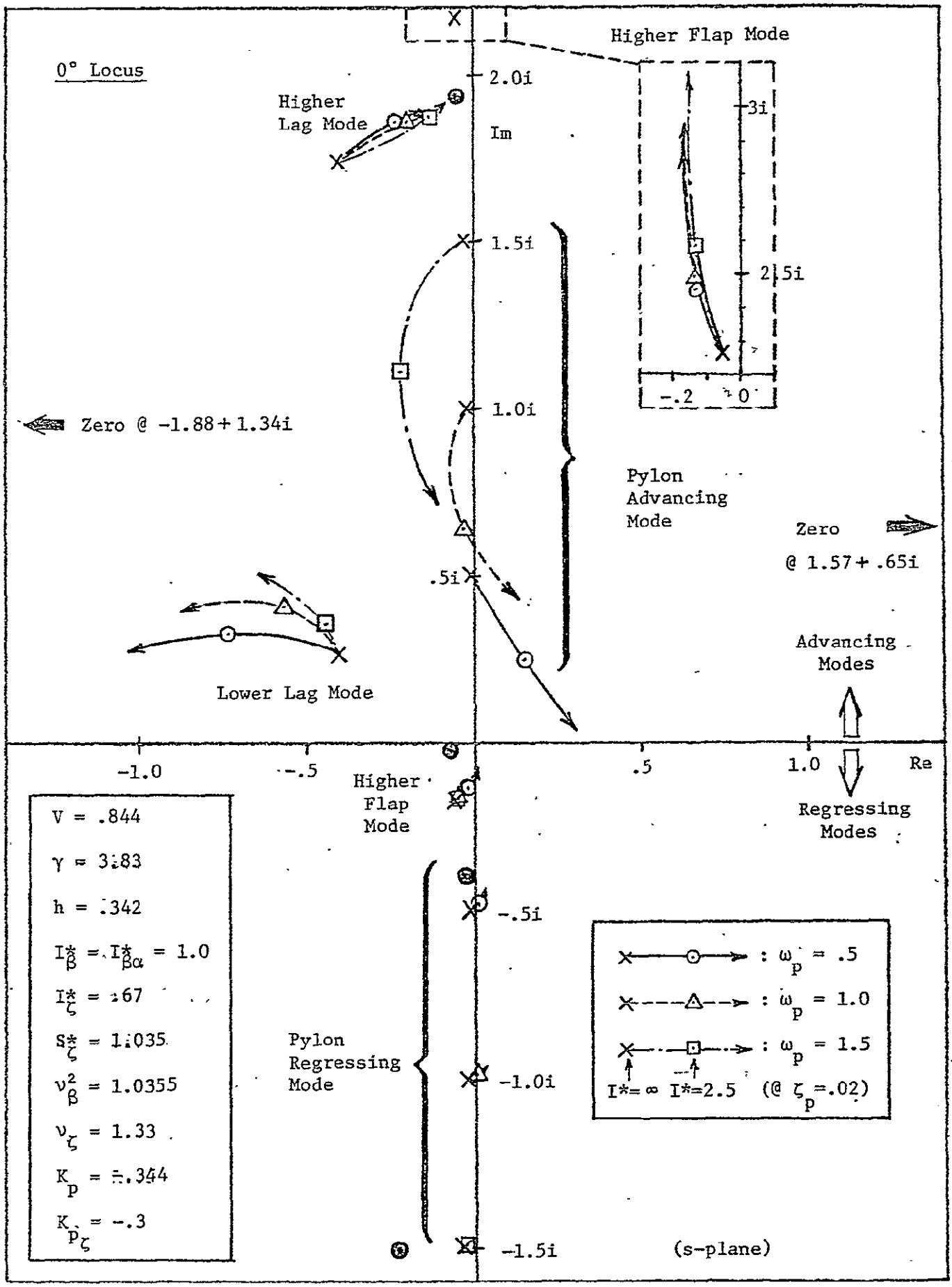

Figure 16. Root Locus: Influence of I* on Coupled Dynamics for Isotropic Pylon; With Cyclic Lag Motion Degree of Freedom and K_p & K_{p_ζ}

1.) Pylon Motion Feedback

We now turn to the question of pylon motion feedback and its influence on the dynamic stability of the pylon proprotor system. First consider the rigid propeller case. The transfer function relating complex pylon motion to complex cyclic pitch is found for the rigid propeller case by taking the limit $\nu_\beta, \nu_\zeta \to \infty$ in equation (20). The transfer function is

$$\frac{\bar{\alpha}}{\bar{\theta}} = - \frac{\gamma M_\theta + ih\gamma H_\theta}{I^* \{\Delta_\alpha\}_{rp}} \tag{33}$$

where the denominator has been discussed previously. The feedback law of interest here is

$$\bar{\theta} = - \bar{K}_d \bar{\alpha}$$

The feedback gain can in general be taken to be a complex number to account for the phasing between pylon deflection and cyclic pitch.

For example, if $\bar{K}_d$ has a purely imaginary value so that $\bar{K}_d = K_d i$ then the feedback law implies

$$\theta_{1c} = -K_d \alpha_x$$

$$\theta_{1s} = -K_d \alpha_y$$

hence cyclic pitch is applied in such a way that the maximum decrease in cyclic occurs at the azimuth position (arg $\bar{K}_d$) greater than the position at which the maximum angular displacement of the pylon occurs. The characteristic equation for the closed loop system from equation (33) is,

$$\{\Delta_\alpha\}_{rp} - \frac{\bar{K}_d}{I^*} (\gamma M_\theta + ih\gamma H_\theta) = 0 \tag{34}$$

This equation may be expanded to yield

$$\Delta_p + \frac{1}{I^*}\left\{ s(s - 2i) + \gamma(h^2 H_\mu - M_{\dot\beta})\left(s - \frac{V(hH_\mu - iM_\mu) + \bar{K}_d(M_\theta + ihH_\theta)}{h^2 H_\mu - M_{\dot\beta}}\right)\right\} = 0 \quad (35)$$

As seen previously, the possibility of whirl flutter is essentially due to the location of one of the complex zeros associated with the quadratic factor (see Fig. 11), i.e., which can be traced to the value of

$$\frac{V(hH_\mu - i\,M_\mu)}{h^2 H_\mu - M_{\dot\beta}}$$

and the sign of $(h^2 H_\mu - M_{\dot\beta})$. Thus if the feedback gain $\bar{K}_d$ is appropriately chosen, such that the quadratic expression has no zeros in the right half plane then the possibility of whirl flutter can be eliminated.

Figure 17 shows the location of the zeros as a function of the feedback gain $\bar{K}_d$ indicating that when $\bar{K}_d = i$, the first order factor has its root in the second quadrant and then the zeros of the quadratic factor are in the left half plane as shown for the parameter values appropriate to the flight condition. With this choice for the feedback gain, the system is stable for any value of the inertia parameter I* as shown in Figure 18 and thus the possibility of whirl flutter is eliminated. Figure 19 then shows the influence of the gain $\bar{K}_d$ on the whirl flutter. It can be seen from the previous figure that the purely imaginary value of $\bar{K}_d$ is of interest. It is interesting to note however that as the gain is increased, the regressing mode is stabilized, and the advancing mode is destablized and that a gain magnitude of less than 1 is desirable.

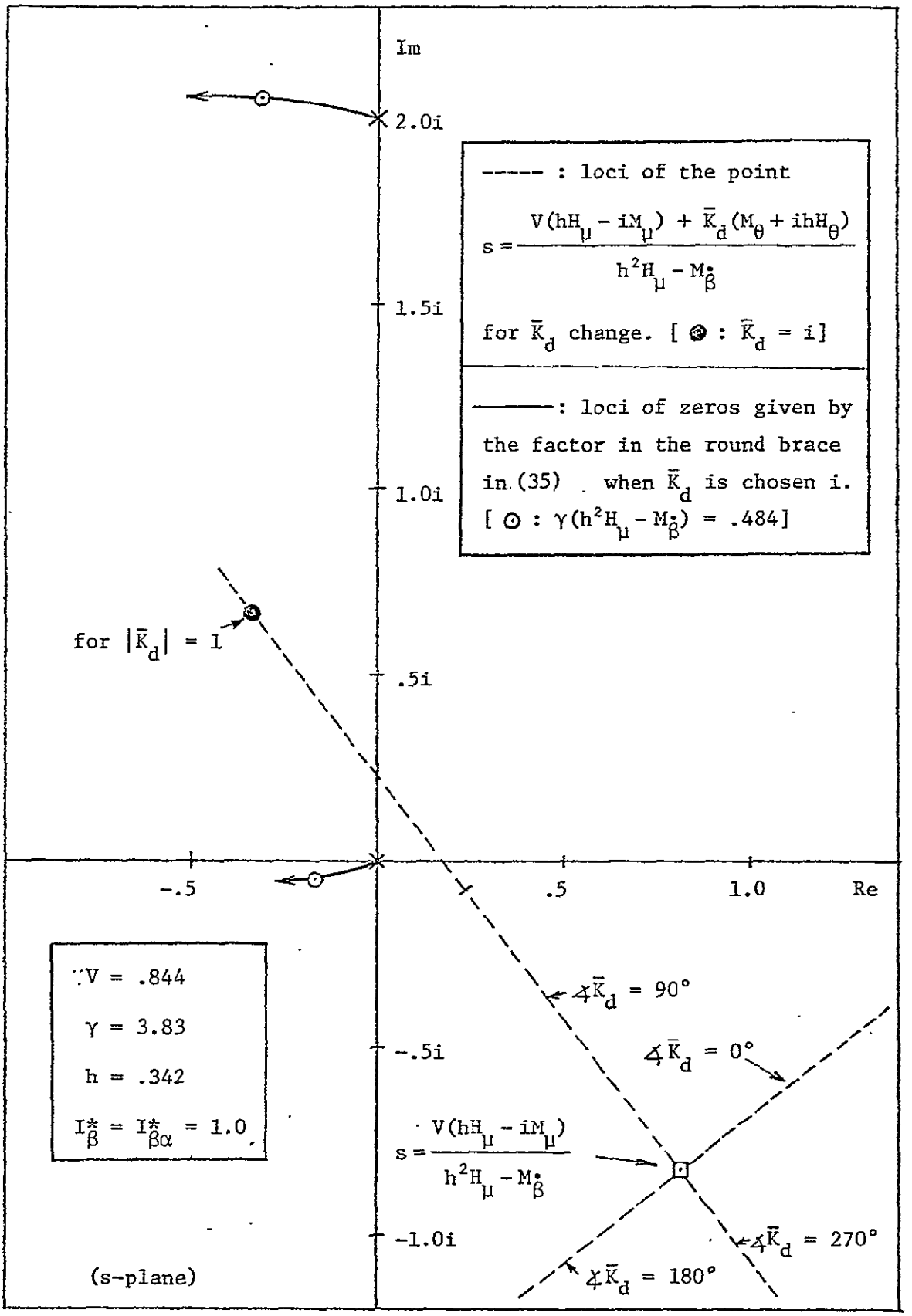

Figure 17. Locus of Zeros: Influence of $\bar{\alpha} \to \bar{\theta}$ Feedback; Isotropic pylon with Rigid Propeller; cf. Eqn. (35)

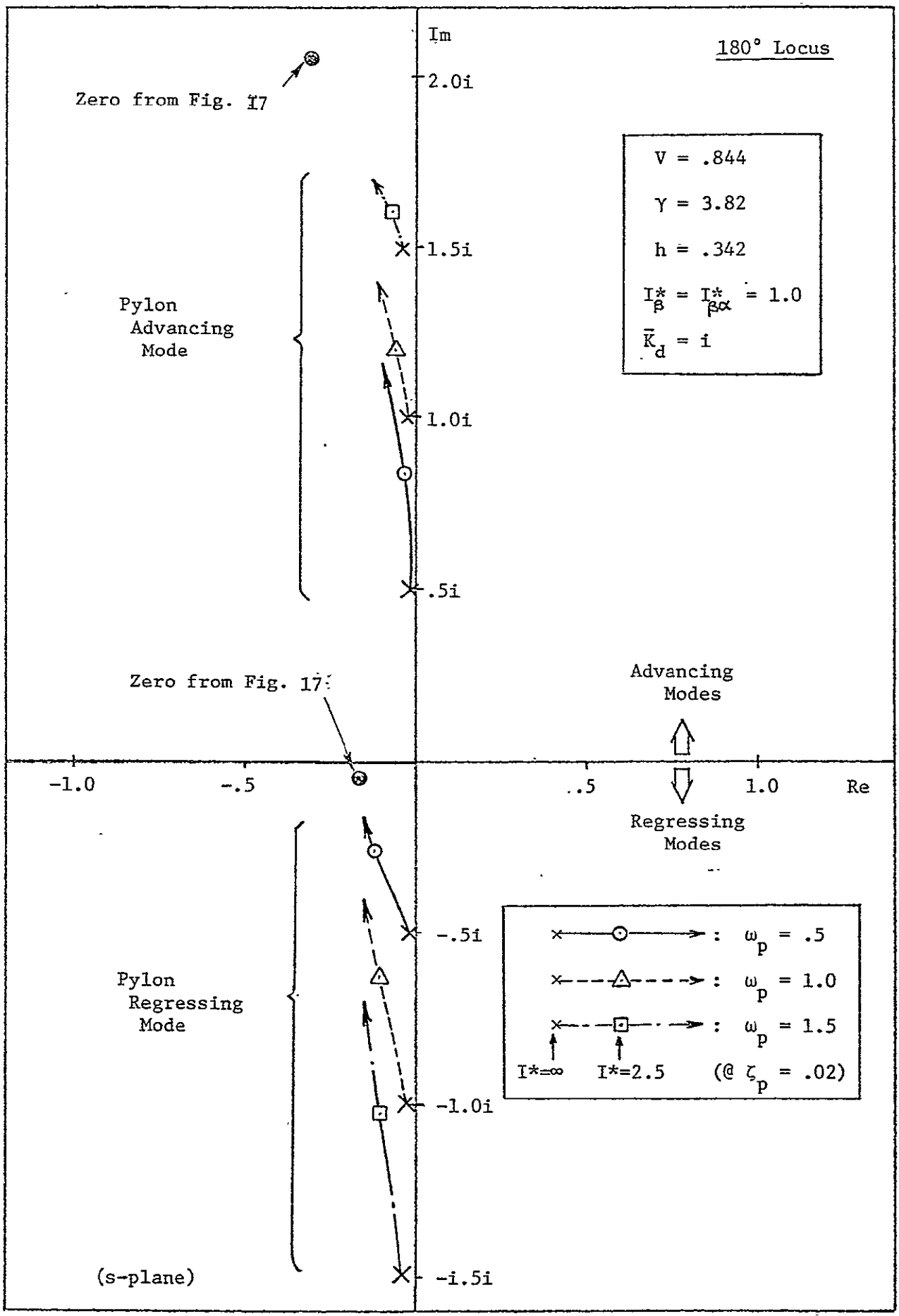

Figure 18. Root Locus: Influence of I* on Pylon Dynamics with $\bar{\alpha} \rightarrow \bar{\theta}$ Feedback ($\bar{K}_d = i$); Isotropic Pylon with Rigid Propeller; cf. Eqn. (35)

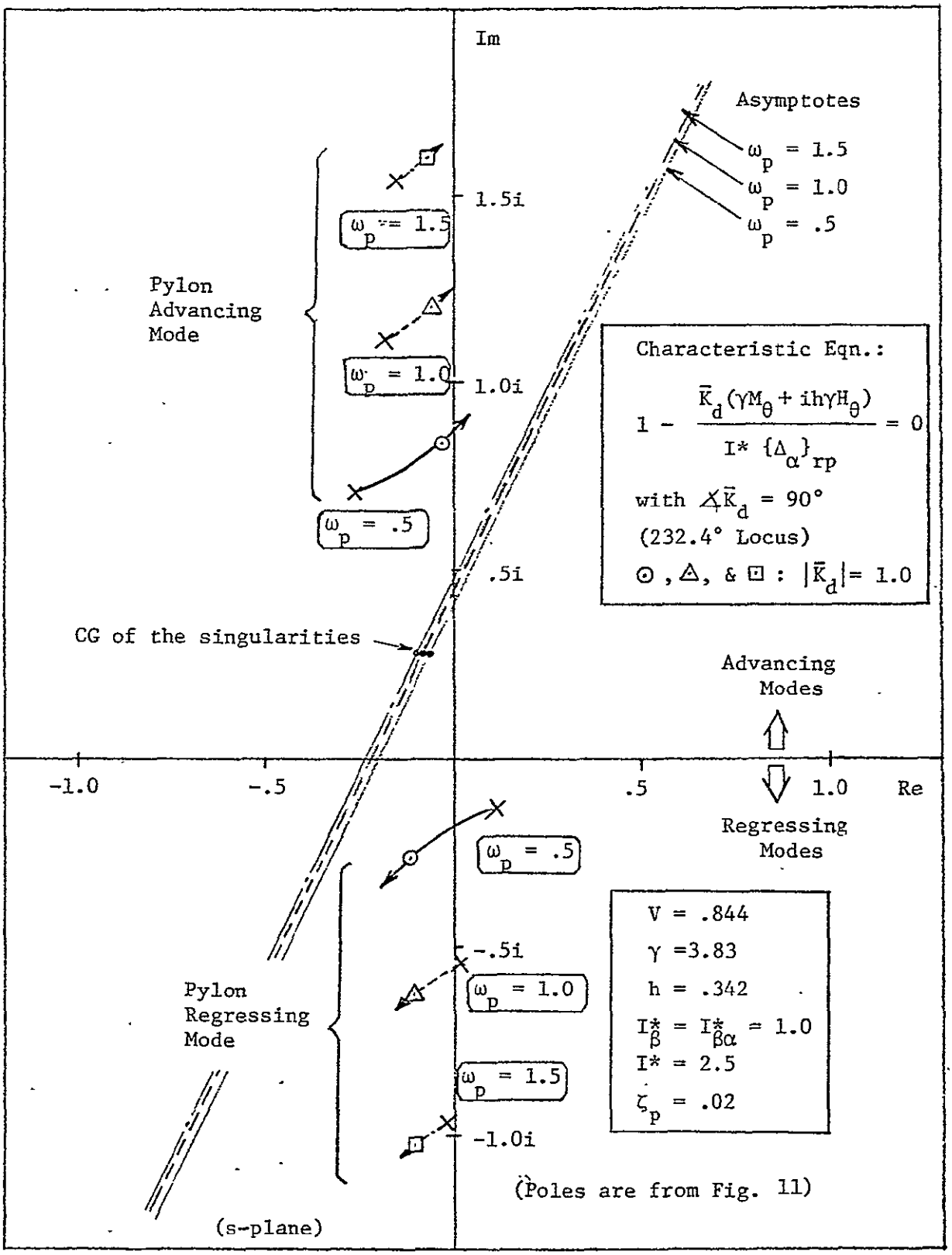

Figure 19. Root Locus: Influence of $\bar{\alpha} \rightarrow \bar{\theta}$ Feedback on Pylon Dynamics; Isotropic Pylon with Rigid Propeller; cf. Eqn. (35)

Now consider the effect of the same feedback law on the gimballed rotor with no lag degree of freedom. The transfer function in this case obtained from equations (20) is

$$\frac{\bar{\alpha}}{\bar{\theta}} = \frac{(N_\theta^\alpha)_{fa}}{(\Delta_{\beta+\alpha})_{fa}} \tag{36}$$

The denominator is given by equation (24) and the numerator is obtained from equations (22),

$$(N_\theta^\alpha)_{fa} = -\frac{ih\gamma H_\theta}{I^*}\{s^2 - [2i + \bar{M}_{\dot{\beta}}(1 - \frac{H_{\dot{\beta}}M_\theta}{M_{\dot{\beta}}H_\theta})]\, s + i\bar{M}_{\dot{\beta}}(1 - \frac{H_{\dot{\beta}}M_\theta}{H_\theta M_{\dot{\beta}}})\} \tag{37}$$

Using the effective radius approximation[1] equation (37) becomes,

$$\cong -\frac{ih\gamma H_\theta}{I^*}\{s^2 - (\frac{1}{9}\bar{M}_{\dot{\beta}} + 2i)\, s + \frac{1}{9} i\bar{M}_{\dot{\beta}}\}$$

The closed loop characteristic equation from (36) is

$$(\Delta_{\beta+\alpha})_{fa} + \bar{K}_d\,(N_\theta^\alpha)_{fa} = 0 \tag{38}$$

Figure 20 shows the root locus for this feedback for various values of gain. It is interesting to note that one of the zeros essentially acts to cancel the higher flap mode and the other zero lies quite close to the origin indicating that this feedback acts more like a damping term than a stiffness change. If $\bar{K}_d$ is real, the feedback law is

$$\theta_{1c} = K_d\,\alpha_y$$

$$\theta_{1s} = -K_d\,\alpha_x$$

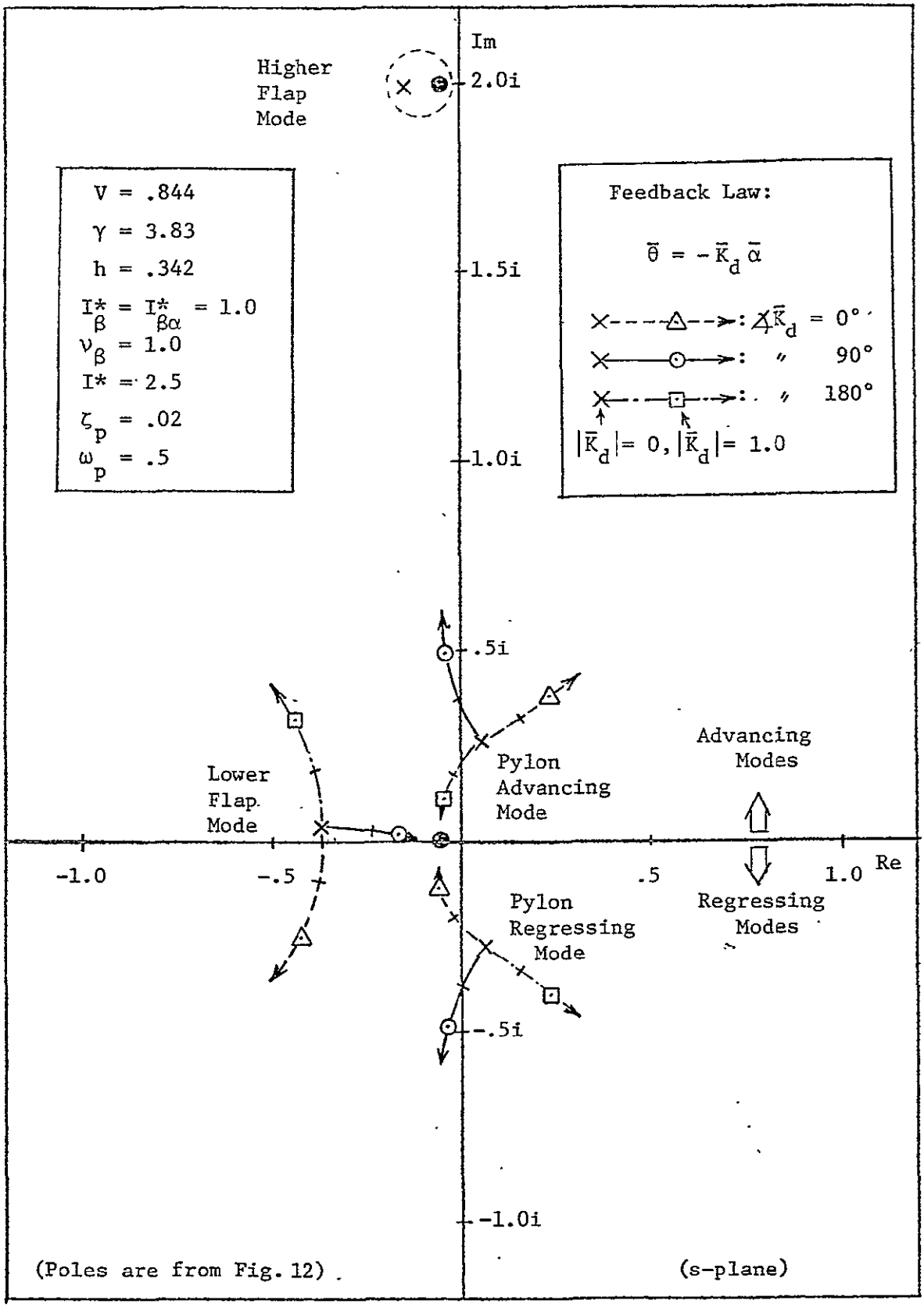

Figure 20. Root Locus: Influence of $\bar{\alpha} \rightarrow \bar{\theta}$ Feedback on Coupled Motion Dynamics; Isotropic Pylon with Gimballed Rotor, cf. Eqn. (38)

This would appear at first glance to be a stiffness effect, however, examination of the nature of the inplane force indicates that the dominant term in the inplane force is proportional to flapping velocity (at low frequency) and since cyclic pitch produces a flap angle this would imply effectively that a feedback proportional to shaft rate is produced by this displacement feedback. Shifting the phase of feedback by 90^{o} produces more of a spring or stiffening effect as would be expected from the above discussion. It is also interesting to note that in general, a feedback phase angle which tends to stabilize one of the modes tends to destabilize the other mode, showing behavior quite analogous to the rigid propeller case (Fig. 19).
Similar behavior is shown in Figure 21 where the effect of various phase feedbacks is shown with different levels of pylon stiffness. In general, the phase of feedback which stabilizes or adds damping to one of the pylon modes, destabilizes or reduces the damping of the other mode.

It is interesting to note the similarity of the results of Figure 21 to the case examined previously in which the coupling term in the pylon equation is dropped ($H_{\dot{\beta}} = 0$). In this case the closed loop characteristic equation is given by

$$\{\Delta_{\alpha}\}_{uc} - \bar{K}_{d}\, ih\bar{H}_{\theta} = 0 \qquad (39)$$

The root loci based on equation (39), i.e., for a dynamically uncoupled pylon is shown in Figure 22 for pylon frequencies $\nu_{p} = 1.0$ and 1.5. It can be seen that the effects of feedback are very similar to the results shown in Figure 21. Of course in this case, the stabilization is not necessary since the increased stiffness has already stabilized the system.

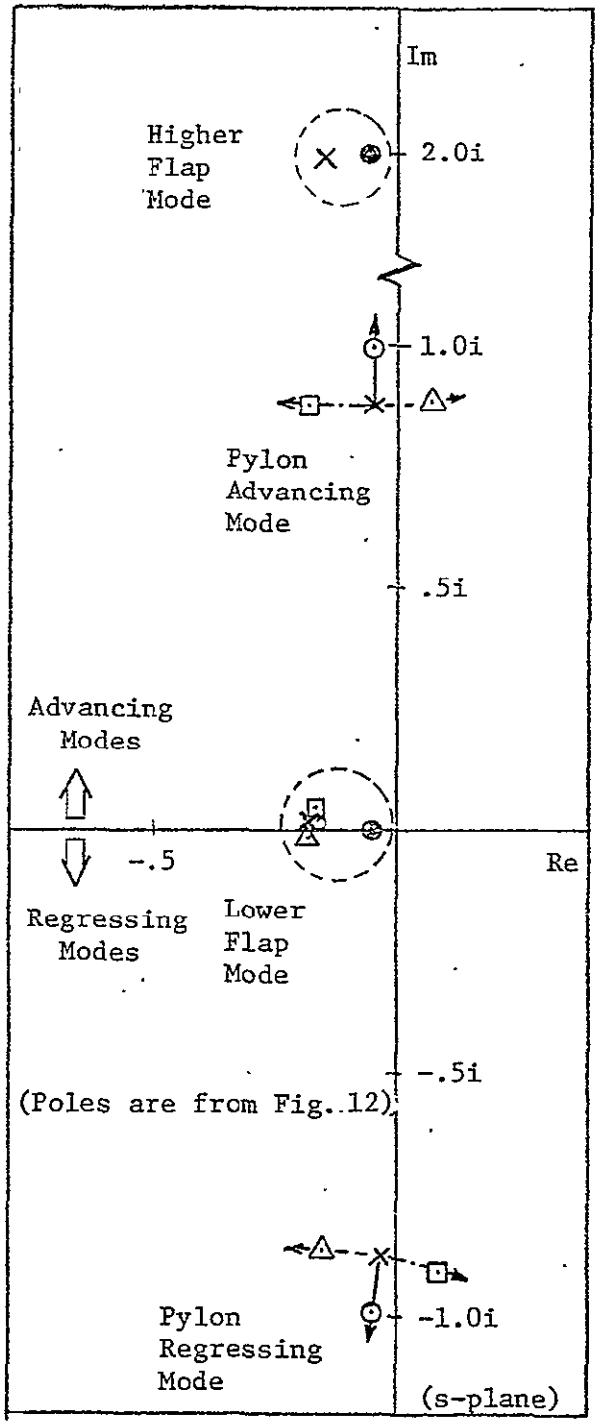

(a) $\omega_p = 1.0$

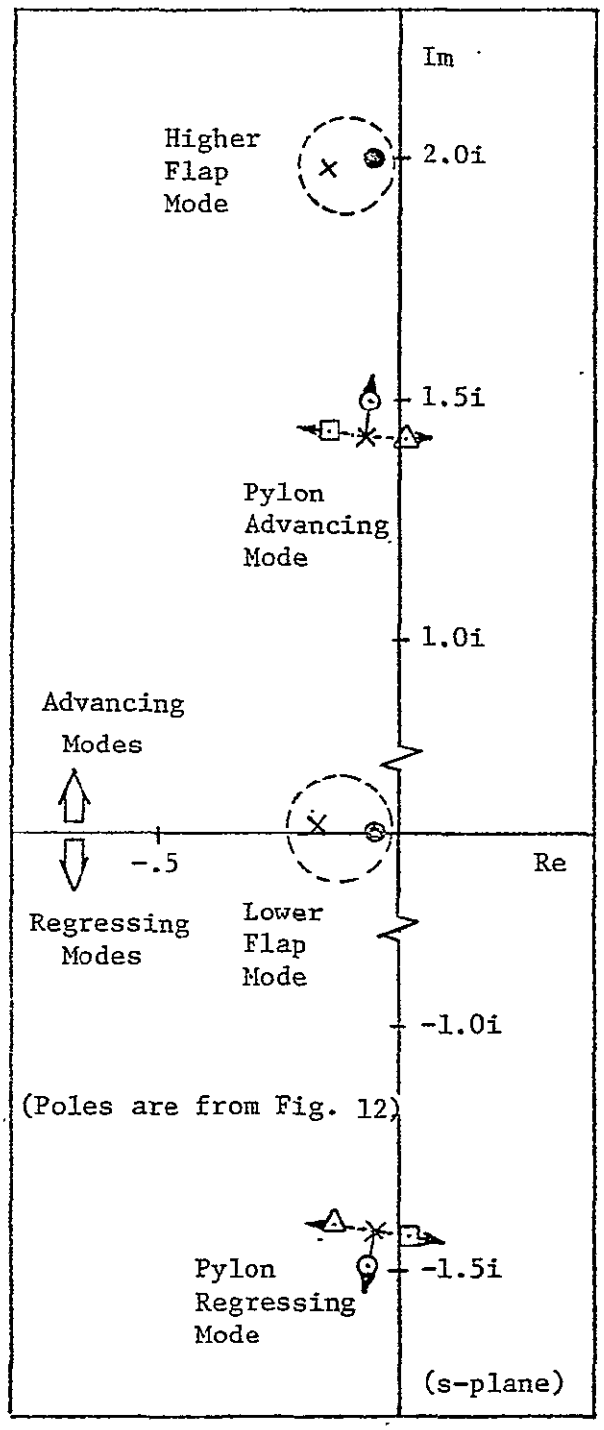

(b) $\omega_p = 1.5$

$V = .844$, $\gamma = 3.83$, $h = .342$, $\nu_\beta = 1.0$

$I^*_\beta = I^*_{\beta\alpha} = 1.0$, $I^* = 2.5$, $\zeta_p = .02$

Feedback Law: $\bar{\theta} = -K_d \bar{\alpha}$

$\times$---$\triangle$---$\rightarrow$: $\measuredangle \bar{K}_d = 0°$

$\times$——$\odot$——$\rightarrow$: $\measuredangle$ 90°

$\times$—·—$\square$—·—$\rightarrow$: $\measuredangle$ 180°

$|\bar{K}_d| = 0, |\bar{K}_d| = 1.0$

Figure 21. Root Locus: Influcence of $\bar{\alpha} \rightarrow \bar{\theta}$ Feedback on Coupled Motion Dynamics; Isotropic Pylon with Gimballed Rotor

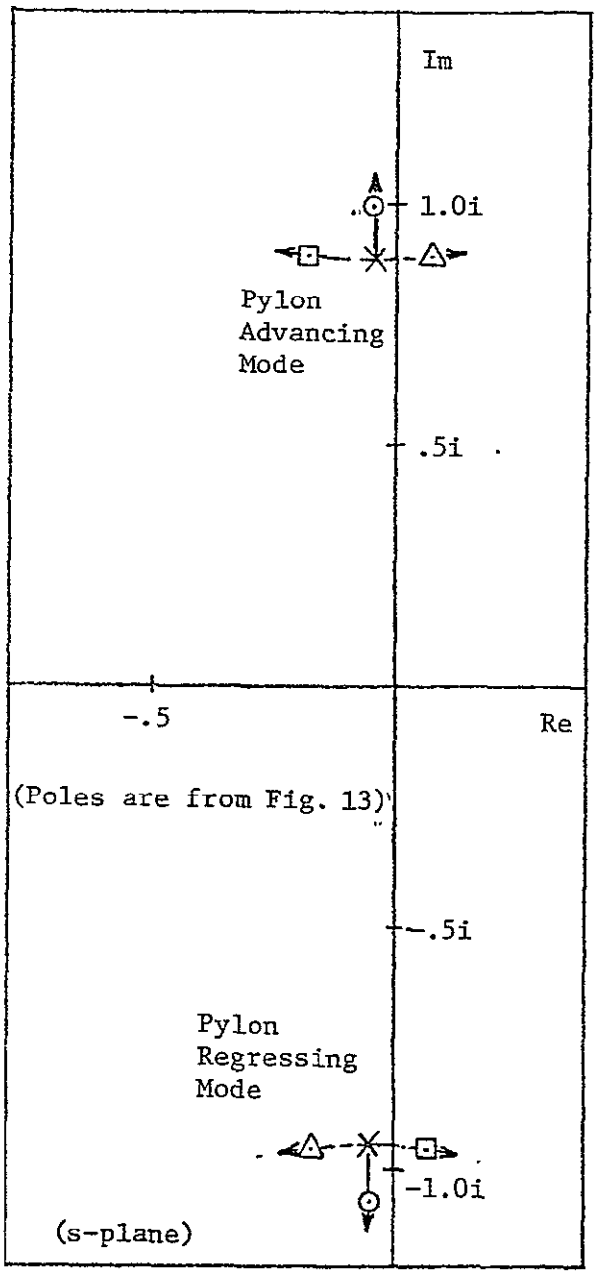

(a) $\omega_p = 1.0$

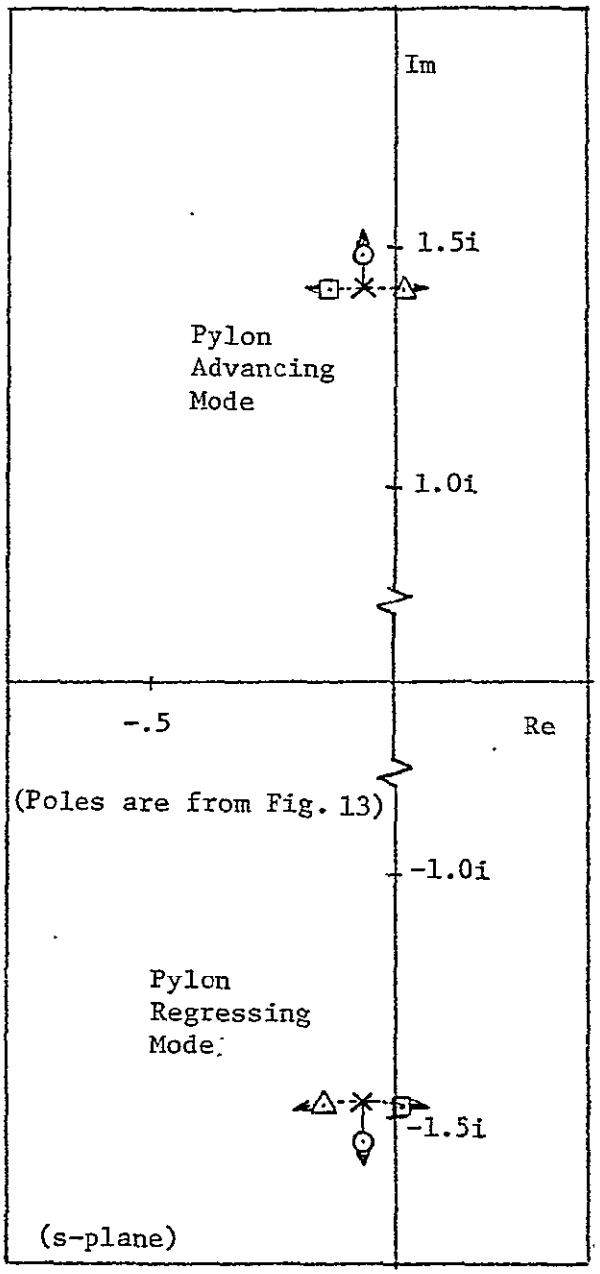

(b) $\omega_p = 1.5$

$V = .844$, $\gamma = 3.83$, $h = .342$

$I^* = 2.5$, $\zeta_p = .02$

Feedback Law: $\bar{\theta} = -\bar{K}_d \bar{\alpha}$

$\times$-----$\triangle$---$\rightarrow$: $\measuredangle \bar{K}_d$ = 0°

$\times$——$\odot$——$\rightarrow$: " 90°

$\times$—·—$\boxdot$—·$\rightarrow$: " 180°

$|\bar{K}_d| = 0$ $|\bar{K}_d| = 1.0$

Figure 22. Root Locus: Influence of $\bar{\alpha} \rightarrow \bar{\theta}$ Feedback on Uncoupled Motion Dynamics; Isotropic Pylon; $(H_{\dot{\beta}} = 0)$

Now as a final topic in this section we examine the effect of the flap frequency in conjunction with feedback. The open loop transfer function is

$$\frac{\bar{\alpha}}{\bar{\theta}} = \frac{N_\theta^\alpha}{\Delta_{\beta + \alpha}} \tag{40}$$

The numerator obtained from equation (22) is expressed as,

$$(N_\theta^\alpha) = (N_\theta^\alpha)_{fa} - \frac{ih\gamma H_\theta}{I^*}(\nu_\beta^2 - 1)\left(1 - \frac{iM_\theta}{hH_\theta}\right) \tag{41}$$

where $(N_\theta^\alpha)_{fa}$ is given by equation (37). Figure 23 shows the root locus for the zeros of the transfer function (equation (40)) as a function of ν_β. The closed loop system equation is obtained from equation (40) as,

$$\Delta_{\beta + \alpha} + \bar{K}_d N_\theta^\alpha = 0 \tag{42}$$

It should be recalled that the system poles given by $\Delta_{\beta + \alpha}$ are also dependent upon ν_β. Root loci are shown in Figure 24 as a function of gain for various values of flapping stiffness with a pylon frequency of 0.5.

The feedback influences the pylon and flapping dynamics. The phase of the feedback which stabilizes the motion shifts as the blade flap frequency is increased as would be expected due to the changing phase angle of the blade response to cyclic. It also may be noted that as the flap frequency is increased, the least stable mode becomes the flapping mode which is stabilized by feedback at the expense of the pylon mode damping.

Figures 25 and 26 show the effect of feedback with increased pylon stiffness indicating that as shown before essentially the uncoupled result is obtained at $\omega_p = 1.0$ and 1.5.

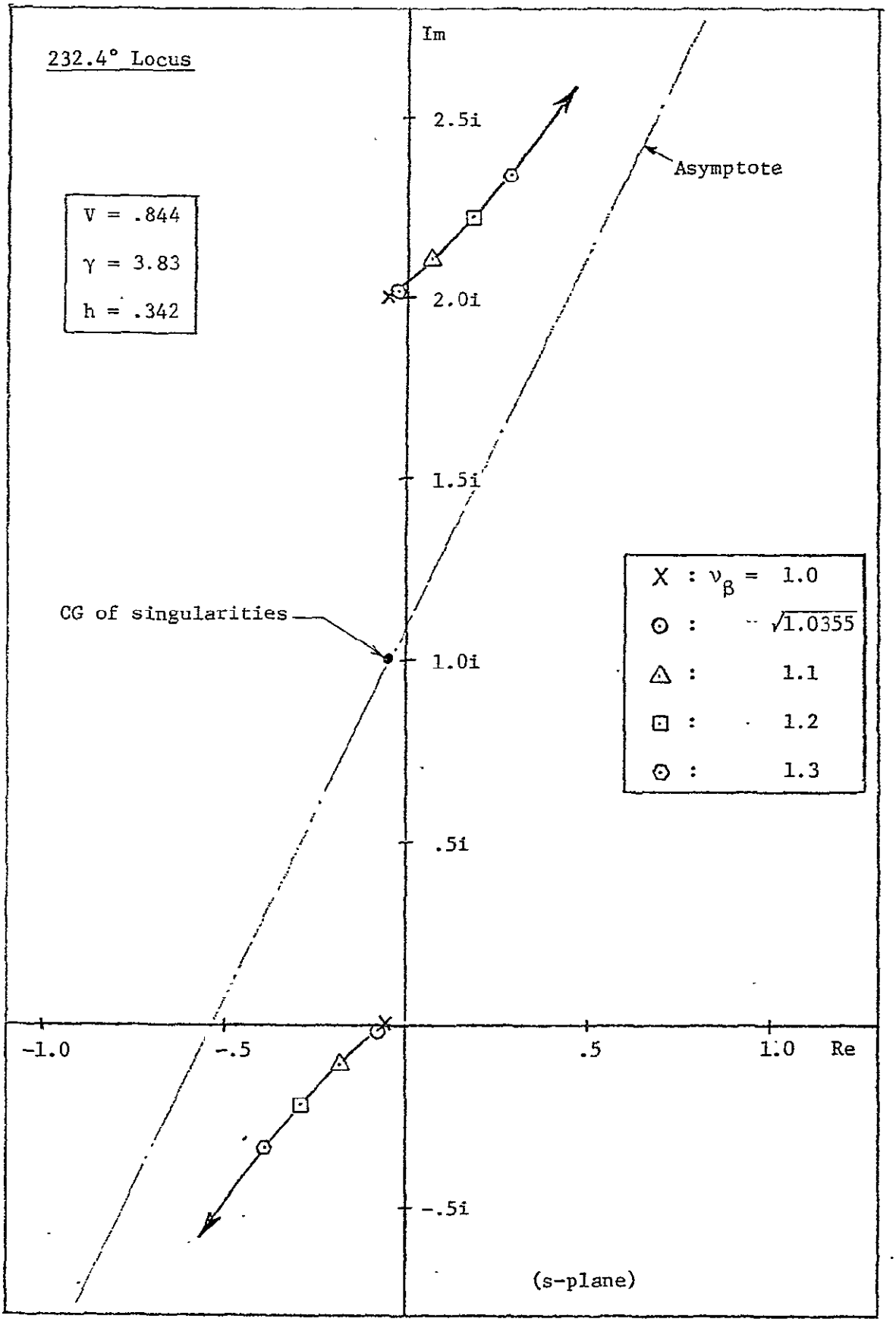

Figure 23. Locus of Zeros: Influence of ν_β Change; Isotropic Pylon; cf. Eqn. (41)

In Figure 27, the articulated rotor case is considered with a combination of displacement and rate feedback.

With a suitable choice of rate and displacement gain the system can be effectively stabilized as shown in Figure 27(c).

The lag degree of freedom is added along with the appropriate pitch-flap and pitch-lag coupling and a root locus is shown in Figure 28. In this case a detailed discussion of the zero location is not possible. However, it can be seen that the primary effect of the additions to the model is to make the 90^{o} phase feedback more effective in damping the unstable advancing mode and in addition to markedly reduce the effect of the feedback on the regressing mode. If the pylon stiffness is increased, the decoupling shown previously does not seem to be present as also shown in Figure 28. The feedbacks have little influence on the regressing modes and the phase of feedback which tends to stabilize the pylon advancing mode, destabilizes the higher lag mode. Thus, with the complete model it appears difficult to provide stabilization for the regressing mode and this result indicates the importance of including all relevant degrees of freedom.

Figure 29 shows the influence of rate feedback and displacement plus rate feedback for the complete system. It is interesting to note that rate feedback alone destabilizes the higher flap and lag modes and has little effect on the pylon mode. The combination of displacement and rate stabilizes the pylon advancing mode while destabilizing the higher flap mode. Thus, the addition of rate feedback does not appear to be useful in this case.

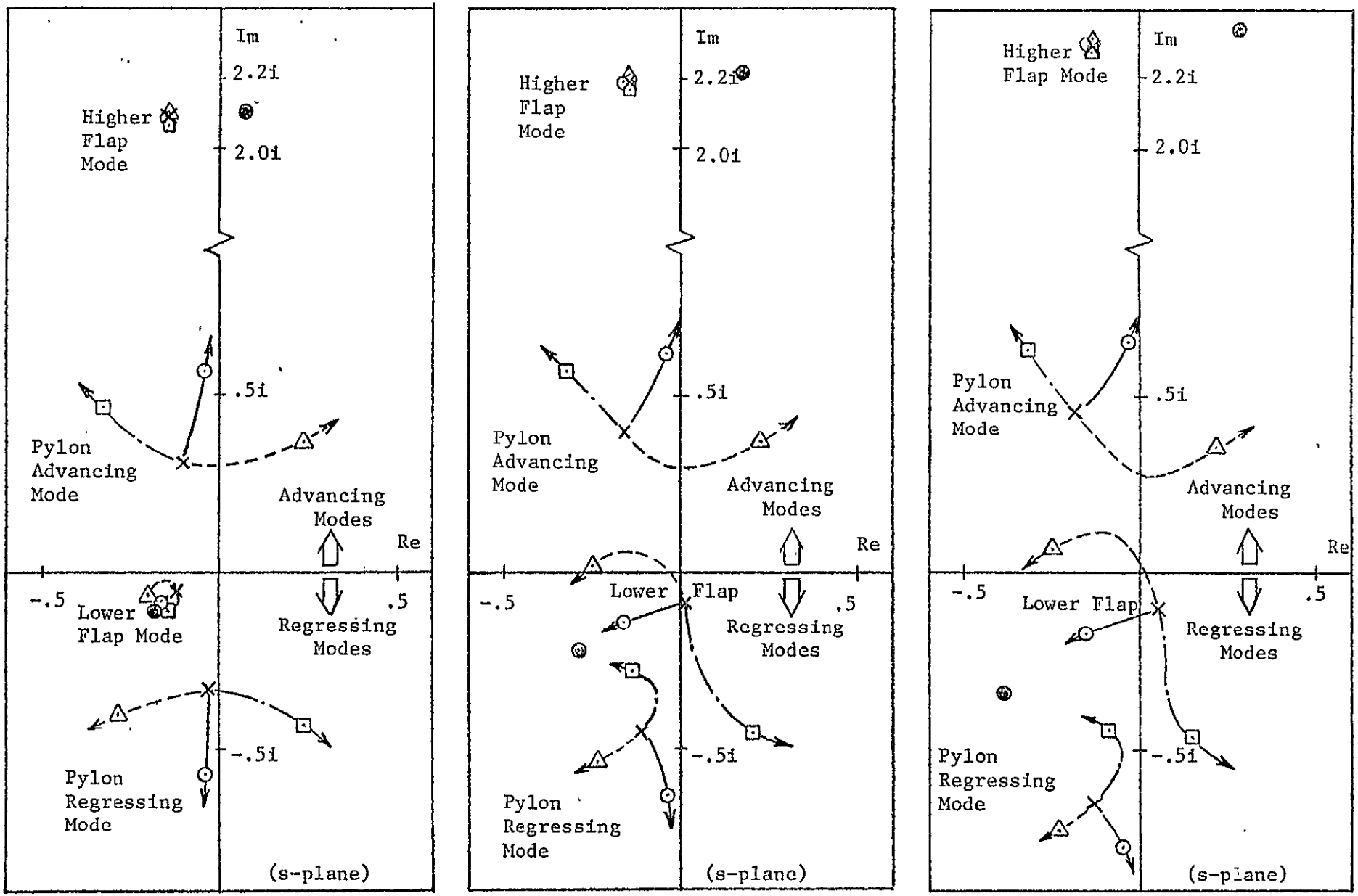

(a) $\nu_\beta = 1.1$ (b) $\nu_\beta = 1.2$ (c) $\nu_\beta = 1.3$

Figure 24. Root Locus: Influence of $\bar{\alpha} \rightarrow \bar{\theta}$ Feedback on Coupled Motion Dynamics

$V = .844$, $\gamma = 3.83$, $h = .342$,
$I^*_\beta = I^*_{\beta\alpha} = 1.0$, $I^* = 2.5$,
$\zeta_p = .02$, $\omega_p = .5$

Feedback Law: $\bar{\theta} = -\bar{K}_d \cdot \bar{\alpha}$
---: $\not\triangleleft K_d = 0°$, ——: $\not\triangleleft K_d = 90°$
—·—: $\not\triangleleft K_d = 180°$; ⊙, △, ⊡: $\bar{K}_d = 1$

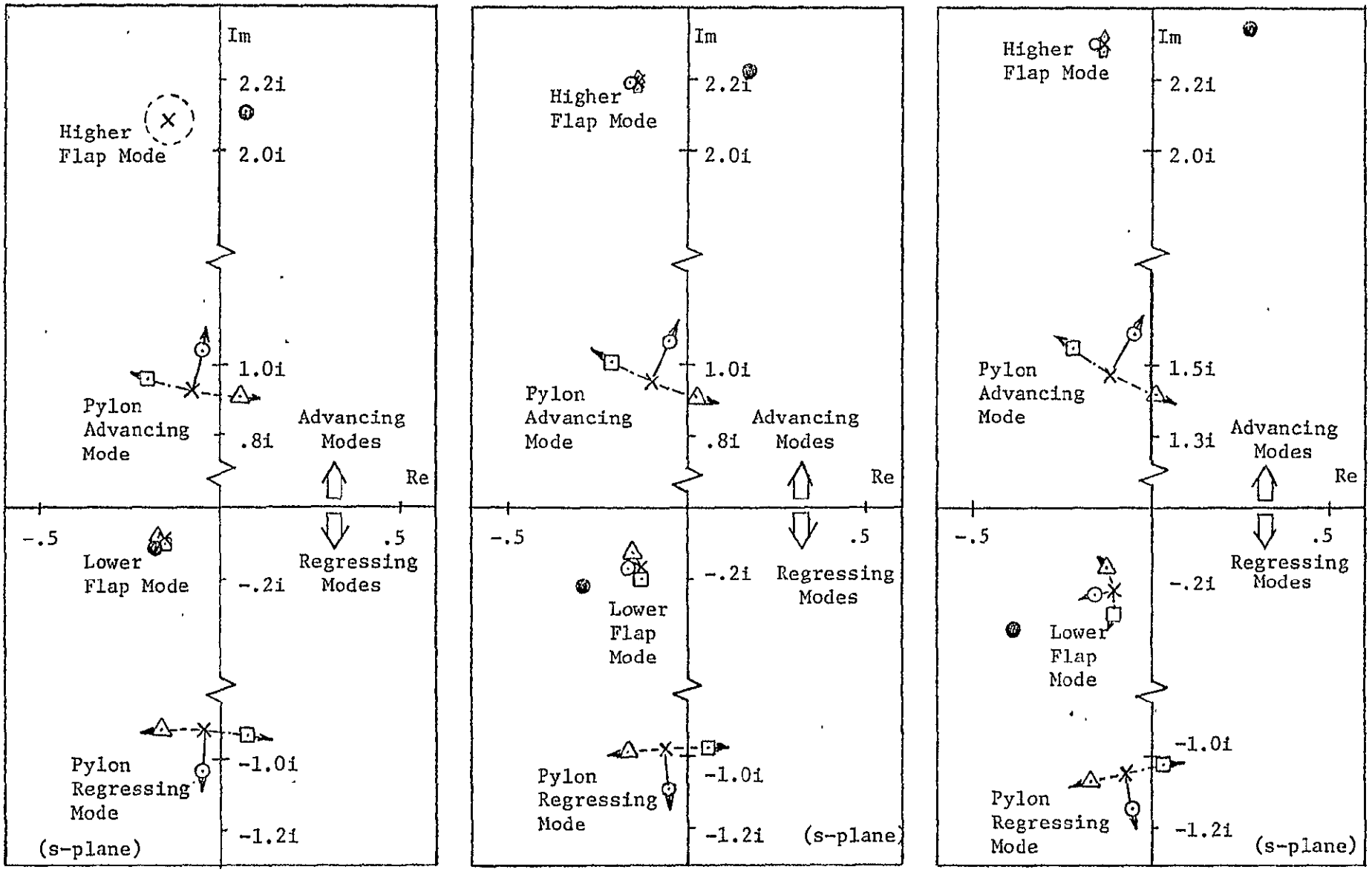

(a) $\nu_\beta = 1.1$ (b) $\nu_\beta = 1.2$ (c) $\nu_\beta = 1.3$

Figure 25. Root Locus: Influence of $\bar{\alpha} \rightarrow \bar{\theta}$ Feedback on Coupled Motion Dynamics

$\bar{V} = .844$, $\gamma = 3.83$, $h = .342$,
$I^*_\beta = I^*_{\beta\alpha} = 1.0$, $I^* = 2.5$,
$\zeta_p = .02$, $\omega_p = 1.0$

Feedback Law: $\bar{\theta} = -\bar{K}_d\bar{\alpha}$
---: $\measuredangle\bar{K}_d = 0°$, ——: $\measuredangle\bar{K}_d = 90°$,
-·-: $\measuredangle\bar{K}_d = 180°$; ⊙, △, ⊡: $|\bar{K}_d| = 1$

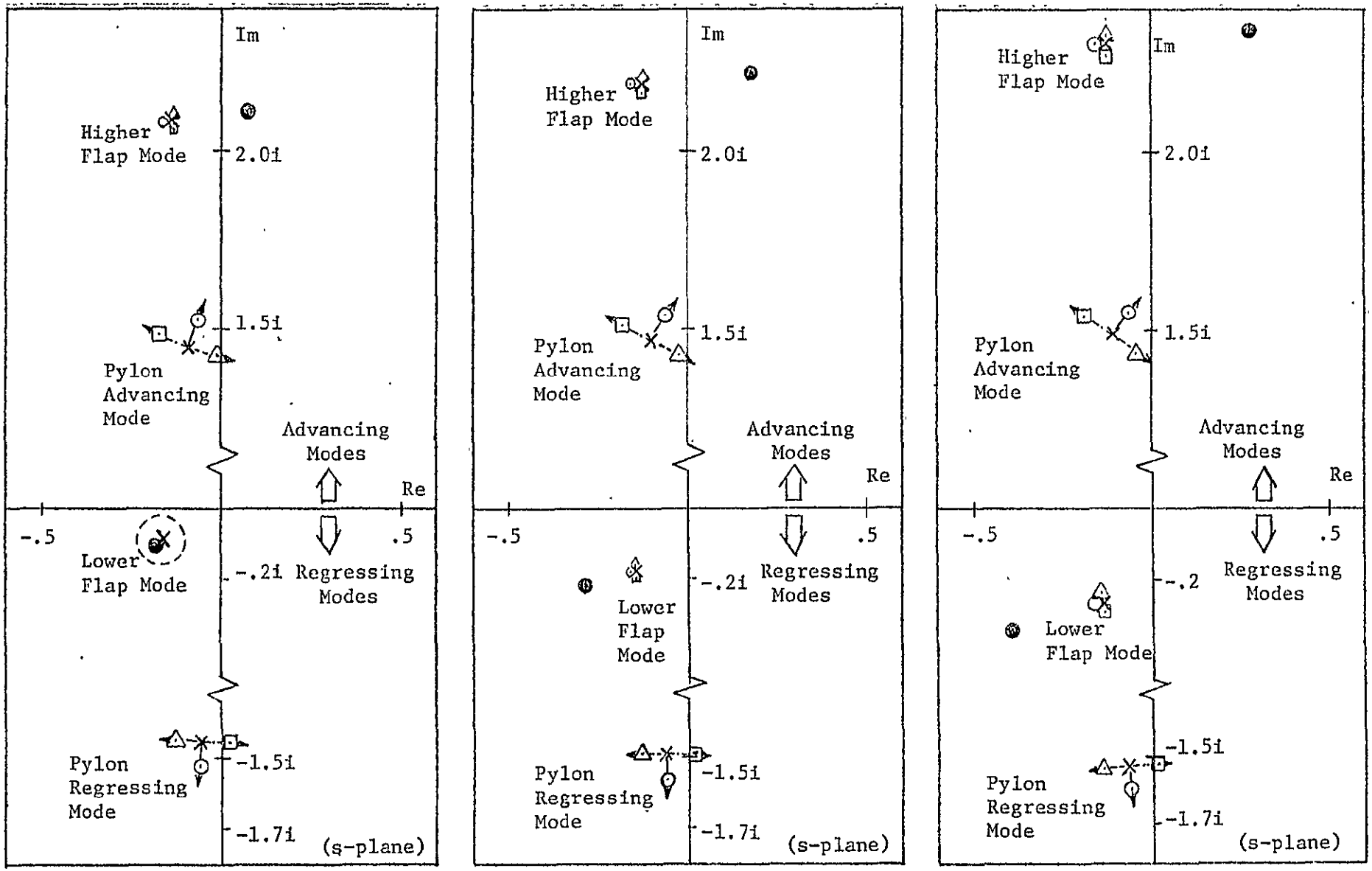

(a) $\nu_\beta = 1.1$ (b) $\nu_\beta = 1.2$ (c) $\nu_\beta = 1.3$

Figure 26. Root Locus: Influence of $\bar{\alpha} \rightarrow \bar{\theta}$ Feedback on Coupled Motion Dynamics

$V = .844$, $\gamma = 3.83$, $h = .342$,
$I^*_\beta = I^*_{\beta\alpha} = 1.0$, $I^* = 2.5$,
$\zeta_p = .02$, $\omega_p = 1.5$

Feedback Law: $\bar{\theta} = -\bar{K}_d\bar{\alpha}$
---: $\measuredangle\bar{K}_d = 0°$, ——: $\measuredangle\bar{K}_d = 90°$,
-·-: $\measuredangle\bar{K}_d = 180°$; ⊙, △, ⊡: $|\bar{K}_d| = 1$

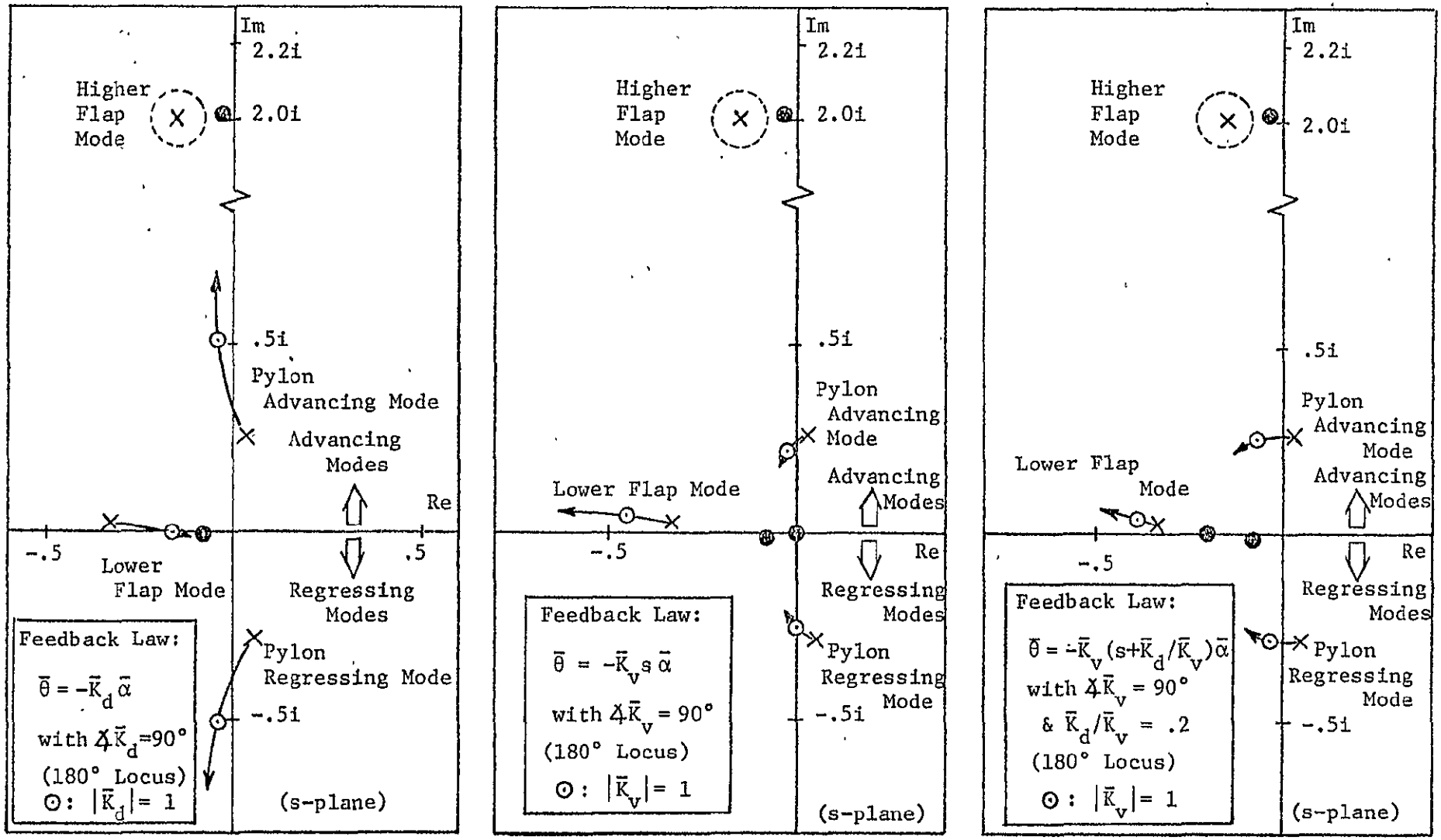

(a) Pylon Displacement Feedback (b) Pylon Rate Feedback (c) Pylon [Dis. + Rate] Feedback

Figure 27. Root Locus: Influence of $\bar{\alpha} \rightarrow \bar{\theta}$ Feedback on Coupled Motion Dynamics; Isotropic Pylon

$V = .844$, $\gamma = 3.83$, $h = .342$,
$I^*_\beta = I^*_{\beta\alpha} = 1.0$, $\nu^2_\beta = 1.0355$,
$I^* = 2.5$, $\zeta_p = .02$, $\omega_p = .5$

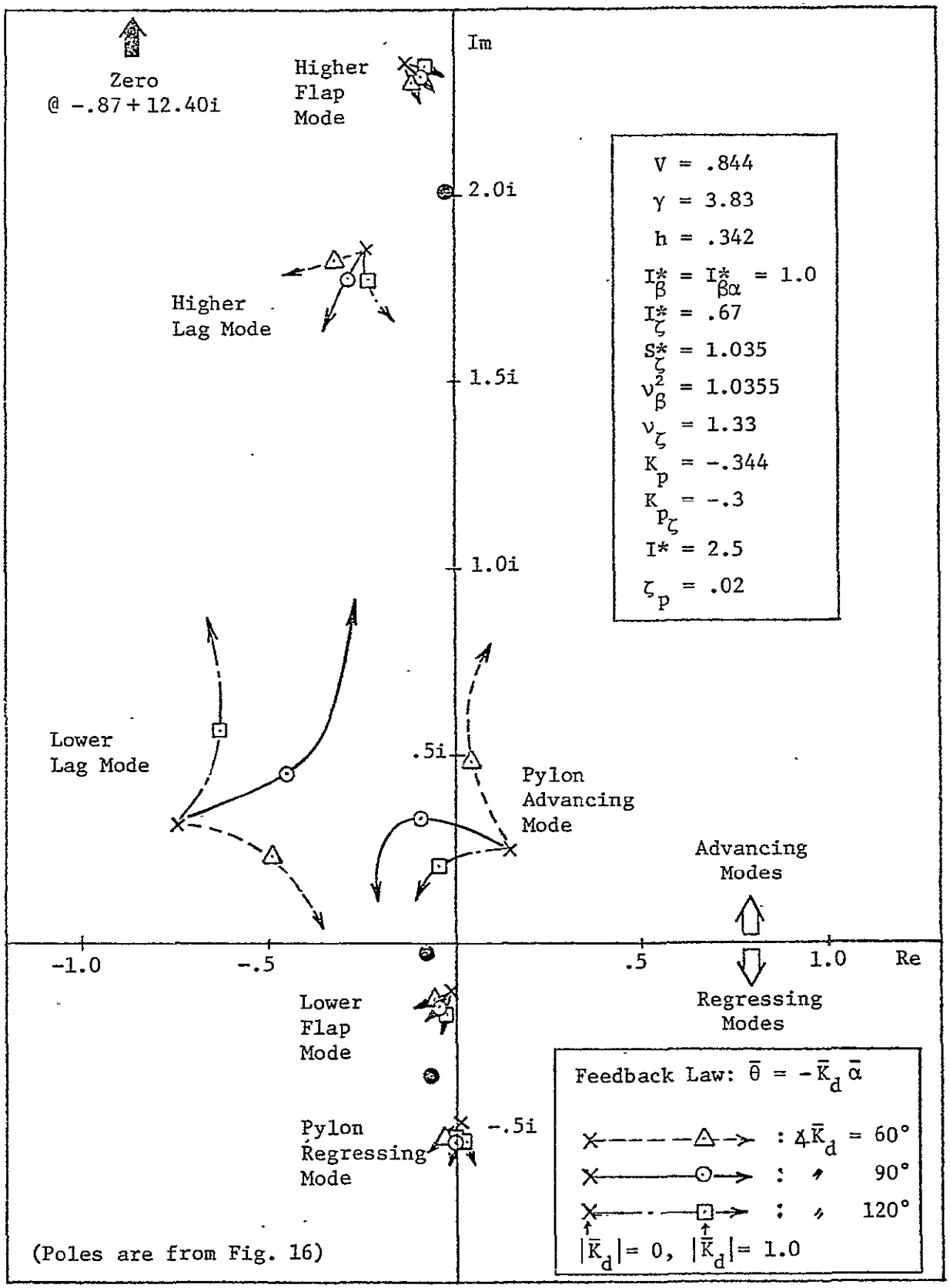

(a) $\omega_p = .5$

Figure 28. Root Locus: Influence of $\bar{\alpha} \rightarrow \bar{\theta}$ Feedback on Coupled Motion Dynamics for Isotropic Pylon; With Lag Motion Degree of Freedom and K_p & K_{p_ζ}

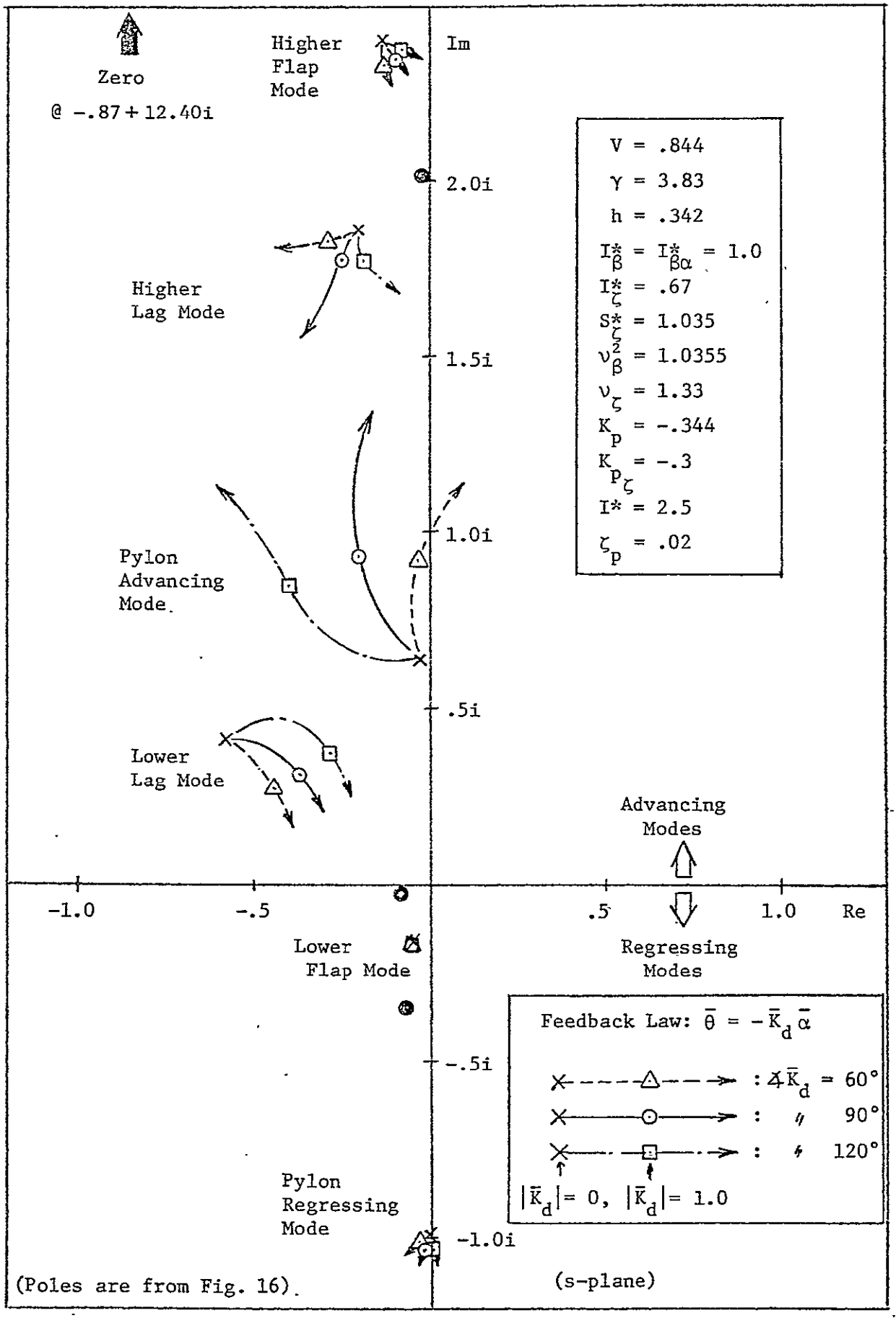

(b) $\omega_p = 1.0$

Figure 28. (continued)

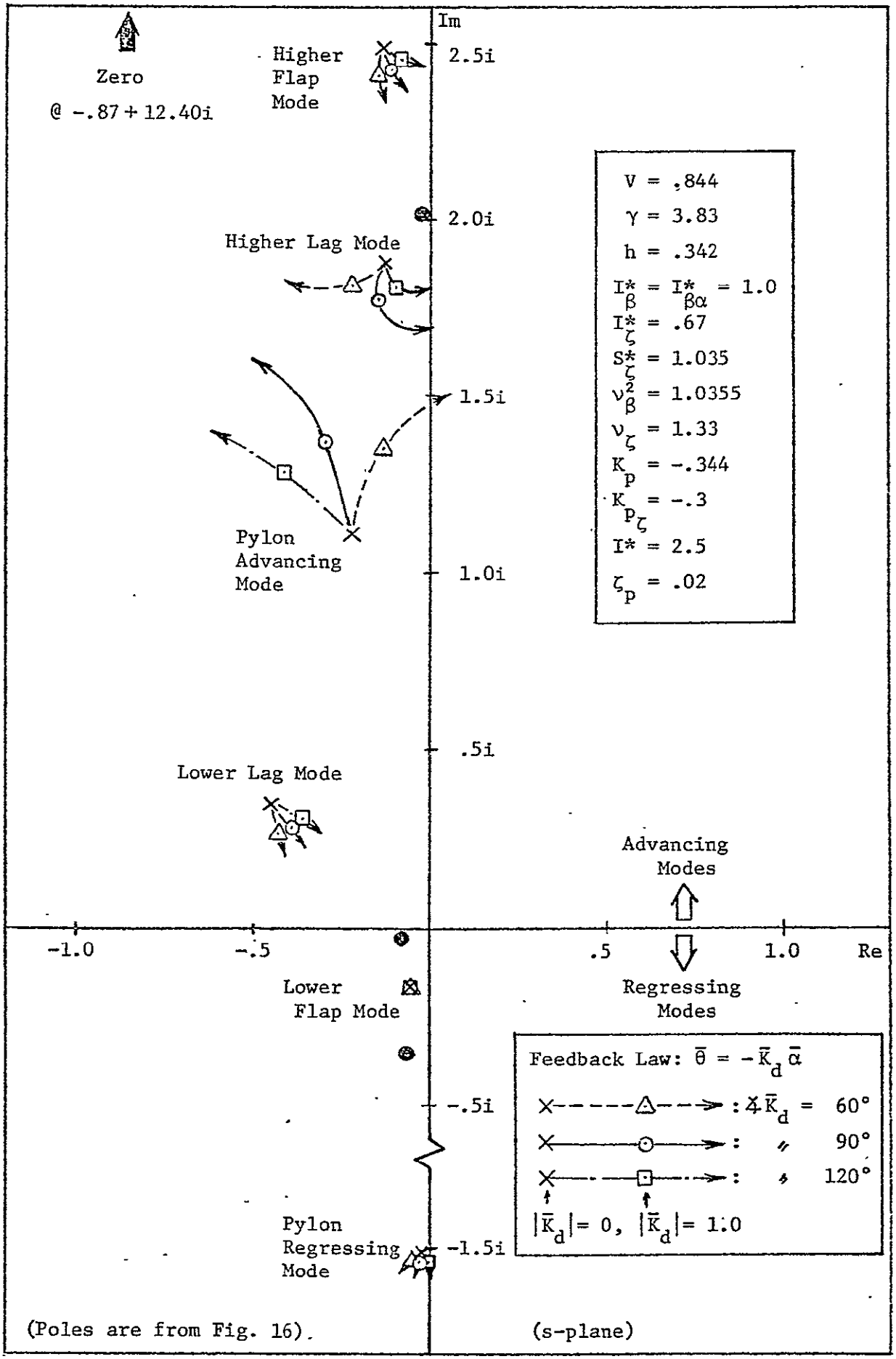

(c) $\omega_p = 1.5$

Figure 28.(concluded)

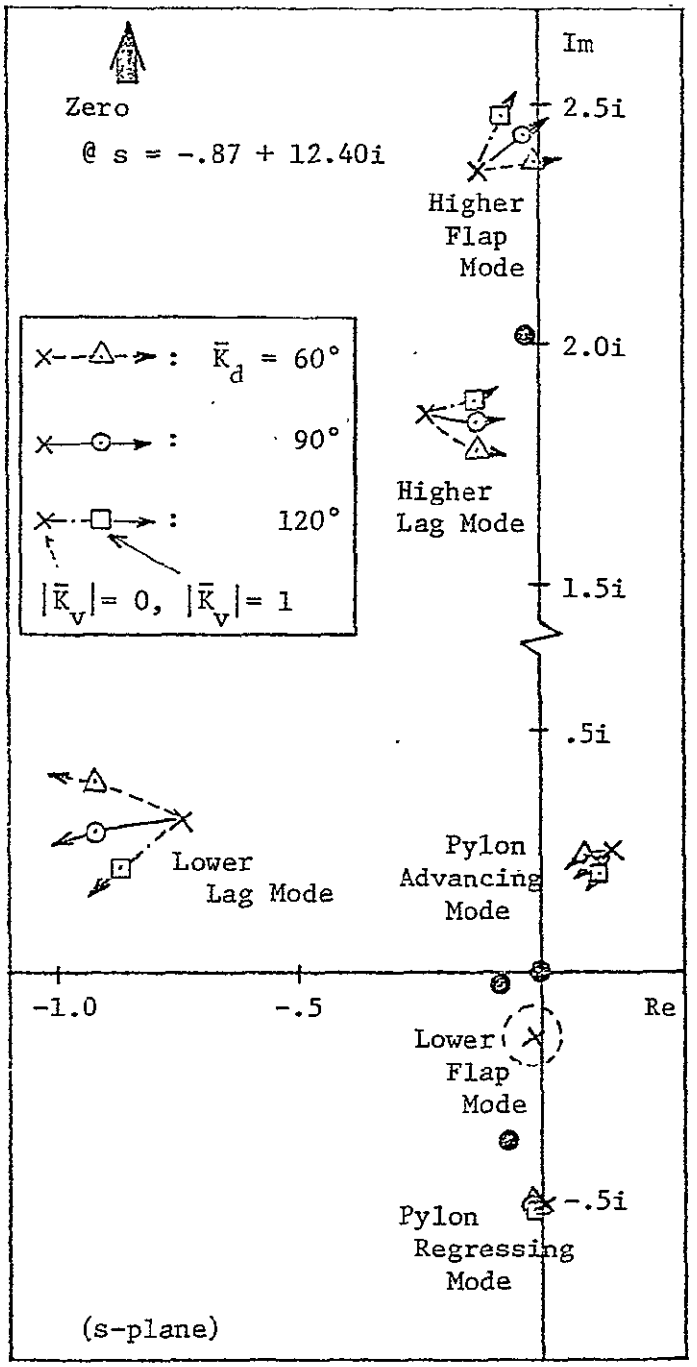

(a) Pylon Rate Feedback;

FB Law: $\bar{\theta} = -\bar{K}_v s \bar{\alpha}$

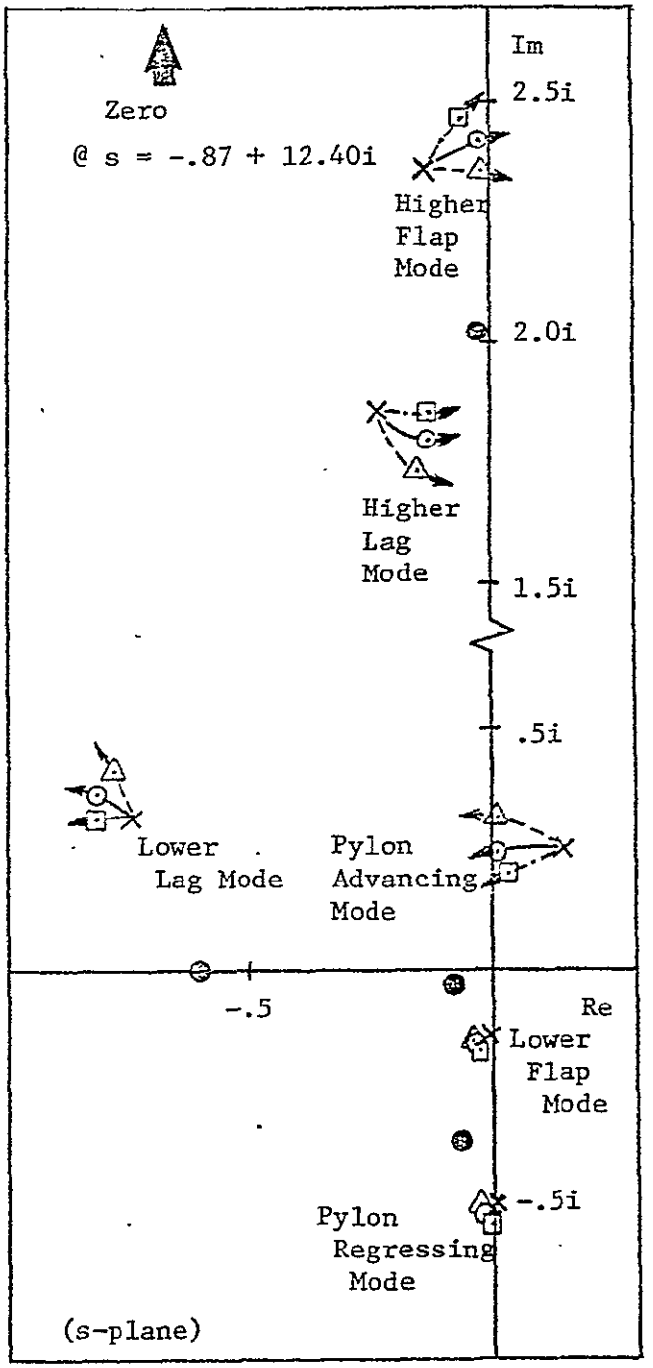

(b) Pylon (Dis. + Rate) Feedback;

FB Law: $\bar{\theta} = -\bar{K}_v(s + \bar{K}_d/\bar{K}_v)\bar{\alpha}$

with $\bar{K}_d/\bar{K}_v = .6$

Figure 29. Root Locus: Influence of $\bar{\alpha} \rightarrow \bar{\theta}$ Feedback on Coupled Motion Dynamics; Isotropic Pylon with Rotor Cyclic Lag Motion DOF and K_p & K_{p_ζ}

$V = .844$, $\gamma = 3.83$, $h = .342$,
$I^*_\beta = I^*_{\beta\alpha} = 1.0$, $I^*_\zeta = .67$,
$S^*_\zeta = 1.035$, $\nu^2_\beta = 1.0355$,
$\nu_\zeta = 1.33$, $K_p = -.344$, $K_{p_\zeta} = -.3$,
$I^* = 2.5$, $\zeta_p = .02$, $\omega_p = .5$

DYNAMICS OF PROPROTOR AND CANTILEVER WING

In this section we now examine the dynamics of the specific physical system of interest, that is, a cantilever wing and proprotor in cruise flight. The primary modification from the previous section is the support model which is a non-isotropic support, i.e, a wing with three degrees of freedom: spanwise bending; chordwise bending; and torsion. First we consider the isolated wing dynamics.

1.) Isolated Wing Dynamics

The wing is modelled using only a single mode in each degree of freedom. The modal amplitudes are denoted by q_1 for spanwise bending, q_2 for chordwise bending and p for torsion.

The torsion and spanwise bending are coupled as a result of the relative locations of the center of gravity and elastic axes. The chordwise degree of freedom is essentially uncoupled from the other two degrees of freedom. The coupled spanwise bending-torsion equations of motion are expressed as

$$\begin{bmatrix} (\Delta_{q_1})_{uc} & \Delta_{q_1 p} \\ \Delta_{p q_1} & (\Delta_p)_{uc} \end{bmatrix} \begin{Bmatrix} q_1 \\ p \end{Bmatrix} = 0 \tag{43}$$

The uncoupled characteristics are given by

$$\begin{aligned} (\Delta_p)_{uc} &= (I^*_{pw} + I^*_{py} + 2M^*_b h^2)\, s^2 + (C^*_p + h^2 \gamma H_\mu - \gamma C_{p\dot{p}})\, s + K^*_p - hV\gamma H_\mu \\ (\Delta_{q_1})_{uc} &= (I^*_{qw} + m^*_p + 2M^*_b y^2_{tw} + 2\eta'^2_{tw})\, s^2 \\ &\quad + (C^*_{q_1} + y^2_{tw}\, \gamma H_\mu - \gamma C_{q_1 \dot{q}_1} + 2\eta'^2_{tw} \gamma Q_\zeta)\, s + K^*_{q_1} \end{aligned} \tag{44}$$

and the coupling terms are,

$$\Delta_{pq_1} = (S_w^* + 2M_b^* h\bar{y}_{tw})s^2 + y_{tw} h\gamma H_\mu s$$

$$\Delta_{q_1 p} = (S_w^* + 2M_b^* h\, y_{tw})\, s^2 + (y_{tw} h\gamma H_\mu - \gamma C_{q_1\dot{p}})\, s - \dot{y}_{tw} V\gamma H_\mu - \gamma C_{q_1 p}$$

The characteristic equation for this system is given by

$$\Delta_{q_1 + p} = (\Delta_{q_1})_{uc} (\Delta_p)_{uc} - \Delta_{pq_1} \Delta_{q_1 p} = 0 \qquad (49)$$

For the physical system under consideration the uncoupled quadratic factors have the following characteristics (at V = 0.844)

$$(\Delta_{q_1})_{uc} = 109\ (s + 0.035 + 0.413i)(s + 0.035 - 0.413i)$$

$$(\Delta_p)_{uc} = 2.66\ (s + 0.055 + 1.10i)(s + 0.055 - 1.10i)$$

It may be noted that the damping of these modes, which arises from aerodynamics is very small.

The coupling terms are

$$\Delta_{pq_1} = 8.50\ s\ (s + 0.074)$$

$$\Delta_{q_1 p} = 8.50\ s\ (s + 0.599)(s - 0.599)$$

The characteristic equation may be written in root locus form to examine the influence of coupling,

$$1 - 0.249 \frac{(s)(s + 0.074)(s + 0.599)(s - 0.587)}{(s^2 + .070s + 0.172)(s^2 + .109s + 1.20)} = 0$$

The root loci shown in Figure 30 illustrate the influence of coupling between the modes. Figure 30(a) shows the dynamics with all of the terms included

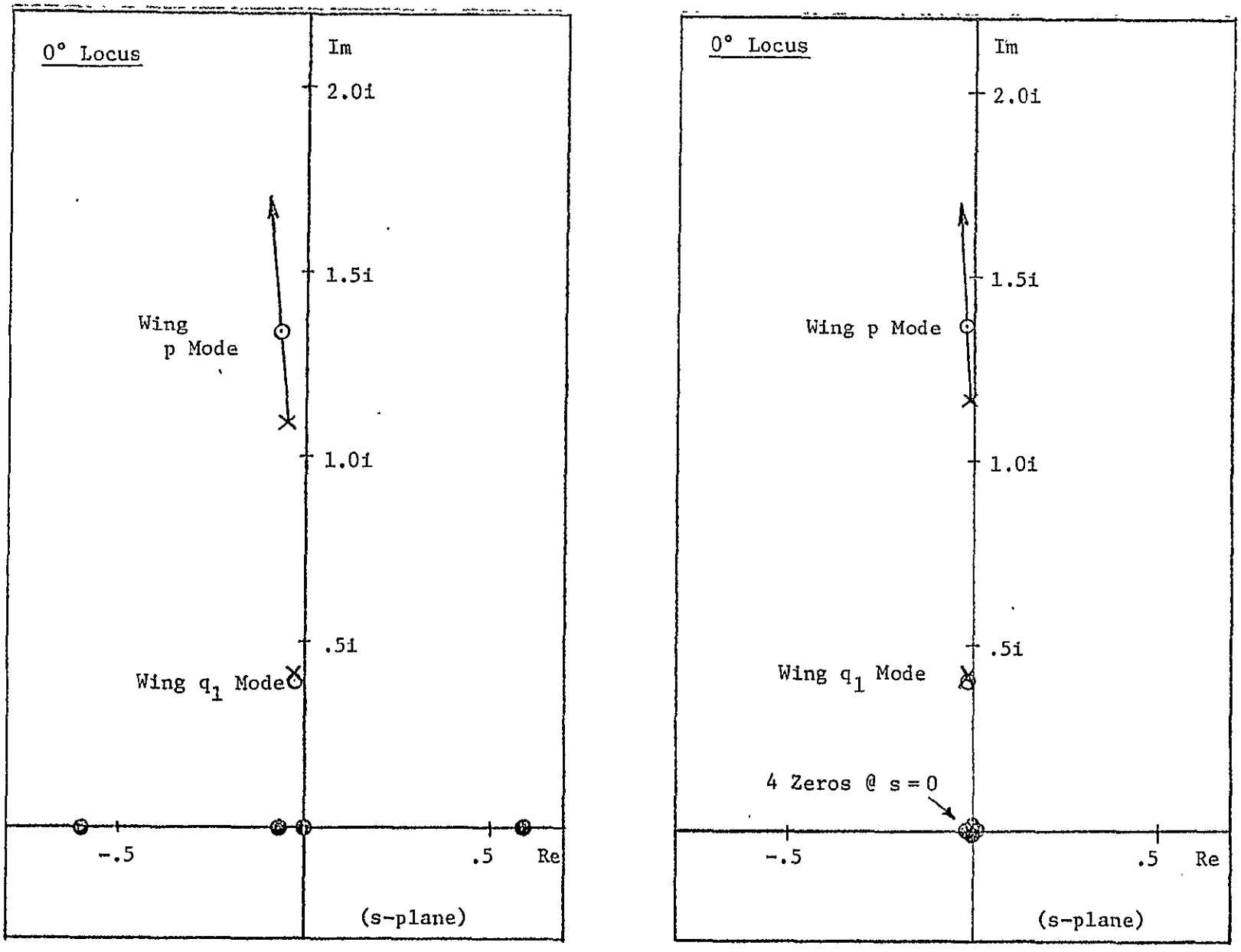

(a) With Aerodynamic Influence (@ V = .844)

(b) Without Aerodynamic Influence

Figure 30. Root Locus: Influence of q_1 ~ p Motion Coupling on Coupled Dynamics

and 30(b) shows the dynamics with the aerodynamic terms neglected, indicating that the coupling is produced by inertial effects arising from the center of gravity displacement from the elastic axis of the wing. The effect of coupling is to raise the p or torsion mode frequency and to produce only a small change in the spanwise or q_1 mode from its uncoupled value. Examining the eigenvectors for these modes is also useful with respect to interpreting some of the results of the feedback analysis which follows.

For the q_1 mode,

$$\frac{p}{q_1} = 1.26\ e^{-5.9^{o}i}$$

and for the p mode

$$\frac{q_1}{p} = 0.09\ e^{-178^{o}i}$$

Thus in the q_1 mode, p and q_1 act almost in phase while for the p mode, q_1 and p are very close to 180^{o} out of phase.

The chordwise mode is essentially uncoupled from the torsion, spanwise motion and the effect of aerodynamic terms is very small so that the chordwise motion degree of freedom motion is described by

$$(\Delta_{q_2})_{uc} \cong [I^*_{qw} + M^*_p + I^*_{px}\,\eta'^{2}_{tw} + 2M^*_b\,(y^2_{tw} + h^2\,\eta'^{2}_{tw})]\ s^2 + C^*_{q_2}\ s + K^*_{q_2} \cong 0 \tag{46}$$

Numerically

$$(\Delta_{q_2})_{uc} = 110\ (s + 0.012 + 0.677i)\ (s + 0.012 - 0.677i)$$

Thus there are three frequencies associated with the wing motion, two associated with spanwise bending and torsion

$$\omega_p = 1.10\ , \quad \omega_{q_1} = 0.413 \quad \text{(uncoupled)}$$

and one associated with chordwise bending

$$\omega_{q_2} = 0.677$$

The support system is, of course, no longer isotropic, however certain similarities can be noted with the isotropic support treated in the previous section as will be noted below.

2.) Wing Proprotor Dynamics

First we examine the influence of adding the wing degrees of freedom to the rotor cyclic motion degrees of freedom. Figure 31 shows the eigenvalues calculated for various degrees of freedom as follows:

4dof: This model includes only the rotor cyclic degrees of freedom (β_{1c}, β_{1s}, ζ_{1c} and ζ_{1s}). The eigenvalues are those discussed previously.

5dof: The wing torsion motion (p) is added to the rotor cyclic dof.

6dof: The wing chordwise bending dof (q_2) is added to the 5dof model.

7dof: The wing spanwise bending dof (q_1) is added to the 6dof model.

Figure 31 indicates that when the torsion degree of freedom is added the higher flap and lag modes are altered and there is little influence on the lower flap and lag modes. Moving to the 6dof case, i.e., adding the chordwise dof has essentially no effect on any of the 5dof eigenvalues. Similarly, for the 7dof case the primary influence on the 6dof eigenvalues is to raise the frequency of the p mode. This is of course, just the trend discussed in the case of the isolated wing.

The complete system also involves the collective dynamics of the rotor and the rotor RPM as degrees of freedom. Figure 32 shows

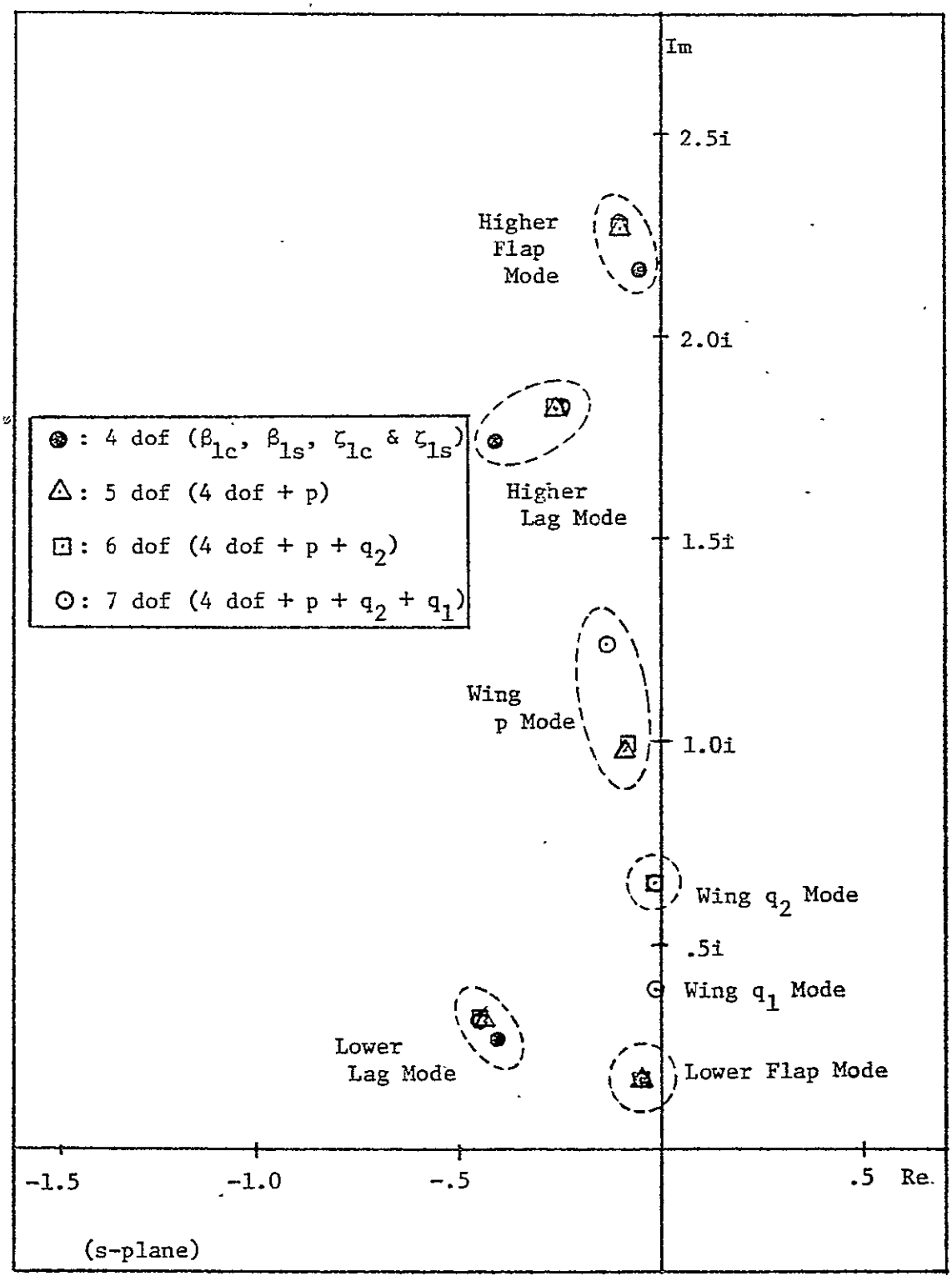

(a) 4, 5, 6 & 7 DOF Models

Figure 31. Comparison of System Eigenvalues for Several Rotor Support Models (@ V = .844)

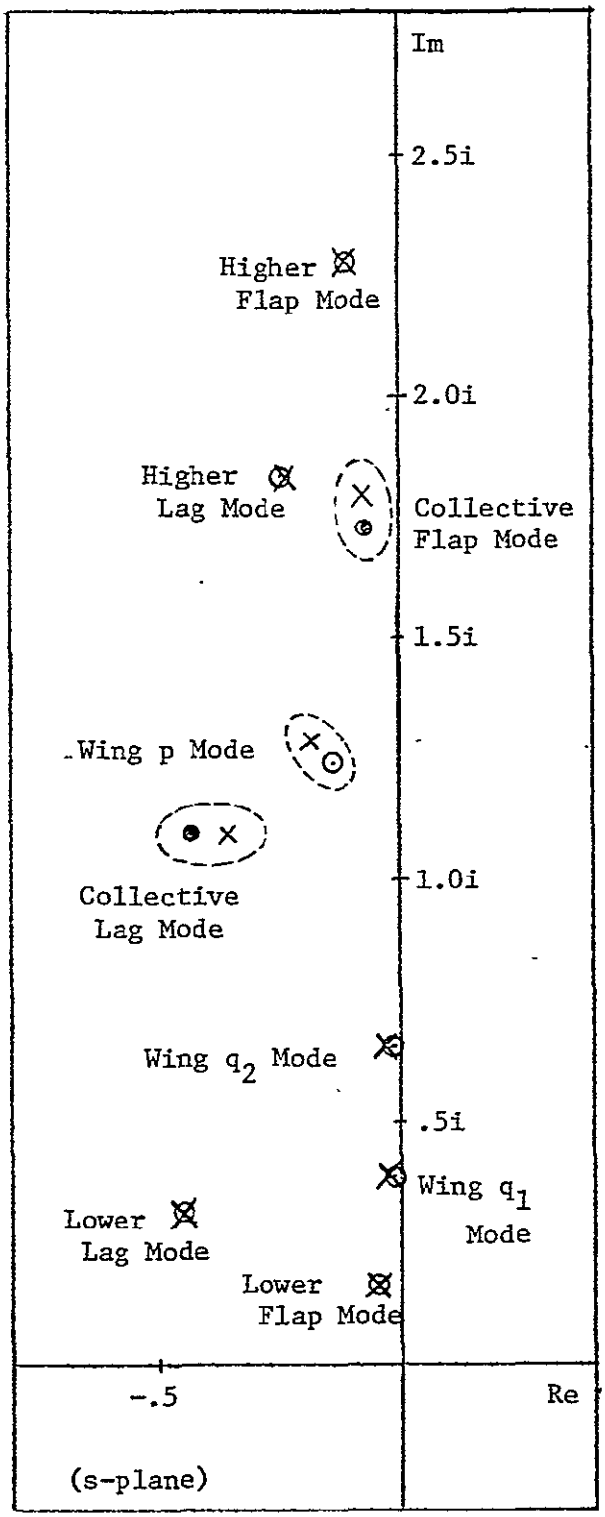

(b) 2, 7 & 9 DOF Models in Constant Rotor RPM Case

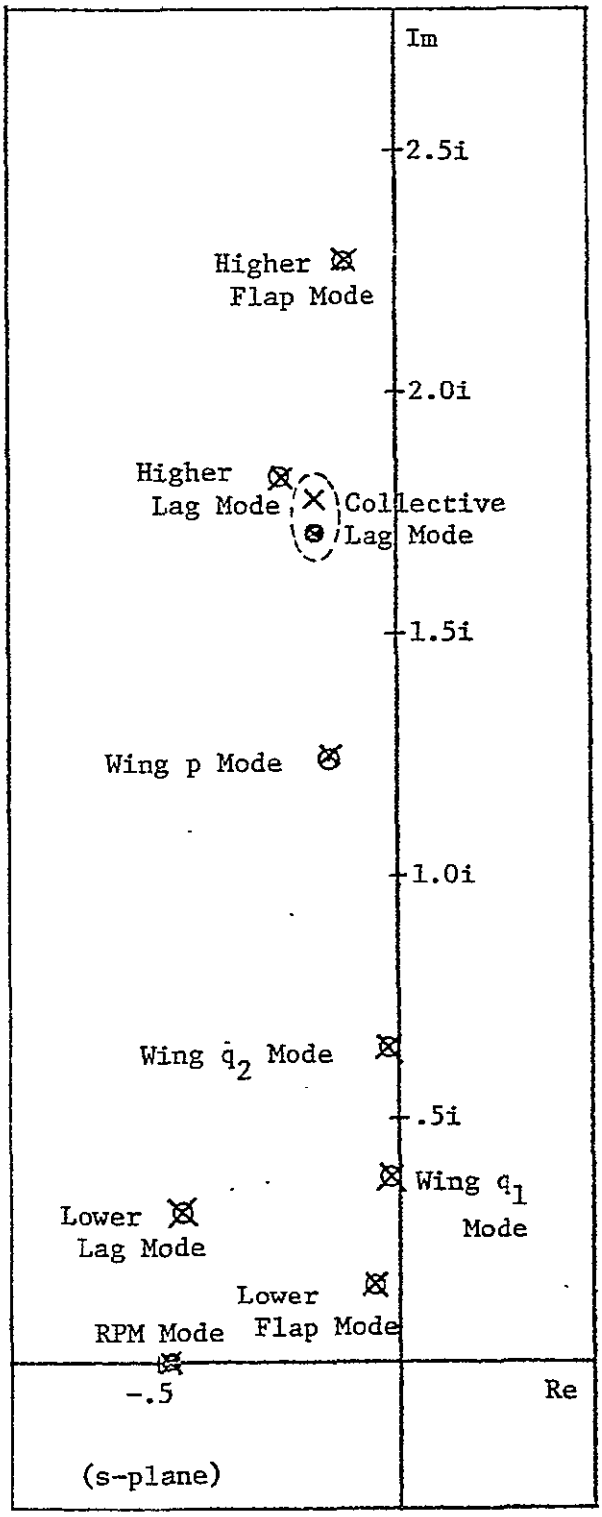

(c) 2, 7 & 9 DOF Models in Free Rotor RPM Case

Figure 32.

● : 2 dof (β_o & ζ_o or Ω_s)

⊙ : 7 dof (same as in Fig. (a))

✕ : 9 dof (7 dof + β_o + ζ_o (or Ω_s))

the two degree of freedom dynamics associated with these additional degrees of freedom for two cases: constant RPM including the collective flap and collective lag modes, and the collective flap plus rotor RPM degrees of freedom. As noted previously, with the rotor RPM degree of freedom, the collective lag mode is essentially not excited and therefore not included when RPM is included as a degree of freedom.

Also shown in Figure 32 are the seven degree of freedom eigenvalues from Figure 31. The dynamics of the complete nine degree of freedom system, i.e., including the coupling between the two collective rotor degrees of freedom and the cyclic-wing motion system are also shown. It can be seen from this figure that there is only weak coupling between these collective dynamics and the 7dof. The eigenvalues of the seven degree of freedom system correspond closely to the same modes in the nine degree of freedom case.

Now we consider in more detail the influence of the support or wing degrees of freedom on the modes of motion and in particular the influence of anisotropy of the support as well as the nature of the coupling. First consider the effect of the addition of the torsion degree of freedom on the blade motion. The problem will be formulated as in the previous section such that the influence of varying the torsional inertia of the wing is employed to evaluate the nature of this coupling. The equations of motion for this system can be written as,

$$\begin{bmatrix} A_{11} & C_{rp} \\ C_{pr} & (\Delta_p)_{uc} \end{bmatrix} \begin{Bmatrix} \beta_{1c} \\ \beta_{1s} \\ \zeta_{1c} \\ \zeta_{1s} \\ \hline p \end{Bmatrix} = 0 \qquad (47)$$

Where A_{11} is the characteristic equation for the flap/lag motion, $(\Delta_p)_{uc}$ is the uncoupled torsion motion. The coupling terms are given in Appendix I.

This various terms are given as

$$C_{pr} = \begin{bmatrix} I^*_{\beta}\,(V^2_{\beta} - 1) + h\gamma H_{\dot{\beta}} \\ -h\gamma\, H_{\dot{\beta}}\, s \\ -h\gamma\, H_{\dot{\zeta}}\, s \\ S^*_{\zeta}\, h\, s^2 + h\gamma H_{\dot{\zeta}} s \end{bmatrix}^T \qquad C_{rp} = \begin{bmatrix} -I^*_{\beta\alpha}\, s^2 + \gamma M_{\dot{\beta}}\, s \\ (2\, I^*_{\beta\alpha} + h\gamma M_{\mu})\, s - \gamma V M_{\mu} \\ \gamma Q_{\dot{\beta}}\, s \\ S^*_{\zeta}\, h\, s^2 + h\gamma Q_{\mu} s - \gamma V Q_{\mu} \end{bmatrix} \tag{48}$$

and

$$(\Delta_p)_{uc} = (I^*_{pw} + I^*_{py} + 2M^*_b\, h^2)\, s^2 + (C^*_p + h^2\, \gamma H_{\mu} - C_{p\dot{p}})\, s + K^*_p - hV\gamma H_{\mu} \tag{49}$$

Pitch-flap and pitch-lag coupling are not included in the above matrices. They can be readily included by modifications to the matrices A_{11} and C_{pr}.

In order to evaluate the influence of the rotor support system dynamics, given by $(\Delta_p)_{uc}$ with the aerodynamic terms omitted (denoted by $(\Delta_p)_o$), the coupled characteristic equation given by equations (47) can be expressed

$$\Delta_{\beta+\zeta+p} = |A_{11}|\,(\Delta_p)_o + \begin{vmatrix} A_{11} & C_{rp} \\ C_{pr} & (h^2\,\gamma H_{\mu} - \gamma C_{p\dot{p}})\, s - h\gamma V H_{\mu} \end{vmatrix} \tag{50}$$

The first term in equation (50) represents the dynamics of the system when the support has infinitely large inertia associated with the torsion degree of freedom of the wing. In this case, the system dynamics are those of the isolated proprotor cyclic modes and the torsion of the wing without aerodynamics. We now examine the influence of the torsion inertia I^*_{po} on the dynamics, maintaining the natural frequency ω_{po} and the damping ratio ζ_{po} constant, following a similar approach to that used for the discussion of the isotropic support.

The root locus varying I^*_{po} is shown in Figure 33. It can be seen that the influence of the torsional motion is primarily in the higher flap and lag modes along with the wing torsion mode. This locus then represents the effect of coupling, in the case where the support has one degree of freedom.

We now examine the effect of additional wing flexibility arising from chordwise or q_2 motion. It is interesting to examine this case as a departure from the isotropic case by formulating the equations in the following way. Let

$$q_2' = - \eta'_{tw} \; q_2$$

The equations of motion can be written as

$$\begin{bmatrix} A_{11} & C_{r q_2'} & C_{rp} \\ C_{q_2' r} & (\Delta_{q_2'})_{uc} & h\gamma H_{\dot{\beta}} \, s \\ C_{pr} & - h\gamma H_{\dot{\beta}} \, s & (\Delta_p)_{uc} \end{bmatrix} \begin{Bmatrix} \beta_{1c} \\ \beta_{1s} \\ \zeta_{1c} \\ \zeta_{1s} \\ \hline q_2' \\ \hline p \end{Bmatrix} = 0 \qquad (51)$$

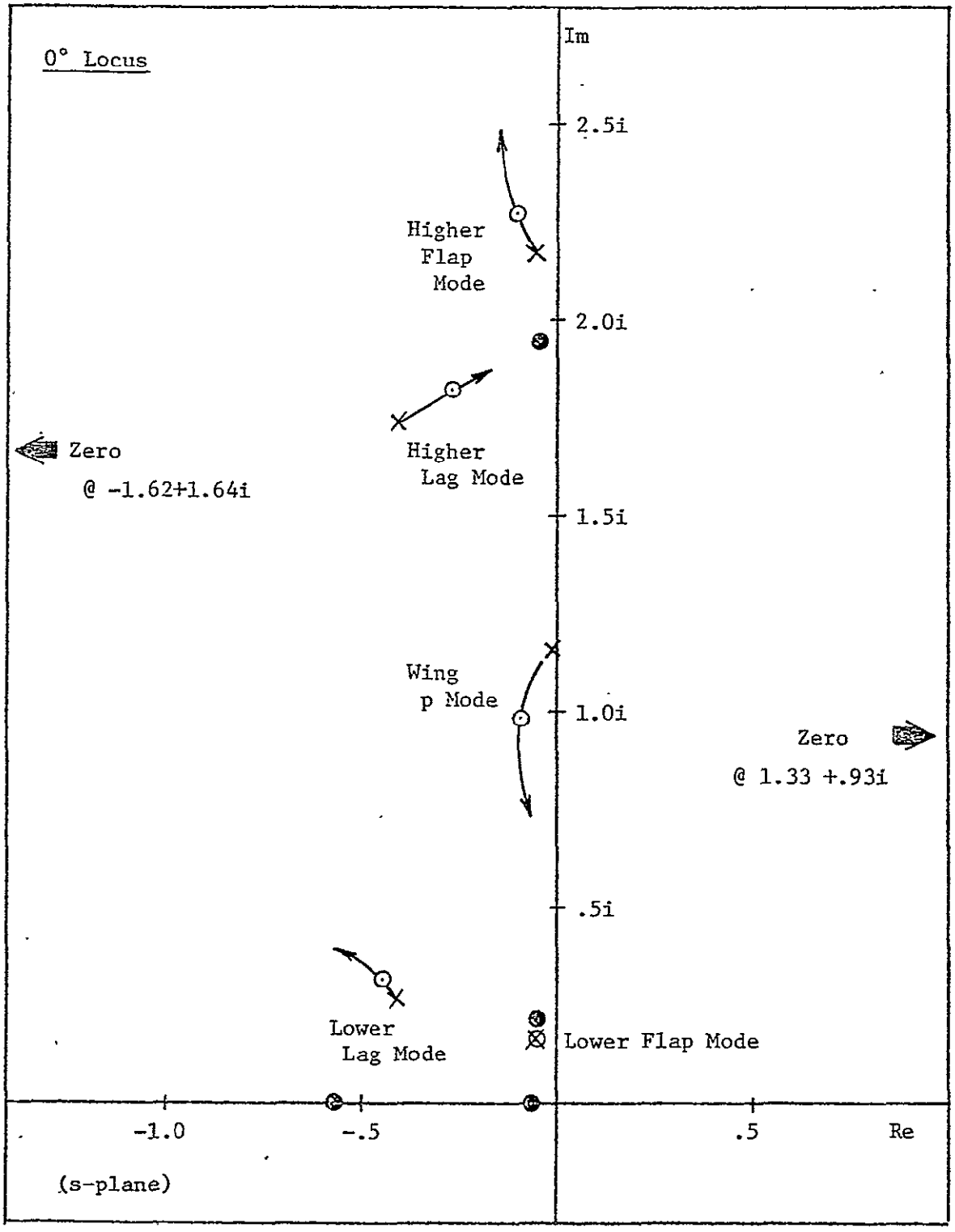

× : $I^*_{p_o}$ = ∞ (corresponding root locus gain is 0)

⊙ : " = 2.66 (" -.0703)

Figure 33. Root Locus: Influence of $I^*_{p_o}$ Change on Coupled Motion Dynamics for 5 DOF Model (@ V = .844; ζ_{p_o} = .015 & ω_{p_o} = 1.16)

It may be noted that if $(\Delta q_2')_{uc} = (\Delta p)_{uc}$, that is, if the support is isotropic, then the method of complex coordinates employed in the previous section could be applied. So it is convenient to examine the real or anisotropic case by splitting $(\Delta q_2')_{uc}$ into two parts, that is,

$$(\Delta_{q_2'})_{uc} = (\Delta_p)_{uc} + (\Delta I^* s^2 + \Delta C^* s + \Delta K^*) \tag{52}$$

where the quadratic factor in parentheses accounts for the anisotropy of the support. Thus the characteristic polynomial for the system, given by equation (51) can be expressed as

$$\Delta_{\beta+\zeta+q_2'+p} = \begin{vmatrix} A_{11} & C_{rq_2'} & C_{rp} \\ C_{q_2'r} & (\Delta_p)_{uc} & h\gamma H_{\dot{\beta}} s \\ C_{pr} & -h\gamma H_{\dot{\beta}} s & (\Delta_p)_{uc} \end{vmatrix} + (\Delta I^* s^2 + \Delta C^* s + \Delta K^*)(\Delta_{\beta+\zeta+p}) \tag{53}$$

where $\Delta_{\beta+\zeta+p}$ is the characteristic polynomial for the five degree of freedom case previously discussed (equation (47)). The first term in equation (53) is the characteristic equation for the case of isotropic supports. Once the eigenvalues are found for this system, then root locus techniques can be employed to examine the influence of the relevant inertia on the isotropic case and then the effect of anisotropy is introduced.

The isotropic case is studied by introducing the complex coordinates as before with the addition of

$$\bar{\alpha}' = p - i\, q_2'$$

The characteristic equation obtained from the first term in equation (53) takes the form of the previous section in the isotropic case,

$$\Delta_{\beta + \zeta + \alpha'} = I^*_\beta I^*_\zeta \Delta_{\beta + \zeta} [\Delta_p]_o - I^*_\beta (S^*_\zeta h)^2 [s^6 + \ldots] \qquad (55)$$

where $\Delta_{\beta + \zeta}$ is the isolated rotor cyclic flap-lag characteristic equation (12), and $(\Delta_p)_o$ is the isotropic support characteristic without aerodynamics with the chordwise stiffness and inertial characteristic (q'_2) the same as p. Figure 34 shows how the system dynamics vary with the support inertia I^*_{po} again maintaining the natural frequency and damping ratio at their proper values. The inflow ratio V = 0.844 and the pitch-flap and pitch-lag coupling are included (K_p = - 0.344 and K_p = - 0.3). For the proper value of the inertia constant (I^*_{po} = 2.66) the eigenvalues are shown. Note that since complex coordinates are employed here, the pole-zero configuration is not symmetric about the real axis. The trends shown are very similar to the isotropic results of the previous section as would be expected. Primarily, the advancing modes are influenced by the coupling and there is little influence on the regressing modes. The trend with inertia in the isotropic case is also very similar to the case with infinite stiffness in one direction as may be seen by comparison with Figure 33, since the rotor support regressing mode is hardly influenced by the coupling.

Now the influence of the anisotropy is examined using the root locus approach described above. The factor under consideration related to the anisotropy is

$$\Delta I^* s^2 + \Delta C^* s + \Delta K^* = 33.8 (s + 0.021 + 0.634i)(s + 0.021 - 0.623i)$$

In the root locus shown in Figure 35, ΔI^* is considered as the gain and $\frac{\Delta C^*}{\Delta I^*}$ and $\frac{\Delta K^*}{\Delta I^*}$ are maintained constant. The root locus is based on equation (53) The root locus gain is given as $\Delta I^* I^*_\zeta / (I^*_\zeta I^*_{po} - S^*_\zeta h)$. Figure 35 then

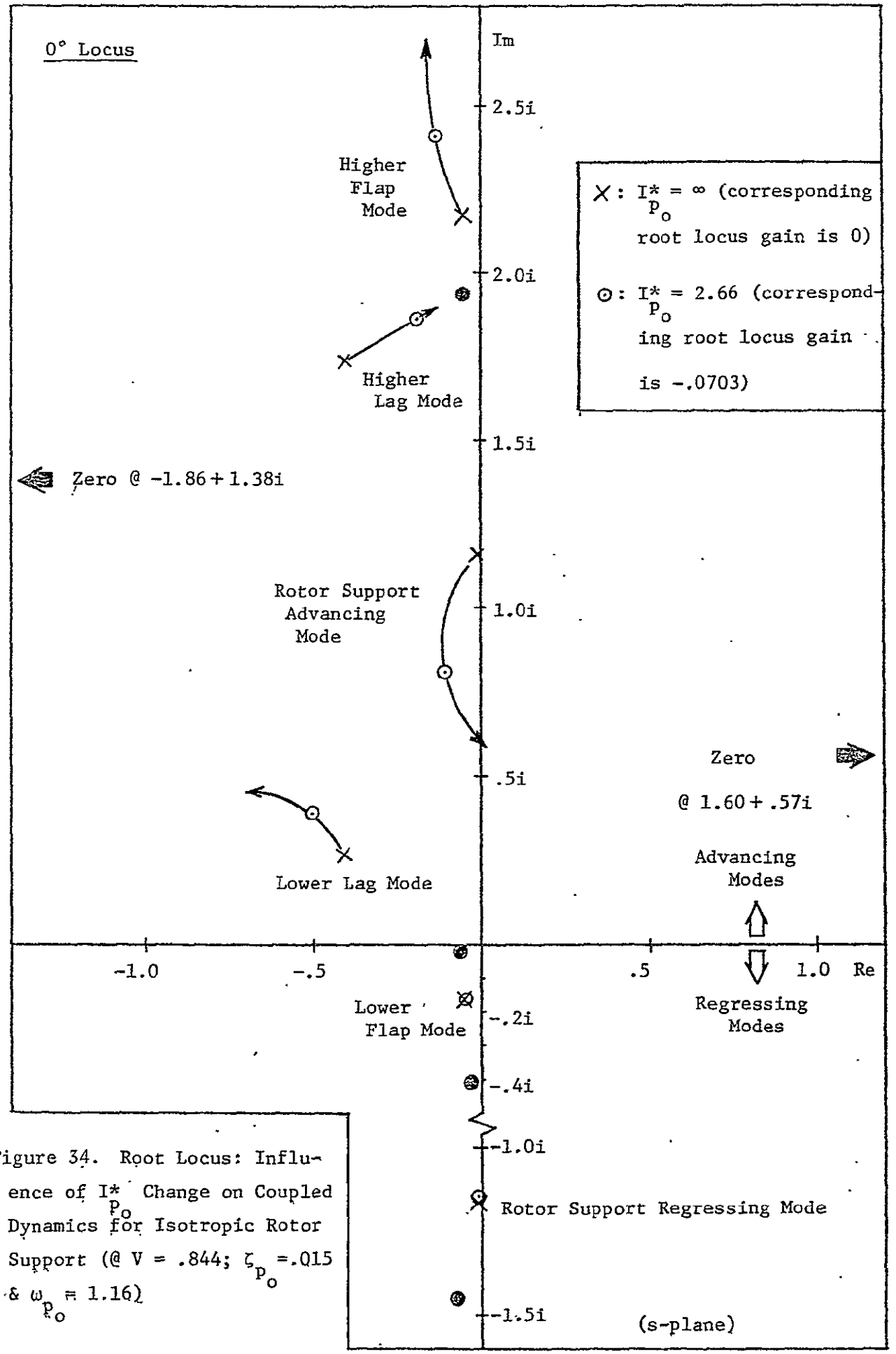

Figure 34. Root Locus: Influence of $I^*_{p_o}$ Change on Coupled Dynamics for Isotropic Rotor Support (@ V = .844; ζ_{p_o} =.015 & ω_{p_o} = 1.16)

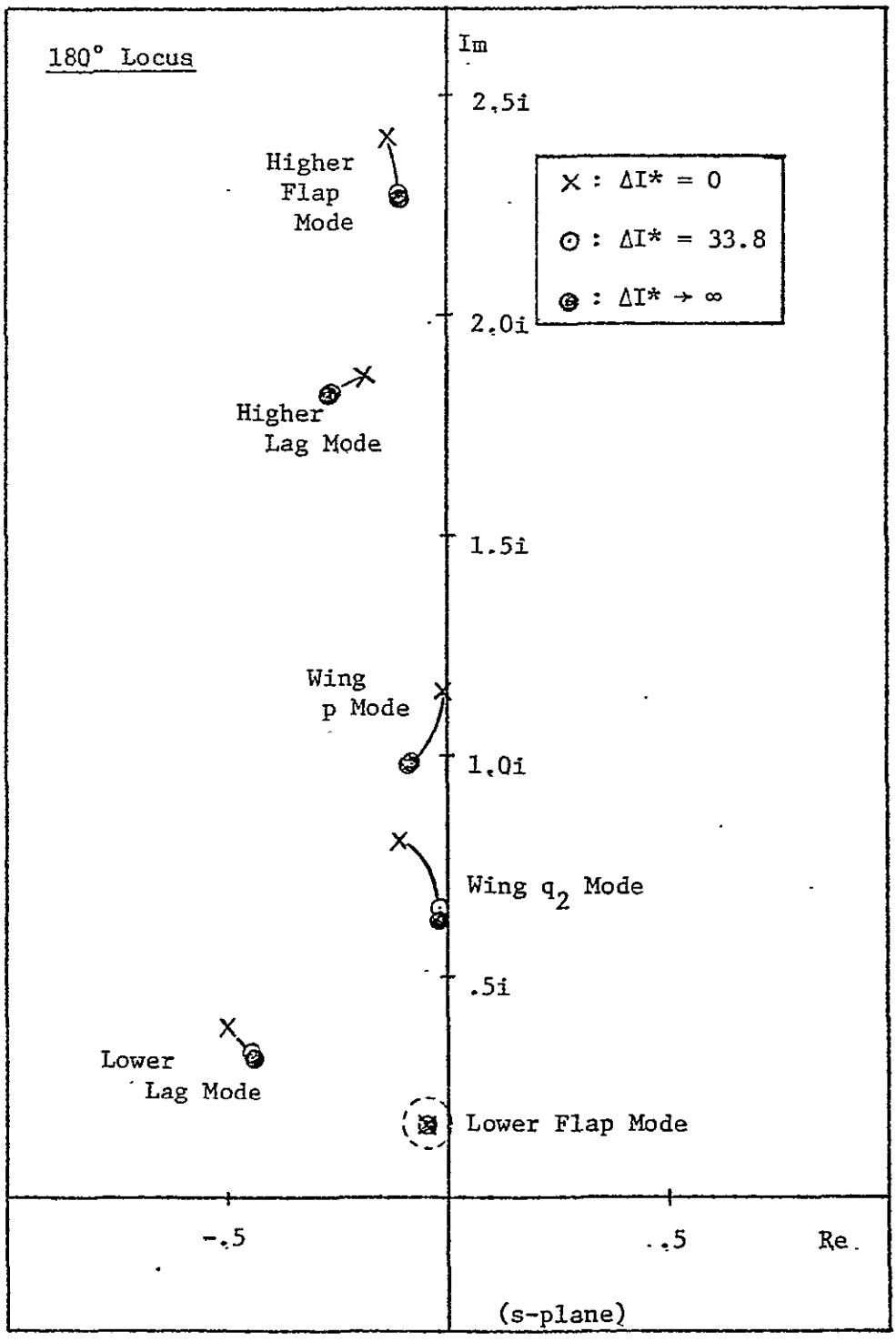

Figure 35. Root Locus: Influence of ΔI* Change on Coupled Motion Dynamics for 6 DOF Model (@ V = .844; $\Delta K^* / \Delta I^* = (.623)^2$ & $\Delta C^* / \Delta I^* = 2(.034)(.623)$)

shows the variation of the eigenvalues as a function of ΔI^*. The isotropic case is represented of course by $\Delta I^* = 0$. The actual difference in support characteristics in the two directions is such that in fact the physical value of the inertia ($\Delta I^* = 33.8$) corresponds very closely to the limiting value of $\Delta I^* = \infty$. This case is the 5dof model and the chordwise parameters of the wing are such that the eigenvalues are close to this limit.

The formulation presented is in general useful in studying the effects of support characteristics.

This investigation appears to indicate the the wing chordwise degree of freedom for the parameters of the physical system of interest is not particularly influential. The chordwise mode does play a role however when the collective modes are examined as will be seen later in this section.

3.) Wing Motion·Cyclic Pitch Feedback

We now turn to the examination of the influence of various single loop feedbacks on the dynamics of the wing proprotor system (nine degrees of freedom). An optimal control theory approach to this problem is presented in Reference 18.

First consider the influence of $q_1 \rightarrow \theta_{1c}$ feedback at the inflow ratio $V = 0.844$. Positive (or negative) feedback represents a feedback law such that the increase in q_1 (positive for upward bending) results in an increase (or decrease) in θ_{1c}. That is, blade pitch takes a maximum value at $\psi = 0^o$ (180^o) in proportion to feedback gain. Figure 36(a) shows the root locus for the influence of this gain. Points are shown for a selected physically reasonable value of the gain. The gain can be interpreted as the ratio of the angular amplitude of cyclic pitch to angular deflection

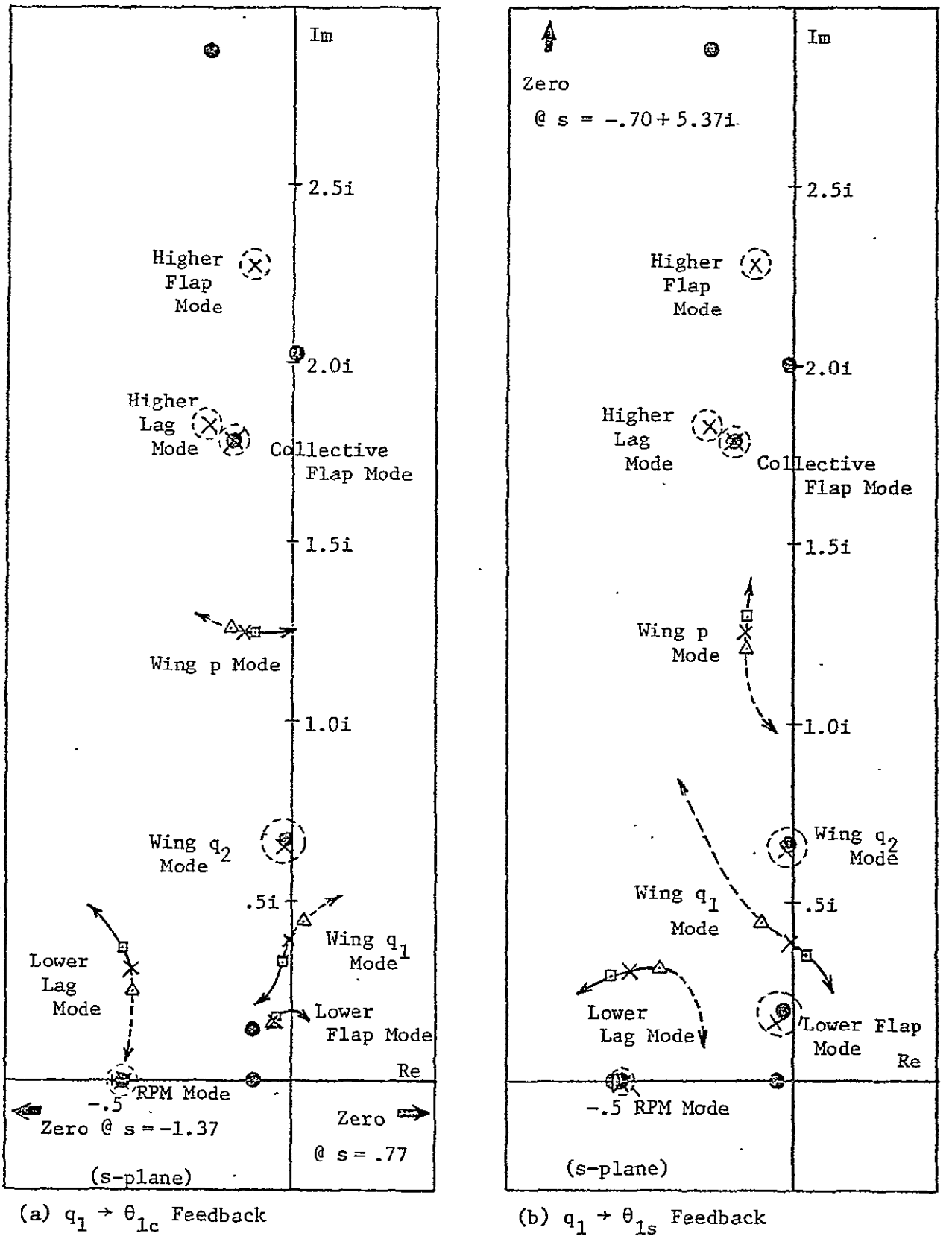

(a) $q_1 \rightarrow \theta_{1c}$ Feedback

(b) $q_1 \rightarrow \theta_{1s}$ Feedback

: Positive FB; : Negative FB, & : FB Gain = 2.51 (8 dB)

Figure 36. Root Locus: Effect of $q_1 \rightarrow \theta_{1c}$ or θ_{1s} Feedback (Proportional); 9 DOF Model @ V = .844

of the wing tip measured from the wing root. It can be seen that the primary influence of cyclic feedback is to change the characteristics of the wing p and q_1 modes and the lower flap and lag modes. This feedback essentially alters the damping of the torsion mode and the stiffness and damping of the spanwise bending mode. Positive feedback increases the torsion mode damping and destabilizes the spanwise mode. There is little influence on the wing chordwise mode, the higher flap and lag cyclic modes, the collective flap mode or the RPM mode. Considering a second feedback, wing bending to θ_{1s}, i.e., a shift in phase of 90^{o}, essentially the root loci effects are shifted by 90^{o}. In this case, the feedback alters the frequency of the p mode and the damping of the q_1 mode. In each case, the larger change occurs in the lower frequency or q_1 mode, and from the standpoint of stabilizing the q_1 mode, θ_{1s} feedback appear to be the best candidate. Now consider the effects of torsion motion feedback shown in Figure 37. The dominant effects of this feedback are to change the torsion mode characteristics as would be expected and there is some influence on the higher lag mode. A positive feedback of θ_{1c} can be employed to provide torsion mode damping. It is interesting to note that the trends with torsion feedback are very similar to the influence of spanwise bending feedback with respect to their influence on the wing modes. Of course, the q_1 feedback causes a larger effect on the q_1 mode and similarly the p feedback causes a larger effect on the p mode. The other difference to be noted is that the torsion mode feedback produces favorable effects on both modes (although the effect on q_1 is small) whereas the q_1 feedback produces opposite effects. This can be explained by noting the eigenvectors for the p, q_1 coupled modes given earlier

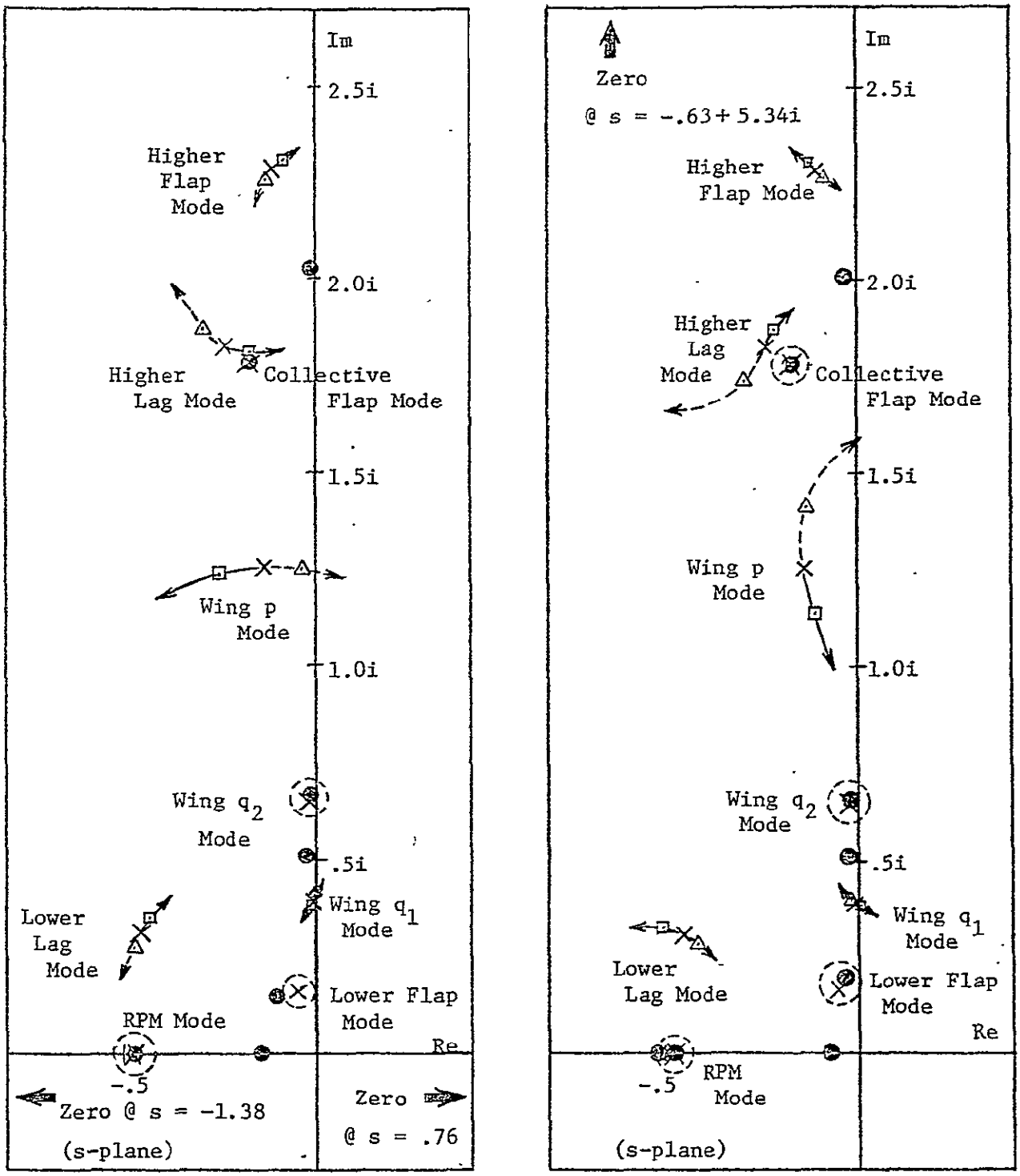

: Positive FB, : Negative FB, & : FB Gain = 1.0 (0 dB).

Figure 37. Root Locus: Effect of $p \rightarrow \theta_{1c}$ or θ_{1s} Feedback (Proportional); 9 DOF Model @ V = .844

where in the q_1 mode, p and q_1 are in phase,whereas in the p mode they are out of phase.

Again the p mode feedback has little influence on many of the modes similar to the q_1 feedback.

Torsion feedback is essentially similar to a single axis version of the focussed pylon mount.

Now we examine chordwise motion feedback. Figure 38 shows the effect of this feedback to each cyclic. The effect is generally small due to the large stiffness noted above. For a reasonable physical value of gain some slight increment in the damping of the chordwise mode can be provided.

These results indicate that owing to the small influence of q_2 feedback a focussed mount system with equal gains on both axes would act essentially like a single axis feedback of torsion or spanwise bending motion.

In considering more generally the influence of these feedbacks it is possible to note some marked similarities between the various feedbacks. Further it is possible to associate certain of the zeros with the wing dynamics and others with the blade dynamics.

Figure 39 shows the zeros for the q_1 transfer functions indicating the source as arising from wing or rotor characteristics. The zeros from the seven and nine degree of freedom models are shown to indicate that there is only a small difference in these two cases. By the symbols H and W the origin of these zeros from the wing or H force transfer function are identified. Figures 40 and 41 show the zeros of the other transfer functions. Each of the transfer functions $\frac{q_1}{\theta_{1c}}$, $\frac{q_2}{\theta_{1s}}$, $\frac{p}{\theta_{1c}}$ has nearly in common the following zeros (denoted by H_s, H_c, Y_s, or Y_c):

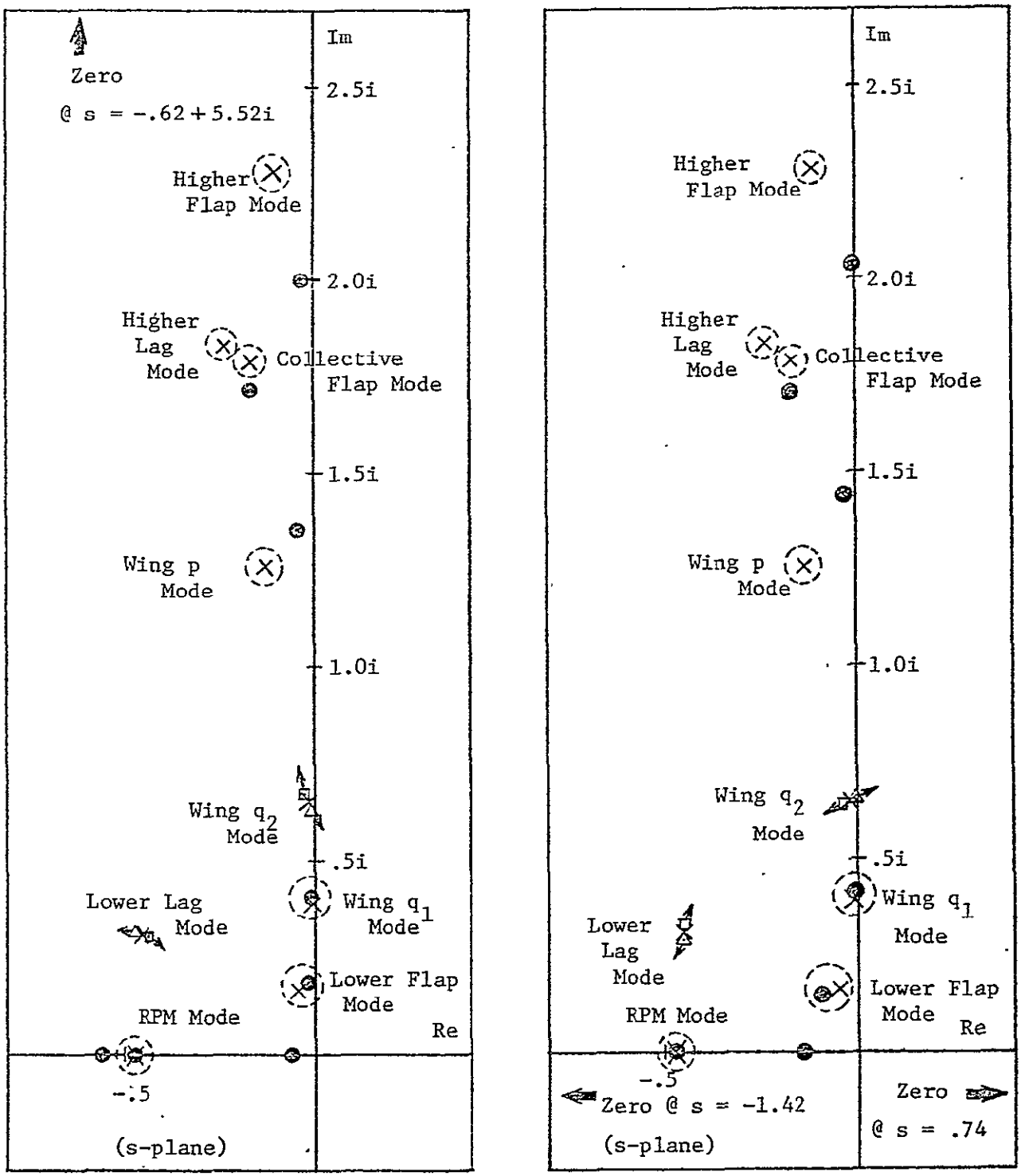

⊠→: Positive FB, ⊠→: Negative FB, △&□: FB Gain = 2.51 (8 dB)

Figure 38. Root Locus: Effect of $q_2 \rightarrow \theta_{1c}$ or θ_{1s} Feedback (Proportional); 9 DOF Model @ V = .844

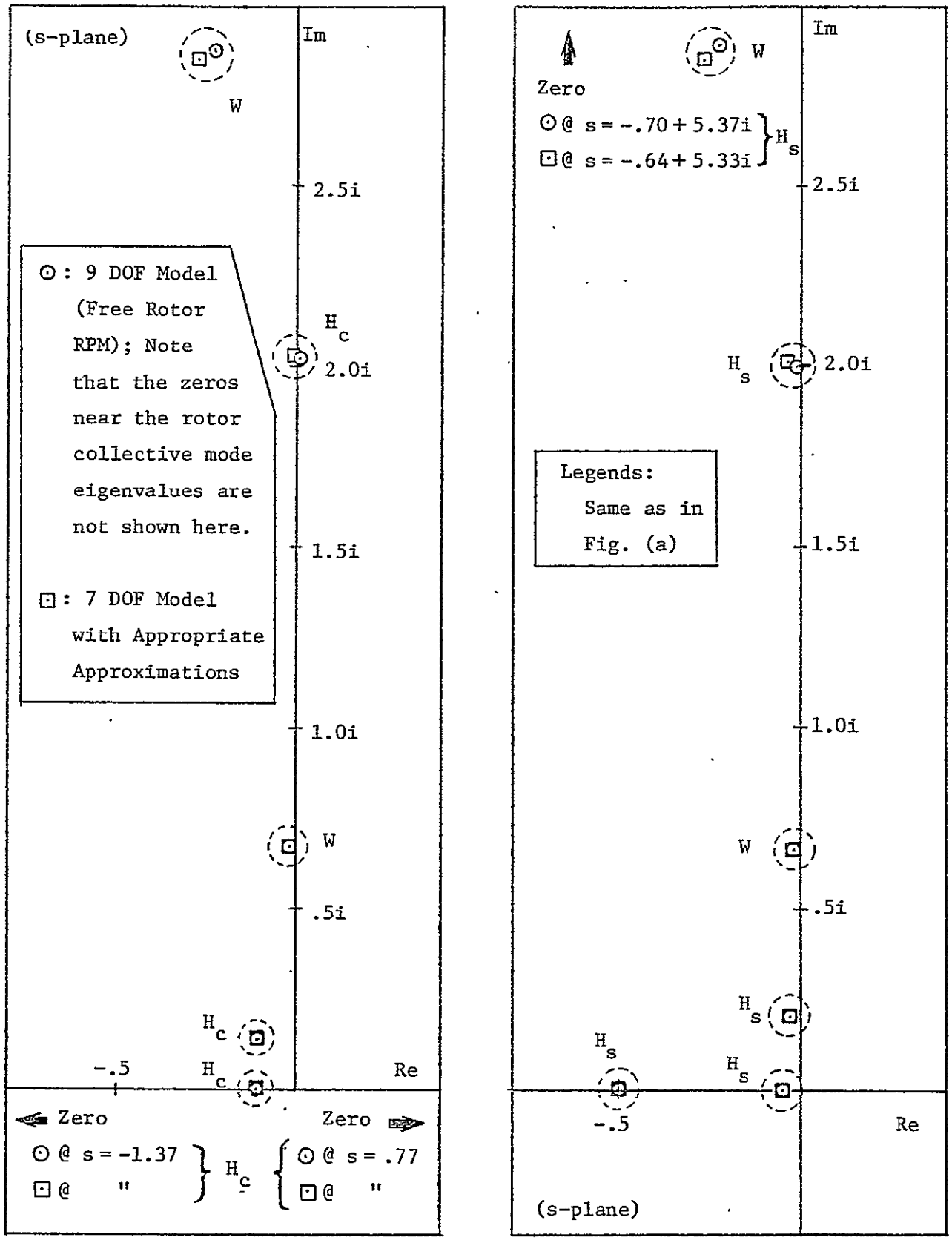

Figure 39. Zeros of Transfer Functions, q_1/θ_{1c} & q_1/θ_{1s}, @ V = .844

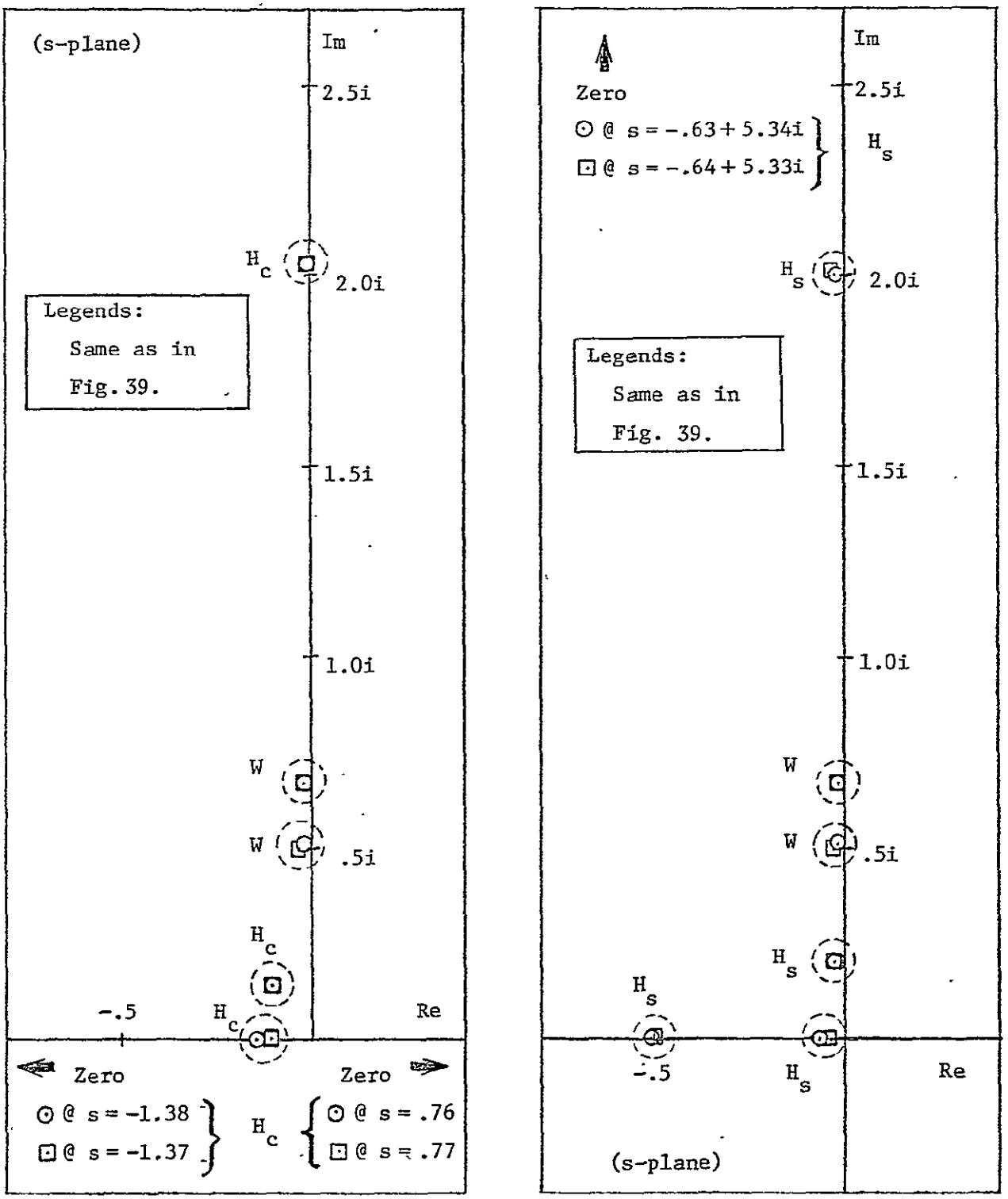

(a) Zeros of p/θ_{1c}

(b) Zeros of p/θ_{1s}

W: Zeros Originating from Wing Dynamics

H_c or H_s: " Rotor " (H Force to θ_{1c} or θ_{1s})

Figure 40. Zeros of Transfer Functions, p/θ_{1c} & p/θ_{1s}, @ V = .844

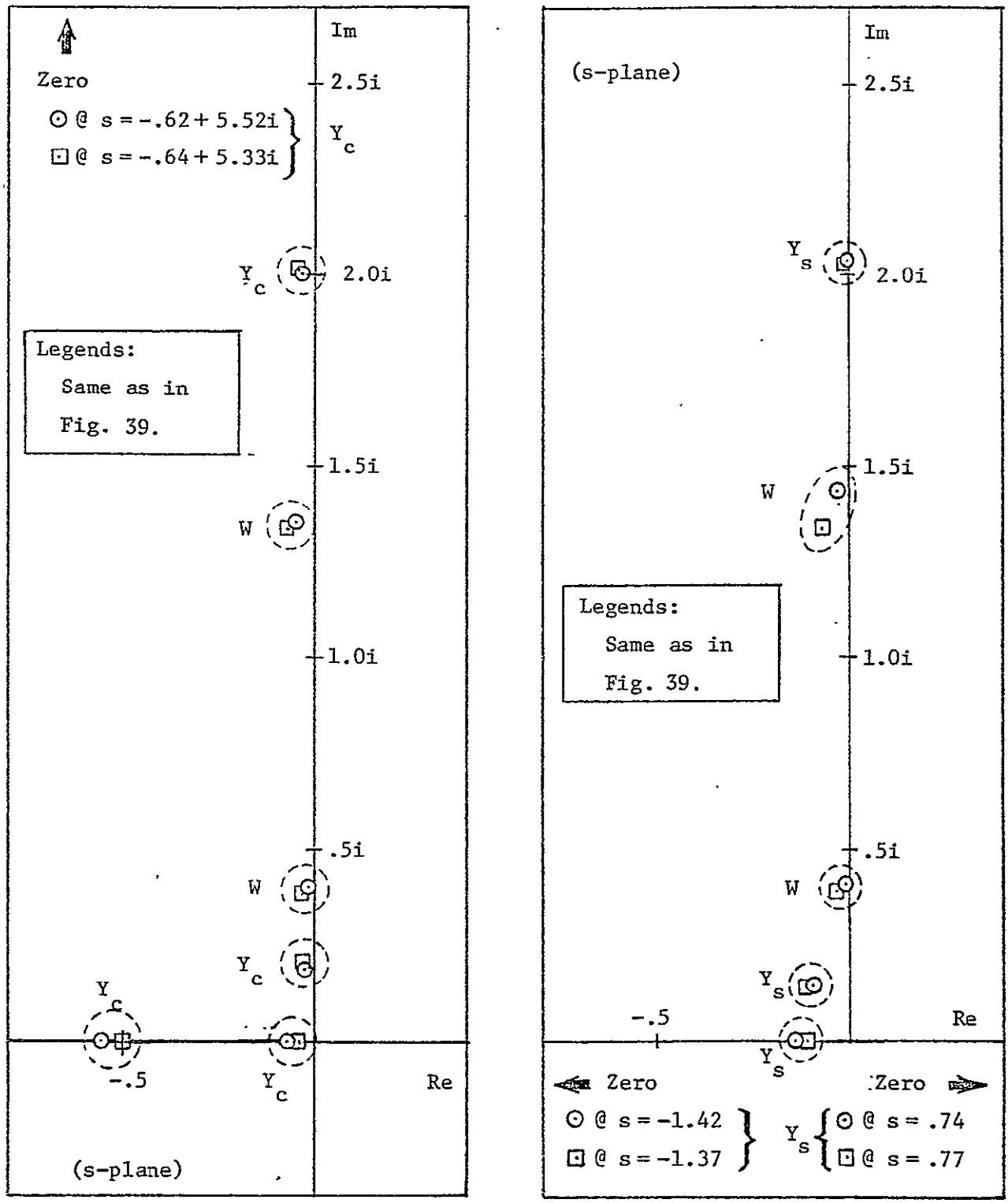

Figure 41. Zeros of Transfer Functions, q_2/θ_{1c} & q_2/θ_{1s}, @ V = .844

1.) Three zeros on the real axis; one on the negative real axis near the origin (s = - 0.1); another farther from the origin (s = - 1.4); and one on the positive real axis (s = 0.8).

2.) One zero near the lower mode flap eigenvalue (s = - 0.1 + 0.14i).

3.) One zero near the point s = 2i.

Similarily for the other three transfer functions, $\frac{q_1}{\theta_{1s}}$, $\frac{q_2}{\theta_{1c}}$, $\frac{p}{\theta_{1s}}$ there are

1.) Two zeros on the negative real axis; one near the origin (s = - 0.05) and one farther to the left (s = - 0.5).

2.) One zero near the lower flap mode eigenvalue (s = - 0.03 + 0.2i).

3.) One zero near the point s = 2i.

4.) One zero far from the origin (s = - 0.6 + 5.3i).

As will be shown below, these zeros in both cases are associated with the rotor dynamics, and are essentially the zeros of the rotor inplane force to cyclic transfer functions. The following section considers this question in more detail.

4.) Transfer Function Zeros for Cyclic Feedback

We now examine some characteristics of the zeros of the transfer functions of the coupled proprotor cyclic and wing motion to illustrate the source of the zeros. The location of these zeros governs the manner in which feedback influences the dynamics of the system.

The coupled system equations of motion may be written as

$$\begin{bmatrix} A_{11} & C_{rq_1} & C_{rq_2} & C_{rp} \\ \hline C_{q_1r} & & & \\ C_{q_2r} & & A_{22}' & \\ C_{pr} & & & \end{bmatrix} \begin{Bmatrix} \underline{x}_r \\ \underline{x}_w \end{Bmatrix} = \begin{bmatrix} B_{11} \\ \hline B_{21}' \end{bmatrix} \{\underline{\delta}\} \qquad (56)$$

where

$$\underline{x}_r = \begin{Bmatrix} \beta_{1c} \\ \beta_{1s} \\ \zeta_{1c} \\ \zeta_{1s} \end{Bmatrix} \qquad \underline{x}_w = \begin{Bmatrix} q_1 \\ q_2 \\ p \end{Bmatrix} \qquad \underline{\delta} = \begin{Bmatrix} \theta_{1c} \\ \theta_{1s} \end{Bmatrix}$$

Only the seven degree of freedom model has been employed, since it has been shown that the collective rotor motion and the RPM degrees of freedom do not influence the dynamics of this system.

Writing the equations (56) in more compact form

$$\begin{bmatrix} A_{11} & A'_{21} \\ A'_{12} & A'_{22} \end{bmatrix} \begin{Bmatrix} \underline{x}_r \\ \underline{x}_w \end{Bmatrix} = \begin{bmatrix} B_{11} \\ B'_{21} \end{bmatrix} \{ \underline{\delta} \} \tag{57}$$

and defining a new rotor motion variable

$$\underline{x}'_r = \underline{x}_r + A_{11}^{-1} A'_{21} \underline{x}_w \tag{58}$$

The equations of motion can be written as

$$\left[A'_{22} - \begin{bmatrix} C_{q_1 r} \\ \hdashline C_{q_2 r} \\ \hdashline C_{pr} \end{bmatrix} A_{11}^{-1} \left[C_{rq_1} \vdots C_{rq_2} \vdots C_{rp} \right] \right] \underline{x}_w = - \begin{bmatrix} C_{q_1 r} \\ C_{q_2 r} \\ C_{pr} \end{bmatrix} \underline{x}'_r + B_{21} \underline{\delta} \tag{59}$$

$$A_{11} \underline{x}'_r = B_{11} \underline{\delta} \tag{60}$$

Now in this form, $\underline{x}_r'$ may be regarded as the isolated rotor motion. Thus to find the input terms on the right hand side of the equation above, in particular as regards the zeros, they can be found from the isolated rotor transfer functions.

For $\nu_\beta = 1$, which is a good approximation to the proprotor under consideration and noting that

$$C_{q_1 r} = C_{pr} \frac{y_{tw}}{h}$$

We can express the right hand side of equation (59) as

$$\begin{bmatrix} C_{q_1 r} \\ \hline C_{q_2 r} \\ \hline C_{pr} \end{bmatrix} \quad \underline{x}_r' + B_{21}' \delta = \begin{bmatrix} f_y & \frac{y_{tw}}{h} \\ \eta_{tw}' f_x & \\ & f_y \end{bmatrix} \tag{61}$$

where

$$\begin{aligned} f_y &= h\gamma \frac{2C_H}{a\sigma} + \gamma \frac{2C_{my}}{a\sigma} \\ f_x &= h\gamma \frac{2C_y}{a\sigma} - \gamma \frac{2C_{mx}}{a\sigma} \end{aligned} \tag{62}$$

The left hand side of equation (59) can be simplified based on the fact noted earlier that, wing chordwise bending (q_2) has almost no effect on the eigenvalues of the rotor wing dynamics, therefore we may drop coupling terms such as C_{rq_2}. Further q_1 motion only effects wing torsion so that

$$A_{22}' \cong \begin{bmatrix} (\Delta_{q_1})_{uc} & 0 & \Delta_{q_1 p} \\ 0 & (\Delta_{q_2})_{uc} & 0 \\ \Delta_{pq_1} & 0 & (\Delta_p)_{uc} \end{bmatrix} \tag{63}$$

$$C_{rq_1} = \{0\}$$

$$C_{rq_2} = \{0\}$$

The hub moment contribution can be neglected due to the low flapping stiffness.

As a result of these approximations equation (59) can be expressed as

$$\left[\begin{array}{c|c|c} (\Delta_{q_1})_{uc} & 0 & \Delta_{q_1 p} - \frac{y_{tw}}{h} C_{pr} A_{11}^{-1} C_{rp} \\ \hline 0 & (\Delta_{q_2})_{uc} & - C_{qr} A_{11}^{-1} C_{rp} \\ \hline \Delta_{pq_1} & 0 & (\Delta_p)_{uc} - C_{pr} A_{11}^{-1} C_{rp} \end{array}\right] \left\{\begin{array}{c} q_1 \\ q_2 \\ p \end{array}\right\}$$

$$= \left[\begin{array}{cc} \frac{y_{tw}}{h} & 0 \\ 0 & \eta'_{tw} \\ 1 & 0 \end{array}\right] \left\{\begin{array}{c} f_y \\ f_x \end{array}\right\} \tag{64}$$

Now the transfer function $\frac{q_1}{\theta_{1c}}$ may be written as

$$\frac{q_1}{\theta_{1c}} = \left(\frac{q_1}{f_y}\right)\left(\frac{f_y}{\theta_{1c}}\right) + \left(\frac{q_1}{f_x}\right)\left(\frac{f_x}{\theta_{1c}}\right) \tag{65}$$

From equation (64) the numerator of $\frac{q_1}{f_y}$ is

$$\frac{q_1}{f_y} = - \frac{y_{tw}}{h} (\Delta_{q_2})_{uc} \left\{ (\Delta_p)_{uc} - \frac{h}{y_{tw}} \Delta_{q_1 p} \right\} \tag{66}$$

and the numerator

$$\frac{q_1}{f_x} = 0 \tag{67}$$

Therefore it can be seen that the $\frac{q_1}{\theta_{1c}}$ transfer function zeros are given by the transfer function $\frac{q_1}{f_y}$ and the zeros of the transfer function $\frac{f_y}{\theta_{1c}}$. Similarly the transfer function

$$\frac{q_1}{\theta_{1s}} = \left(\frac{q_1}{f_y}\right)\left(\frac{f_y}{\theta_{1s}}\right) + \left(\frac{q_1}{f_x}\right)\left(\frac{f_x}{\theta_{1s}}\right) \tag{68}$$

since $\frac{q_1}{f_x} \simeq 0$ the zeros of $\frac{q_1}{\theta_{1s}}$ consist of the same wing zeros as for the $\frac{q_1}{\theta_{1c}}$ with the rotor zero contribution given by $\frac{f_y}{\theta_{1s}}$.

The approximate zeros given by this approach are

From

$$(\Delta_{q_2})_{uc} = 111\ s^2 + 5.17s + 49.5$$

$$s = -0.02 \pm 0.67i$$

From

$$(\Delta_p)_{uc} - \frac{h}{y_{tw}}\ \Delta_{q_1 p} = 0.481\ s^2 + 0.265\ s + 3.96$$

$$s = -0.28 \pm 2.86i$$

The zeros of the transfer function $\frac{f_y}{\theta_{1c}}$

$$s = -0.11,\ 0.77,\ -1.37,\ -0.11 \pm 0.14i,\ -0.01 \pm 2.03i$$

The zeros in the figure are labelled W or H as to whether they arise from the wing dynamics or the rotor dynamics on the figures. The physical origin of the zeros can be seen. The wing motion response to cyclic can

be considered to be a product of cascaded transfer functions, i.e, the product of the wing response to rotor force times the rotor force to cyclic where the zeros can be calculated based on a decoupling assumption.

Now consider the torsion transfer functions

$$\frac{p}{\theta_{1c}} = \frac{p}{f_y}\,\frac{f_y}{\theta_{1c}} + \frac{p}{f_x}\,\frac{f_x}{\theta_{1c}} \tag{69}$$

From equation (64), we obtain the numerator of

$$\frac{p}{f_y} = (\Delta_{q_2})_{uc}\left\{(\Delta_{q_1})_{uc} - \frac{y_{tw}}{h}\,\Delta_{pq_1}\right\} \tag{70}$$

and similarly the numerator of

$$\frac{p}{f_x} = 0 \tag{71}$$

Again the zeros are given by the wing contributions

$$(\Delta_{q_2})_{uc} \text{ and} \left\{(\Delta_{q_1})_{uc} - \frac{y_{tw}}{h}\,\Delta_{pq_1}\right\}$$

and the zeros of the transfer function $\frac{f_y}{\theta_{1c}}$. Similarly

$$\frac{p}{\theta_{1s}} = \left(\frac{p}{f_y}\right)\left(\frac{f_y}{\theta_{1s}}\right) + \left(\frac{p}{f_x}\right)\left(\frac{f_x}{\theta_{1s}}\right) \tag{72}$$

So the wing contributions are the same as above and in addition we have the zeros of the transfer function $\frac{f_y}{\theta_{1s}}$.

Thus the torsion to cyclic transfer functions have the sets of zeros from the rotor which are identical and differ only in the wing contributions.

In a similar fashion we can examine the chordwise transfer functions

P-2

$$\frac{q_2}{\theta_{1c}} = \left(\frac{q_2}{f_y}\right)\left(\frac{f_y}{\theta_{1c}}\right) + \left(\frac{q_2}{f_x}\right)\left(\frac{f_x}{\theta_{1c}}\right)$$

$$\frac{q_2}{\theta_{1s}} = \left(\frac{q_2}{f_y}\right)\left(\frac{f_y}{\theta_{1s}}\right) + \left(\frac{q_2}{f_x}\right)\left(\frac{f_x}{\theta_{1s}}\right) \tag{73}$$

If we assume that $C_{rp} = 0$ then the numerator of

$$\frac{q_2}{f_y} = 0 \tag{74}$$

and the numerator of

$$\frac{q_2}{f_x} = \eta'_{tw} \quad [(\Delta_{q_1})_{uc} \ (\Delta_p)_{uc} - \Delta_{pq_1} \ \Delta_{q_1 p}] \tag{75}$$

so it can be seen that the zeros for chordwise feedback are:

The zeros of the factor $[(\Delta_{q_1})_{uc} \ (\Delta_p)_{uc} - \Delta_{pq_1} \ \Delta_{q_1 p}]$ which are in fact the zeros of the characteristic polynomial $\Delta_{q_1 + p}$, i.e, the coupled wing torsion bending motion. And the zeros of the transfer function $\frac{f_x}{\theta_{1c}}$, which because of symmetry is equal to $-\frac{f_y}{\theta_{1s}}$.

Similarly the zeros for the $\frac{q_2}{\theta_{1s}}$ transfer function have the same wing contributions (the uncoupled wing torsion bending zeros) and the zeros of the transfer function $\frac{f_x}{\theta_{1s}}$ which is equivalent to $\frac{f_y}{\theta_{1c}}$. The zeros obtained from this approximation agree well with the results obtained from the complete model.

Thus the source of the similarity in the zeros can be seen. To summarize the results, $\frac{q_1}{\theta_{1c}}$, $\frac{q_2}{\theta_{1s}}$, $\frac{p}{\theta_{1c}}$ all have essentially the same zero contributions from the inplane response characteristics and differ in the wing zeros. $\frac{q_1}{\theta_{1s}}$, $\frac{q_2}{\theta_{1c}}$, and $\frac{p}{\theta_{1s}}$ also have similar characteristics, indicating that the zeros may be derived from a cascaded system in which the

coupling terms appearing in the numerators can be neglected, i.e., the zeros in the rotor force to cyclic transfer functions can be estimated ignoring wing motion.

It should be noted that these conclusions depend upon a number of assumptions which may not be true for other proprotor aircraft with markedly different characteristics. It appears that $\nu_\beta = 1$ is one of the crucial assumptions.

In this particular case, the difference in the action of each of these feedbacks is essentially due to the role of the wing dynamics. Chordwise feedback has little effect on the other wing modes owing to the fact that the approximate zeros of the chordwise transfer functions lie on the q_1,p modes. The torsion and spanwise feedbacks have one pair of zeros very near the q_2 mode. The other pair is basically related to the wing response to rotor force, and produces the nature of the feedback effect.

To summarize,the essential difference in the effects of the various wing motion to cyclic feedbacks appears to be due to the location of the zeros due to the wing dynamics, and these can be estimated from the wing motion transfer functions in response to forces applied at the rotor hub. Both the q_1 and p feedbacks give a zero at the uncoupled chordwise mode. The second pair of wing zeros for q_1 feedback is at rather high frequency while for p feedback the zeros are at relatively low frequency near the q_1 mode, sufficiently close in fact such that p feedback has only a relatively weak influence on the q_1 mode. q_2 feedback results in zeros from the wing dynamics which are near the q_1 and p modes as would be expected.

It is also interesting to note that the rotor force to cyclic transfer functions yield a zero quite close to the origin implying that the response

of the rotor force to cyclic is close to being a rate dependent effect. A simple model for the rotor in-plane force implies that for low frequency motions the inplane force is proportional to flapping rate, and since cyclic produces a flap angle for low frequency inputs, the rotor force transfer function is more like a damping feedback than a stiffness change. This would be quite different if the rotor produced appreciable hub moments through a flapping spring.

Thus it can be seen that cyclic pitch feedback could be effective in controlling the wing torsion and spanwise bending modes but has little influence on the chordwise mode. Therefore it seems desirable to examine the effect of chordwise motion to collective pitch feedback.

5.) Chordwise Motion to Rotor Collective Feedback

The root loci shown in Figure 42 illustrates the influence of proportional feedback of wing q_2 motion to collective pitch for the nine degree of freedom model in the free rotor RPM case at advance ratio V = 0.844. The sign convention for positive (or negative) feedback is such that an increase in q_2 (positive for aft bending) results in an increase (or decrease) in blade collective pitch.

It can be seen from this complete model that essentially only the chordwise mode, collective flap and RPM modes are involved and pole zero cancellations eliminate the effects on other modes. Thus it appears that this feedback can be adequately examined using only a three degree of freedom model.

Figure 43 shows some results using this three degree of freedom model. It is interesting to note from Figure 42 the zero configuration involved in this feedback. There is a zero at the origin implying that this feedback

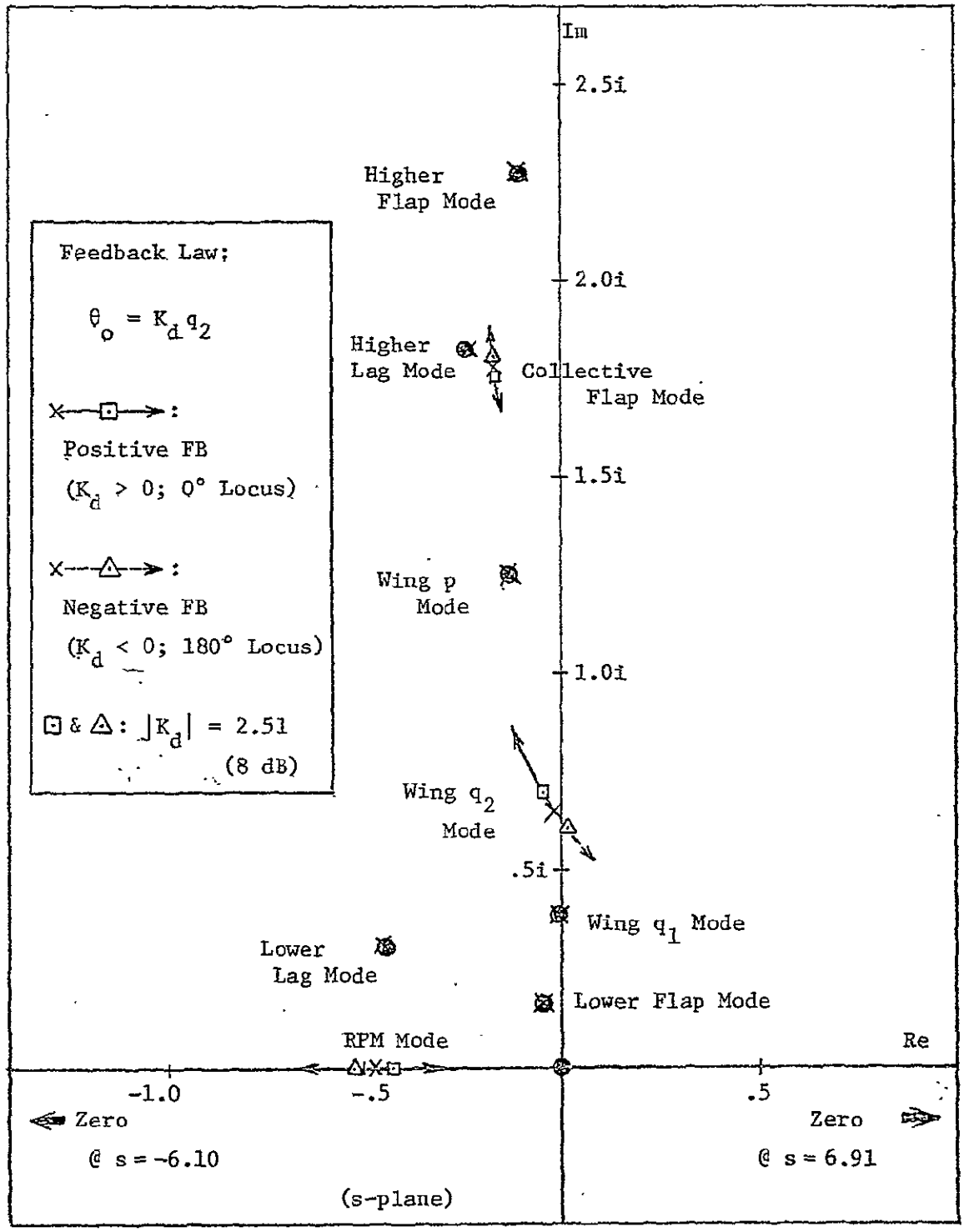

Figure 42. Root Locus: Effect of $q_2 \rightarrow \theta_o$ Feedback (Proportional); 9 DOF Model (in Free Rotor RPM Case) @ V = .844

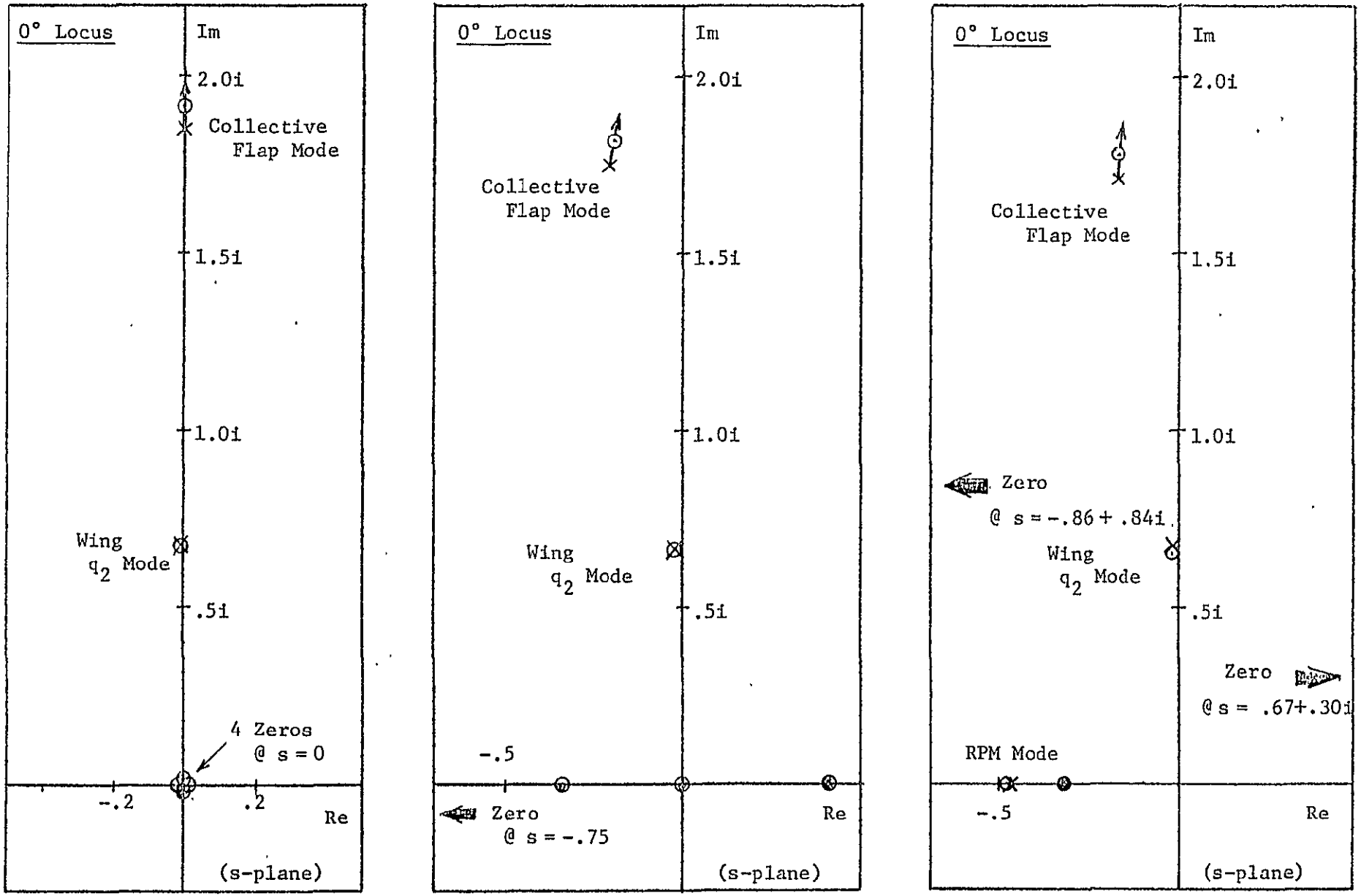

(a) $q_2 \sim \beta_o$ (Without Aero-Dynamic Influence)

(b) $q_2 \sim \beta_o$ (With Aerodynamic Influence; @ V = .844)

(c) $q_2 \sim \beta_o$ & Ω_s (@ V = .844)

Figure 43. Root Locus: Influence of $q_2 \sim \beta_o$ & Ω_s Motion Coupling on Coupled Dynamics

is essentially a rate feedback. That is, that a collective pitch change gives no steady state thrust. This is a consequence of the free RPM assumption. That is, in the steady state no thrust change is produced by a collective pitch change. The two real axis zeros indicate the presence of a non-minimum phase effect. These trends can be readily explained by considering the three degree of freedom dynamics in more detail

The equations of motion can be written as

$$[A] \begin{Bmatrix} \beta_o \\ \Omega_s \\ q_2 \end{Bmatrix} = \begin{bmatrix} \gamma M_\theta \\ -\gamma Q_\theta \\ -2\, y_{tw}\, \gamma T_\theta \end{bmatrix} \theta_o \tag{76}$$

Since this is a relatively simple system,we do not consider the cascade approach used in a previous section.

The numerator of the $\frac{q_2}{\theta_o}$ transfer functions, denoted by $N_{\theta_o}^{q_2}$ is given by

$$N_{\theta_o}^{q_2} = \begin{vmatrix} I^*_{\beta_o} (\Delta_{\beta_o})_{uc} & -\gamma M_{\dot\zeta} & \gamma M_\theta \\ \gamma Q_{\dot\beta}\, s & (\Delta\Omega)_{uc} & -\gamma Q_\theta \\ 2\, y_{tw}(-S^*_{\beta_o} s^2 + \gamma T_{\dot\beta} s) & 2\, y_{tw}\, T_{\dot\zeta} & -2\, y_{tw}\gamma T_\theta \end{vmatrix} \tag{77}$$

But since the Q derivatives are proportional to the T derivatives[1], i.e.,

$$Q_{(\,)} = V\, T_{(\,)}$$

equation (77) can be simplified to,

$$N^{q_2}_{\theta_o} = \begin{vmatrix} I^*_{\beta_o} & (\Delta_{\beta_o})_{uc} & -\gamma M_{\dot{\zeta}} & \gamma M_\theta \\ V S^*_{\beta_o} & s^2 & s & 0 \\ 2\, y_{tw}(-S^*_{\beta_o} & s^2 + \gamma T_{\dot{\beta}}\, s) & 2\, y_{tw}\gamma T_{\dot{\zeta}} & -2\, y_{tw}\gamma T_\theta \end{vmatrix} \tag{78}$$

Expanding

$$N^{q_2}_{\theta_o} = -2\, y_{tw}\gamma T_\theta s \left[(I^*_{\beta_o} - S^*_{\beta_o} \frac{M_\theta}{T_\theta})\, s^2 + \left(\gamma \left(\frac{T_{\dot{\beta}} M_\theta}{T_\theta} - M_{\dot{\beta}}\right) - V S^*_{\beta_o} \left(\frac{T_{\dot{\zeta}} M_\theta}{T_\theta}\right) - M_{\dot{\zeta}} \right) s + I^*_{\beta_o}\, \nu^2_{\beta_o} \right] \tag{79}$$

The damping term in the second factor is very small, i.e., if the effective radius approximation is employed this term vanishes, so that the numerator is given by

$$N^{q_2}_{\theta_o} = 2\, y_{tw}\, \gamma T_\theta I^*_{\beta_o} \left[\left(\frac{S^*_{\beta_o} M_\theta}{I^*_{\beta_o} T_\theta} - 1 \right) s \left\{ s^2 - \frac{\nu^2_{\beta_o}}{\frac{S^*_{\beta_o}}{M_\theta}(I^*_{\beta_o} T_\theta - 1)} \right\} \right] \tag{80}$$

Inserting numerical values we find that the zeros are

$$s = 0, \pm 6.49$$

which compares well with the more exact result obtained by retaining all of the aerodynamic terms

$$s = 0, -6.06, 6.95$$

The zero located at the origin gives a zero static gain indicating that a step input in collective produces no steady state chordwise deflection implying that in the steady state condition there is no thrust change.

It can also be seen that the nonminimum phase effect, or zero in the right half plane arises from the blade inertia. A step increase in pitch input causes the blades to accelerate forward and the inertial reaction of the wing occurs in the opposite direction or to the rear.

Consider the equations of motion for the three degrees of freedom, neglecting aerodynamic terms on the left hand side,

$$\begin{bmatrix} I^*_{\beta_o} (\Delta_\beta)_{uc} & 0 & -y_{tw} S^*_{\beta_o} s^2 \\ 0 & (\Delta_\Omega)_{uc} & 0 \\ -2 y_{tw} S^*_{\beta_o} s^2 & 0 & (\Delta_{q_2})_{uc} \end{bmatrix} \begin{Bmatrix} \beta_o \\ \Omega_s \\ q_2 \end{Bmatrix} \tag{81}$$

$$= \begin{bmatrix} \gamma M_\theta \\ -\gamma Q_\theta \\ -2 y_{tw} \gamma T_\theta \end{bmatrix} \theta_o$$

Figure 43 shows the influence of coupling for this model, including aerodynamics, with and without the Ω_s degree of freedom. The primary effect of coupling is to raise the frequency of the collective flap mode, as the neglect of the aerodynamic terms decouples the Ω_s degree of freedom. It also can be seen that the $S^*_{\beta_o}$ term representing the blade inertial characteristics is responsible for the non-minimum phase term.

The complete system analysis of Figure 42 shows an influence on the q_2 mode, a positive feedback, i.e., aft bending of the wing producing an increase in collective pitch results in a stabilizing effect. Figure 44 considers the influence of rate feedback as well as a combination of rate and displacement indicating that a combination of rate plus displacement is most effective in increasing the damping of the wing chordwise mode although the damping of the collective blade mode is slightly reduced. A physically reasonable value of gain produces a rather small effect however, owing to the high chordwise stiffness of the wing.

To summarize the results of this section, it generally appears that spanwise or torsion bending to cyclic feedback could be effective in controlling the dynamic characteristics of these modes. Owing to the high stiffness of the chordwise mode, it appears difficult to obtain much change in the chordwise mode owing to the high stiffness. Collective pitch feedback appears more effective, for reasonable gain values, in controlling the chordwise mode.

Other possible feedbacks have not been considered since they primarily influence the isolated modes, i.e., cyclic feedback to blade motion alters the blade motion itself and wing flap feedback will largely only influence the wing torsion-spanwise bending motion.

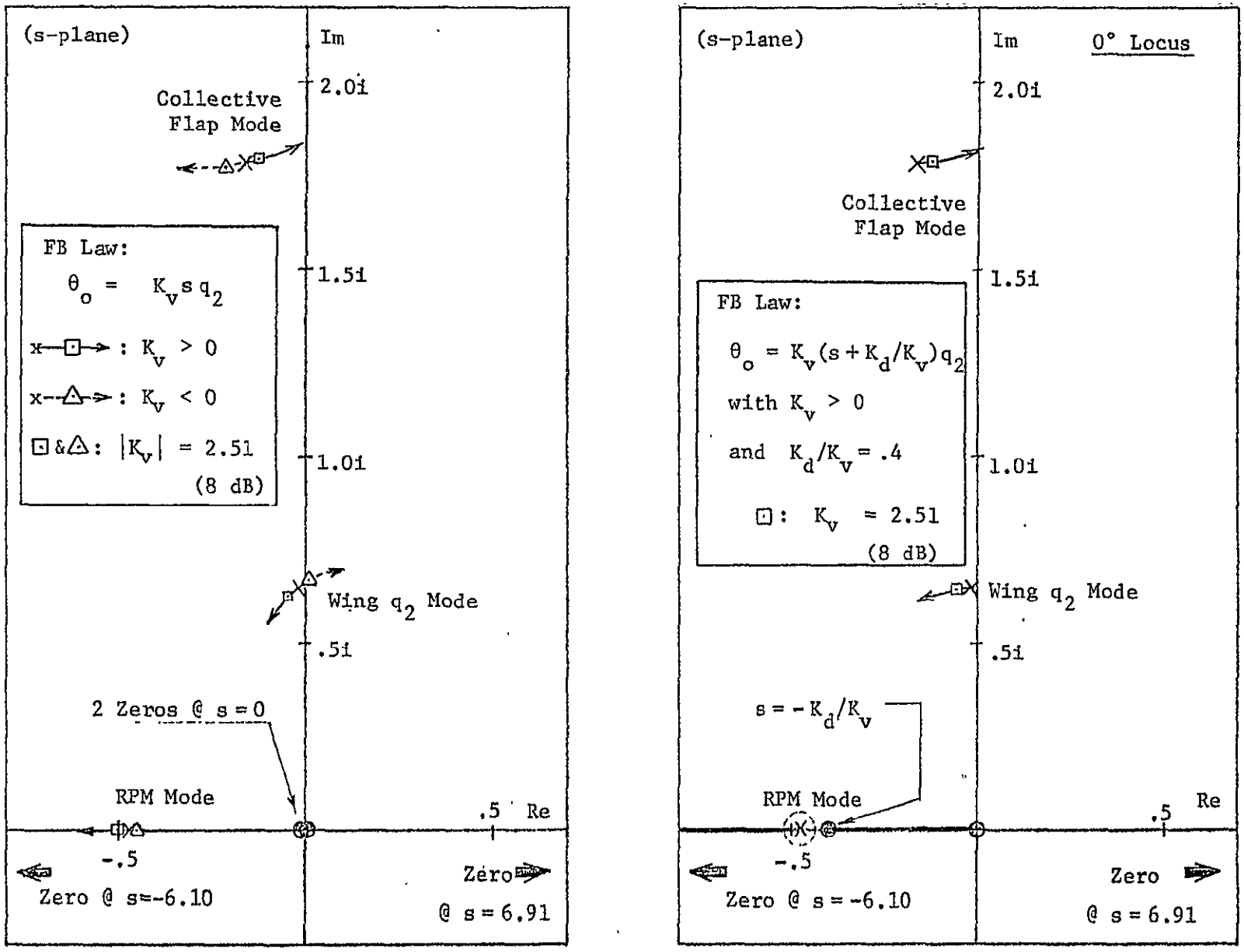

(a) Rate Feedback

(b) [Rate + Dis.] Feedback

Figure 44. Root Locus: Effect of $q_2 \rightarrow \theta_o$ Feedback; 9 DOF Model (in Free Rotor RPM Case) @ V = .844

PROPROTOR DYNAMICS WITH FUSELAGE FREEDOM

In this section we examine the influence of freeing the fuselage on the overall dynamics of the proprotor aircraft with flexibility. Only the symmetric degrees of freedom of the fuselage are considered, i.e., pitch, vertical translation, and horizontal translation. Further, additional blade degrees of freedom have been included to more precisely represent the influence of the blade torsion degree of freedom. The proprotor wing model is now that of Reference 2. Rather than using an effective pitch-lag coupling as in the previous sections, additional blade degrees of freedom including modal coupling between flap and lag bending as well as control system flexibility are incorporated. This increases the complexity of the basic model with free proprotor RPM. Fifteen degrees of freedom are now involved. Therefore with the fuselage free, we have an eighteen degree of freedom system. The inclusion of additional blade degrees of freeom, while changing quantitative aspects of the results does not give any essential qualitative differences from the nine degree of freedom model with pitch-lag coupling.

Of particular interest here is the influence of freeing the fuselage on the dynamics and stability of the overall system especially as regards its influence on the whirl flutter speed. In addition, the influence of the flexibility on the dynamics of the aircraft, especially with respect to the lowest frequency modes which are related to the stability and control of the aircraft are examined and an approximate model discussed which considers the primary influence of flexibility.

Figure 45 shows the eigenvalues of the eighteen degree of freedom (fuselage free) and fifteen degree of freedom (fuselage fixed) motions

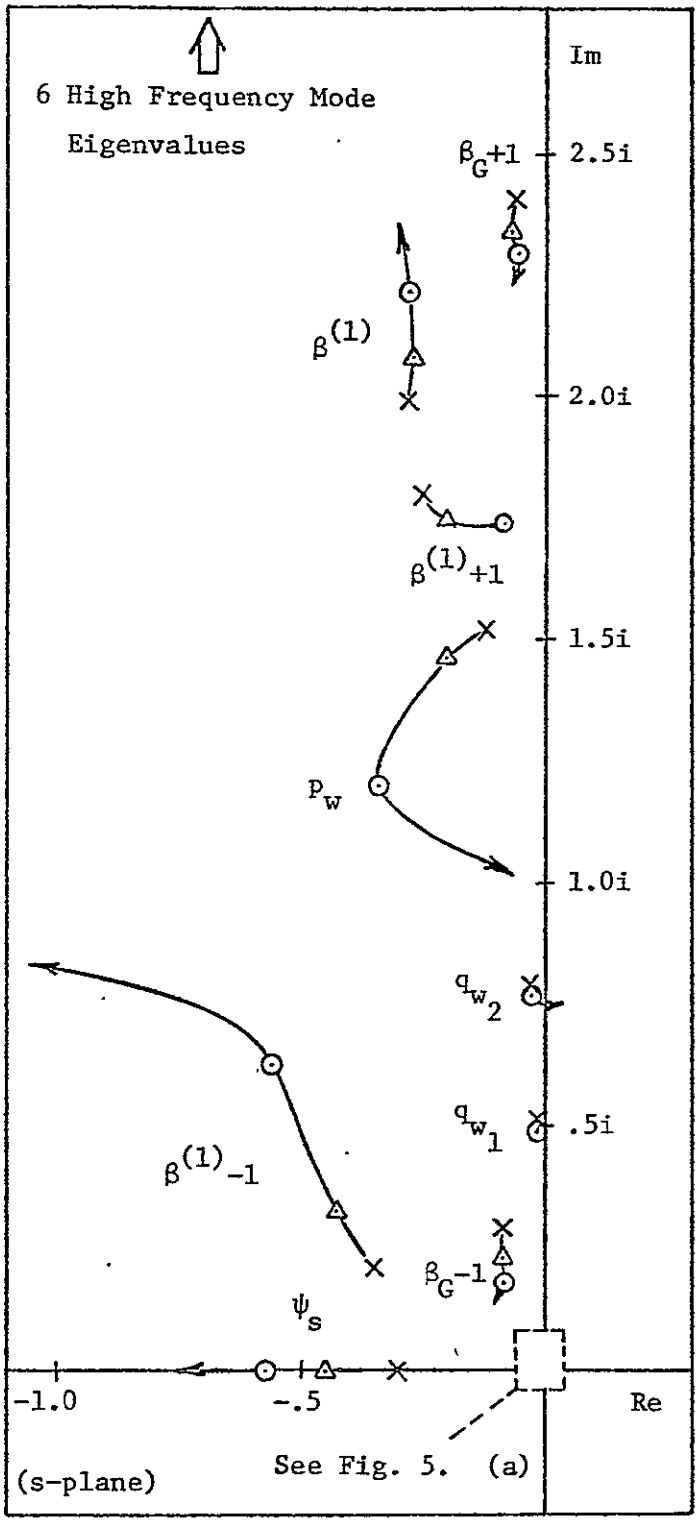

(a) 18 DOF Model; With Aircraft Longitudinal Rigid Body Motion DOF

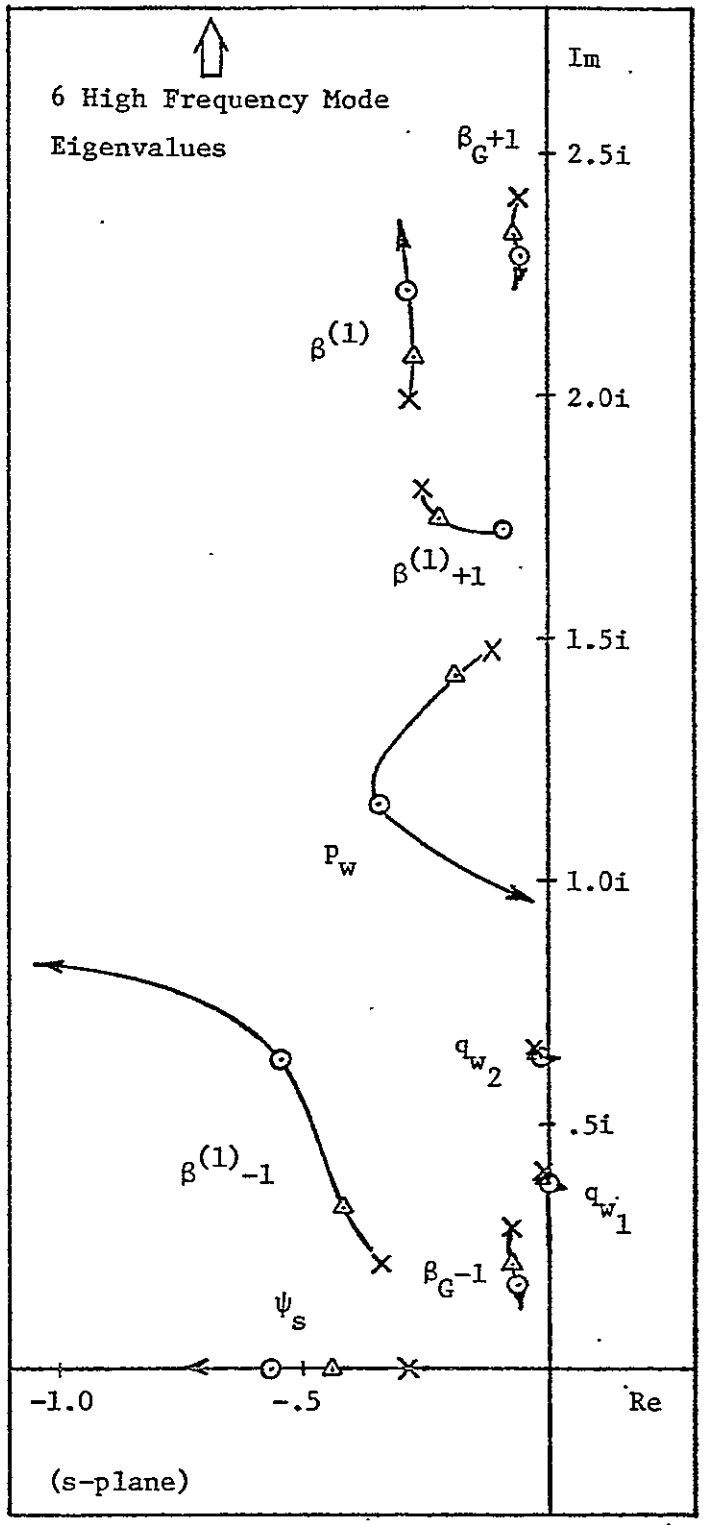

(b) 15 DOF Model; Without Aircraft Longitudinal Rigid Body Motion DOF

Figure 45. Root Locus for Velocity Sweep; @ Free Rotor RPM

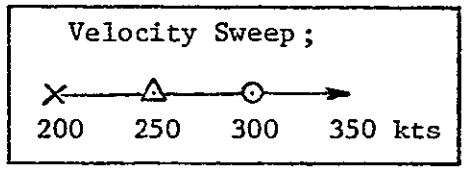

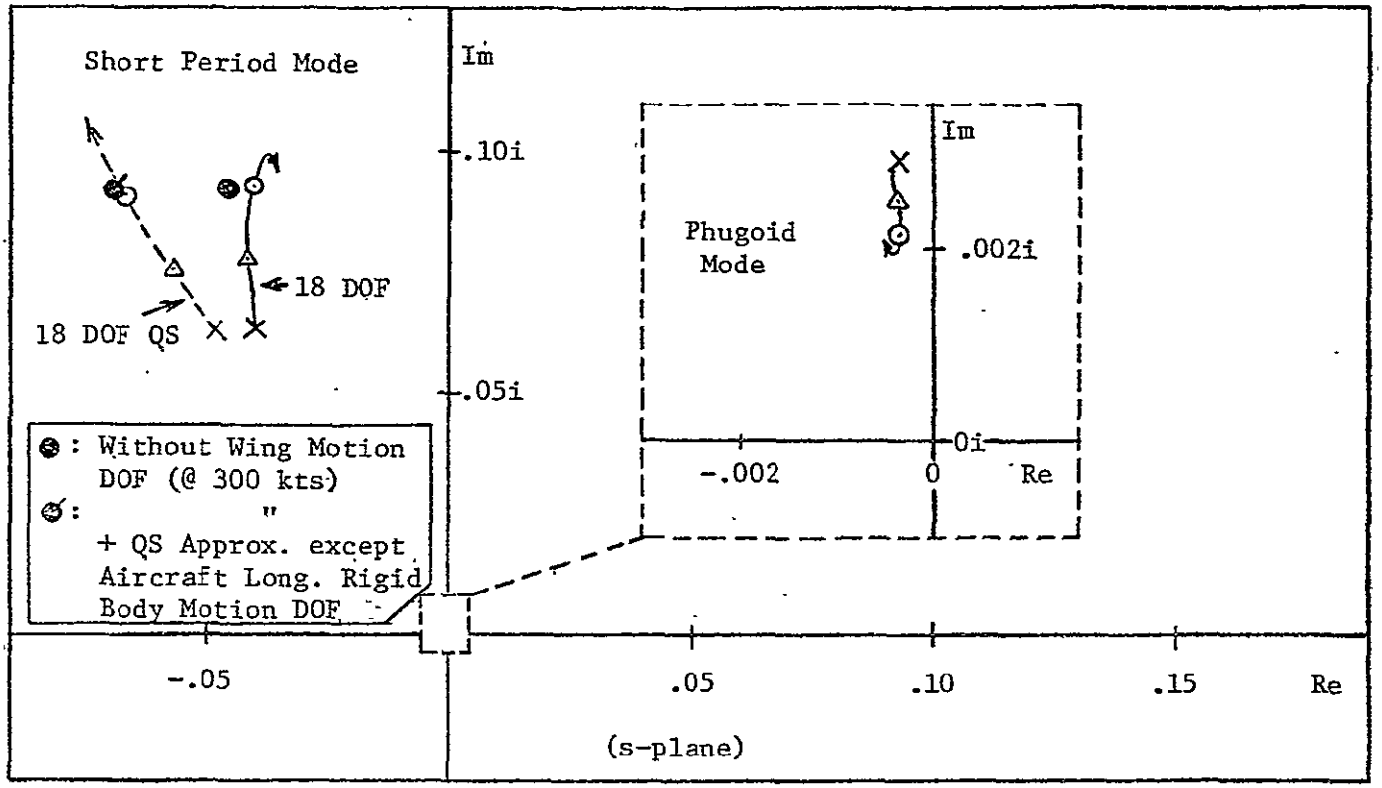

(a) @ Free Rotor RPM (18 DOF Model)

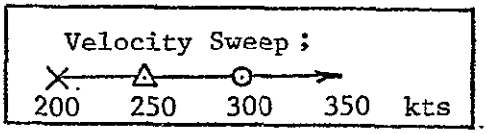

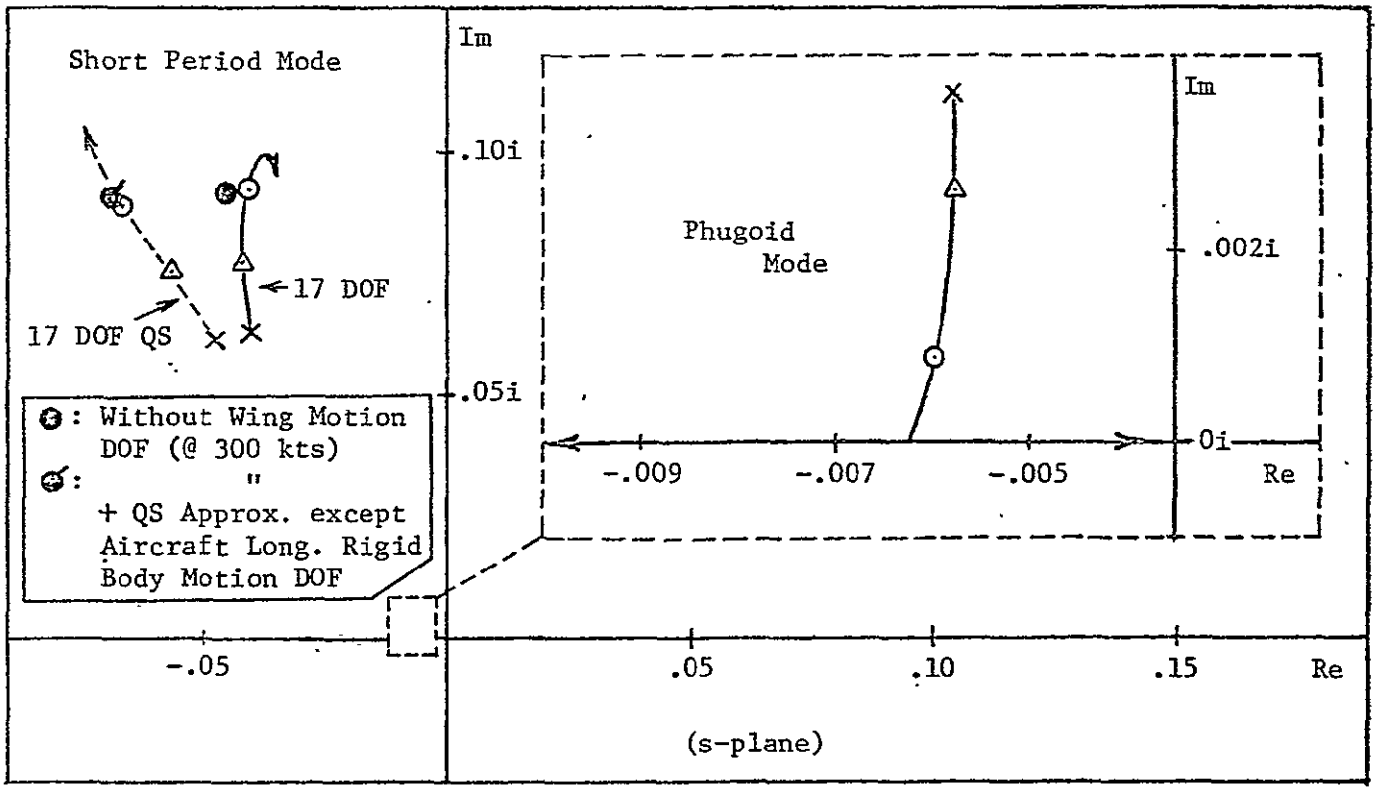

(b) @ Constant Rotor RPM (17 DOF Model)

Figure 45. Root Locus for Velocity Sweep; Aircraft Longitudinal Rigid Body Motion Modes

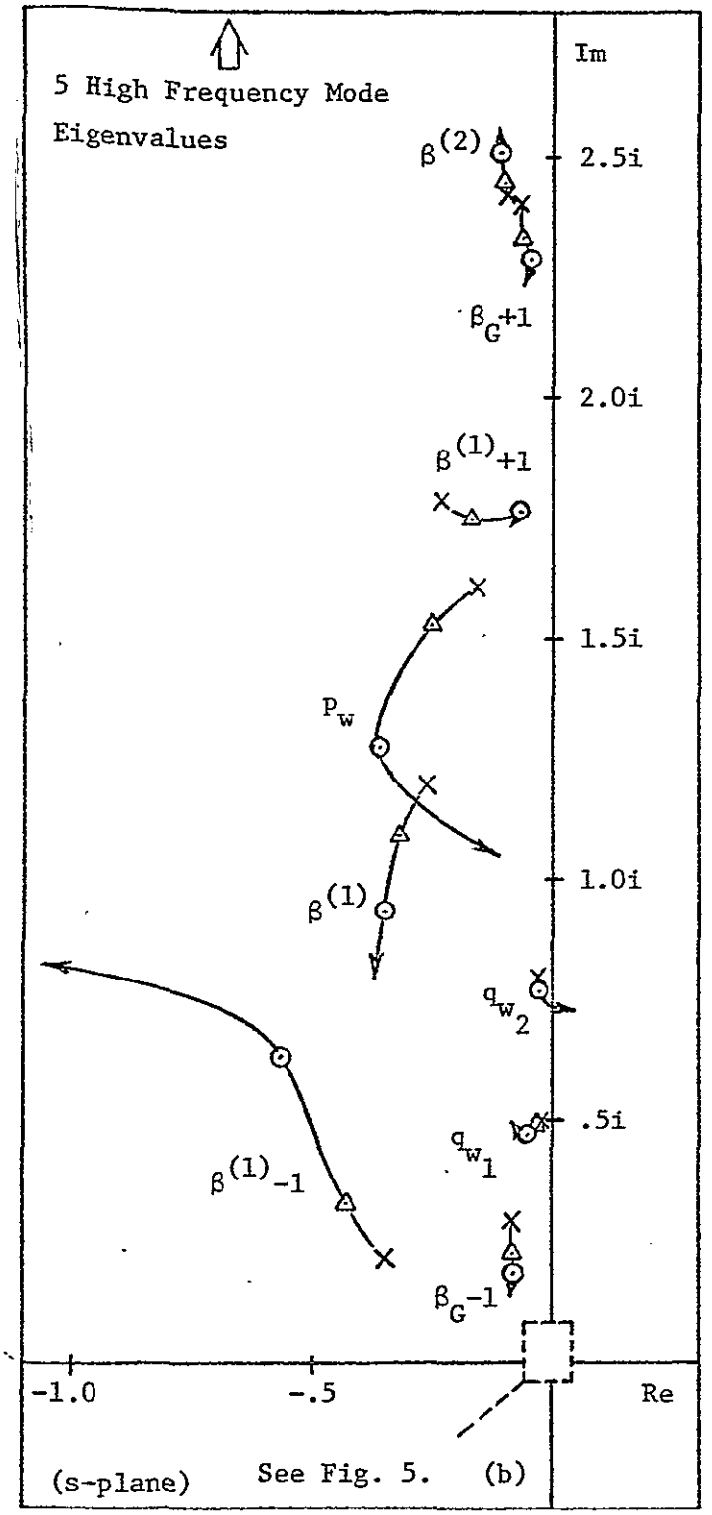

(a) 17 DOF Model; With Aircraft Longitudinal Rigid Body Motion DOF

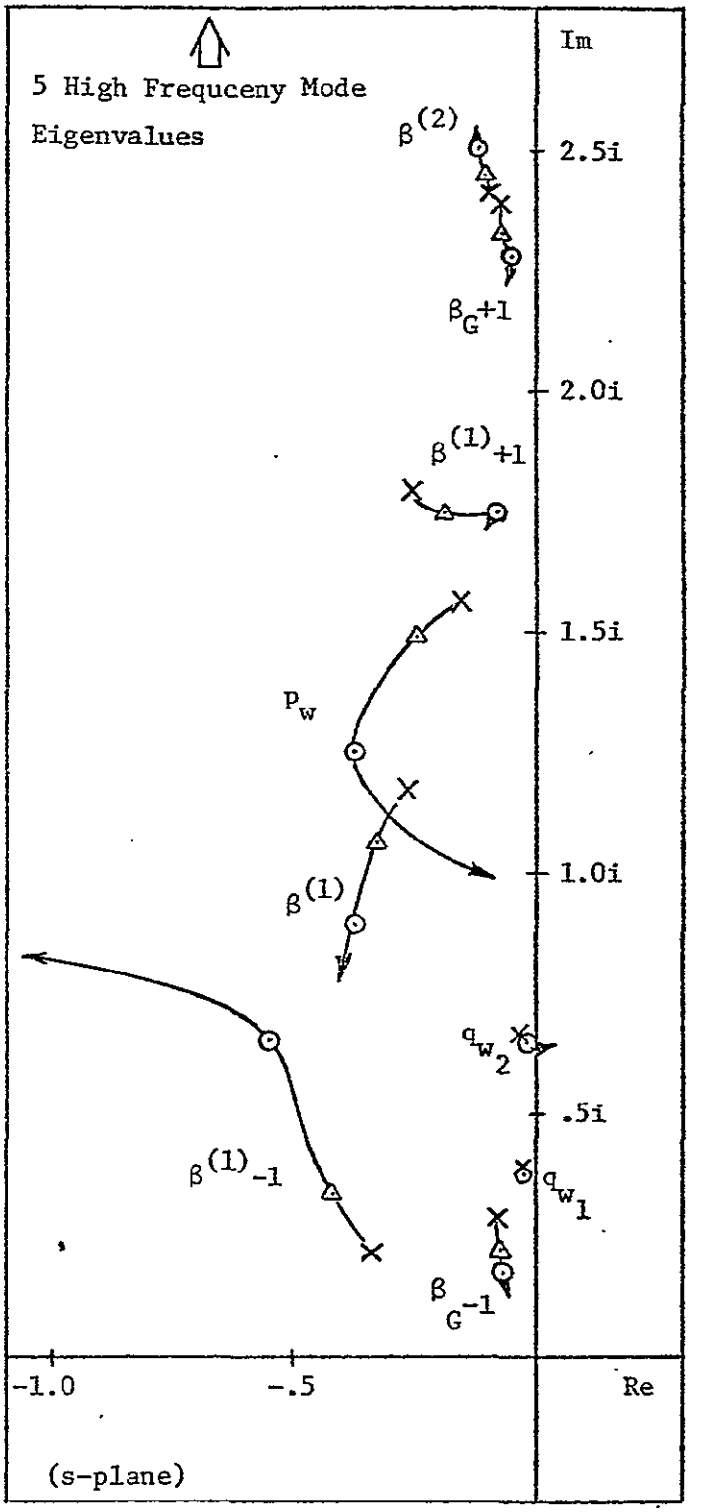

(b) 14 DOF Model; Without Aircraft Longitudinal Rigid Body Motion DOF

Figure 45. Root Locus for Velocity Sweep; @ Constant Rotor RPM

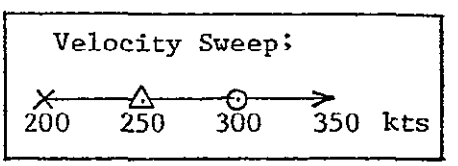

as a function of trimmed flight velocity and also the case with rotor RPM assumed constant (seventeen and fourteen degrees of freedom). It can be seen that there is little influence on many of the eigenvalues with the exception of the wing bending modes and of course the addition of the classical longitudinal modes of motion of the airframe.

In particular it can be noted that upon freeing the fuselage both of the wing bending modes (q_{w_1} and q_{w_2}) are raised in frequency and their damping ratios are increased. This increase in frequency is simply explained by considering the way in which the natural frequencies of a beam undergoing symmetric vibration are influenced by a mass located at the center of the beam. If we compare the lowest natural frequency of a cantilever beam which is given by

$$\omega_{N_c} = 3.52 \sqrt{\frac{EI}{m\ell^4}}$$

which would correspond to the limiting case of an infinite mass at the center of a free-free beam to the natural frequency of a free-free beam with no mass at the center, its natural frequency is

$$\omega_{N_{ff}} = 22.4 \sqrt{\frac{EI}{m\ell^4}}$$

indicating the lowest mode natural frequency increases as the effect of fuselage freedom is included. This effect can be seen in the complete model by comparing the frequencies of the q_{w_1} and q_{w_2} modes in Figures 45(a) and (b). Figure 46 shows these results more explicitly giving the frequency of there two modes obtained from the fifteen and eighteen degree of freedom models.

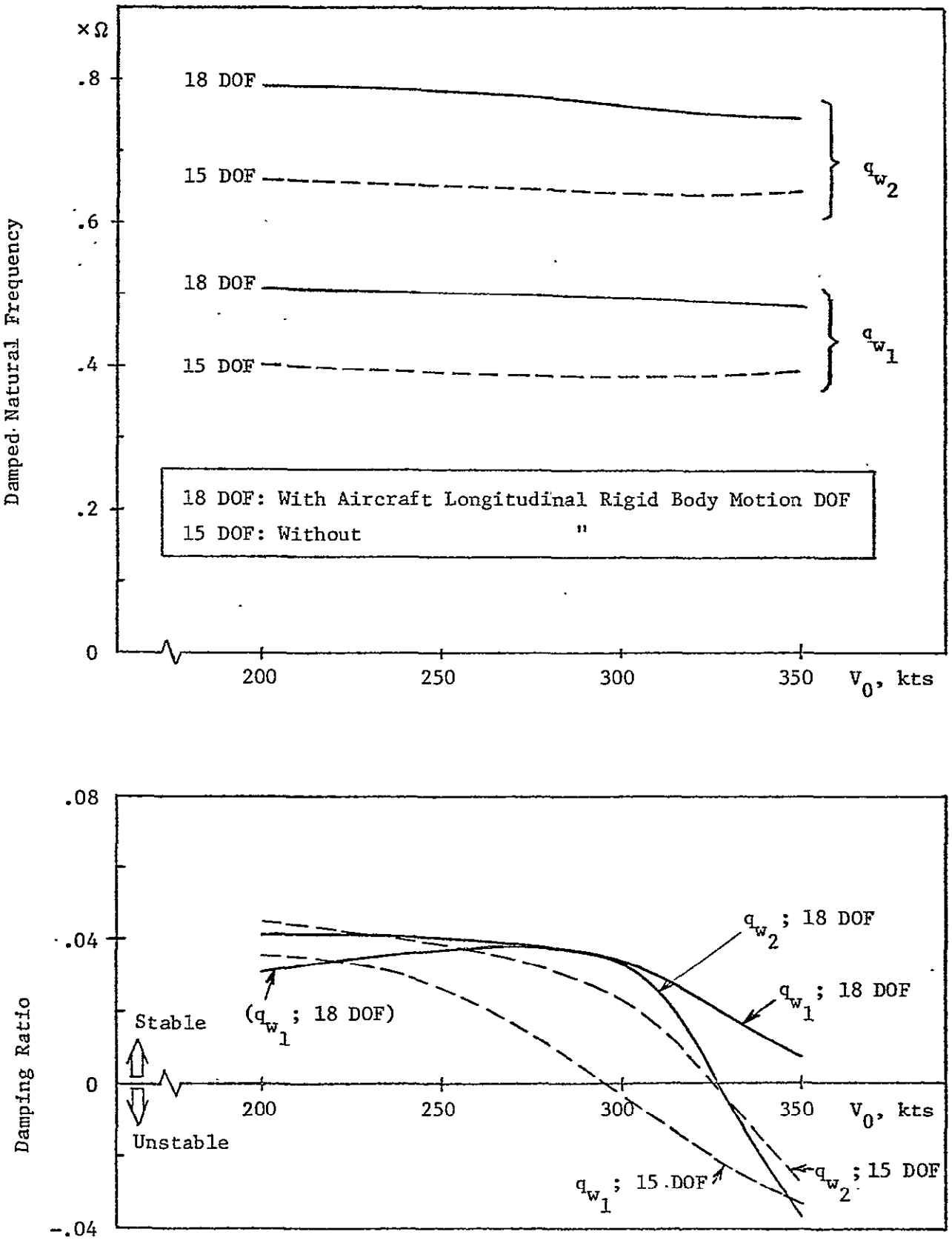

Figure 46. Wing q_{w_1} & q_{w_2} Motion Mode Characteristics; @ Free Rotor RPM

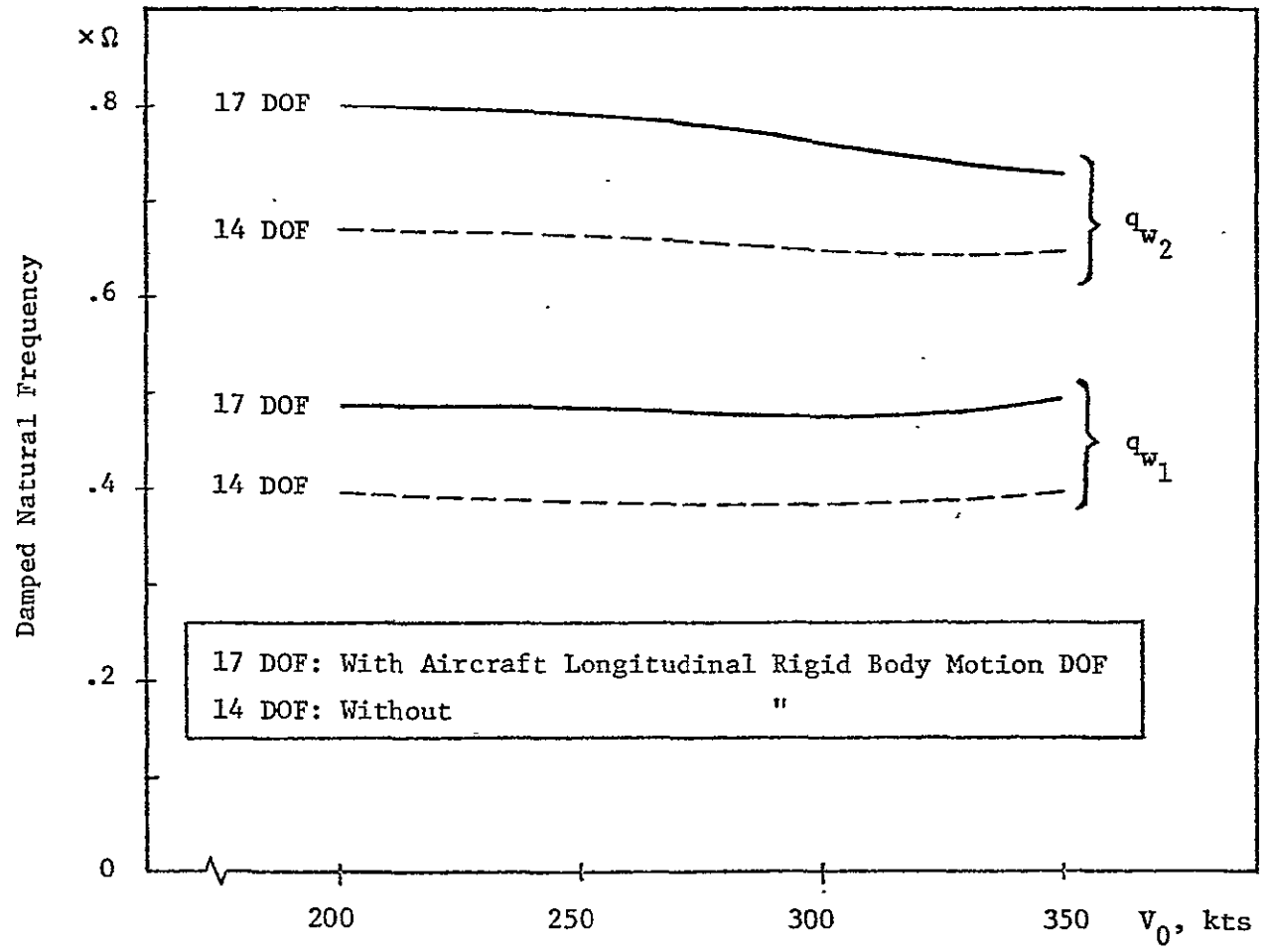

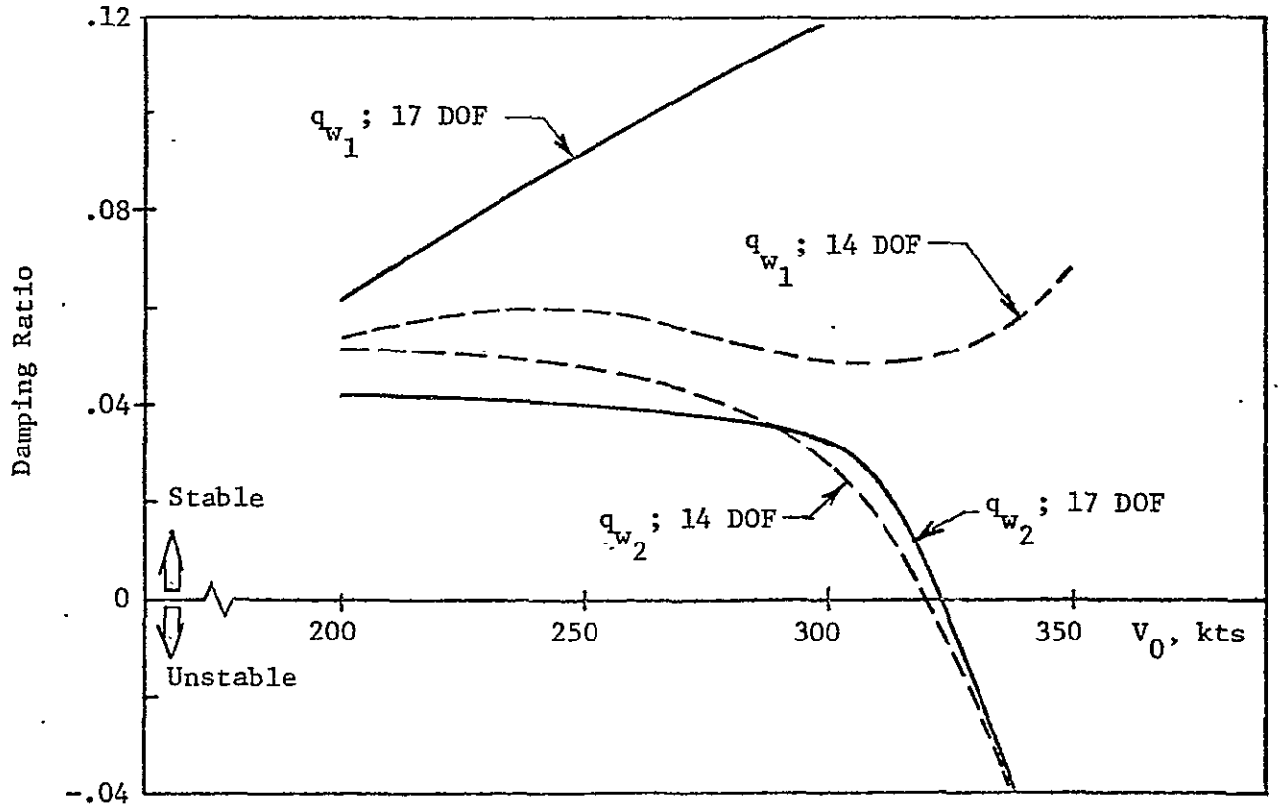

Figure 46. Wing q_{w_1} & q_{w_2} Motion Mode Characteristics; @ Constant Rotor RPM

Also shown is the influence of freeing the fuselage on the damping of the two modes. There is little effect shown on the damping of the chordwise mode however the damping of the spanwise mode is increased quite significantly apparently obtaining some additional damping from the freeing of the fuselage

The other case of interest here is that with the rotor RPM constant, i.e., the case of perfect engine governor. The eigenvalues in this case with the fuselage fixed and fuselage free are also shown in Figure 45. The general trend of the eigenvalues with speed are similar to the RPM free case. There is a difference in the collective mode ($\beta^{(1)}$) for reasons explained earlier.

As far as the stability of the system, or in other words the whirl flutter speed, there is little change in the damping of the q_{w_2} mode as shown in Figure 46. There is however a marked increase in damping of the q_{w_1} mode. This increase in damping arises apparently from the fact that wing spanwise bending causes a rotation of the rotor shaft with respect to space and thus if the proprotor RPM is assumed constant aerodynamic damping appears in the spanwise mode. If the RPM is free, then in effect no aerodynamic forces appear as a result of this rotation.

The constant RPM assumption also has a marked influence on the proprotor contribution to the phugoid damping as may be seen from Figure 47. At the higher flight speeds the phugoid becomes critically damped due to the large thrust variation with airspeed which does not appear for the free rotor RPM case.

Figure 47 compares the time to half amplitude in these two cases for the phugoid and the short period where it can be seen that the only significant difference between the eighteen and seventeen degree of freedom models occurs in the phugoid mode. The period change in the phugoid between the two cases is of course due to the difference in damping.

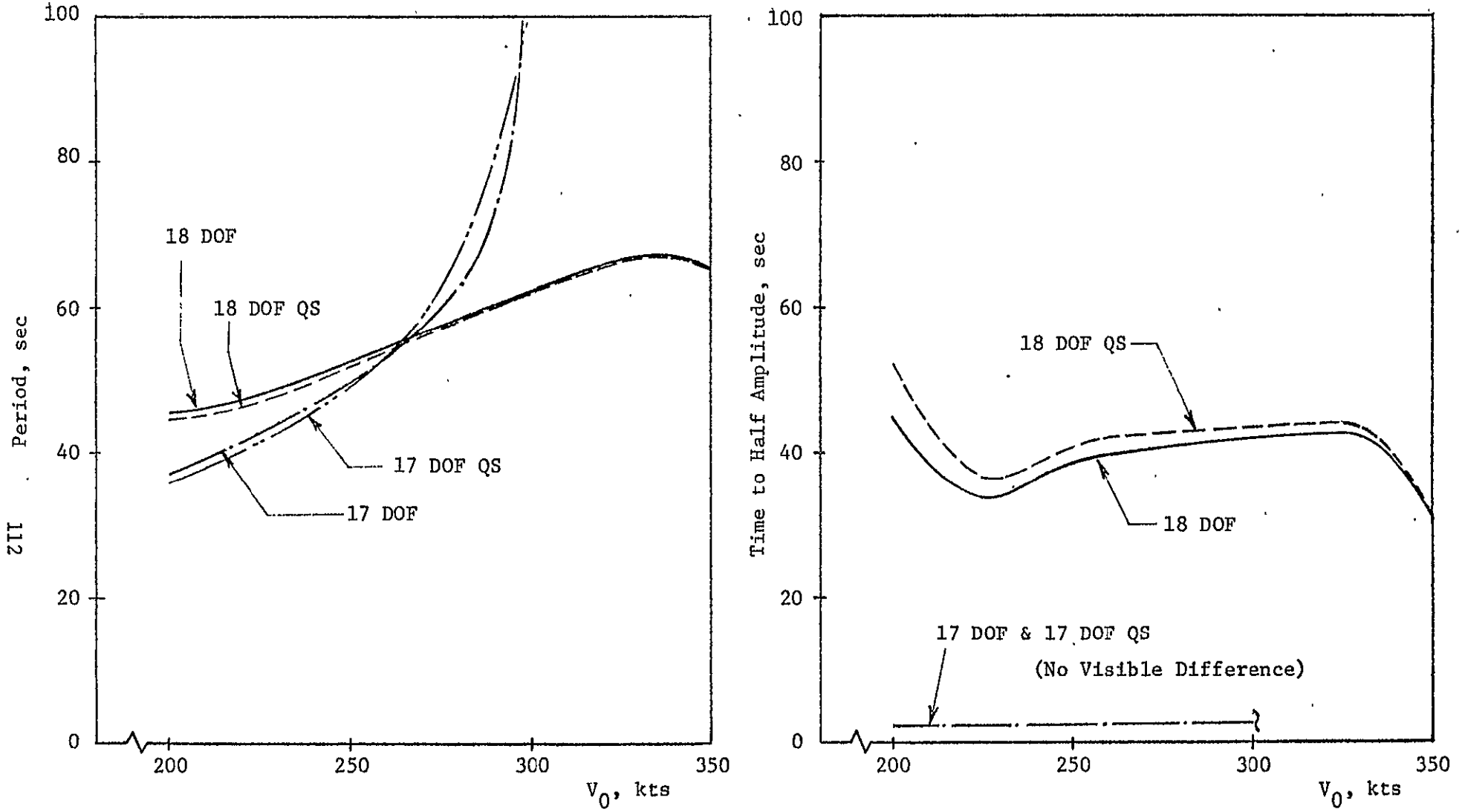

"QS" indicates that the Qasi-Static Approximation is applied to All Motion DOF except the Aircraft Longitudinal Rigid Body Motion DOF

Figure 47. Phugoid Mode Characteristics

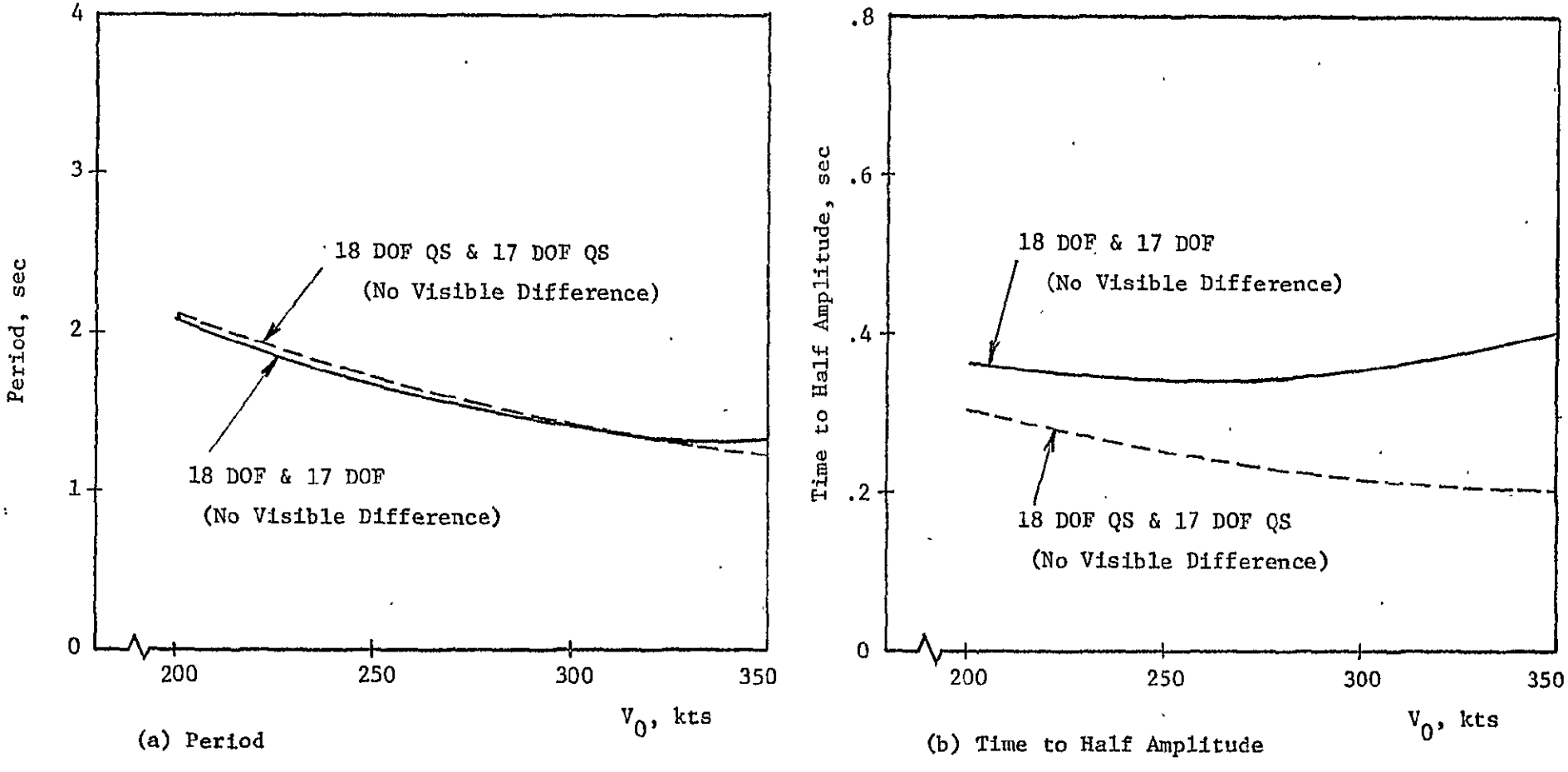

(a) Period

(b) Time to Half Amplitude

"QS" indicates that the Quasi-Static Approximation is Applied to All Motion DOF except the Aircraft Longitudinal Rigid Body Motion DOF

Figure 47. Short Period Mode Characteristics

We also examine at this point the influence of the aeroelastic degrees of freedom on the two low frequency modes associated with the stability and control characteristics of the aircraft. Also shown in Figure 47 are the quasistatic approximations to the low frequency motions, i.e., the dynamic terms associated with the aeroelastic effects are eliminated. This approximation must be made with care since we must retain the proper rate dependent aerodynamic contributions from the various modes. It can be seen that the only significant difference between the quasistatic approximation and the complete system dynamics is associated with the short period damping. Use of the quasistatic approximation results in an overestimation of the short period damping or time to half amplitude. It would be highly desirable in order to obtain insight into the aircraft dynamics to obtain a low order approximation to the short period motion including the effect of aeroelasticity. The following section considers this question in detail.

1.) Short Period Motion

First we consider the quasi-static approximation to the short period motion in order to justify an approximate way in which to account for the dynamics of the aircraft associated with its flexibility and then proceed to develop this approximation.

The short period equations of motion in an inertial frame of reference may be written as

$$\begin{bmatrix} (1 - \tilde{Z}_{\dot{w}})\,\tilde{s} - \tilde{Z}_{w} & -\tilde{Z}_{\dot{\theta}}\,\tilde{s} - \tilde{Z}_{\theta} \\ -\tilde{M}_{\dot{w}}\,\tilde{s} - \tilde{M}_{w} & \tilde{s}^2 - \tilde{M}_{\dot{\theta}}\,\tilde{s} - \tilde{M}_{\theta} \end{bmatrix} \begin{Bmatrix} \tilde{w}_f \\ \tilde{\theta}_f \end{Bmatrix} = 0 \qquad (82)$$

where

$$\tilde{Z}_{(\,)} = \frac{1}{M}\frac{\partial Z}{\partial (\,)} \qquad \tilde{M}_{(\,)} = \frac{1}{I}\frac{\partial M}{\partial (\,)}$$

These equations are written in dimensional real time ($\tilde{s} = s\Omega$). It is of course assumed that the center of gravity of the aircraft is fixed at one point and thus M is the total aircraft mass and the moment of inertia includes the rotor contributions as a point mass. Thus the rotor inplane force does not contain any inertia terms. The rotor blade inertia terms are included in the moment. This is important to keep in mind when we examine the dynamic form of the inplane force and moment in the following.

Note again that the conventional Eulerian frame is not being used for the short period which accounts for the fact that pitch attitude dependence of the aerodynamics appears in the equations and there is no inertial term depending on pitch rate in the normal force equation.

$\tilde{Z}_{\dot{w}}$ and $\tilde{M}_{\dot{w}}$ are the usual downwash lag derivatives. Note that the angle of attack change of the aircraft is equal to $(\theta_f - \frac{\tilde{w}_f}{V})$ so that the derivatives $\tilde{Z}_{\dot{\theta}}$ and $\tilde{M}_{\dot{\theta}}$ also include downwash lag effects in addition to the direct effects of pitch rate.

If we convert these equations of motion into dimensionless form consistant with the notation of the rest of this report,

$$\begin{bmatrix} (1 - Z_{\dot{w}})\, s - Z_w & -Z_{\dot{\theta}}\, s - Z_\theta \\ -M_{\dot{w}}\, s - M_w & s^2 - M_{\dot{\theta}} s - M_\theta \end{bmatrix} \begin{Bmatrix} w_f \\ \theta_f \end{Bmatrix} = 0 \qquad (82')$$

where

$$w_f = \frac{\tilde{w}_f}{V\Omega R}$$

$$Z_{\dot{w}} = \tilde{Z}_{\dot{w}} = \frac{y^2}{m^* V} \frac{2\gamma}{a\sigma} \frac{\partial C_Z}{\partial \dot{w}_f}$$

$$Z_w = \frac{\tilde{Z}_w}{\Omega} = (") \ (") \frac{\partial C_Z}{\partial w_f}$$

$$Z_{\dot{\theta}} = \frac{\tilde{Z}_{\dot{\theta}}}{V\Omega R}$$

$$Z_\theta = \frac{Z_\theta}{V\Omega^2 R}$$

$$M_{\dot{w}} = \tilde{M}_{\dot{w}} \ VR = \frac{1}{I^*} \frac{2\gamma}{a\sigma} \frac{\partial C_M}{\partial \dot{w}_f}$$

$$M_w = \tilde{M}_w \frac{VR}{\Omega}$$

$$M_{\dot{\theta}} = \frac{\tilde{M}_{\dot{\theta}}}{\Omega}$$

$$M_\theta = \frac{\tilde{M}_\theta}{\Omega^2}$$

and

$$m^* = \frac{M}{(y_{tw} R)^2 / \frac{N}{2} I_b} \qquad I^* = \frac{I}{\frac{N}{2} I_b}$$

$$C_Z = \frac{Z}{\rho \pi R^2 (\Omega R)^2} \qquad C_M = \frac{M}{\rho \pi R^3 (\Omega R)^2}$$

The various derivatives can be expressed as follows:

1.) The vertical acceleration derivatives ($\dot{w}_f$) are due to downwash lag and arise from the horizontal tail contributions. They are given by

$$\frac{2}{a\sigma} \frac{\partial C_Z}{\partial \dot{w}_f} = - \frac{\gamma V}{\pi a \sigma} S_H \ell_t \ c_w \ a_t \frac{d\varepsilon}{d\alpha}$$

$$\frac{2}{a\sigma} \frac{\partial C_M}{\partial \dot{w}_f} = \frac{\gamma V}{\pi a \sigma} S_H \ell_t^2 \ c_w^2 \ a_t \frac{d\varepsilon}{d\alpha}$$

2.) The vertical velocity derivatives (w_f) arise from the horizontal tail, rotors, wing and fuseage.

a.) horizontal tail

$$\frac{2\gamma}{a\sigma}\frac{\partial C_Z}{\partial w_f}\bigg|_{hT} = -\frac{\gamma V^2}{\pi a\sigma} S_H a_t \left(1 - \frac{d\varepsilon}{d\alpha}\right)$$

$$\frac{2\gamma}{a\sigma}\frac{\partial C_M}{\partial w_f}\bigg|_{hT} = \frac{\gamma V^2}{\pi a\sigma} S_H \ell_T c_w a_T \left(1 - \frac{d\varepsilon}{d\alpha}\right)$$

b.) rotor

$$\frac{2\gamma}{a\sigma}\frac{\partial C_Z}{\partial w_f}\bigg|_r = -\frac{2\gamma}{a\sigma}\frac{\partial C_H}{\partial \alpha_g}$$

$$\frac{2\gamma}{a\sigma}\frac{\partial C_M}{\partial w_f}\bigg|_r = -\frac{2\gamma}{a\sigma}\frac{\partial C_{MY}}{\partial \alpha_g}$$

owing to the equivalence between a gust input α_g and a vertical velocity of the aircraft w_f

c.) wing

$$\frac{2\gamma}{a\sigma}\frac{\partial C_Z}{\partial w_f}\bigg|_w = -\frac{\gamma V^2}{\pi a\sigma} 2 S_w a_w$$

$$\frac{2\gamma}{a\sigma}\frac{\partial C_M}{\partial w_f}\bigg|_w = -\frac{\gamma V^2}{\pi a\sigma} 2 S_w \ell_w c_w a_w$$

where ℓ_w is the distance between the aircraft center of gravity and the wing MAC (divided by $c_w R$)

d.) fuselage

$$\frac{2\gamma}{a\sigma}\frac{\partial C_Z}{\partial w_f}\bigg|_f = -\frac{\gamma V^2}{\pi a\sigma} S_f C_{\ell_{f_\alpha}}$$

$$\frac{2\gamma}{a\sigma}\frac{\partial C_M}{\partial w_f}\bigg|_f = -\frac{\gamma V^2}{\pi a\sigma} S_f c_w C_{M_{f_\alpha}}$$

3.) The pitch rate derivatives ($\dot{\theta}_f$) arise from the horizontal tail and the rotors with a small contribution from the wing

a.) horizontal tail

$$\frac{2\gamma}{a\sigma}\left.\frac{\partial C_Z}{\partial \dot{\theta}_f}\right|_{h_t} = \frac{\gamma V}{\pi a\sigma} S_H \ell_T c_w a_T\left(1 - \frac{d\varepsilon}{d\alpha}\right)$$

$$\frac{2\gamma}{a\sigma}\left.\frac{\partial C_M}{\partial \dot{\theta}_f}\right|_{h_t} = -\frac{\gamma V}{\pi a\sigma} S_H \ell_T^2 c_w^2 a_T\left(1 + \frac{d\varepsilon}{d\alpha}\right)$$

b.) rotors. Noting the equivalence between $\dot{\theta}_f$ and $\dot{\alpha}_y$

$$\frac{2\gamma}{a\sigma}\left.\frac{\partial C_Z}{\partial \dot{\theta}_f}\right|_{r} = \frac{2\gamma}{a\sigma}\frac{\partial C_H}{\partial \dot{\alpha}_y}$$

$$\frac{2\gamma}{a\sigma}\left.\frac{\partial C_M}{\partial \dot{\theta}_f}\right|_{r} = \frac{2\gamma}{a\sigma}\frac{\partial C_M}{\partial \dot{\alpha}_y}$$

c.) The wing produces a small contribution

$$\frac{2\gamma}{a\sigma}\left.\frac{\partial C_Z}{\partial \dot{\theta}_f}\right|_{w} = -\frac{\gamma V}{\pi a\sigma} 2 S_w \ell_w c_w a_w$$

$$\frac{2\gamma}{a\sigma}\left.\frac{\partial C_Z}{\partial \dot{\theta}_f}\right|_{w} = -\frac{\gamma V}{\pi a\sigma} 2 S_w \ell_w^2 c_w^2 a_w$$

The fuselage contribution is neglected.

4.) The pitch attitude derivatives are directly related to the vertical velocity derivatives,

$$\frac{2\gamma}{a\sigma}\frac{\partial C_Z}{\partial \theta_f} = -\frac{2\gamma}{a\sigma}\frac{\partial C_Z}{\partial w_f}$$

$$\frac{2\gamma}{a\sigma}\frac{\partial C_M}{\partial \theta_f} = -\frac{2\gamma}{a\sigma}\frac{\partial C_M}{\partial w_f}$$

These various derivatives are numerically evaluated using the parameters of the aircraft given in Table III to yield the results given in Table IV.

We now proceed to examine the characteristic equation for the short period motion.

Using the equivalences, $Z_w = - Z_\theta$, $M_w = - M_\theta$, and noting that the derivative $Z_{\dot{w}}$ is negligible compared to 1, the characteristic equation for the short period mode is obtained from equation (82') is

$$\Delta_{Sp} = s^2 + [- Z_w - M_{\dot{\theta}} - Z_{\dot{\theta}} M_{\dot{w}}] \; s + [Z_w M_{\dot{\theta}} - M_\theta - Z_{\dot{\theta}} M_w - Z_\theta M_{\dot{w}}] = 0 \qquad (83)$$

Consider the numerical contributions of the derivatives to the stiffness and damping terms in this quadratic equation

$$(- Z_w) + (- M_{\dot{\theta}}) + (- Z_{\dot{\theta}} M_{\dot{w}})$$

$$(0.0362) + (0.108) + (- 0.0012) = 0.143$$

$$Z_w M_{\dot{\theta}} + (- M_\theta) + (- Z_{\dot{\theta}} M_w) + (- Z_\theta M_{\dot{w}})$$

$$(0.00391) + (0.0106) + (0.00039) + (- 0.00121) = 0.0129$$

The characteristic roots are

$$s_{1,2} = - 0.072 \pm 0.088 \; i$$

The damping ratio and natural frequency are

$$\zeta_{sp} = 0.63 \qquad \omega_{sp} = 0.114$$

Total Aircraft:	Horizontal Tail:
AFT CG (FS 298.2, WL 73.63) $m_a^* = 712$ (Gross Weight 13000 lbs) $I_a^* = 81.9$ ($I_a = 12903$ slug×ft^2) $V = .844$ (300 kts when $\Omega R = 600$ ft/sec)	$S_H = .322$ $\ell_t = 4.23$ $a_t = 4.13$ $\frac{d\epsilon}{d\alpha} = .335$
Rotor:	**Wing:**
$N = 3$ $a = 5.7$ $\sigma = .089$ $I_b = 105$ slug×ft^2 $\gamma = 3.83$ $I_\beta^* = I_{\beta\alpha}^* = 1.0$ $I_\zeta^* = .67$ $\nu_\beta^2 = 1.0355$ $\nu_\zeta = 1.33$ $h = .361$ $K_p = -.344$ $K_{p_\zeta} = -.3$	$2S_w = 1.101$ ($= 2\, y_{Tw}\, c_w$) $y_{Tw} = 1.333$ $c_w = .413$ $\ell_w = .107$ $a_w = 4.58$
	Fuselage:
	$S_f = .206$ $C_{Lf_\alpha} = 3.64$ $C_{mf_\alpha} = 7.10$

Table III. Data Used for the Evaluation of the Derivatives Shown in Table IV.

	Horizontal Tail	Rotors (Two)	Wing	Fuselage	Total
$\frac{2\gamma}{a\sigma}\frac{\partial C_z}{\partial \hat{w}_f}$	- 1.57	(*)	(*)	(*)	- 1.57
$\hat{Z}_{\dot{w}}$	-.00465				-.00465
$\frac{2\gamma}{a\sigma}\frac{\partial C_z}{\partial w_f}$	- 1.51	-.406 × 2	- 8.64	- 1.28	-12.2
$\hat{Z}_w$	-.00446	-.00240	-.0255	-.00379	-.0362
$\frac{2\gamma}{a\sigma}\frac{\partial C_z}{\partial \dot{\theta}_f}$	6.27	3.29 × 2	-.454	(*)	12.4
$\hat{Z}_{\dot{\theta}}$	.0185	.0194	-.0013		.0366
$\frac{2\gamma}{a\sigma}\frac{\partial C_z}{\partial \theta_f}$	1.51	.406 × 2	8.64	1.28	12.2
$\hat{Z}_{\theta}$	.00446	.00240	.0255	.00379	.0362
$\frac{2\gamma}{a\sigma}\frac{\partial C_m}{\partial \hat{w}_f}$	2.75	(*)	(*)	(*)	2.75
$\hat{M}_{\dot{w}}$	.0335				.0335
$\frac{2\gamma}{a\sigma}\frac{\partial C_m}{\partial w_f}$	2.64	-.175 × 2	-.382	- 1.03	.869
$\hat{M}_w$	.0322	-.00427	-.00467	-.0126	.0106
$\frac{2\gamma}{a\sigma}\frac{\partial C_m}{\partial \dot{\theta}_f}$	- 10.9	1.05 × 2	-.0200	(*)	-8.86
$\hat{M}_{\dot{\theta}}$	-.133	.0256	-.0002		-.108
$\frac{2\gamma}{a\sigma}\frac{\partial C_m}{\partial \theta_f}$	- 2.64	.175 × 2	.382	1.03	-.869
$\hat{M}_{\theta}$	-.0322	.00427	.00467	.0126	-.0106

(*) : neglected

Table IV. Derivatives: Results of Numerical Evaluation for the Case Given in Table III.

This is the quasi-static prediction of the short period characteristic. Noting from previous sections that the low frequency rotor flapping mode has a frequency approximately equal to 0.18 it can be seen that this frequency is reasonably close to the short period motion and would be expected therefore that including in some approximate way the coupling of this mode to the short period would be the source of the discrepancy in damping between the complete model and the quasi-static model described previously.

First consider the relative magnitude of the contributions of the various derivatives to the short period motion and in particular the rotor contributions. The primary contribution to the damping is $M_{\dot{\theta}}$ and next in importance is Z_w. The influence of $Z_{\dot{\theta}}M_{\dot{w}}$ is small. From Table IV it can also be seen that the rotor contribution to these three terms are 18%, 1.7% and 0.5% respectively. Therefore we can conclude that the important contribution of the rotor to the damping term is through $M_{\dot{\theta}}$.

In the stiffness term, the most important contribution is M_θ. The rotor contribution to this term is approximately 42% of the total. The next term in order of size is $Z_w M_{\dot{\theta}}$ and from Table IV the rotor contribution to Z_w is about 6% and 24% of $M_{\dot{\theta}}$. Therefore it can be assumed that the primary contribution of the rotor to this term is through $M_{\dot{\theta}}$. The last two terms in the stiffness are relatively small and especially when the rotor contributions to them are considered (Table IV) it is found that they may be neglected. Thus we may conclude that the important rotor contributions to the stiffness are through the terms M_θ and $M_{\dot{\theta}}$.

Now in order to include the rotor dynamics in the short period motion we consider the following approach. The rotor contribution to the pitch attitude and pitch rate derivatives are expressed as

$$-\frac{2\gamma}{a\sigma}\frac{\partial C_M}{\partial \dot{\theta}_f} = -A\, G_{\dot{\theta}_f}(s)$$

$$-\frac{2\gamma}{a\sigma}\frac{\partial C_M}{\partial \theta_f} = -A'\, G_{\theta_f}(s)$$

where A and A' are the rotor derivatives when the quasi-static approximation is made and $G_{\dot{\theta}_f}$ and G_{θ_f} are transfer frunctions which include the effect of rotor dynamics.

Since there is an equivalence such that

$$\frac{\partial(\ )}{\partial \dot{\alpha}_y} = \frac{\partial(\ )}{\partial \dot{\theta}_f}$$

and

$$\frac{\partial(\ )}{\partial \alpha_g} = \frac{\partial(\ )}{\partial \theta}$$

we can obtain approximations to the dynamic effects by considering the rotor hub moment frequency response characteristics to $\dot{\alpha}_y$ and α_g which can be calculated from expressions previously given.

Figures 48 and 49 show the frequency response characteristics of the rotor hub moment to sinusoidal inputs in $\dot{\alpha}_y$ and α_g. Since many factors contribute to these frequency response characteristics it is difficult to obtain simple analytical expressions for the transfer characteristics $G_{\dot{\theta}_f}(s)$ and $G_{\theta_f}(s)$. However, second order approximations can be developed

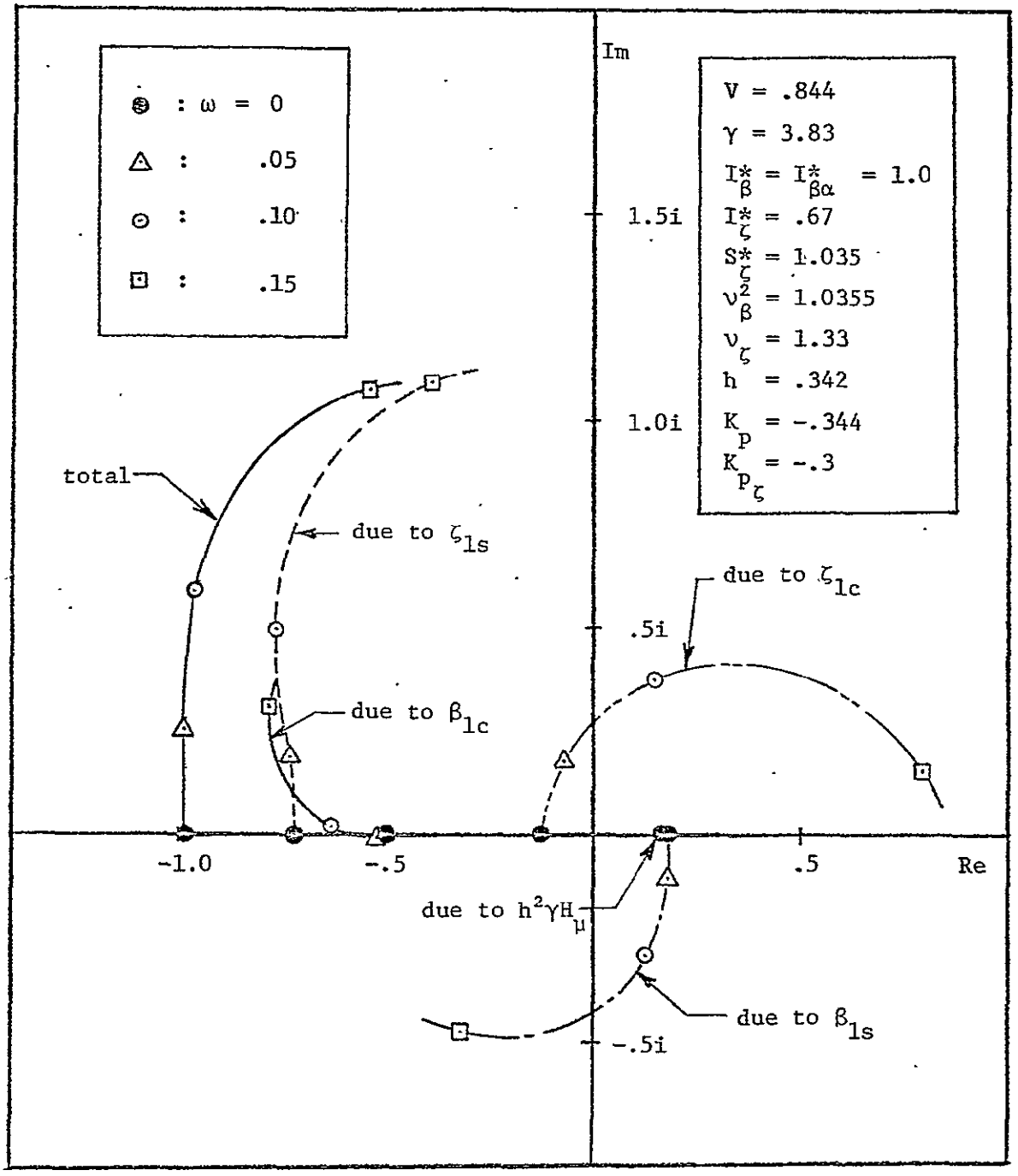

Figure 48. Polar Plot: Frequency Response of the Pivot Pitching Moment to the Shaft Pitch Rate Input

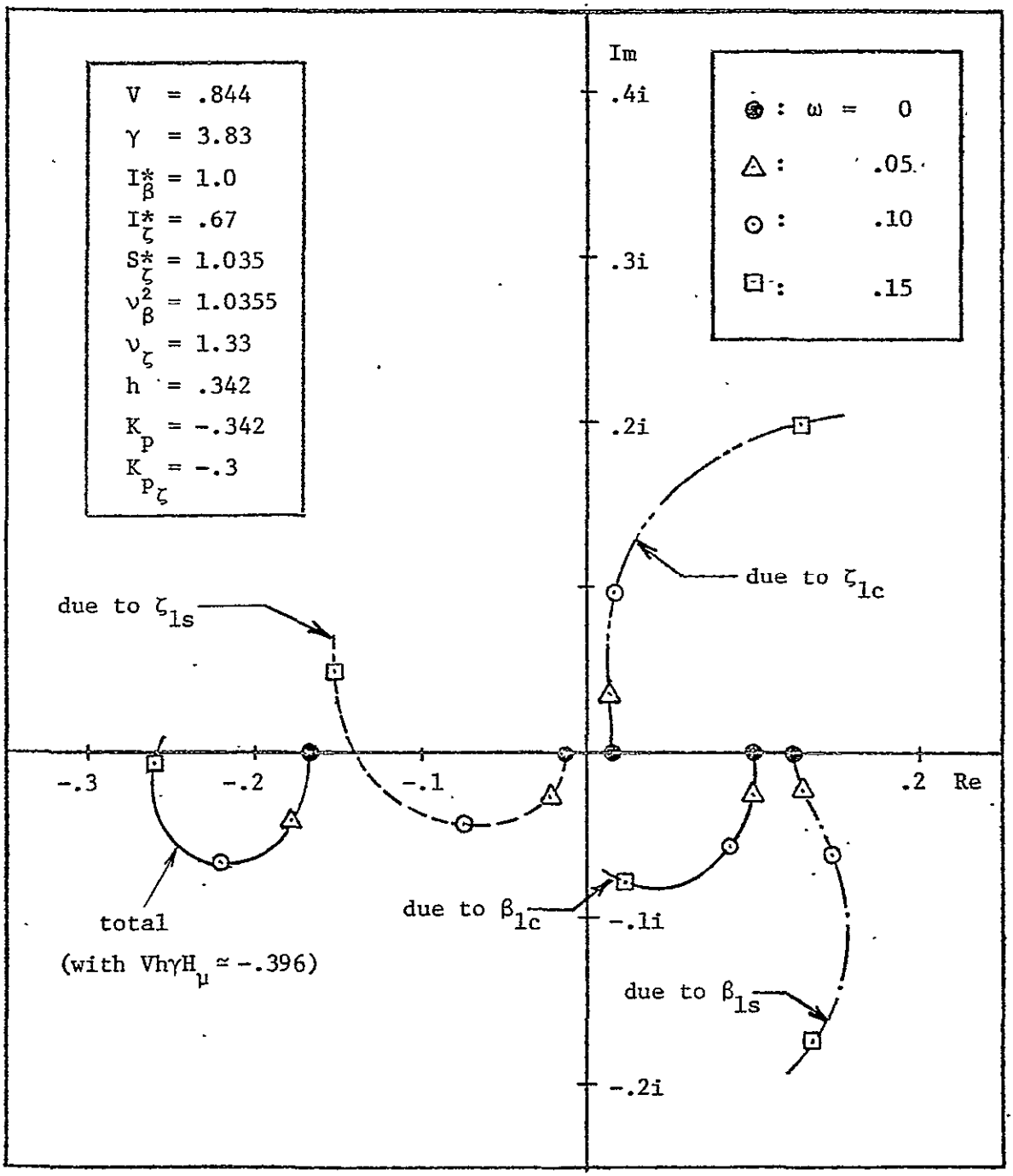

Figure 49. Polar Plot: Frequency Response of the Pivot Pitching Moment to Normal Gust Input.

so that,

$$G_{\dot{\theta}_f}(s) = \frac{(0.20)^2}{s^2 + (2)(0.46)(0.20)\ s + (0.20)^2}$$

$$G_{\theta_f}(s) = \frac{0.76\ s^2 + 0.37\ s + (0.20)^2}{s^2 + 2\ (0.46)(0.20)\ s + (0.20)^2} \tag{84}$$

The agreement between these approximate transfer functions and the exact ones are shown in Figure 50 indicating that a good match is obtained by second order form up to a frequency of 0.1.

We can now use root locus techniques to examine the effect of rotor dynamics on the short period motion.

First consider only the rate effect of the rotor written as

$$(M_{\dot{\theta}})_R \left\{\frac{(0.20)^2}{s^2 + (2)(0.46)(0.20)\ s + (0.20)^2}\right\}$$

$$= (M_{\dot{\theta}})_R - (M_{\dot{\theta}})_R \left\{\frac{(s)\ (s + 2\ (0.46)(0.20))}{s^2 + (2)(0.46)(0.20)\ s + (0.20)^2}\right\} \tag{85}$$

So that the total pitch damping can be written as

$$M_{\dot{\theta}} - (M_{\dot{\theta}})_R \left\{\frac{(s)\ (s + 2\ (0.46)(0.20))}{s^2 + (2)(0.46)(0.20)\ s + (0.20)^2}\right\}$$

$M_{\dot{\theta}}$ is the quasi-static damping. The characteristic equation may be written in root locus form as

$$1 + (M_{\dot{\theta}})_R \left\{\frac{(s)\ (s - Z_w)\ (s + 0.184)}{\Delta_{sp}\ [s^2 + 2\ (0.46)(0.20)\ s + (0.20)^2]}\right\} = 0 \tag{86}$$

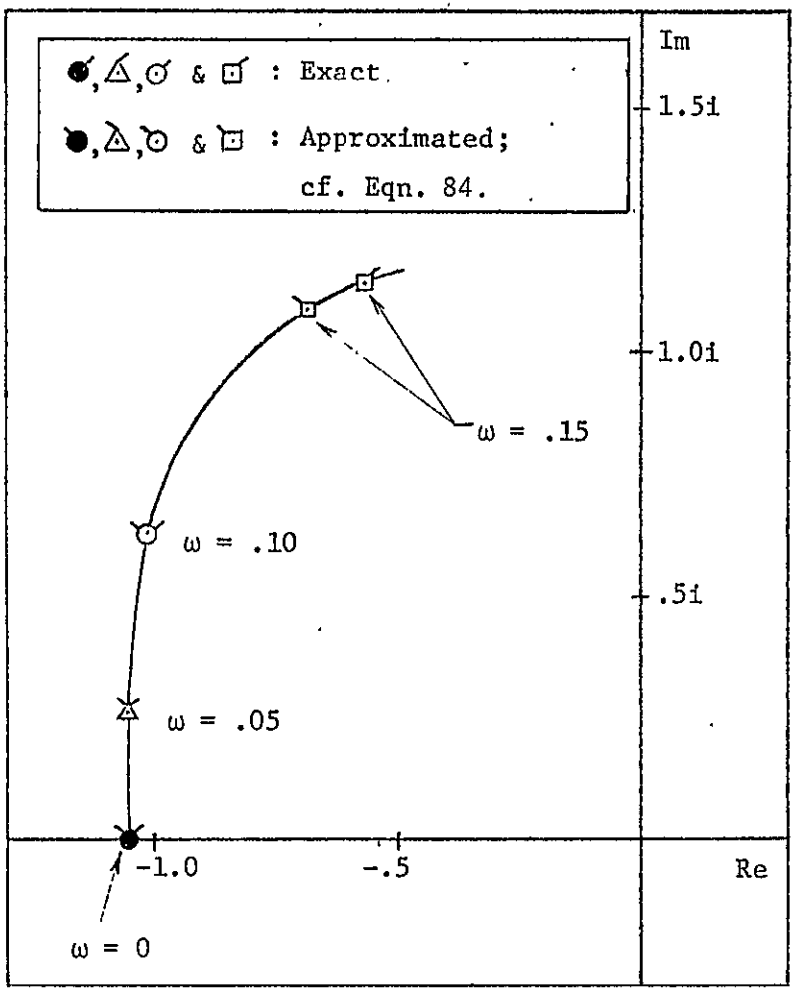

(a) Pitching Moment to $\dot{\theta}_f$ Input

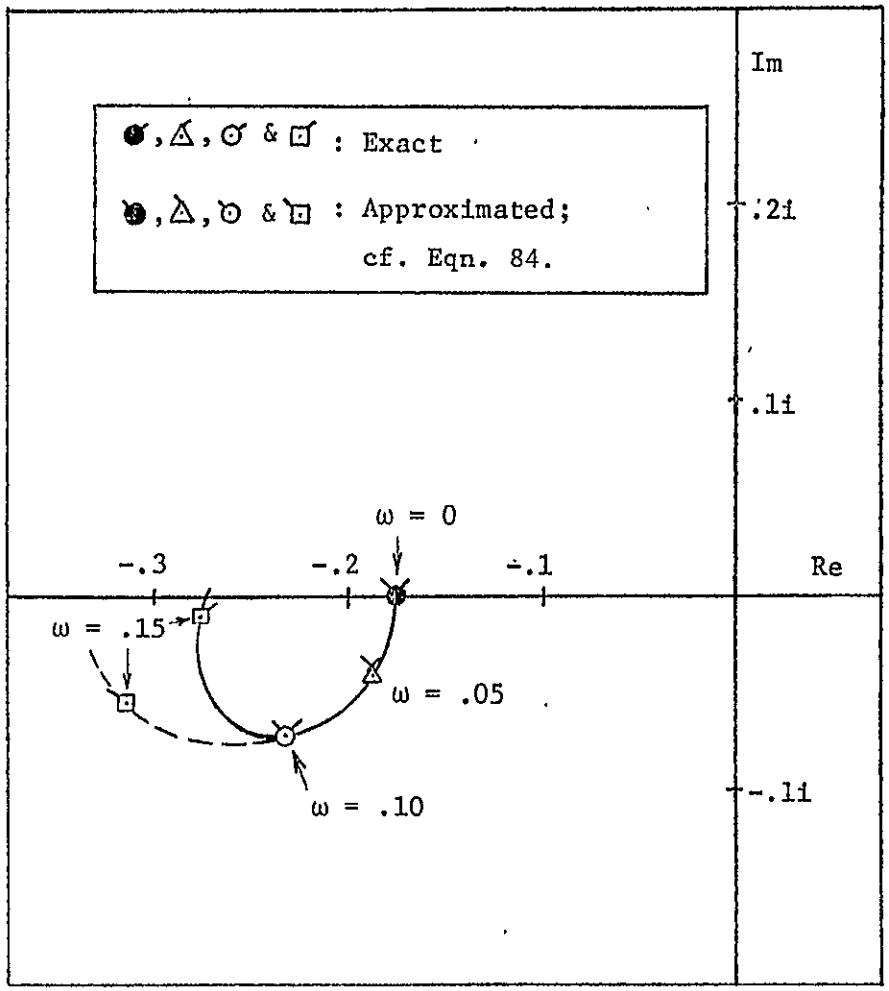

(b) Pitching Moment to θ_f Input

Figure 50. Polar Plot: Frequency Response of Pitching Moment due to Rotor about Aircraft CG to $\dot{\theta}_f$ and θ_f Inputs; Comparison with the Approximate Transfer Functions

$V = .844$, $\gamma = 3.83$, $I^*_\beta = I^*_{\beta\alpha} = 1.0$
$I^*_\zeta = .67$, $S^*_\zeta = 1.035$, $\nu^2_\beta = 1.0355$,
$\nu_\zeta = 1.33$, $\underline{h = .361}$, $K_p = -.344$, $K_{p_\zeta} = -.3$

where Δ_{sp} is the quasi-static short period motion.

The root locus shown in Figure 51 shows the effect of the gain $(M_{\dot{\theta}})_R$ indicating that the dynamic response of the rotor force to pitch rate and consequently coupling between the rotor dynamics and the short period produces a loss in damping.

If we now also include the influence of the rotor dynamics in the attitude derivative M_{θ} , the characteristic equation can be expressed as

$$\Delta_{sp} + (M_{\dot{\theta}})_R \left\{ \frac{s\left[(s + 0.184)(s - Z_w) + 0.24\ (s - 0.78)\ \frac{(M_{\theta})_R}{(M_{\dot{\theta}})_R}\right]}{s^2 + 2\ (0.46)(0.20)\ s + 0.20)^2} \right\} = .0 \qquad (87)$$

This can be placed in root locus form with the ratio $(\frac{M_{\theta}}{M_{\dot{\theta}}})_R$ constant and the results of the influence of these terms on the short period are also shown in Figure 51. Using values from Table IV gives the short period dynamics shown. The characteristic roots are now

$$s = - 0.063 \pm 0.088i$$

giving a damping ratio and a natural frequency

$$\zeta'_{sp} = 0.58$$

$$\omega'_{sp} = 0.108$$

Thus using this approximate model indicates a loss in short period damping due to the coupling between the rotor modes and the body modes. The approximate results also agree well with the complete dynamic model.

Unfortunately, the amount of algebra involved precluded finding analytical expressions for these transfer functions representing the blade

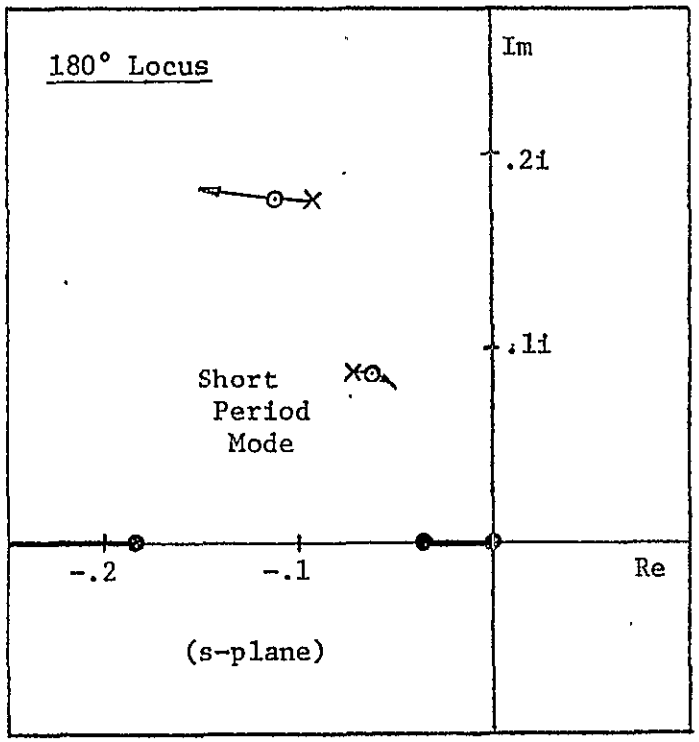

(a) With Rotor Dynamics Reflected in $M_{\dot{\theta}}$ Only; cf. Characteristic Eqn. (86);

⊙ : $[M_{\dot{\theta}}]_R$ = .0256

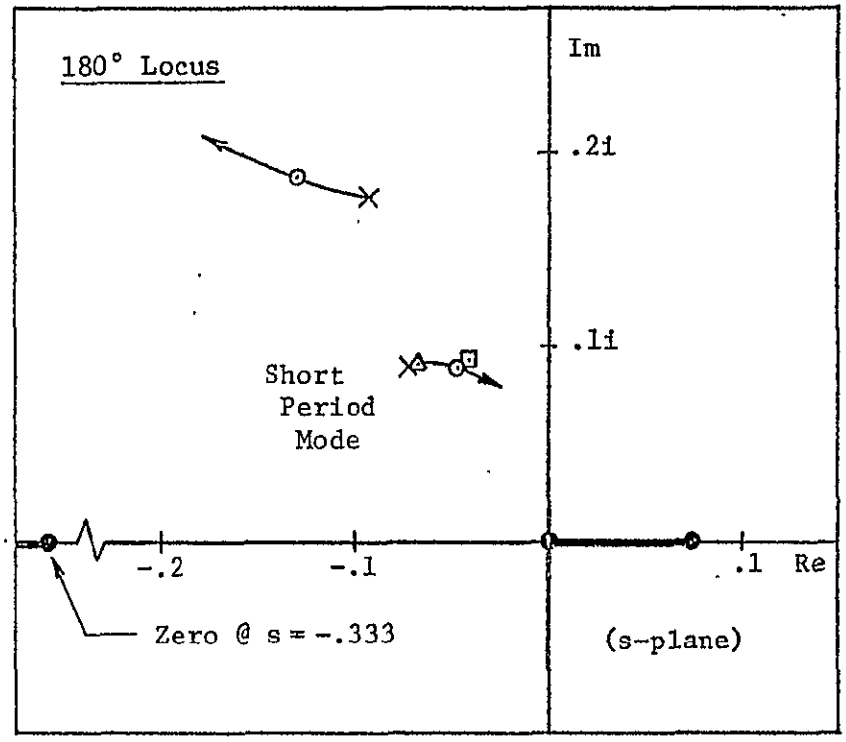

(b) With Rotor Dynamics Reflected in Both $M_{\dot{\theta}}$ and M_{θ}; cf. Characteristic Eqn. (86);

⊙ : $[M_{\dot{\theta}}]_R$ = .0256 (@ $[M_{\theta}]_R/[M_{\dot{\theta}}]_R$ = .167)

⊡ : Result of Fig. 47 with Complete Rotor Dynamics Retained (18 DOF Model)

△ : Same as Above, but with QS Approximation Applied to All Motion DOF except Aircraft Longitudinal Rigid Body Motion DOF

Figure 51. Root Locus: Influence of Rotor Dynamics on Aircraft Short Period Mode Characteristics for the Case Given in Table III. V_o = 300 kts.

dynamics. It can be seen that the natural frequency in the denominator lies relatively close to the lower flap mode.

It then appears that the rotor dynamics should be included in predicing the short period characteristics of this type of vehicle. It is not clear at this time how the flap natural frequency ν_β would influence this conclusion. Other studies on helicopters have indicated that as the flap frequency is increased it becomes important to include this coupling between blade motion and fuselage motion.

It is further interesting to note that the trend of the two modes, the short period and the lower gimbal mode (β_G - 1) are such that the coupling increases with airspeed. It can be seen from Figure 45 that the lower gimbal mode frequency decreases with airspeed and the short period frequency increases with airspeed and thus there is more significant coupling between these two modes as airspeed increases. This trend is also supported by the increasing departure of the short period dynamics predicted by the quasi-static model compared to the complete model as shown in Figure 45.

INFLUENCE OF FEEDBACK WITH FUSELAGE FREE

We now examine the influence of various feedbacks using the complete or eighteen degree of freedom model.

First we consider the effect of body motion feeback such as might be employed to improve the stability and control characteristics of the aircraft. Figure 52 shows the influence of a combination of pitch rate and pitch attitude feedback to the elevator on the dynamics. This feedback of course improves the damping of the phugoid as shown in the figure and also increases the short period damping and frequency. The only other significant changes occur in the two wing bending modes, where as might be expected, as the gain is increased, the frequencies are lowered and the spanwise bending mode is destabilized. Infinite gain essentially corresponds to the fuselage fixed case and so the trends with increasing gain are essentially the reverse of those shown in Figure 46 with respect to freeing the fuselage. As indicated in Figure 52 a large value of the feedback gain does produce an instability.

Figures 53 through 59 show the influence of various wing motion feedbacks considered earlier for the complete system dynamics.

In general it may be noted that there is little change from the simpler model with fuselage fixed considered earlier, particularly for any reasonable level of gain. Compare for example Figures 53 with Figure 36. It can be seen that there is very little change in the influence of wing motion feedbacks on the dynamics of the system whether the fuselage is free or fixed.

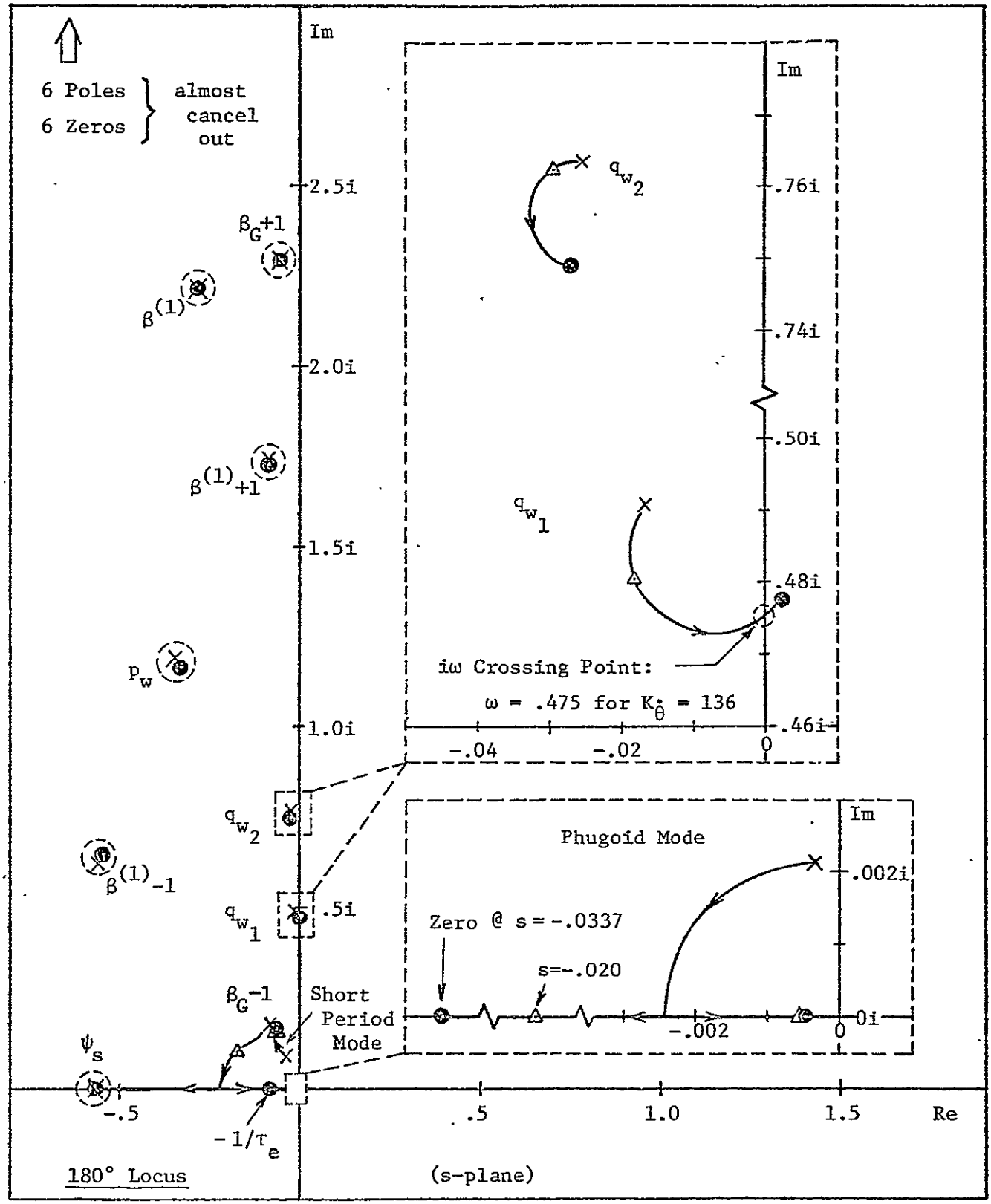

Feedback Law: $\delta_e = K_{\dot\theta}\ (s + 1/\tau_e)\ \theta_f$ with $K_{\dot\theta} > 0$ & $1/\tau_e = .0833\ (\rightarrow 4.0\ \text{sec}^{-1})$

Δ: $K_{\dot\theta} = 10$ (20 dB) → { Pitch Rate: .20°/(°/sec)
Pitch Attitude: .83°/°

Figure 52. Root Locus: Effect of $\theta_f \rightarrow \delta_e$ Feedback; 18 DOF Model @ V = .844 (300 kts)

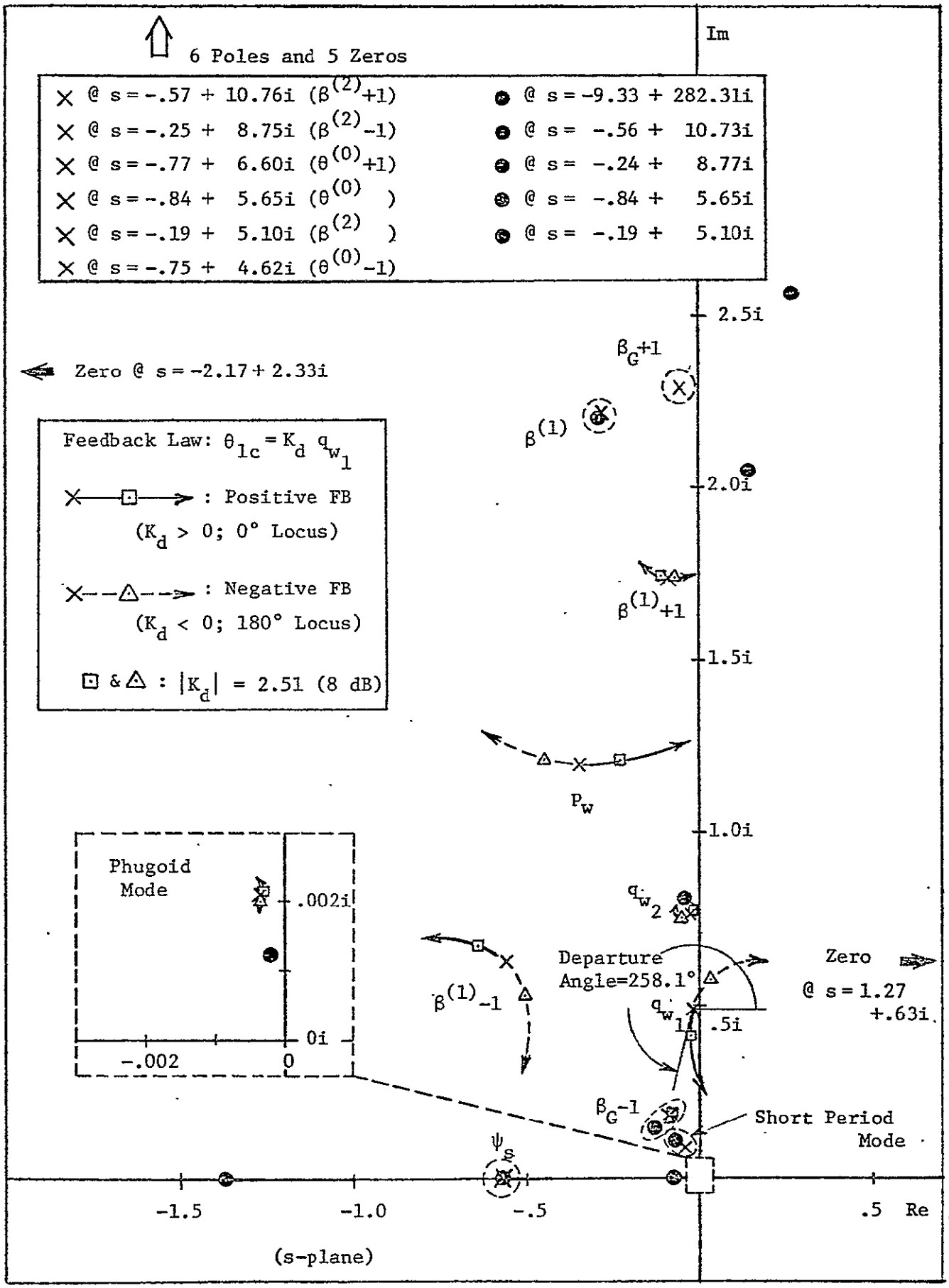

Figure 53. Root Locus: Effect of $q_{w_1} \rightarrow \theta_{1c}$ Feedback (Proportional); 18 DOF Model @ V = .844 (300 kts)

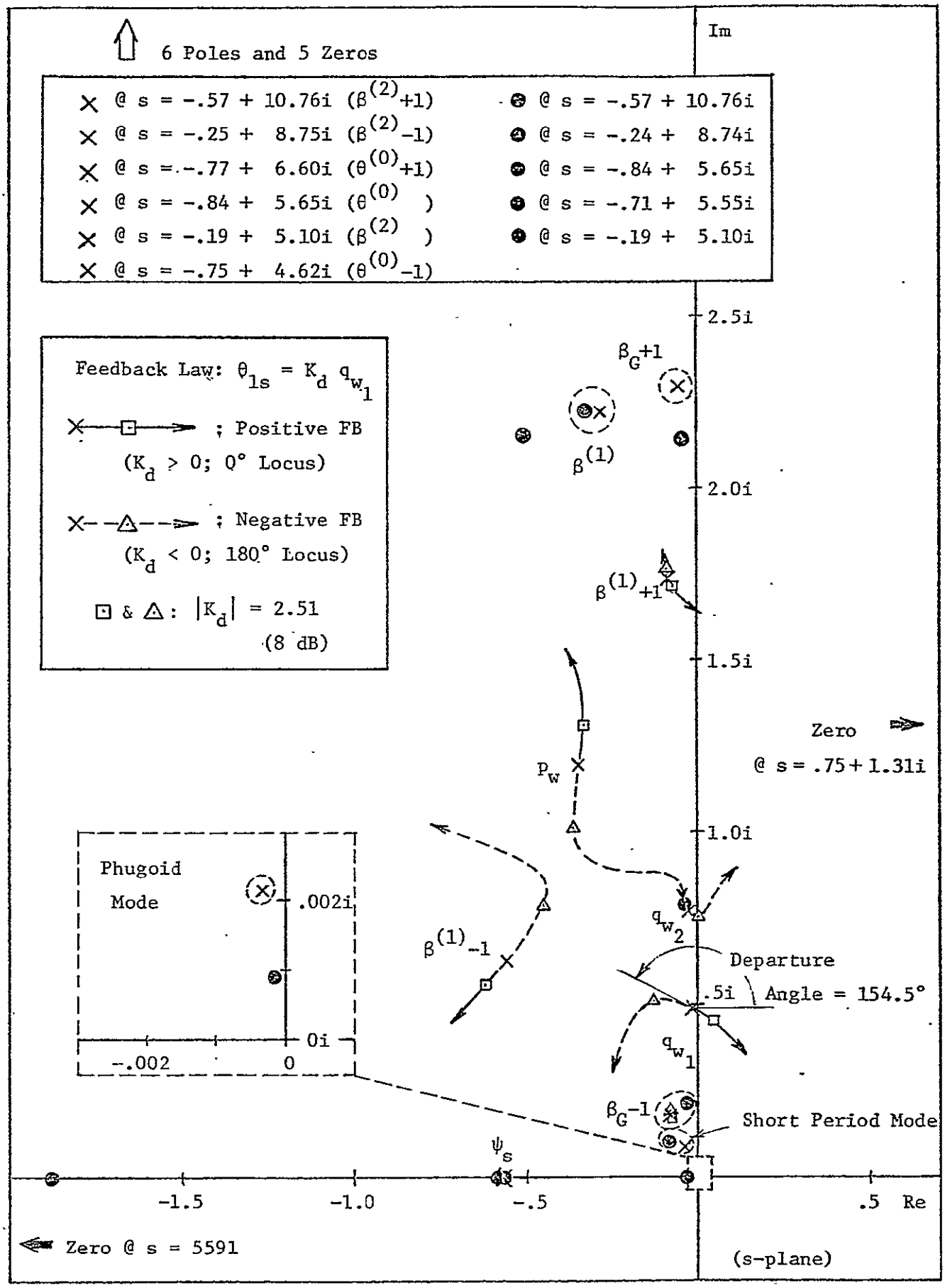

Figure 54. Root Locus: Effect of $q_{w_1} \rightarrow \theta_{1s}$ Feedback (Proportional); 18 DOF Model @ V = .844 (300 kts)

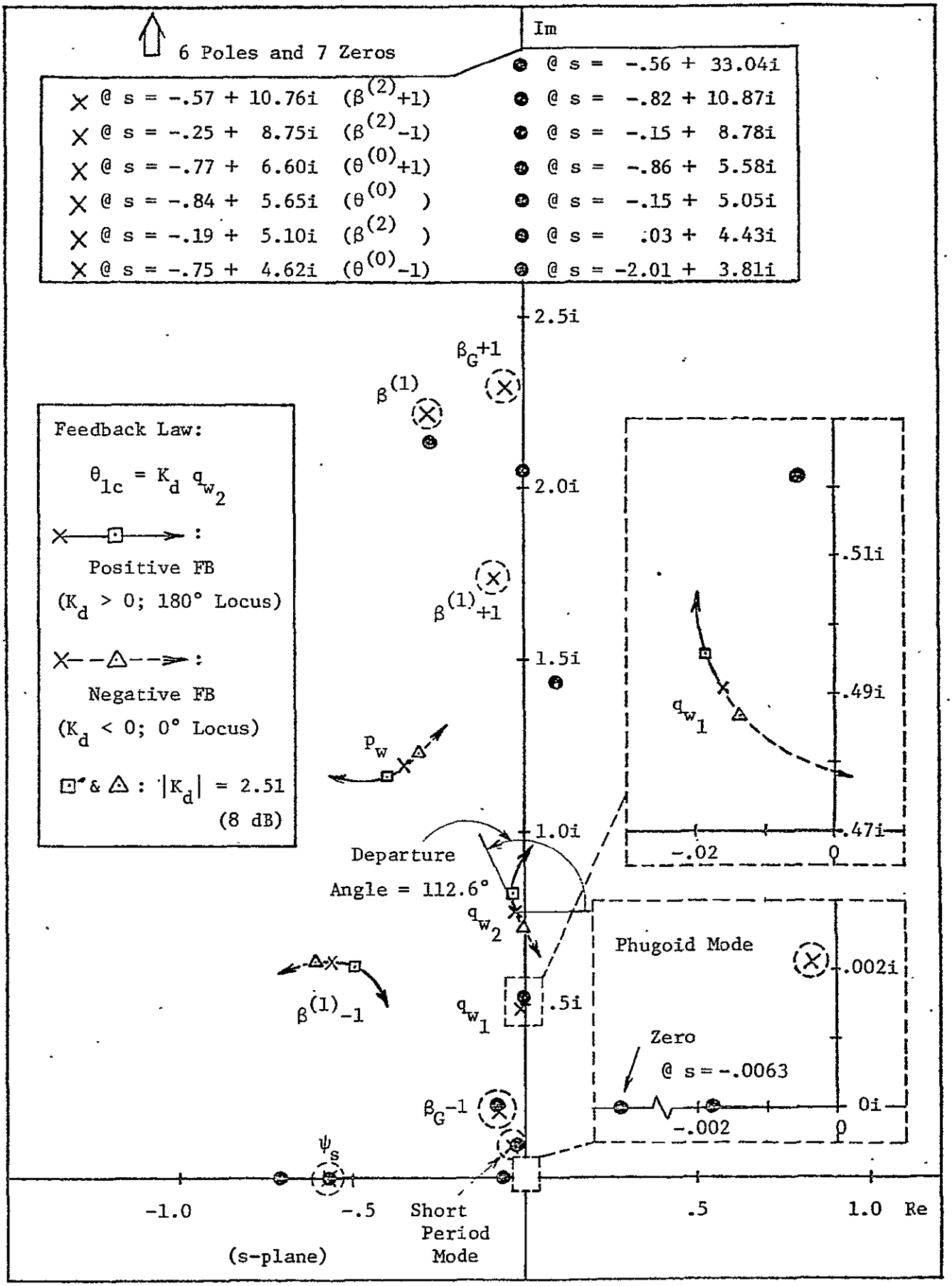

Figure 55. Root Locus: Effect of $q_{w_2} \rightarrow \theta_{1c}$ Feedback (proportional); 18 DOF Model @ V = .844 (300 kts)

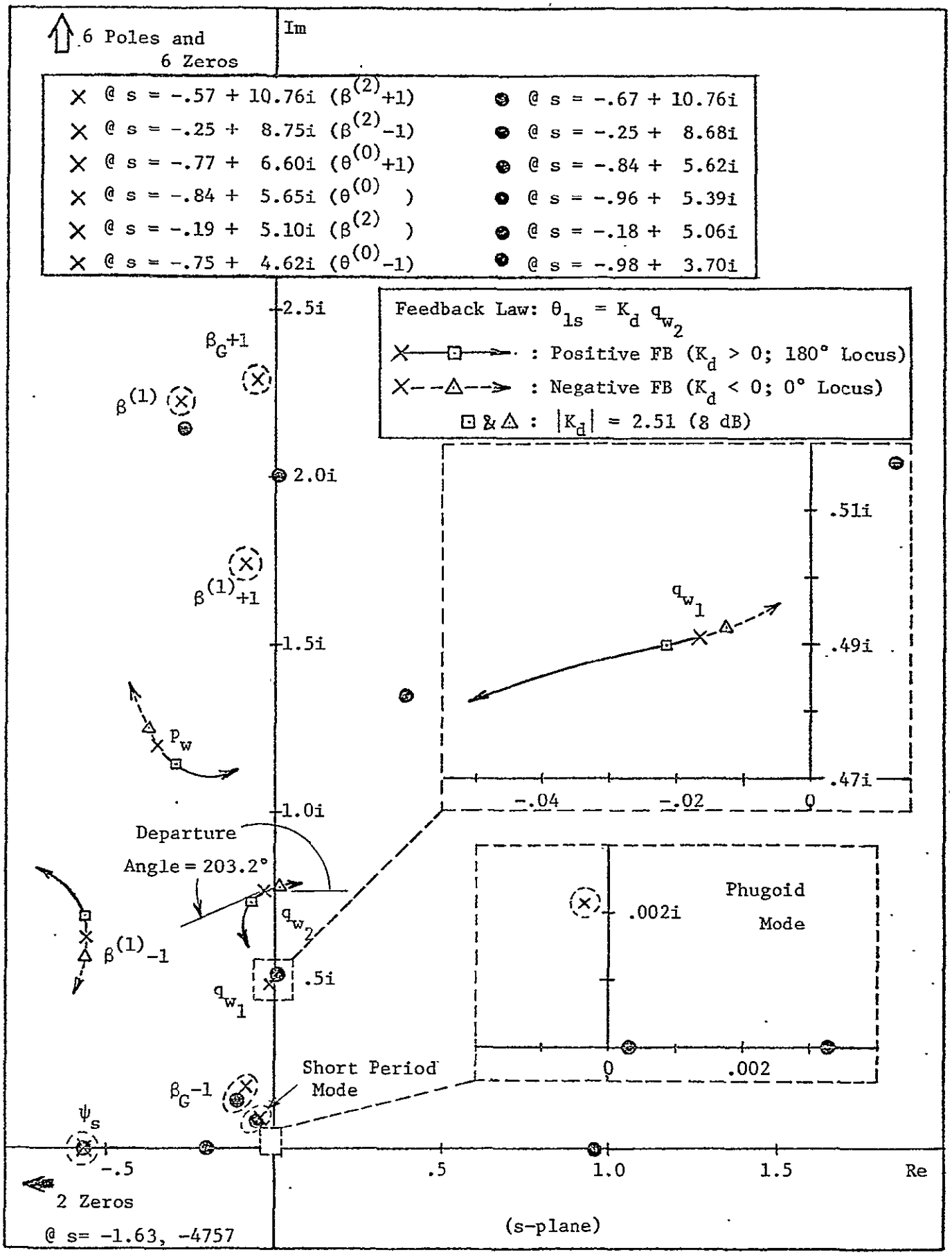

Figure 56. Root Locus: Effect of $q_{w_2} \rightarrow \theta_{1s}$ Feedback (Proportional); 18 DOF Model @ V = .844 (300 kts)

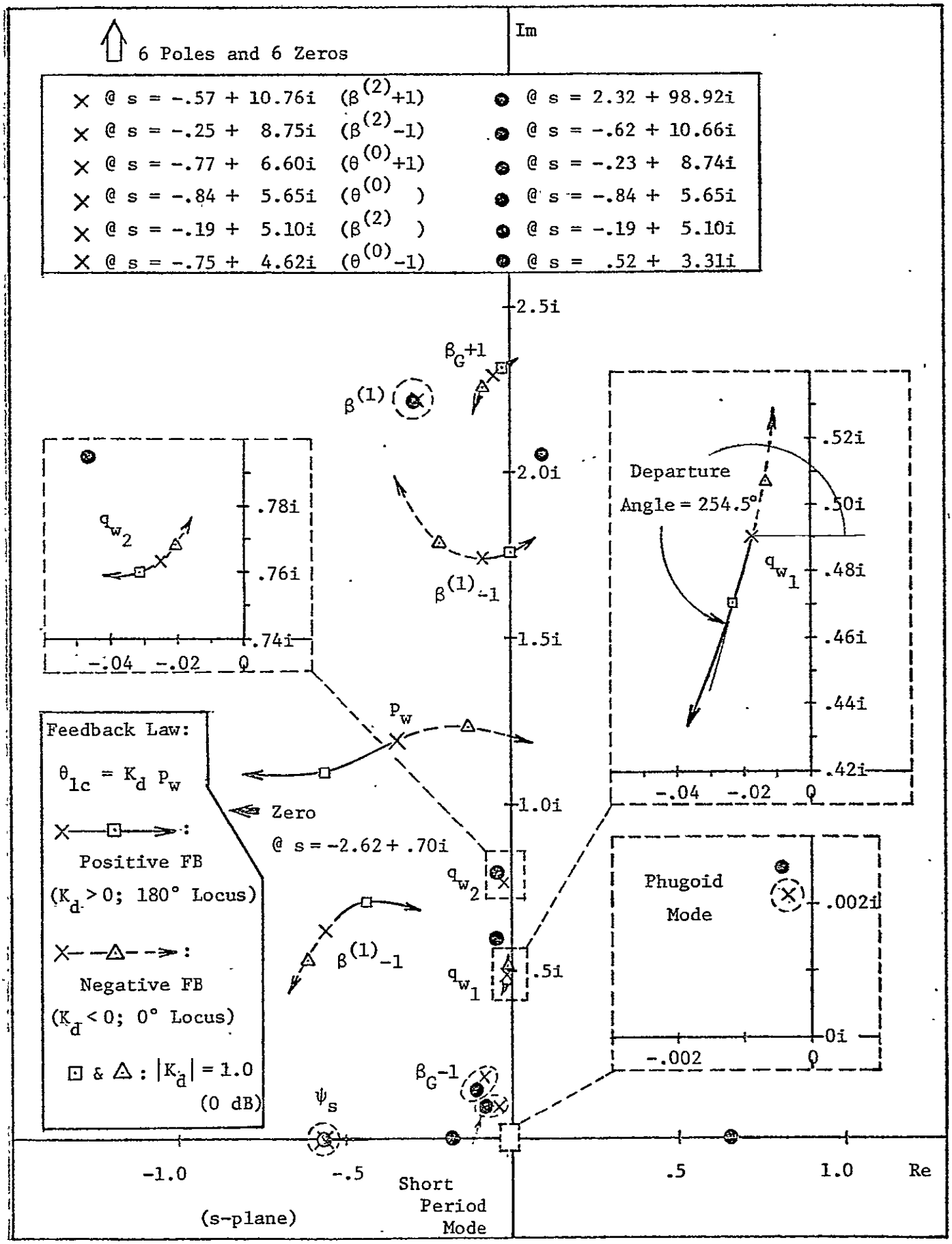

Figure 57. Root Locus: Effect of $p_w \rightarrow \theta_{1c}$ Feedback (proportional);

18 DOF Model @ V = .844 (300 kts)

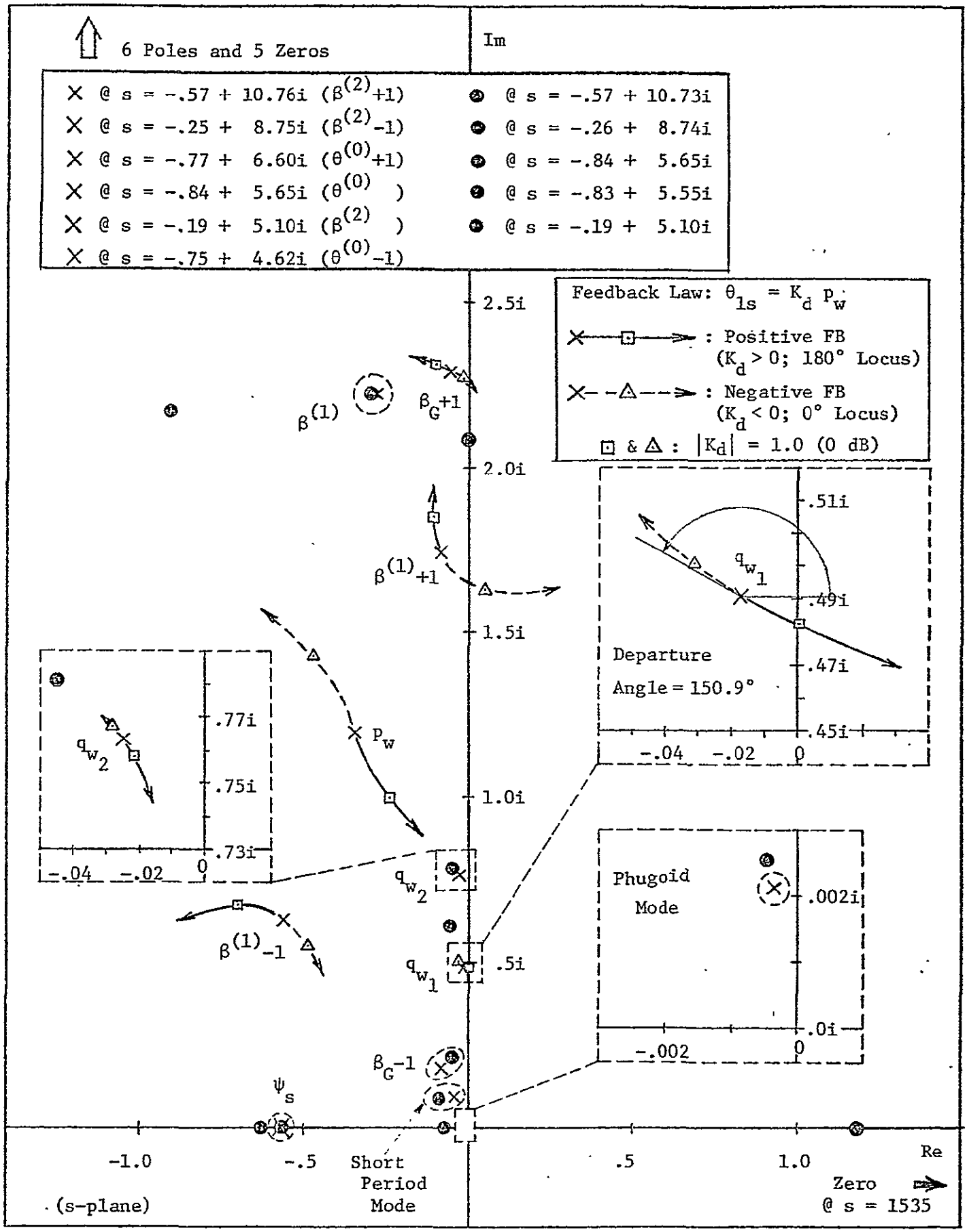

Figure 58. Root Locus: Effect of $p_w \rightarrow \theta_{1s}$ Feedback (Proportional); 18 DOF Model @ V = .844 (300 kts)

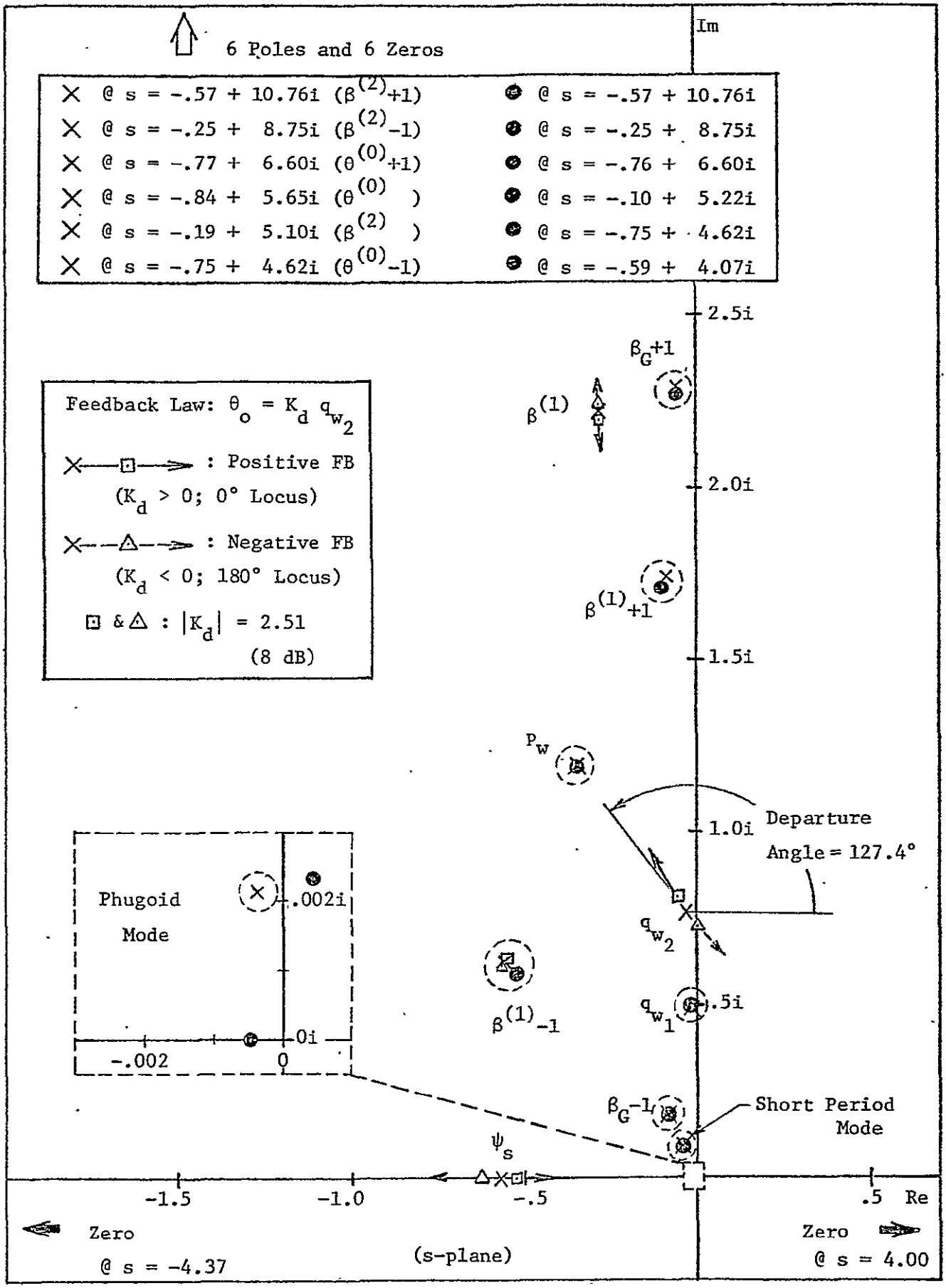

Figure 59. Root Locus: Effect of $q_{w_2} \rightarrow \theta_o$ Feedback (Proportional);
18 DOF Model @ V = .844 (300 kts)

CONCLUSIONS

Classical feedback techniques, combined with the introduction of complex coordinates are valuable in providing insight into the factors influencing the dynamic stability of this complex aeroelastic system.

Simplified or lower order dynamic models can be conveniently developed using these techniques which provide qualitative insight into the important parameters in the problem, however a large number of degrees of freedom appear necessary for quantitative accuracy.

The essential features of the whirl flutter problem, for the range of physical parameters studied are shown by considering the proprotor cyclic flapping degrees of freedom coupled with wing torsion and spanwise bending. The wing chordwise mode is primarily coupled to the collective rotor modes. The complexity of the coupling effects is largely associated with the fact that the uncoupled wing modes have natural frequencies near or below once per revolution.

Single loop feedbacks of wing motion to cyclic pitch generally appear to stabilize one particular wing mode while destabilizing another.

Adding fuselage degrees of freedom tends to raise the natural frequencies of the wing modes and to increase the damping of the wing spanwise mode while exerting little influence on the damping of the chordwise mode. Including fuselage freedom has only a small influence on the effects of wing motion feedback.

Relevant to the stability and control characteristics of the aircraft, the flexible modes couple with the short period mode of the vehicle and

influence the damping ratio of this mode. Use of the quasi-static assumption for the flexible modes of the vehicle results in an overestimation of the short period damping and this coupling tends to increase with flight speed.

REFERENCES

1. Johnson, W.: "Dynamics of Tilting Proprotor Aircraft in Cruise Flight", NASA TN D-7677, May 1974.

2. Johnson, W.: "Analytical Model for Tilting Proprotor Aircraft Dynamics, Including Blade Torsion and Coupled Bending Modes, and Conversion Mode Operation", NASA TM X-62,369, August 1974.

3. Johnson, W.: "Analytical Modelling Requirements for Tilting Proprotor Aircraft Dynamics", NASA TN D-8013, July 1975.

4. Edenborough, H. D.: "Investigation of Tilt-Rotor VTOL Aircraft Rotor-Pylon Stability", Journal of Aircraft, Vol. 5, No. 6, March-April 1968.

5. Hall, W. E., Jr.: "Prop-Rotor Stability at High Advance Ratios", Journal of the American Helicopter Society, Vol. 11, No. 2, April 1966.

6. Reed, W. H., III: "Review of Propeller-Rotor Whirl Flutter", NASA TR R-264, February 1967.

7. Young, M. I. and Lytwyn, R. T.: "The Influence of Blade Flapping Restraint on the Dynamic Stability of Low Disc Loading Propeller-Rotors", Journal of the American Helicopter Society, Vol. 12, No. 4, December 1967.

8. Wernicke, K. G. and Edenborough, H. K.: "Full-Scale Prop Rotor Development", Journal of the American Helicopter Society, Vol. 17, No. 1, January 1972.

9. Johnson, W.: "Theory and Comparisons with Tests of Two Full-Scale Prop Rotors", AHS/NASA-Ames Specialists Meeting on Rotorcraft Dynamics, February 13-15, 1974.

10. Kvaternik, R. V.: "Experimental and Analytical Studies on Tilt-Rotor Elasticity", AHS/NASA-Ames Specialists Meeting on Rotorcraft Dynamics, February 13-15, 1974.

11. Gaffey, T. M.: "The effects of Positive-Pitch-Flap Coupling (Negative δ_3) on Rotor Blade Motion Stability and Flaping", Proceedings of 24th Annual National Forum of American Helicopter Society, May 1968.

12. Alexander, R. H., Hengen, L. M. and Weiberg, J. A.: "Aeroelastic-Stability Characteristics of a V/STOL Tilt-Rotor Aircraft With Hingeless Blades: Correlation of Analysis and Test", American Helicopter Society Preprint 835, May 1974.

13. Curtiss, H. C., Jr.: "The Longitudinal Equations of Motion of a Tilt Proprotor Aircraft Including the Effects of Wing and Proprotor Blade Flexibility", Technical Report 1273, Princeton University, Department of Aerospace and Mechanical Sciences, April 1976.

14. Briczinski, S., and Cooper, D. E.: "Flight Investiations of Rotor/Vehicle State Feedback", NASA CR-132546, September 1976.

15. Maisel, M.: "Tilt Rotor Research Aircraft Familiarization Document, NASA TM X-62,407.

16. Curtiss, H. C., Jr.: "Complex Coordinates in Near Hovering Rotor Dynamics", Journal of Aircraft, Vol. 10, No. 5, May 1973.

17. Dowell, E. H., Curtiss, H. C., Jr., Scanlan, R. H., and Sisto, F.: A MODERN COURSE IN ELASTICITY", Sijthoff and Noordhoff, 1978.

18. Frick, J. K. and Johnson, W.: "Optimal Control Theory Investigation of Proprotor/Wing Response to Vertical Gust", NASA TM X-62,384, September 1974.

19. Johnson, W.: "The Influence of Engine/Transmission/Governor on Tilting Proprotor Aircraft Dynamics", NASA TM X-62,455, June 1975.

APPENDIX I

BASIC THEORY FOR PROPROTOR DYNAMICS IN HIGH INFLOW

1.1 Introduction

In this Appendix we will develop linearized equations of motion for a proprotor and its support in axial flow at high inflow ratio, employing a relatively simple analytical model. Although the derivation of these equations of motion is shown in detail in Ref. 1, it is briefly recapitulated in this Appendix to show the basic analytical approach and also for use in the main body of the report for a study of the fundamental dynamics of the proprotor in high inflow. The derivation of the more elaborate model including aircraft longitudinal dynamics is given in References 2 and 13.

The analytical model employed here consists of a proprotor with three blades and the rotor support which is either a pivotted pylon or a cantilevered elastic wing. We consider pure out-of-plane ("flap") and pure in-plane ("lag") motion for each blade which is represented by the deflection of the blade spar with no torque offset, no droop, and no sweep, retaining only lowest modes of their motion. The rotor support motion comprises pylon pitch and yaw motion degrees of freedom for the isotropic pylon, and elastic bending (in spanwise and chordwise) and torsion motion degrees of freedom for the cantilevered wing with only their lowest modes retained.

For a typical proprotor aircraft operation in airplane cruise mode, the rotor induced velocity is negligibly small compared with the forward velocity even for the powered flight, owing to the high inflow and low thrust required (the ratio of the rotor thrust in airplane cruise to that in hover is inversely proportional to the aircraft lift-drag ratio). If simple momentum theory is applied to estimate the ratio of the rotor induced velocity to the forward velocity, it is approximated for high inflow as $v/V \approx C_T/(2V^2)$ which is typically of order 0.001. When we consider a proprotor in autorotation where the rotor torque is zero, the rotor produces a negative thrust, however, its magnitude is much smaller than that for the powered flight, which then makes it more valid to neglect the rotor induced velocity in high inflow.

From the proprotor dynamics point of view it appears that there is no significant difference between the powered flight and the autorotation, and since the latter provides a more simplified treatment we assume an autorota-

ting proprotor in axial flow at high inflow ratio in the following, and consequently the rotor induced velocity is neglected.

1.2 Rotor Equations of Motion

Rotating Frame

Consider a model of a proprotor on its support as shown in Fig. 1.1. When the rotor support is in motion represented by linear displacements of the pivot and angular displacements about it (both assumed small) as defined in the figure, the equations of motion of the flap and lag motion (also assumed small) for the m-th blade at azimuth position $\psi = \psi_m$, as is illustrated in Fig. 1.2, can then be written in dimensionless form as follows (in the rotating frame) :

$$\text{Flap:}\quad I^*_\beta\{\ddot{\beta}_m + \nu^2_\beta \beta_m\} + I^*_{\beta\alpha}\{-(\ddot{\alpha}_y - 2\dot{\alpha}_x)\cos\psi_m + (\ddot{\alpha}_x + 2\dot{\alpha}_y)\sin\psi_m\} + S^*_\beta \ddot{z}_p = \gamma \frac{M_F}{ac}$$

$$\text{Lag:}\quad I^*_\zeta\{\ddot{\zeta}_m + \nu^2_\zeta \zeta_m\} + S^*_\zeta\{(\ddot{x}_p + h\ddot{\alpha}_y)\sin\psi_m - (\ddot{y}_p - h\ddot{\alpha}_x)\cos\psi_m\} - I^*_{\zeta\alpha}\ddot{\alpha}_z = \gamma \frac{M_L}{ac} \qquad (1.1)$$

where

$$I^*_\beta \equiv \int_0^1 \eta^2_\beta m_b\, dr / \bar{I}_b\,,\quad I^*_{\beta\alpha} \equiv \int_0^1 \eta_\beta r m_b\, dr / \bar{I}_b\,,\quad S^*_\beta \equiv \int_0^1 \eta_\beta m_b\, dr / \bar{I}_b\,,$$

$$I^*_\zeta \equiv \int_0^1 \eta^2_\zeta m_b\, dr / \bar{I}_b\,,\quad I^*_{\zeta\alpha} \equiv \int_0^1 \eta_\zeta r m_b\, dr / \bar{I}_b\,,\quad S^*_\zeta \equiv \int_0^1 \eta_\zeta m_b\, dr / \bar{I}_b\,,$$

$$\bar{I}_b \equiv I_b / R^2 = \int_0^1 r^2 m_b\, dr\,,\quad \gamma \equiv \rho a (cR) R^4 / I_b$$

$$(\dot{}) \equiv d(\quad)/d(\Omega t)\,,\quad (\ddot{}) \equiv d^2(\quad)/d(\Omega t)^2$$

r : blade radial position, normalized by R
m_b : blade section mass per unit dimensionless length
ν_β : blade flap rotating natural frequency, normalized by Ω
ν_ζ : " lag " , "
η_β : flap mode shape, normalized to 1 at the blade tip ($r = 1$)
η_ζ : lag " , "
M_F : aerodynamic flap moment on the blade, normalized by $\rho\Omega^2 R^5$
M_L : " lag " , "
x_p, y_p, z_p, h and c are normalized by R

and the Coriolis inertia coupling of the flap and lag motion is ignored, since it is of order $\gamma C_T/a\sigma$ and negligible compared with the aerodynamic coupling terms of the flap and lag motion which are of order 1 as will be shown later ($\gamma M_{\dot{\zeta}}$ & $\gamma Q_{\dot{\beta}}$). In conjunction with this, the influence of the blade precone is also neglected. The influence of the blade precone becomes important if the blade pitch motion dynamics, specifically due to the blade pitch control system flexibility, is considered; however, its first order effect can be examined by introducing the "pitch-lag coupling parameter," which is an approximate treatment for a relatively stiff control system.

Nonrotating Frame

When the number of the blades is equal to or greater than 3, i.e., $N \geq 3$, it is possible to transform the motion variables described in the rotating frame to those in the nonrotating frame by applying the Fourier type coordinate transformation or the "Mulitiblade Coordinate Transformation" (Ref. 1) whose advantage lies in the simplification it provides in the equations of motion.

As to the flapping motion, for example, the new degrees of freedom in the nonrotating frame are defined as follows:

$$\beta_o \equiv \frac{1}{N}\sum_m \beta_m , \qquad \beta_{nc} \equiv \frac{2}{N}\sum_m \beta_m \cos n\psi_m$$

$$\beta_{ns} \equiv \frac{2}{N}\sum_m \beta_m \sin n\psi_m , \qquad \beta_{N/2} \equiv \frac{1}{N}\sum_m \beta_m (-1)^m \quad \text{(only for } N \text{ even)} \tag{1.2}$$

With these new degrees of freedom, β_m can be given as

$$\beta_m = \beta_o + \sum_n \{\beta_{nc}\cos n\psi_m + \beta_{ns}\sin n\psi_m\} + \beta_{N/2}(-1)^m \tag{1.3}$$

where the last term on the right hand side appears only if N is even, and the summation is from $n = 1$ to $n = (N-1)/2$ for N odd and to $n = (N-2)/2$ for N even.

The relations for the lag motion degrees of freedom are also found in a like manner.

In the present case where $N = 3$ is assumed, the new degrees of freedom for the flap and lag motion in the nonrotating frame are the following:

Flap : β_o : collective flap or coning

β_{1c} : cyclic flap or longitudinal tip path plane tilt

β_{1s} : " lateral

Lag : ζ_o : collective lag

ζ_{1c} : cyclic lag

ζ_{1s} : "

with which β_m and ζ_m are given as

$$\begin{aligned} \beta_m &= \beta_o + \beta_{1c}\cos\psi_m + \beta_{1s}\sin\psi_m \\ \zeta_m &= \zeta_o + \zeta_{1c}\cos\psi_m + \zeta_{1s}\sin\psi_m \end{aligned} \tag{1.4}$$

Now we will convert the equations (1.1) to those in the nonrotating frame. Consider the flap equation. From Eqn. (1.4.1) the time derivatives (with respect to the dimensionless time, Ωt) of β_m are as follows:

$$\begin{aligned} \dot{\beta}_m &= \dot{\beta}_o + (\dot{\beta}_{1c} + \beta_{1s})\cos\psi_m + (\dot{\beta}_{1s} - \beta_{1c})\sin\psi_m \\ \ddot{\beta}_m &= \ddot{\beta}_o + (\ddot{\beta}_{1c} + 2\dot{\beta}_{1s} - \beta_{1c})\cos\psi_m + (\ddot{\beta}_{1s} - 2\dot{\beta}_{1c} - \beta_{1s})\sin\psi_m \end{aligned} \tag{1.5}$$

Substituting Eqns. (1.4.1) and (1.5) into the flap equation in (1.1) and applying the operations $\frac{1}{N}\sum_m(\ldots)$, $\frac{2}{N}\sum_m(\ldots)\cos\psi_m$, and $\frac{2}{N}\sum_m(\ldots)\sin\psi_m$ to the resulting equation with following relations:

$$\begin{aligned} &\frac{1}{N}\sum_m \sin\psi_m = \frac{1}{N}\sum_m \cos\psi_m = \frac{2}{N}\sum_m \sin\psi_m\cos\psi_m = 0 , \\ &\frac{2}{N}\sum_m \sin^2\psi_m = \frac{2}{N}\sum_m \cos^2\psi_m = 1 , \qquad (\because \psi_m = \psi_{m-1} + \frac{2\pi}{N}) \end{aligned} \tag{1.6}$$

we obtain the flap equation of motion in the nonrotating frame as follows:

Coning :
$$I^*_{\beta o}(\ddot{\beta}_o + \nu^2_{\beta o}\beta_o) + S^*_{\beta o}\ddot{z}_p = \gamma\frac{M_{Fo}}{ac}$$

Cyclic Flap :
$$\begin{aligned} &I^*_\beta\{\ddot{\beta}_{1c} + 2\dot{\beta}_{1s} + (\nu^2_\beta - 1)\beta_{1c}\} + I^*_{\beta\alpha}(-\ddot{\alpha}_y + 2\dot{\alpha}_x) = \gamma\frac{M_{F1c}}{ac} \\ &I^*_\beta\{\ddot{\beta}_{1s} - 2\dot{\beta}_{1c} + (\nu^2_\beta - 1)\beta_{1s}\} + I^*_{\beta\alpha}(\ddot{\alpha}_x + 2\dot{\alpha}_y) = \gamma\frac{M_{F1s}}{ac} \end{aligned} \tag{1.7.1}$$

where

$$M_{Fo} \equiv \frac{1}{N} \sum_m M_F \;,\quad M_{F1c} \equiv \frac{2}{N} \sum_m M_F \cos\psi_m \;,\quad M_{F1s} \equiv \frac{2}{N} \sum_m M_F \sin \psi_m \tag{1.8.1}$$

The subscript o added to the inertia constants and to the (rotating)natural frequency in the coning equation reflects that the different mode shape and natural frequency might be used, according to how the blade root is restrained. That is, if the blade is cantilevered at its root to the hub which is fixed to the rotor shaft, then the coning mode and the cyclic flap mode are both the elastic bending mode, hence, there is no difference in the mode shapes and natural frequencies to be used. However, for the gimballed rotor the cyclic flap mode is almost equal to that of an articulated blade which is hinged at the center of rotation, i.e., rigid body mode ($\eta_\beta = r$), whereas the coning mode is still an elastic bending mode. In such a case the appropriate mode shapes and natural frequencies to describe each motion properly might be different.

In a similar manner the lag equations of motion in the nonrotating frame may be given as follows:

Collective Lag :

$$I^*_{\zeta o} (\ddot{\zeta}_o + \nu^2_{\zeta o} \zeta_o) - I^*_{\zeta o\alpha} \ddot{\alpha}_z = \gamma \frac{M_{Lo}}{ac}$$

Cyclic Lag :

$$\begin{aligned} I^*_\zeta \{ \ddot{\zeta}_{1c} + 2\dot{\zeta}_{1s} + (\nu^2_\zeta - 1)\zeta_{1c}\} + S^*_\zeta (-\ddot{y}_p + h\ddot{\alpha}_x) &= \gamma \frac{M_{L1c}}{ac} \\ I^*_\zeta \{ \ddot{\zeta}_{1s} - 2\dot{\zeta}_{1c} + (\nu^2_\zeta - 1)\zeta_{1s}\} + S^*_\zeta (\ddot{x}_p + h\ddot{\alpha}_y) &= \gamma \frac{M_{L1s}}{ac} \end{aligned} \tag{1.7.2}$$

where

$$M_{Lo} \equiv \frac{1}{N} \sum_m M_L \;,\quad M_{L1c} \equiv \frac{2}{N} \sum_m M_L \cos\psi_m \;,\quad M_{L1s} \equiv \frac{2}{N} \sum_m M_L \sin \psi_m \tag{1.8.2}$$

Again the subscript o added to the inertia constants and to the (rotating) natural frequency in the collective lag equation indicates that the different mode shape and natural frequency might be used. For an autorotating rotor, rigid body mode shape ($\eta_\zeta = r$) is used for which $I^*_{\zeta o} = I^*_{\zeta o\alpha} = 1$ and $\nu_{\zeta o} = 0$, and now $\dot{\zeta}_o$ represents the rotor shaft rotational velocity perturbation (with reapect to the rotor support). If there is no shaft speed perturbation considered (i.e., perfect rotor rpm governor is assumed) then the mode shape and the natural frequency in the collective lag equation of motion are same

as those in the cyclic lag equations of motion.

Aerodynamic Flap and Lag Moments

Now we will find the expressionsfor the aerodynamic forcing terms on the right hand sides of Eqns. (1.7). By making use of the quasi-steady aerodynamics and applying the strip theory with the tip loss neglected, the dimensionless aerodynamic flap and lag moments on the blade are given as

$$M_F = \int_0^1 \eta_\beta F_z \, dr , \qquad M_L = \int_0^1 \eta_\zeta F_x \, dr$$

where F_z and F_x are the dimensionless section forces resolved into the hub plane, and they are related to the section lift and drag (also dimensionless) as

$$F_z = \frac{L u_T - D u_P}{U} , \quad F_x = \frac{L u_P + D u_T}{U}$$

where

$$L = \frac{1}{2} c U^2 C_l , \quad D = \frac{1}{2} c U^2 C_d , \quad U^2 = u_T^2 + u_P^2$$

(cf. Fig. 1.3).

In the following evaluation we will use the rigid body mode shape for η_β and η_ζ, since the most significant aerodynamic loading occurs near the blade tip where the mode shape is very mich like that of the rigid body mode. Therefore, from the relations given in the above, we have

$$\begin{aligned} \frac{M_F}{ac} &\simeq \int_0^1 r \frac{F_z}{ac} dr = \int_0^1 r U \left(u_T \frac{C_l}{2a} - u_P \frac{C_d}{2a} \right) dr \\ \frac{M_L}{ac} &\simeq \int_0^1 r \frac{F_x}{ac} dr = \int_0^1 r U \left(u_P \frac{C_l}{2a} + u_T \frac{C_d}{2a} \right) dr \end{aligned} \tag{1.9}$$

where the blade chord is assumed constant over the blade span.

In the trim condition where the rotor is operating in axial flow, the velocity components and the angle-of-attack at the section r, are given as

$$\begin{aligned} u_T &= r , \quad u_P = V + v \simeq V , \quad U \simeq \sqrt{r^2 + V^2} , \\ \alpha &= \theta - \phi \simeq \theta - \tan^{-1}(V/r) \end{aligned} \tag{1.10}$$

for which the moment coefficients in Eqns. (1.9) become

$$\left(\frac{M_F}{ac}\right)_{@trim} \equiv M_o \simeq \int_0^1 r\sqrt{r^2 + V^2}\left(r\frac{C_{lo}}{2a} - V\frac{C_{do}}{2a}\right)dr$$
$$\left(\frac{M_L}{ac}\right)_{@trim} \equiv Q_o \simeq \int_0^1 r\sqrt{r^2 + V^2}\left(V\frac{C_{lo}}{2a} + V\frac{C_{do}}{2a}\right)dr \qquad (1.11)$$

where C_{lo} and C_{do} are the section lift and drag coefficients at trim, respectively.

Now consider small perturbations from the equilibrium. In order to evaluate the variations of the aerodynamic flap and lag moments on the blade for those perturbations, it is apparently necessary from Eqns. (1.9) to find the variations, δU, δu_T, δu_P, δC_l, and δC_d, in terms of the motion variables and in the control and gust inputs.

First, recalling that a rigid body mode shape is assumed for η_β and η_ζ, δu_T and δu_P are written as follows:

$$\delta u_T = r\,\delta u_{TA} + \delta u_{TB}\,, \qquad \delta u_P = r\,\delta u_{PB} + \delta u_{PA} \qquad (1.12)$$

where
$$\delta u_{TA} \equiv \dot{\alpha}_z - \dot{\zeta}_m$$

$$\delta u_{TB} \equiv (-h\dot{\alpha}_x + V\alpha_x + \dot{y}_p + V\beta_g)\cos\psi_m + (-h\dot{\alpha}_y + V\alpha_y - \dot{x}_p + V\alpha_g)\sin\psi_m \qquad (1.13)$$

$$\delta u_{PB} \equiv \dot{\beta}_m - \dot{\alpha}_y\cos\psi_m + \dot{\alpha}_x\sin\psi_m$$

$$\delta u_{PA} \equiv V u_g + \dot{z}_p$$

The variation, δU, is obtained from the relation, $U^2 = u_T^2 + u_P^2$, as

$$\delta U = \frac{r\,\delta u_T + V\,\delta u_P}{\sqrt{r^2 + V^2}} \qquad (1.14)$$

The blade section lift and drag coefficients may be considered as functions of the angle-of-attack and Mach number at that section, hence,

$$\delta C_l = C_{l\alpha}\delta\alpha + C_{lM}\,\delta M\,, \qquad \delta C_d = C_{d\alpha}\delta\alpha + C_{dM}\,\delta M \qquad (1.15)$$

where

$$\delta\alpha = \delta\theta - \delta\{\tan^{-1}(u_P/u_T)\} = \delta\theta - \frac{r\,\delta u_P - V\,\delta u_T}{r^2 + V^2} \tag{1.16}$$

$$\delta M = M_{tip}\,\delta U\ , \quad \text{where } M_{tip} \equiv \Omega R / a_s\ , \quad a_s\text{: speed of sound}$$

It should be noted that from Eqns. (1.13), (1.14), (1.15) and (1.16) the variations, δU, δC_l, and δC_d can be eventually expressed in terms of the variations, δu_{TA}, δu_{TB}, δu_{PB}, δu_{PA}, and $\delta\theta$. Therefore, the variational quantities in the flap and lag moments on the blade may be expanded as follows:

$$\begin{aligned}
\delta\left\{\frac{M_F}{ac}\right\} &\equiv M_\mu\,\delta u_{TB} + M_{\dot\zeta}\,\delta u_{TA} + M_\lambda\,\delta u_{PA} + M_{\dot\beta}\,\delta u_{PB} + M_\theta\,\delta\theta \\
\delta\left\{\frac{M_L}{ac}\right\} &\equiv Q_\mu\,\delta u_{TB} + Q_{\dot\zeta}\,\delta u_{TA} + Q_\lambda\,\delta u_{PA} + Q_{\dot\beta}\,\delta u_{PB} + Q_\theta\,\delta\theta
\end{aligned} \tag{1.17}$$

where the aerodynamic derivatives in the above expressions can be found by the integration along the blade span of the integrands which comprise r, V, C_{l_0}, C_{l_α}, C_{l_M}, C_{d_0}, C_{d_α}, C_{d_M} and M_{tip}, as easily seen from the above. However, the most important and dominant term in each derivative comes from the section lift change due to the angle-of-attack change, hence, we retain only C_{l_α} term in the evaluation of each derivative, using the relation $C_{l_\alpha} / 2a \simeq 1/2$, although it is a function of the Mach number.

Thus, the variations of the aerodynamic flap and lag moments may be written as follows:

$$\begin{aligned}
\delta\left\{\frac{M_F}{ac}\right\} &= \int_0^1 r\sqrt{r^2+V^2}\ r\,\frac{C_{l_\alpha}}{2a}\ \delta\alpha\,dr \\
&\simeq \int_0^1 r^2\sqrt{r^2+V^2}\ \frac{1}{2}\left\{\delta\theta - \frac{r}{r^2+V^2}\,(r\,\delta u_{PB} + \delta u_{PA}) + \frac{V}{r^2+V^2}\,(r\,\delta u_{TA} + \delta u_{TB})\right\} dr \\
&\simeq \left\{\frac{V}{2}\int_0^1 \frac{r^2}{\sqrt{r^2+V^2}}\,dr\right\}\delta u_{TB} + \left\{\frac{V}{2}\int_0^1 \frac{r^3}{\sqrt{r^2+V^2}}\,dr\right\}\delta u_{TA} \\
&\quad + \left\{-\frac{1}{2}\int_0^1 \frac{r^3}{\sqrt{r^2+V^2}}\,dr\right\}\delta u_{PA} + \left\{-\frac{1}{2}\int_0^1 \frac{r^4}{\sqrt{r^2+V^2}}\,dr\right\}\delta u_{PB} \\
&\quad + \left\{\frac{1}{2}\int_0^1 r^2\sqrt{r^2+V^2}\,dr\right\}\delta\theta
\end{aligned} \tag{1.18.1}$$

and similarly,

$$\delta\left\{\frac{M_L}{ac}\right\} \simeq \int_0^1 r\sqrt{r^2+V^2}\; V\frac{C_{l\alpha}}{2a}\;\delta\alpha\; dr$$

$$\simeq \left\{\frac{V^2}{2}\int_0^1 \frac{r}{\sqrt{r^2+V^2}}\,dr\right\}\delta u_{TB} + \left\{\frac{V^2}{2}\int_0^1 \frac{r^2}{\sqrt{r^2+V^2}}\,dr\right\}\delta u_{TA}$$

$$+\left\{-\frac{V}{2}\int_0^1 \frac{r^2}{\sqrt{r^2+V^2}}\,dr\right\}\delta u_{PA} + \left\{-\frac{V}{2}\int_0^1 \frac{r^3}{\sqrt{r^2+V^2}}\,dr\right\}\delta u_{PB}$$

$$+\left\{\frac{V}{2}\int_0^1 r\sqrt{r^2+V^2}\,dr\right\}\delta\theta \qquad (1.18.2)$$

Comparing Eqns. (1.17) and (1.18), the derivatives are identified as

$$\begin{aligned}
M_\mu &\simeq V f_2 & Q_\mu &\simeq V^2 f_1\\
M_{\dot\zeta} &\simeq V f_3 & Q_{\dot\zeta} &\simeq V^2 f_2\\
M_\lambda &\simeq -f_3 & Q_\lambda &\simeq -V f_2\\
M_{\dot\beta} &\simeq -f_4 & Q_{\dot\beta} &\simeq -V f_3\\
M_\theta &\simeq g_2 & Q_\theta &\simeq V g_1
\end{aligned} \qquad (1.19)$$

where

$$f_n \equiv \frac{1}{2}\int_0^1 \frac{r^n}{\sqrt{r^2+V^2}}\,dr\,, \qquad g_n \equiv \frac{1}{2}\int_0^1 r^n\sqrt{r^2+V^2}\,dr \qquad (1.20)$$

If we use the inflow angle at the effective radius position for the evaluation of the integrals involved in the rotor aerodynamic derivatives, then the following expressions result:

$$\begin{aligned}
M_\mu &\simeq (\sin\phi_e)/6 & Q_\mu &\simeq (V\sin\phi_e)/4\\
M_{\dot\zeta} &\simeq (\sin\phi_e)/8 & Q_{\dot\zeta} &\simeq (V\sin\phi_e)/6\\
M_\lambda &\simeq -(\cos\phi_e)/6 & Q_\lambda &\simeq -(\sin\phi_e)/6\\
M_{\dot\beta} &\simeq -(\cos\phi_e)/8 & Q_{\dot\beta} &\simeq -(\sin\phi_e)/8\\
M_\theta &\simeq 1/(8\cos\phi_e) & Q_\theta &\simeq V/(6\cos\phi_e)
\end{aligned} \qquad (1.21)$$

where

$$\cos\phi_e \equiv r_e/\sqrt{r^2+V^2}\,, \qquad \sin\phi_e \equiv V/\sqrt{r^2+V^2}$$

and r_e is usually taken as 3/4.

Since the trim values of the aerodynamic flap and lag moments and their variations from the trim values, as are given in Eqns. (1.11) and (1.17), respectively, are derived in the rotating frame, we will convert them to those in the nonrotating frame, again applying the Fourier type coordinate transformation. Noting that the trim values, M_o and Q_o, and the derivatives, $M_{(\ )}$'s, and $Q_{(\ )}$'s, are all constants and independent of the blade azimuth position (this is owing to the axial flow assumed in the trim condition), we need the transformed expressions only for δu_{TB}, δu_{TA}, δu_{PA}, δu_{PB} and $\delta\theta$. Using relations given in Eqns. (1.6), (1.5.1) for $\dot{\beta}_m$, and a similar relationship for $\dot{\zeta}_m$, we obtain the following expressions from Eqns. (1.13):

Operations On	$\frac{1}{N}\sum_m(\ldots)$	$\frac{2}{N}\sum_m(\ldots)\cos\psi_m$	$\frac{2}{N}\sum_m(\ldots)\sin\psi_m$
δu_{TB}	0	$-h\dot{\alpha}_x + V\alpha_x + \dot{y}_p + V\beta_g$	$-h\dot{\alpha}_y + V\alpha_y - \dot{x}_p + V\alpha_g$
δu_{TA}	$\dot{\alpha}_g - \dot{\zeta}_o$	$-\dot{\zeta}_{1c} - \zeta_{1s}$	$-\dot{\zeta}_{1s} + \zeta_{1c}$
δu_{PA}	$V u_g + \dot{z}_p$	0	0
δu_{PB}	$\dot{\beta}_o$	$\dot{\beta}_{1c} + \beta_{1s} - \dot{\alpha}_y$	$\dot{\beta}_{1s} - \beta_{1c} + \dot{\alpha}_x$

(1.22)

For $\delta\theta$ we define the following:

$$\theta_o \equiv \frac{1}{N}\sum_m \delta\theta \quad : \text{collective pitch}$$

$$\theta_{1c} \equiv \frac{2}{N}\sum_m \delta\theta\cos\psi_m \quad : \text{lateral cyclic pitch} \qquad (1.23)$$

$$\theta_{1s} \equiv \frac{2}{N}\sum_m \delta\theta\sin\psi_m \quad : \text{longitudinal cyclic pitch}$$

Therefore, the aerodynamic flap and lag moments in the nonrotating frame which have appeared on the right hand sides of Eqn. (1.7) are written in terms of the motion variables and the control and gust inputs as follows:

$$
\begin{aligned}
\gamma \frac{M_{Fo}}{ac} &= \gamma M_o + \gamma M_{\dot\zeta} (\dot\alpha_z - \dot\zeta_o) + \gamma M_\lambda (V u_g + \dot z_p) + \gamma M_{\dot\beta} \dot\beta_o + \gamma M_\theta \theta_o \\
\gamma \frac{M_{F1c}}{ac} &= \gamma M_\mu (-h\dot\alpha_x + V\alpha_x + \dot y_p + V\beta_g) + \gamma M_{\dot\zeta} (-\dot\zeta_{1c} - \zeta_{1s}) \\
&\quad + \gamma M_{\dot\beta} (\dot\beta_{1c} + \beta_{1s} - \dot\alpha_y) + \gamma M_\theta \theta_{1c} \\
\gamma \frac{M_{F1s}}{ac} &= \gamma M_\mu (-h\dot\alpha_y + V\alpha_y - \dot x_p + V\alpha_g) + \gamma M_{\dot\zeta} (-\dot\zeta_{1s} + \zeta_{1c}) \\
&\quad + \gamma M_{\dot\beta} (\dot\beta_{1s} - \beta_{1c} + \dot\alpha_x) + \gamma M_\theta \theta_{1s} \\
\gamma \frac{M_{Lo}}{ac} &= \gamma Q_o + \gamma Q_{\dot\zeta} (\dot\alpha_z - \dot\zeta_o) + \gamma Q_\lambda (V u_g + \dot z_p) + \gamma Q_{\dot\beta} \dot\beta_o + \gamma Q_\theta \theta_o \\
\gamma \frac{M_{L1c}}{ac} &= \gamma Q_\mu (-h\dot\alpha_x + V\alpha_x + \dot y_p + V\beta_g) + \gamma Q_{\dot\zeta} (-\dot\zeta_{1c} - \zeta_{1s}) \\
&\quad + \gamma Q_{\dot\beta} (\dot\beta_{1c} + \beta_{1s} - \dot\alpha_y) + \gamma Q_\theta \theta_{1c} \\
\gamma \frac{M_{L1s}}{ac} &= \gamma Q_\mu (-h\dot\alpha_y + V\alpha_y - \dot x_p + V\alpha_g) + \gamma Q_{\dot\zeta} (-\dot\zeta_{1s} + \zeta_{1c}) \\
&\quad + \gamma Q_{\dot\beta} (\dot\beta_{1s} - \beta_{1c} + \dot\alpha_x) + \gamma Q_\theta \theta_{1s}
\end{aligned}
\tag{1.24}
$$

Thus the rotor flap and lag equations of motion are now fully described in the nonrotating frame by Eqns. (1.7) and (1.24). It should be noted here that these linear equations have only constant coefficients as a result of the application of the Fourier type coordinate transformation, which is made possible by the assumptions on the number of blades ($N \geq 3$) and the rotor operating condition in equilibrium (axial flow).

1.3 Rotor Hub Forces and Moments

Before developing the equations of motion for the rotor support, we will derive the expressions for the rotor hub forces and moments in the nonrotating frame which will appear as forcing terms in the support equations.

Hub Pitch and Yaw Moments

The rotor hub pitch and yaw moments originate from the bending moment at the blade root due to the flapping motion, and with the nonrotating frame degrees of freedom they can be written in dimensionless form (normalized by $\frac{N}{2} I_b \Omega^2$) as follows:

$$\gamma \frac{2C_{My}}{a\sigma} = - I^*_\beta (\nu^2_\beta - 1) \beta_{1c}$$

$$\gamma \frac{2C_{Mx}}{a\sigma} = I^*_\beta (\nu^2_\beta - 1) \beta_{1s} \qquad (1.25)$$

where $\sigma \equiv N(cR)R / \pi R^2 = Nc / \pi$.

Torque, Thrust, H Force and Y Force

The rotor torque, thrust, H force, and Y force transmitted to the rotor hub comprise inertia and aerodynamic contributions.

First, the inertia contributions to these forces and moment are given in coefficient form as follows:

$$\gamma\{\frac{C_Q}{a\sigma}\}_{in} = - I^*_{\zeta o\alpha} \ddot{\zeta}_o + \ddot{\alpha}_z$$

$$\gamma\{\frac{C_T}{a\sigma}\}_{in} = - S^*_{\beta o} \ddot{\beta}_o - M^*_b \ddot{z}_p$$

$$\gamma\{\frac{2C_H}{a\sigma}\}_{in} = - S^*_\zeta \ddot{\zeta}_{1s} - 2M^*_b (\ddot{x}_p + h\ddot{\alpha}_y) \qquad (1.26)$$

$$\gamma\{\frac{2C_Y}{a\sigma}\}_{in} = S^*_\zeta \ddot{\zeta}_{1c} - 2M^*_b (\ddot{y}_p - h\ddot{\alpha}_x)$$

where $M^*_b \equiv \int_0^1 m_b \, dr \; / \; \overline{I}_b$.

The aerodynamic contributions are written as

$$\gamma\{\frac{C_Q}{a\sigma}\}_{aero} = \gamma \frac{1}{N} \sum_m \{ \int_0^1 r \frac{F_x}{ac} dr \}$$

$$\gamma\{\frac{C_T}{a\sigma}\}_{aero} = \gamma \frac{1}{N} \sum_m \{ \int_0^1 \frac{F_z}{ac} dr \}$$

$$\gamma\{\frac{2C_H}{a\sigma}\}_{aero} = \gamma \frac{2}{N} \sum_m \{ \int_0^1 \frac{F_x}{ac} dr \} \sin \psi_m \qquad (1.27)$$

$$\gamma\{\frac{2C_Y}{a\sigma}\}_{aero} = - \gamma \frac{2}{N} \sum_m \{ \int_0^1 \frac{F_x}{ac} dr \} \cos \psi_m$$

where F^C_x and F^C_z are the dimensionless section aerodynamic forces in the hub plane already introduced before. The expression for the torque above is same as given in Eqn. (1.24.4), i.e.,

$$\gamma\{\frac{C_Q}{a\sigma}\}_{aero} = \gamma Q_o + \gamma Q_\zeta (\dot{\alpha}_z - \dot{\zeta}_o) + \gamma Q_\lambda (V u_g + \dot{z}_p) + \gamma Q_{\dot{\beta}} \dot{\beta}_o + \gamma Q_\theta \dot{\theta}_o \qquad (1.28.1)$$

For the evaluation of the forces in Eqns. (1.27) we will take a similar approach as we did in the derivation of the aerodynamic flap and lag moments. That is, expanding the integrals as

$$\begin{aligned}\int_0^1 \frac{F_z}{ac}\,dr &\equiv T_o + T_\mu\,\delta u_{TB} + T_{\dot\zeta}\,\delta u_{TA} + T_\lambda\,\delta u_{PA} + T_{\dot\beta}\,\delta u_{PB} + T_\theta\,\delta\theta \\ \int_0^1 \frac{F_x}{ac}\,dr &\equiv H_o + H_\mu\,\delta u_{TB} + H_{\dot\zeta}\,\delta u_{TA} + H_\lambda\,\delta u_{PA} + H_{\dot\beta}\,\delta u_{PB} + H_\theta\,\delta\theta\end{aligned} \tag{1.29}$$

and applying the operations of the Fourier-type coordinate transformation, we obtain the following:

$$\begin{aligned}\gamma\left\{\frac{C_T}{a\sigma}\right\}_{aero} &= \gamma T_o + \gamma T_{\dot\zeta}\,(\dot\alpha_z - \dot\zeta_o) + \gamma T_\lambda\,(V u_g + \dot z_p) + \gamma T_{\dot\beta}\,\dot\beta_o + \gamma T_\theta\,\theta_o \\ \gamma\left\{\frac{2C_H}{a\sigma}\right\}_{aero} &= \gamma H_\mu\,(-h\dot\alpha_y + V\alpha_y - \dot x_p + V\alpha_g) + \gamma H_{\dot\zeta}\,(-\dot\zeta_{1s} + \zeta_{1c}) \\ &\quad + \gamma H_{\dot\beta}\,(\dot\beta_{1s} - \beta_{1c} + \dot\alpha_x) + \gamma H_\theta\,\theta_{1s} \\ \gamma\left\{\frac{2C_Y}{a\sigma}\right\}_{aero} &= -\gamma H_\mu\,(-h\dot\alpha_x + V\alpha_x + \dot y_p + V\beta_g) - \gamma H_{\dot\zeta}\,(-\dot\zeta_{1c} - \zeta_{1s}) \\ &\quad - \gamma H_{\dot\beta}\,(\dot\beta_{1c} + \beta_{1s} - \dot\alpha_y) - \gamma H_\theta\,\theta_{1c}\end{aligned} \tag{1.28.2,3,\&4}$$

where

$$\begin{aligned}T_o &\simeq \int_0^1 \sqrt{r^2 + V^2}\,\left\{r\,\frac{C_{lo}}{2a} - V\,\frac{C_{do}}{2a}\right\}dr \\ H_o &\simeq \int_0^1 \sqrt{r^2 + V^2}\,\left\{V\,\frac{C_{lo}}{2a} + r\,\frac{C_{do}}{2a}\right\}dr\end{aligned} \tag{1.30}$$

and the derivatives are found as

$$\begin{aligned} T_\mu &\simeq V f_1 & H_\mu &\simeq V^2 f_0 \\ T_{\dot\zeta} &\simeq V f_2 & H_{\dot\zeta} &\simeq V^2 f_1 \\ T_\lambda &\simeq -f_2 & H_\lambda &\simeq -V f_1 \\ T_{\dot\beta} &\simeq -f_3 & H_{\dot\beta} &\simeq -V f_2 \\ T_\theta &\simeq g_1 & H_\theta &\simeq V g_0 \end{aligned} \tag{1.31}$$

where f_n's and g_n's are already defined by Eqns. (1.20). The integrals required for the evaluation of the aerodynamic derivatives in Eqns. (1.19)

and (1.31) are given as follows:

$$
\begin{aligned}
f_0 &= \frac{1}{2}\, ln\, \frac{1+\sqrt{1+V^2}}{V} \\
f_1 &= \frac{1}{2}\, (\sqrt{1+V^2} - V) \\
f_2 &= \frac{1}{4}\sqrt{1+V^2} - \frac{1}{2} V^2 f_0 \\
f_3 &= \frac{1}{6}\{\sqrt{1+V^2}\,(1-2V^2) + 2V^3\} \\
f_4 &= \frac{1}{16}\sqrt{1+V^2}\,(2-3V^2) + \frac{3}{8} V^4 f_0 \\
g_0 &= \frac{1}{4}\sqrt{1+V^2} + \frac{1}{2} V^2 f_0 \\
g_1 &= \frac{1}{6}\{(\sqrt{1+V^2})^3 - V^3\} \\
g_2 &= \frac{1}{16}\sqrt{1+V^2}\,(2+V^2) - \frac{1}{8} V^4 f_0
\end{aligned}
\qquad (1.32)
$$

Again, if the effective radius is used for the evaluation of the integrals, then the following expressions result:

$$
\begin{aligned}
T_\mu &\simeq (\sin\phi_e)/4 & H_\mu &\simeq (V\sin\phi_e)/2 \\
T_{\dot\zeta} &\simeq (\sin\phi_e)/6 & H_{\dot\zeta} &\simeq (V\sin\phi_e)/4 \\
T_\lambda &\simeq -(\cos\phi_e)/4 & H_\lambda &\simeq -(\sin\phi_e)/4 \\
T_{\dot\beta} &\simeq -(\cos\phi_e)/6 & H_{\dot\beta} &\simeq -(\sin\phi_e)/6 \\
T_\theta &\simeq 1/(6\cos\phi_e) & H_\theta &\simeq V/(4\cos\phi_e)
\end{aligned}
\qquad (1.33)
$$

Thus, combining the inertia and aerodynamic contributions, we have

$$
\begin{aligned}
\gamma \frac{C_Q}{a\sigma} &= \gamma Q_o + \gamma Q_{\dot\zeta}\,(\dot\alpha_z - \dot\zeta_o) + \gamma Q_\lambda\,(V u_g + \dot z_p) \\
&\quad + \gamma Q_{\dot\beta}\,\dot\beta_o + \gamma Q_\theta\,\theta_o - I^*_{\zeta o\alpha}\ddot\zeta_o + \ddot\alpha_z \\
\gamma \frac{C_T}{a\sigma} &= \gamma T_o + \gamma T_{\dot\zeta}\,(\dot\alpha_z - \dot\zeta_o) + \gamma T_\lambda\,(V u_g + \dot z_p) \\
&\quad + \gamma T_{\dot\beta}\,\dot\beta_o + \gamma T_\theta\,\theta_o - S^*_{\beta o}\,\ddot\beta_o - M^*_b\,\ddot z_p \\
\gamma \frac{2C_H}{a\sigma} &= \gamma H_\mu\,(-h\dot\alpha_y + V\alpha_y - \dot x_p + V\alpha_g) + \gamma H_{\dot\zeta}\,(-\dot\zeta_{1s} + \zeta_{1c}) \\
&\quad + \gamma H_{\dot\beta}\,(\dot\beta_{1s} - \beta_{1c} + \dot\alpha_x) + \gamma H_\theta\,\theta_{1s} - S^*_\zeta\,\ddot\zeta_{1s} - 2M^*_b\,(\ddot x_p + h\ddot\alpha_y)
\end{aligned}
\qquad (1.34.1,\ 2,\ \&\ 3)
$$

$$\gamma \frac{2C_Y}{a\sigma} = -\gamma H_\mu (-h\dot{\alpha}_x + V\alpha_x + \dot{y}_p + V\beta_g) - \gamma H_{\dot{\zeta}}(-\dot{\zeta}_{1c} - \zeta_{1s}) - \gamma H_{\dot{\beta}} (\dot{\beta}_{1c} + \beta_{1s} - \dot{\alpha}_y) - \gamma H_\theta \dot{\theta}_{1c} + S^*_\zeta \ddot{\zeta}_{1c} - 2M^*_b (\ddot{y}_p - h\ddot{\alpha}_x) \tag{1.34.4}$$

1.4 Equations of Motion for Proprotor and Pivoted Pylon Support

Support Equations of Motion

For the pivoted pylon support we consider only its pitch and yaw motion about the pivot. The pylon pitch and yaw equations of motion are written in dimensionless form as follows (normalized by $\frac{N}{2} I_b \Omega^2$):

$$\text{Pitch:} \quad I^*_{py} \ddot{\alpha}_y + C^*_y \dot{\alpha}_y + K^*_y \alpha_y = \gamma \frac{2C_{My}}{a\sigma} + h\gamma \frac{2C_H}{a\sigma}$$

$$\text{Yaw:} \quad I^*_{px} \ddot{\alpha}_x + C^*_x \dot{\alpha}_x + K^*_x \alpha_x = \gamma \frac{2C_{Mx}}{a\sigma} - h\gamma \frac{2C_Y}{a\sigma} \tag{1.35}$$

where I^*_{py} : pylon pitch moment of inertia about the pivot, normalized by $\frac{N}{2} I_b$

I^*_{px} : " yaw " , "

C^*_y : " pitch damping, normalized by $\frac{N}{2} I_b \Omega$

C^*_x : " yaw " , "

K^*_y : " pitch spring constant, normalized by $\frac{N}{2} I_b \Omega^2$

K^*_x : " yaw " , "

and the forcing terms on the right hand sides above are given in Eqns. (1.25) and (1.34) with x_p, y_p, z_p and α_z degrees of freedom dropped. It should be noted again that the coefficients of the support equations are all constant.

Combined Equations of Motion

Dropping x_p, y_p, z_p and α_z degrees of freedom also in the rotor equations of motion (Eqns. (1.7) & (1.24)), we obtain the combined equations of motion for a model considered here in operational form as follows:

$$\left[\begin{array}{c|c|c} A_{11} & A_{12} & \underline{0} \\ \hline A_{21} & A_{22} & \underline{0} \\ \hline \underline{0} & \underline{0} & A_{33} \end{array}\right] \underline{\dot{x}} = \left[\begin{array}{c|c} B_{11} & \underline{0} \\ \hline B_{21} & \underline{0} \\ \hline \underline{0} & B_{32} \end{array}\right] \underline{v} \tag{1.36}$$

where

$$\underline{x} \equiv \begin{pmatrix} \beta_{1c} \\ \beta_{1s} \\ \zeta_{1c} \\ \zeta_{1s} \\ \hline \alpha_y \\ \alpha_x \\ \hline \beta_o \\ \zeta_o \end{pmatrix}, \qquad \underline{v} \equiv \begin{pmatrix} \theta_{1c} \\ \theta_{1s} \\ \alpha_g \\ \beta_g \\ \hline \theta_o \\ u_g \end{pmatrix}$$

$$A_{11} \equiv \left(\begin{array}{c|c|c|c} I^*_\beta s^2 - \gamma M^*_{\dot\beta} s + I^*_\beta (\nu^2_\beta - 1) & 2 I^*_\beta s - \gamma M^*_{\dot\beta} & \gamma M^*_{\dot\zeta} s & \gamma M^*_{\dot\zeta} \\ \hline - 2 I^*_\beta s + \gamma M^*_{\dot\beta} & I^*_\beta s^2 - \gamma M^*_{\dot\beta} s + I^*_\beta (\nu^2_\beta - 1) & - \gamma M^*_{\dot\zeta} & \gamma M^*_{\dot\zeta} s \\ \hline - \gamma Q^*_{\dot\beta} s & - \gamma Q^*_{\dot\beta} & I^*_\zeta s^2 + \gamma Q^*_{\dot\zeta} s + I^*_\zeta (\nu^2_\zeta - 1) & 2 I^*_\zeta s + \gamma Q^*_{\dot\zeta} \\ \hline \gamma Q^*_{\dot\beta} & - \gamma Q^*_{\dot\beta} s & - 2 I^*_\zeta s - \gamma Q^*_{\dot\zeta} & I^*_\zeta s^2 + \gamma Q^*_{\dot\zeta} s + I^*_\zeta (\nu^2_\zeta - 1) \end{array}\right) \tag{1.37.1}$$

$$A_{21} \equiv \left(\begin{array}{c|c|c|c} I^*_\beta (\nu^2_\beta - 1) + h \gamma H^*_{\dot\beta} & - h \gamma H^*_{\dot\beta} s & - h \gamma H^*_{\dot\zeta} & S^*_\zeta h s^2 + h \gamma H^*_{\dot\zeta} s \\ \hline - h \gamma H^*_{\dot\beta} s & - I^*_\beta (\nu^2_\beta - 1) - h \gamma H^*_{\dot\beta} & S^*_\zeta h s^2 + h \gamma H^*_{\dot\zeta} s & h \gamma H^*_{\dot\zeta} \end{array}\right) \tag{1.37.2}$$

$$A_{12} \equiv \left(\begin{array}{c|c} - I^*_{\beta\alpha} s^2 + \gamma M^*_{\dot\beta} s & (2 I^*_{\beta\alpha} + h \gamma M_\mu) s - V \gamma M_\mu \\ \hline (2 I^*_{\beta\alpha} + h \gamma M_\mu) s - V \gamma M_\mu & I^*_{\beta\alpha} s^2 - \gamma M^*_{\dot\beta} s \\ \hline \gamma Q^*_{\dot\beta} s & S^*_\zeta h s^2 + h \gamma Q_\mu s - V \gamma Q_\mu \\ \hline S^*_\zeta h s^2 + h \gamma Q_\mu s - V \gamma Q_\mu & - \gamma Q^*_{\dot\beta} s \end{array}\right) \tag{1.37.3}$$

$$A_{22} \equiv \left(\begin{array}{c|c} (I^*_{py} + 2 M^*_b h^2) s^2 + (C^*_y + h^2 \gamma H_\mu) s + K^*_y - hV \gamma H_\mu & - h \gamma H^*_{\dot\beta} s \\ \hline h \gamma H^*_{\dot\beta} s & (I^*_{px} + 2 M^*_b h^2) s^2 + (C^*_x + h^2 \gamma H_\mu) s + K^*_x - hV \gamma H_\mu \end{array}\right) \tag{1.37.4}$$

$$A_{33} \equiv \begin{bmatrix} I^*_{\beta o}\, s^2 - \gamma M^*_{\dot\beta}\, s + I^*_{\beta o}\, \nu^2_{\beta o} & \gamma M^*_{\dot\zeta}\, s \\ -\gamma Q^*_{\dot\beta}\, s & I^*_{\zeta o}\, s^2 + \gamma Q^*_{\dot\zeta}\, s + I^*_{\zeta o}\, \nu^2_{\zeta o} \end{bmatrix} \tag{1.37.5}$$

$$B_{11} \equiv \begin{bmatrix} \gamma M_\theta & 0 & 0 & V\,\gamma M_\mu \\ 0 & \gamma M_\theta & V\,\gamma M_\mu & 0 \\ \gamma Q_\theta & 0 & 0 & V\,\gamma Q_\mu \\ 0 & \gamma Q_\theta & V\,\gamma Q_\mu & 0 \end{bmatrix} \tag{1.37.6}$$

$$B_{21} \equiv \begin{bmatrix} 0 & h\,\gamma H_\theta & hV\,\gamma H_\mu & 0 \\ h\,\gamma H_\theta & 0 & 0 & hV\,\gamma H_\mu \end{bmatrix} \tag{1.37.7}$$

$$B_{32} \equiv \begin{bmatrix} \gamma M_\theta & V\,\gamma M_\lambda \\ \gamma Q_\theta & V\,\gamma Q_\lambda \end{bmatrix} \tag{1.37.8}$$

In the collective flap and lag equations above, M_o and Q_o terms are omitted, since they only affect the trim values of β_o and ζ_o, respectively. It should be noted that the collective flap and lag motion does not couple with the pylon motion for the present model, and that the final set of equations of motion has only constant coefficients.

1.5 Equations of Motion for Proprotor and Cantilevered Elastic Wing Support

Support Equations of Motion

Consider an elastic wing which is cantilevered at its root to a certain fixed support (Fig. 1.4). We assume for simplicity that the wing is rectangular and has no sweep, no dihedral, and no incidence, and that its motion is represented by the elastic bending and torsion of the wing elastic axis. Retaining only lowest motion modes, they are expressed as

$$z_w = \eta_w\, q_1, \quad x_w = \eta_w\, q_2, \quad \theta_w = \xi_w\, p$$

where z_w : wing vertical displacement

x_w : " chordwise "

θ_w : " torsion "

η_w : " bending mode shape, normalized to $y_{Tw}R$ at the wing tip

ξ_w : " torsion " , " 1 "

q_1 : " spanwise bending degree of freedom, positive upward

q_2 : " chordwise " , " rearward

p : " torsion degree of freedom, positive leading edge up

If it is further assumed that the pylon is rigidly attached to the wing tip such that the pivot is located at the wing tip elastic axis, then the pivot linear and angular displacements are expressed in terms of the wing motion as follows:

$$\begin{aligned} x_p &= y_{Tw}\, q_1 \;,\; y_p = 0 \;,\; z_p = -\, y_{Tw}\, q_2 \\ \alpha_x &= -\, \eta'_{Tw}\, q_2 \;,\; \alpha_y = p \;,\; \alpha_z = -\, \eta'_{Tw}\, q_1 \end{aligned} \tag{1.38}$$

where η'_{Tw} is the slope of the bending mode shape at the wing tip, and the rotor rotational direction is assumed clockwise on the right wing.

The wing equations of motion may be written in dimensionless form as follows (normalized by $\frac{N}{2} I_b \Omega^2$) :

$$\begin{aligned} (I^*_{q\omega} + m^*_p)\, \ddot{q}_1 + C^*_{q_1} \dot{q}_1 + K^*_{q_1} q_1 + S^*_w \ddot{p} &= M^*_{q_1 w.aero} + M^*_{q_1 rotor} \\ (I^*_{q\omega} + I^*_{px}\, \eta'^2_{Tw} + m^*_p)\, \ddot{q}_2 + C^*_{q_2} \dot{q}_2 + K^*_{q_2} q_2 &= M^*_{q_2 w.aero} + M^*_{q_2 rotor} \\ (I^*_{p\omega} + I^*_{py})\, \ddot{p} + C^*_p \dot{p} + K^*_p p + S^*_w \ddot{q}_1 &= M^*_{p\, w.aero} + M^*_{p\, rotor} \end{aligned} \tag{1.39}$$

where $I^*_{q\omega} \equiv \int_0^{y_{Tw}R} \eta_w^2\, m_w\, dy_w \,/\, \frac{N}{2} I_b$, $I^*_{p\omega} \equiv \int_0^{y_{Tw}R} \xi_w^2\, I_{\theta\omega}\, dy_w \,/\, \frac{N}{2} I_b$,

$m^*_p \equiv m_p\, y^2_{Tw} \,/\, \frac{N}{2} \bar{I}_b$, $S^*_w \equiv m_p\, y_{Tw}\, z_{PEA} \,/\, \frac{N}{2} \bar{I}_b$

$C^*_{q_1}$: wing spanwise beding damping, normalized by $\frac{N}{2} I_b \Omega$

$C^*_{q_2}$: " chordwise " , "

C^*_p : " torsion damping , "

$K^*_{q_1}$: wing spanwise bending spring constant, normalized by $\frac{N}{2} I_b \Omega^2$

$K^*_{q_2}$: " chordwise " , "

K^*_p : " torsion spring constant , "

m_w : " section mass per unit spanwise length

$I_{\theta w}$: " moment of inertia about EA per unit spanwise length

m_p : pylon mass

The wing aerodynamic terms on the right hand sides in the above equations may be found as

$$M^*_{q_1 w.aero} = \gamma C_{q_1 \dot{q}_1} \dot{q}_1 + \gamma C_{q_1 \dot{p}} \dot{p} + \gamma C_{q_1 p} p + \gamma C_{q_1 \alpha} \alpha_g$$

$$M^*_{q_2 w.aero} = 0 \quad , \qquad M^*_{p\, w.aero} = \gamma C_{p\dot{p}} \dot{p} \tag{1.40}$$

where $C_{q_1 \dot{q}_1} = - d_{13} V a_w e_2$, $C_{q_1 \dot{p}} = d_{12} V a_w \frac{3}{4} e_4$

$C_{q_1 p} = d_{12} V a_w e_4$, $C_{q_1 \alpha} = d_{12} V a_w e_1$

$C_{p\dot{p}} = - d_{31} V a_w \frac{1}{8} f^*_3$

a_w : wing 3-dimensional lift curve slope

$d_{mn} \equiv (c_w)^m (y_{Tw})^n / (\pi \sigma a)$

$$e_1 \equiv \int_0^{y_{Tw}R} \eta_w \, dy_w / (y_{Tw}R)^2 \simeq \frac{1}{3}$$

$$e_2 \equiv \int_0^{y_{Tw}R} \eta_w^2 \, dy_w / (y_{Tw}R)^3 \simeq \frac{1}{5}$$

$$e_4 \equiv \int_0^{y_{Tw}R} \eta_w \xi_w \, dy_w / (y_{Tw}R)^2 \simeq \frac{1}{4}$$

$$f^*_3 \equiv \int_0^{y_{Tw}R} \xi_w^2 \, dy_w / (y_{Tw}R) \simeq \frac{1}{3}$$

where the integrals above are evaluated by using the approximated mode shapes for η_w and ξ_w , i.e., $\eta_w \simeq y_w^2 / (y_{Tw}R)$ and $\xi_w \simeq y_w / (y_{Tw}R)$.

The rotor force and moment contributions are written as follows:

$$
\begin{aligned}
M^*_{q_1\,rotor} &= 2\,\eta'_{Tw}\,\gamma\,\frac{C_Q}{a\sigma} + y_{Tw}\,\gamma\,\frac{2\,C_H}{a\sigma} \\
M^*_{q_2\,rotor} &= -\,\eta'_{Tw}\,\{\gamma\,\frac{2\,C_{Mx}}{a\sigma} - h\,\gamma\,\frac{2\,C_Y}{a\sigma}\} - 2\,y_{Tw}\,\gamma\,\frac{C_T}{a\sigma} \qquad (1.41) \\
M^*_{p\,rotor} &= \gamma\,\frac{2\,C_{My}}{a\sigma} + h\,\gamma\,\frac{2\,C_H}{a\sigma}
\end{aligned}
$$

where the rotor hub forces and moments are found in Eqns. (1.25) and (1.34) with the relations given in Eqns. (1.38) substituted. Again it should be noted that the support equations have only constant coefficients.

Combined Equations of Motion

Using relations given in Eqns. (1.38), we obtain from Eqns. (1.7), (1.24), (1.34), (1.39), (1.40), & (1.41) the combined equations of motion for the prop-rotor and the cantilevered elastic wing support in operational form as follows:

$$
\left[\begin{array}{c|c|c}
A_{11} & A'_{12} & \underline{0} \\ \hline
A'_{21} & A'_{22} & A'_{23} \\ \hline
\underline{0} & A'_{32} & A_{33}
\end{array}\right]
\left\{\begin{array}{c}
\beta_{1c} \\ \beta_{1s} \\ \zeta_{1c} \\ \zeta_{1s} \\ \hline
q_1 \\ q_2 \\ p \\ \hline
\beta_o \\ \zeta_o
\end{array}\right\}
=
\left[\begin{array}{c|c}
B_{11} & \underline{0} \\ \hline
B'_{21} & B'_{22} \\ \hline
\underline{0} & B_{32}
\end{array}\right]
\left\{\begin{array}{c}
\theta_{1c} \\ \theta_{1s} \\ \alpha_g \\ \beta_g \\ \hline
\theta_o \\ u_g
\end{array}\right\} \qquad (1,42)
$$

where A_{11} is same as given in Eqn. (1.37.1)
A_{33} " (1.37.5)
B_{11} " (1.37.6)
B_{32} " (1.37.8)

$$
A'_{21} \equiv
\left[\begin{array}{c|c|c|c}
y_{Tw}\,\gamma H_{\dot\beta} & -\,y_{Tw}\,\gamma H_{\dot\beta}\,s & -\,y_{Tw}\,\gamma H_{\dot\zeta} & S^*_\zeta\,y_{Tw}\,s^2 + y_{Tw}\,\gamma H_{\dot\zeta}\,s \\ \hline
h\,\eta'_{Tw}\,\gamma H_{\dot\beta}\,s & \eta'_{Tw}\,I^*_\beta\,(\nu^2_\beta - 1) + h\,\eta'_{Tw}\,\gamma H_{\dot\beta} & -\,S^*_\zeta\,h\,\eta'_{Tw}\,s^2 - h\,\eta'_{Tw}\,\gamma H_{\dot\zeta}\,s & -\,h\,\eta'_{Tw}\,\gamma H_{\dot\zeta} \\ \hline
I^*_\beta\,(\nu^2_\beta - 1) + h\,\gamma H_{\dot\beta} & -\,h\,\gamma H_{\dot\beta}\,s & -\,h\,\gamma H_{\dot\zeta} & S^*_\zeta\,h\,s^2 + h\,\gamma H_{\dot\zeta}\,s
\end{array}\right] \qquad (1.43.1)
$$

$$A'_{12} \equiv \begin{bmatrix} 0 & -\eta'_{T\omega}(2I^*_{\beta\alpha} + h\,\gamma M_\mu)\,s + \eta'_{T\omega} V\,\gamma M_\mu & -I^*_{\beta\alpha}\,s^2 + \gamma M_{\dot\beta}\,s \\ y_{T\omega}\,\gamma M_\mu\,s & \eta'_{T\omega}(-I^*_{\beta\alpha}s^2 + \gamma M_{\dot\beta}\,s) & (2I^*_{\beta\alpha} + h\,\gamma M_\mu)\,s - V\,\gamma M_\mu \\ 0 & -\eta'_{T\omega}(S^*_\zeta h\,s^2 + h\,\gamma Q_\mu\,s - V\,\gamma Q_\mu) & \gamma Q_{\dot\beta}\,s \\ y_{T\omega}(S^*_\zeta s^2 + \gamma Q_\mu\,s) & \eta'_{T\omega}\,\gamma Q_{\dot\beta}\,s & S^*_\zeta h\,s^2 + h\,\gamma Q_\mu\,s - V\,\gamma Q_\mu \end{bmatrix}$$

(1.43.2)

$$A'_{22} \equiv \begin{bmatrix} (I^*_{q\omega} + m^*_p + 2M^*_b y^2_{T\omega} + 2\eta'^2_{T\omega})\,s^2 + (C^*_{q_1} + y^2_{T\omega}\,\gamma H_\mu - \gamma C_{q_1\dot q_1} + 2\eta'^2_{T\omega}\,\gamma Q_{\dot\zeta})\,s + K^*_{q_1} & y_{T\omega}\eta'_{T\omega}\,(2\gamma Q_\lambda + \gamma H_{\dot\beta})\,s & (S^*_\omega + 2M^*_b h\,y_{T\omega})\,s^2 + (y_{T\omega} h\,\gamma H_\mu - \gamma C_{q_1\dot p})\,s - y_{T\omega} V\,\gamma H_\mu - \gamma C_{q_1 p} \\ -2y_{T\omega}\,\eta'_{T\omega}\,\gamma T_{\dot\zeta}\,s & \{I^*_{q\omega} + m^*_p + I^*_{px}\,\eta'^2_{T\omega} + 2M^*_b(y^2_{T\omega} + h^2\eta'^2_{T\omega})\}\,s^2 + (C^*_{q_2} + h^2\eta'^2_{T\omega}\,\gamma H_\mu - 2y^2_{T\omega}\,\gamma T_\lambda)\,s + K^*_{q_2} - \eta'^2_{T\omega} hV\,\gamma H_\mu & -h\,\eta'_{T\omega}\,\gamma H_{\dot\beta}\,s \\ (S^*_\omega + 2M^*_b h\,y_{T\omega})\,s^2 + y_{T\omega} h\,\gamma H_\mu\,s & h\,\eta'_{T\omega}\,\gamma H_{\dot\beta}\,s & (I^*_{p\omega} + I^*_{py} + 2M^*_b h^2)\,s^2 + (C^*_p + h^2\gamma H_\mu - \gamma C_{p\dot p})\,s + K^*_p - hV\,\gamma H_\mu \end{bmatrix}$$

(1.43.3)

$$A'_{32} \equiv \begin{bmatrix} \eta'_{T\omega}\,\gamma M_{\dot\zeta}\,s & y_{T\omega}(-S^*_{\beta o}\,s^2 + \gamma M_\lambda\,s) & 0 \\ \eta'_{T\omega}\,(I^*_{\zeta o\alpha}\,s^2 + \gamma Q_{\dot\zeta}\,s) & y_{T\omega}\,\gamma Q_\lambda\,s & 0 \end{bmatrix}$$

(1.43.4)

$$A'_{23} \equiv \begin{bmatrix} -2\eta'_{Tw}\,\gamma Q_{\dot{\beta}}\,s & 2\eta'_{Tw}\,(I^*_{\zeta o\alpha}\,s^2 + \gamma Q_{\dot{\zeta}}\,s) \\ 2y_{Tw}\,(-S^*_{\beta o}\,s^2 + \gamma T_{\dot{\beta}}\,s) & -2y_{Tw}\,\gamma T_{\dot{\zeta}}\,s \\ 0 & 0 \end{bmatrix} \tag{1.43.5}$$

$$B'_{21} \equiv \begin{bmatrix} 0 & y_{Tw}\,\gamma H_\theta & y_{Tw}V\gamma H_\mu + \gamma C_{q_1\alpha} & 0 \\ -\eta'_{Tw}\,h\,\gamma H_\theta & 0 & 0 & -\eta'_{Tw}\,hV\,\gamma H_\mu \\ 0 & h\,\gamma H_\theta & hV\,\gamma H_\mu & 0 \end{bmatrix} \tag{1.43.6}$$

$$B'_{22} \equiv \begin{bmatrix} 2\eta'_{Tw}\,\gamma Q_\theta & 2\eta'_{Tw}\,V\,\gamma Q_\lambda \\ -2y_{Tw}\,\gamma T_\theta & -2y_{Tw}\,V\,\gamma T_\lambda \\ 0 & 0 \end{bmatrix} \tag{1.43.7}$$

Again it should be mentioned that the final set of the equations of motion for the present model has only constant coefficients.

1.6 Summary

In this Appendix we have developed linearized equations of motion for a simple analytical model of a proprotor and its support in axial flow at high inflow ratio. First, rotor blade flap and lag equations of motion which are described in the rotating frame are Fourier type coordinate transformed to those in the nonrotating frame by introducing new motion degrees of freedom in that frame. The expressions for the aerodynamic flap and lag moments involeved in these equations are also obtained in the nonrotating frame. Then, rotor hub forces and moments are found in the nonrotating frame, and using these hub forces and moments, rotor support equations of motion are presented for two support models, i.e., for a pivotted pylon support and for a cantilevered elastic wing support. Finally, the rotor and support equations of motion are combined to give a set of linear, second order ordinary differential equations with constant coefficients, thus, standard techniques can be applied to examine the dynamics of the system,

It should be mentioned here that we have not considered any coupling between pitch and flap or lag in the above. This is because their influences can be conveniently dealt with by using conventional feedback techniques.

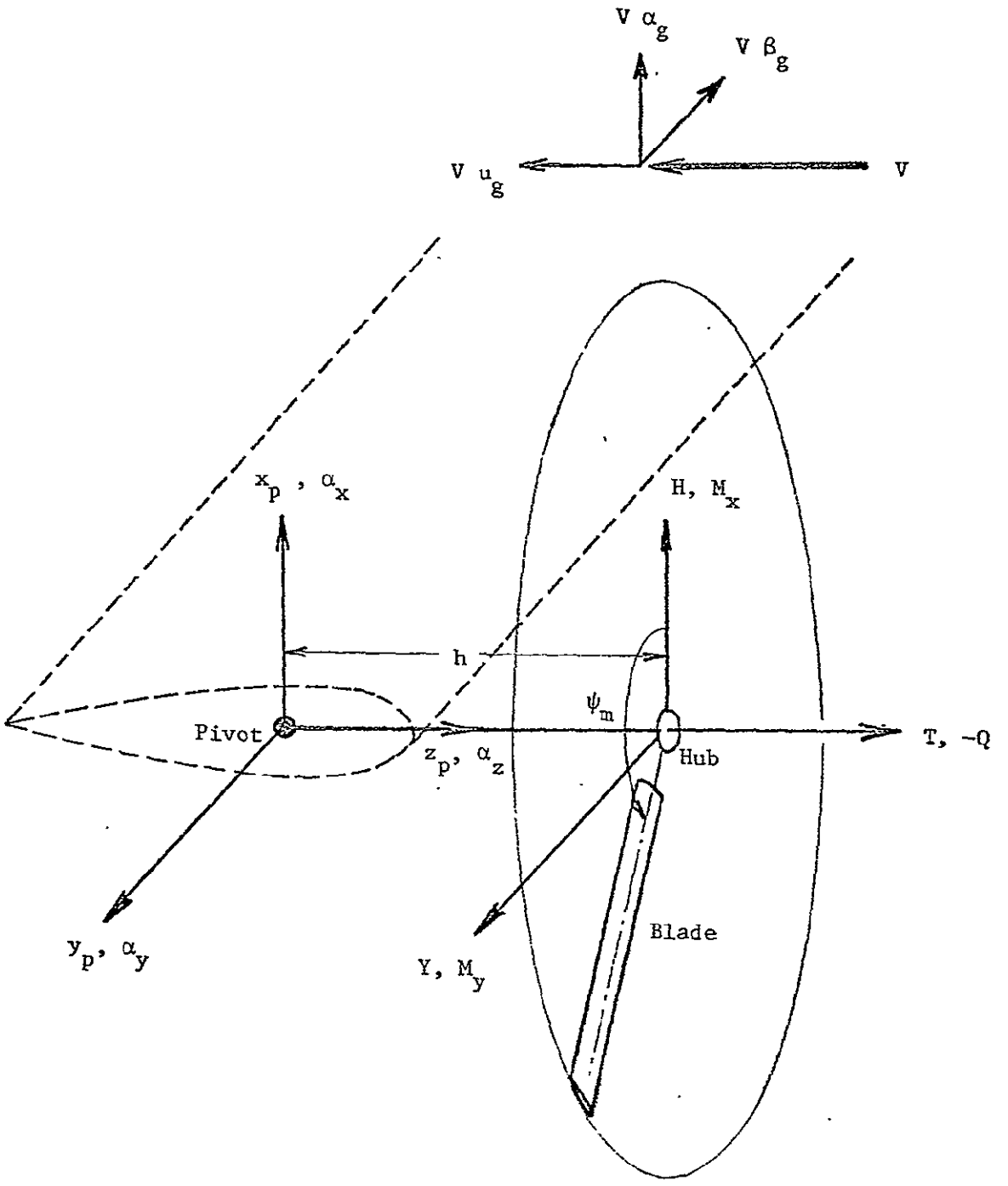

Fig. 1.1 A Model of Proprotor on Its Support: Definition of Hub Forces and Moments, Pylon Linear and Angular Displacements, and Gust Velocities; Only m-th Blade is shown.

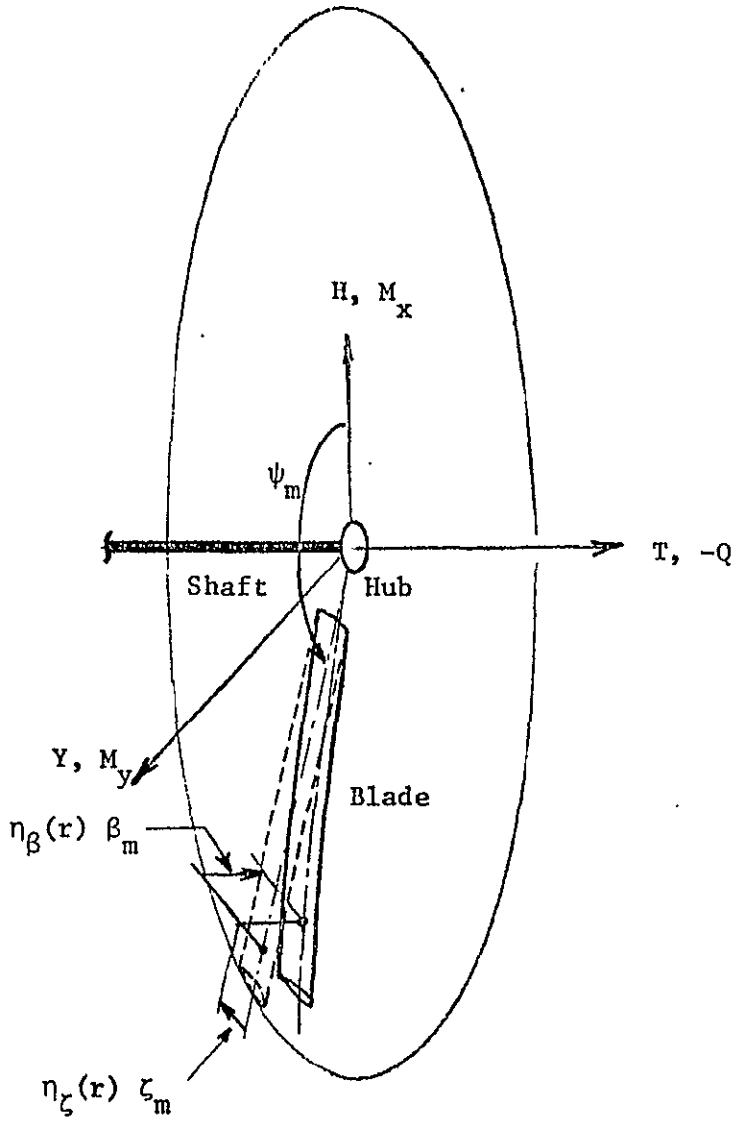

Fig. 1.2 Blade Flap and Lag Deformations (m-th Blade)

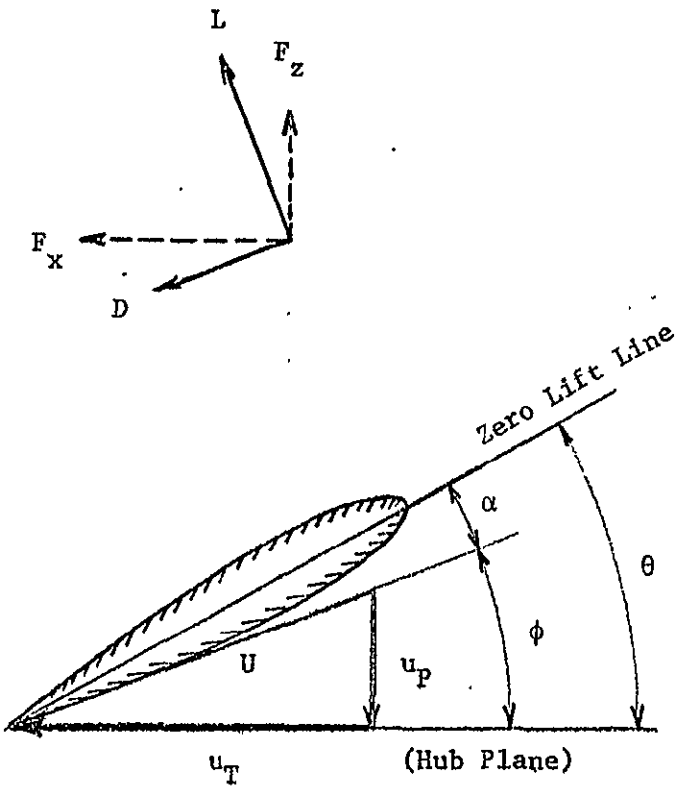

Fig. 1.3 Typical Blade Section: Velocities, and the Resulting Aerodynamic Forces. (Looking Inboard)

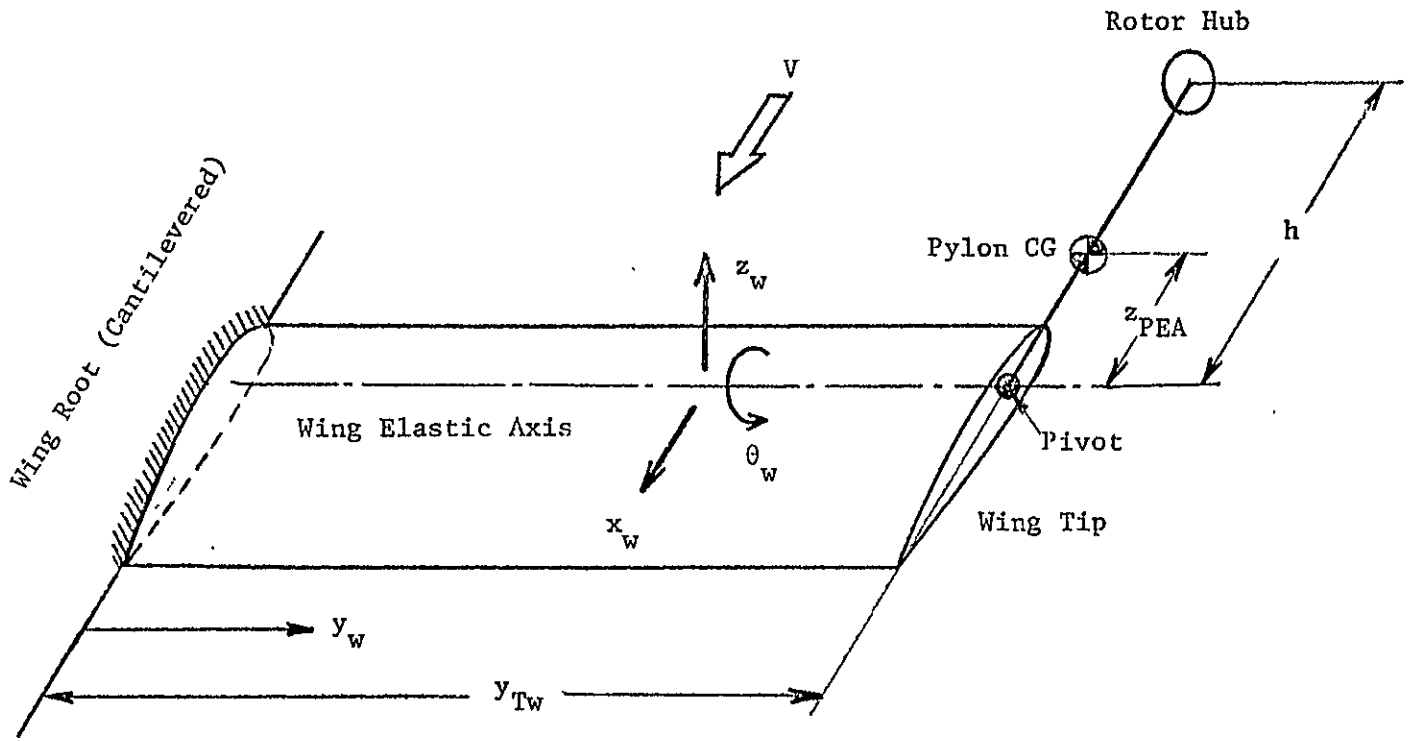

Fig. 1.4 A Model of Cantilevered Elastic Wing As A Proprotor Support

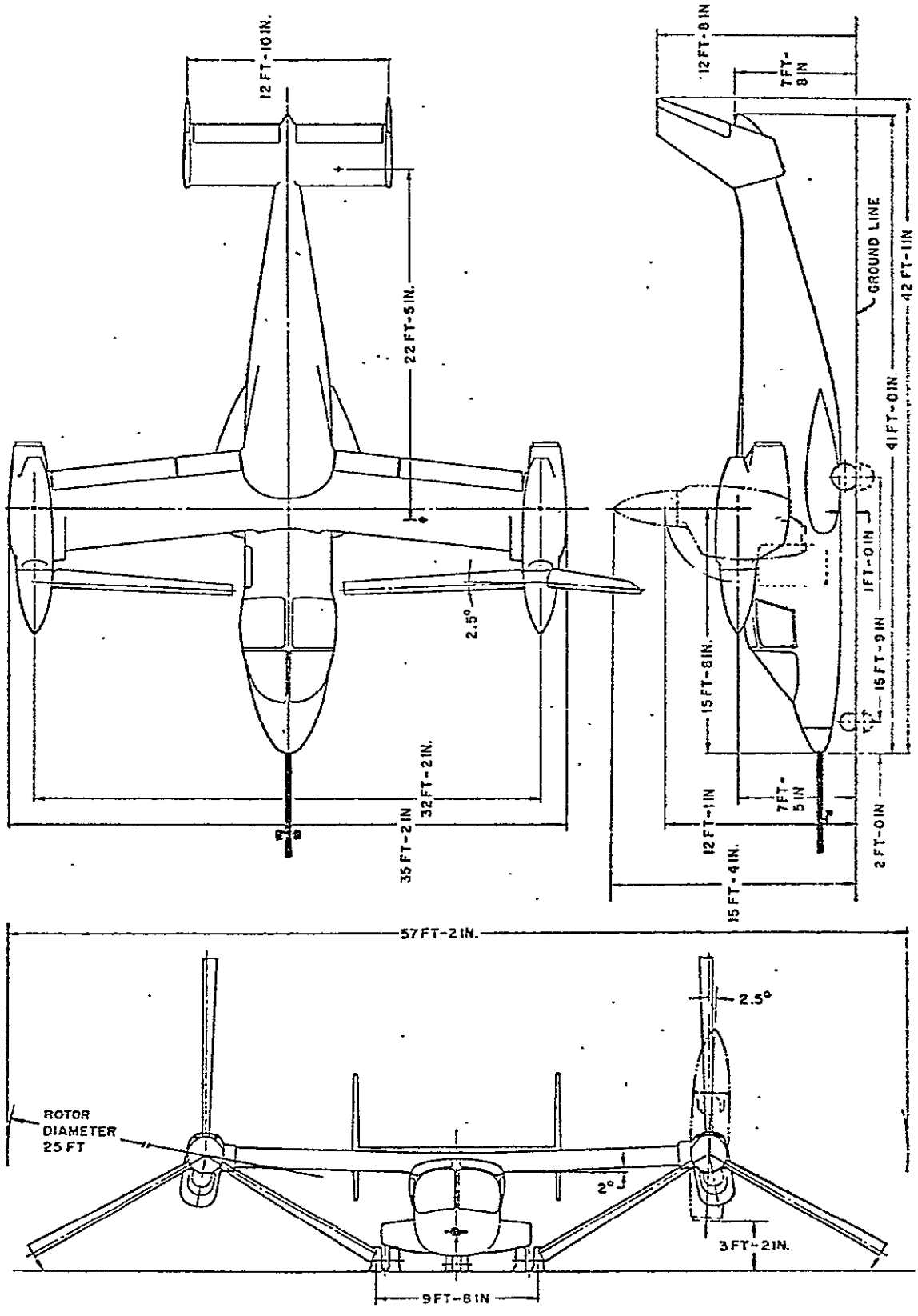

Figure 1.5. XV-15 Aircraft General Arrangement